The role of Ezrin phosphorylation in regulating the relationship between biophysical properties and cell migration

Xiaoli Zhang

This thesis is submitted as part of the requirement for the degree of Doctor of Philosophy

School of Engineering and Materials Science
Queen Mary University of London

Supervisor: Dr. Núria Gavara

2019

Statement of originality

I, Xiaoli Zhang, confirm that the research included within this thesis is my own work or that where it has been carried out in collaboration with, or supported by others, that this is duly acknowledged below, and my contribution indicated.

I attest that I have exercised reasonable care to ensure that the work is original and does not to the best of my knowledge break any UK law, infringe any third party's copyright or other Intellectual Property Right, or contain any confidential material.

I accept that the College has the right to use plagiarism detection software to check the electronic version of the thesis.

I confirm that this thesis has not been previously submitted for the award of a degree by this or any other university.

Xiaoli Zhang

Date:

Abstract

Ezrin, a member of the ERM (Ezrin/Radixin/Moesin) family of proteins, serves as a crosslinker between plasma membrane and actin cytoskeleton. It provides structural links to connect cell cortex and plasma membrane, acting as a signal transducer in multiple pathways during migration, proliferation, and development. Ezrin is also considered crucial during cancer metastasis, due to its altered expression levels and subcellular localization. Nevertheless, the mechanism how Ezrin promotes cancer progression remains unclear. In this thesis, the primary role of Ezrin phosphorylation in the relationship between cell motility, cell mechanical properties and cytoskeleton organization was investigated as follows:

Firstly, long-term live-cell imaging was used to evaluate the effect of Ezrin phosphorylation on cell migration. The key results showed that cells expressing active Ezrin T567D migrated faster, with more protein accumulating at the cell rear.

Secondly, the changes of cell mechanical properties caused by Ezrin were explored by atomic force microscopy (AFM). It revealed that transfection of active Ezrin T567D decreased cortical stiffness but increased cytoskeleton stiffness.

Thirdly, image quantification approaches were carried out to study the effect of Ezrin on three cytoskeleton (actin filaments, microtubules and vimentin) as well as nuclear mechanical properties. The results showed that Ezrin T567D transfection led to thicker actin stress fibers and longer vimentin filaments.

In the end, a sandwich model was developed to study bleb based migration in which Ezrin is also involved. Bleb based migration was observed by confining cells between two pieces of polyacrylamide gels. This model showed potential for the future investigation of Ezrin phosphorylation in bleb based migration.

Altogether, we have fundamentally revealed that dynamic regulation of phosphorylated Ezrin played a pivotal role in cell motility and cell mechanical properties by altering the cytoskeleton's microstructure. These findings are useful for a better understanding of how Ezrin is biophysically involved in cancer progression.

Contents

Acknowledgements

Foremost, I would like to express my sincere gratitude to my supervisor, Dr Núria Gavara, for providing this opportunity to do the PhD with her. Núria is the best example of a good researcher with her immense knowledge across different fields and endless enthusiasm in science. Also she is the best supervisor I have ever met who guided my work and helped me whenever she was needed during the past four years. Particularly, I would like to thank her for her support on my writing of this thesis during my pregnancy in the last year of my PhD study. Núria is a good friend too who shares the life wisdom and experience in carrying and educating a baby.

I would also like to thank Prof. Martin Knight and Prof. Wen Wang for introducing me to Queen Mary University of London and helping me apply for the finance support from Chinese Scholarship Council.

Furthermore, I would like to thank all the colleagues in our group who have provided me with help, inspiration, advice, and encouragement, and who have so generously shared their knowledge and technical expertise with me. Special thanks go to Dr Luís Rafael Pereira do Carmo Flores and Mr Michael Keeling who helped me a lot on the experiment and data analysis.

I would also like to acknowledge Dr Stephen Thorpe, Dr Weiqi Li, Dr Jing Xu, Dr Jordi Gonzalez-Molina, Dr Dexu Kong and Mr Su Fu for their help in the lab.

Great thanks go to Mr Chris Mole, Dr Dongshen Wu, Mr Shafir Iqbal and Mr Jonathon Hills for providing the best lab and office conditions in the School of Engineering and Materials Science.

I would like to thank my parents and my brother for their unconditional love and support, for always believing in me.

At last, I would like to thank my son who is thirteen month old, Muen, for his company during my PhD final year. Despite all the suffering from morning sickness or the happiness for feeling the first fetal movement, you are the biggest surprise in my life. I would like to thank my amazing husband Dr.Mingwen Bai. Thank you for your love and support in my life, for your professional help and suggestion in the writing, for being the best husband and father.

I would also like to acknowledge the Chinese Scholarship Council (CSC) which financially supported my PhD studentship.

List of Figures

List of Tables

List of abbreviations

2D	Two dimension
3D	Three dimension
ABP	Actin binding proteins
AFM	Atomic force microscopy
APS	Ammonium persulfate
Arp2/3 complex	Actin-related protein 2/3 complex
BF	bright field
BM	basement membrane
BSA	Bovine serum albumin
CCD	Charged Coupled Device
CSK	Cytoskeleton
DMEM	Dulbecco's modified eagle's medium
DMSO	Dimethyl sulfoxide
DNA	Deoxyribonucleic acid
E3KARP	NHE3 kinase A regulatory protein
EBP50 protein	ERM-binding phosphoprotein 50
ECM	Extracellular matrix
EMT	Epithelial-mesenchymal transition
ERK1/2	extracellular signal regulated kinase1/2
ERM family	Ezrin Radixin Moesin family
ERULS	ezrin-rich uropod like structure
FACS	Fluorescence-activated cell sorting
FAK	focal adhesion kinase
FBS	Fetal bovine serum
FERM	Four-point one, Ezrin, Radixin, Moesin
FIM	Fluorescence Intensity Manager
FITC	Fluorescein isothiocyanate
GAPs	GTPase-activating proteins
GDIs	GDP dissociation inhibitors
GEFs	Guanine nucleotide exchange factors

GFAP	Glial fibrillary acidic protein
GTDs	Globular tail domains
HCC	Hepatocellular carcinoma cell
HEPES	4-(2-hydroxyethyl)-1-piperazineethanesulfonic acid
HGF	Hepatocyte growth factor
IL-8	interleukin 8
LB	Luria Broth
MAPs	Microtubule associated proteins
MEM	Minimum Essential Media
MGF	mechano-growth factor
MMPs	matrix metalloproteinases
MSDs	Mean squared displacements
MTOCs	Microtubule organizing centers
NES	nuclear export signal
NHE3	sodium–hydrogen exchanger 3
NLS	nuclear localization signal
NMII	non-muscle myosin II
NPFs	Nucleation promoting factors
NTA-Ni	nickel nitrilotriacetic acid
N-WASP	Neuronal WASP
PBS	Phosphate buffer solution
PCR	Polymerase chain reaction
PDGF	platelet derived growth factor
PDMS	Polydimethylsiloxane
PDZ domain	PSD-95/Drosophila discs large/ZO-1 domains
PFA	Paraformaldehyde
PLA2	Phospholipases A2
PLEKHG6	pleckstrin homology domain containing family G with RhoGef domain member 6
PTB	phosphotyrosine-binding
PTEN	phosphatase and tensin homolog deleted on chromosome 10
RPMI 1640	Roswell Park Memorial Institute
SOS	Son of sevenless
SSM	solid-supported membrane
TEMED	Tetramethylethylenediamine
TGF-β	transforming growth factor β
TRITC	tetramethyl rhodamin isothiocyanate
ULFs	Unit-length filaments
VEGF	vascular endothelial growth factor

VEGFR1	vascular endothelial growth factor receptor 1
WASP	Wiskott-Aldrich Syndrome protein
WAVEs	Verprolin homologs
β-DG	β-Dystroglycan

Chapter 1

Introduction

Ezrin, along with other two closely related proteins Radixin and Moesin, constitutes the Ezrin-Radixin-Moesin (ERM) family. In its active state, Ezrin is able to connect actin filaments to the plasma membrane through various membrane proteins, such as CD44. Therefore, Ezrin is important in the regulation of cell morphology and signalling pathways. Overexpression of Ezrin, and especially phosphorylation at amino acid T567,has been reported to be involved in cancer metastasis in recent years [1]. In addition, cancer cells with high metastasis ability were found to be much softer [2]. However, it remains unclear about the exact role of Ezrin in regulation of the relationship between migration and stiffness.

This thesis therefore focuses on the effect of active Ezrin, which is phosphorylated at amino acid T567, on cell migration, cell mechanical properties and three types of cytoskeleton structures. Ezrin has also been involved in bleb based migration as an alternative mechanism when lamellipodium based migration is inhibited. So, another goal of the study is to build a sandwich model aiming to find out the role of Ezrin in bleb based migration. In order to achieve these goals, a combination of long-term live-cell imaging, AFM and image quantification approaches were utilized. Firstly, long-term live-cell imaging is a powerful technique that can be used to directly visualize biological phenomena of single cells over a long period time. A compact microscope has been placed into an incubator where both CO_2 and temperature are well maintained, and the cells are also free of disturbance. Furthermore, high-throughput experimental data have been obtained from multiple fields of view. Moreover, the dynamic behavior of certain protein can be visualized directly through fluorescent cell labelling such as transfection. Secondly, an image analysis pipeline, which was recently developed by our group, was applied for single cell quantification, which can generate 18 parameters including information about cell morphology, cytoskeleton features

and nuclear properties. This useful information could provide explanation for the changes in migration and mechanical properties. Thirdly, a new generation of AFM, with the features of large scanning range, integration with epifluorescence microscopes, well controlled temperature system and various choices of tips, has been employed for mechanical properties analysis. It is superior to traditional cell biological tools, which provides cell topography, stiffness and adhesion force.

Overall, the work in this thesis is divided into two main parts: the first part including chapter 4-6 describes the role of Ezrin phosphorylation in cell migration, cell mechanical properties and cell cytoskeleton, respectively. The results obtained in these chapters constitute the basis of a submitted manuscript which which is now published in the International Journal of Molecular Sciences [3]; Another part, which is chapter 7, describes the development and construction of a sandwich model to study bleb based migration in order to study the role of Ezrin and its mutants in bleb based migration in the future.

Chapter 2

Literature Review

2.1 Introduction of Ezrin

The ERM (Ezrin, Radixin, Moesin) proteins are a family of widely distributed cell membrane-actin filament crosslinking proteins involved in regulating biological processes like cell migration, adhesion and development. The ERM proteins are highly homologous revealing from sequencing analysis, which indicates that the three proteins might arise from gene duplication through the whole evolution. What's more, the first 300 amino acids of ERM proteins share more than 70% similarities [4] (Figure 2.1). Along with other proteins which also contain FERM (Four point one, Ezrin, Radixin, Moesin) domains, ERM proteins belong to the band 4.1 superfamily, involving in connecting proteins to the plasma membrane [5]. Most cell types express multiple ERM proteins and it is believed that ERM proteins have at least partially overlapping functions [6]. Also it has been reported that ERM proteins are expressed in a developmental and tissue-special manner, with many epithelial cells expressing predominantly Ezrin, many endothelial cells expressing predominantly Moesin, and hepatocytes only expressing Radixin [7, 8]. Among the three proteins, Ezrin, is the best and the most widely studied member of the ERM proteins. Especially more and more attentions are drawn on its link to cancer.

Ezrin, a $\sim$80 kDa protein which is encoded by the vil2 (EZR) gene, was first purified from minor components of isolated chicken intestinal microvilli and characterized as a cytoskeletal protein which was concentrated in actin-rich cell surface structures, such as microvilli [9]. It was then shown as a substrate of the protein tyrosine kinases concentrated at surface projections [10]. With the increasing interest in studying Ezrin and the development of new research technologies, Ezrin is now better understood, including its structure, the regulation of its activity, func-

tion, as well as its relationship with cancer progression.

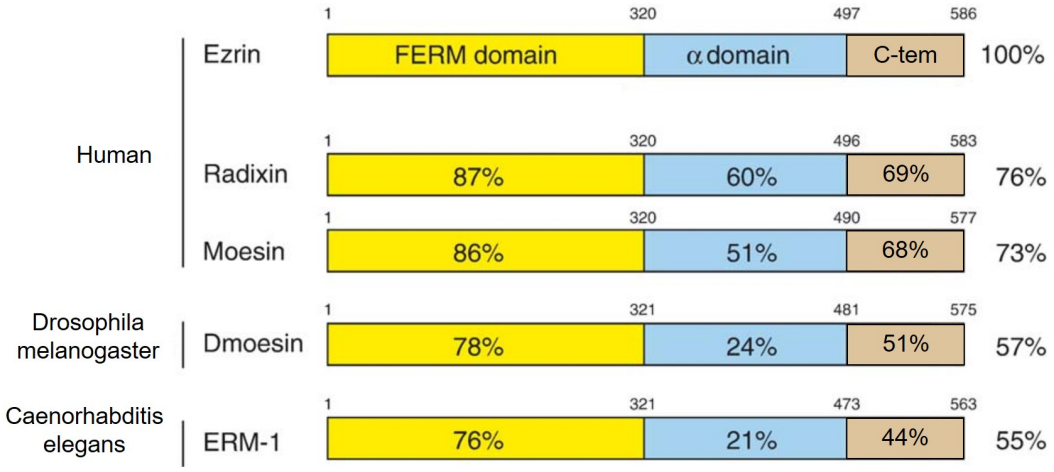

Figure 2.1: ERM proteins are highly conserved through evolution. Overall sequence identity to human Ezrin for human moesin, human radixin, Drosophila melanogaster moesin and Caenorhabditis elegans ERM protein is indicated. The FERM domain and the C-terminal domain share the highest conservation throughout species, from the percentage of sequence identity. Image adapted from Fiévet et al, BBA-Molecular Cell Research, 2007 [4].

2.1.1 The structure of Ezrin

Now the full-length structure of Ezrin protein has been revealed through the rapid progress of structural studies. As shown in Figure 2.2A, Ezrin is composed of three distinct domains: 1) a FERM domain, $\sim$ 300 amino acids, situates at the N-terminus, sharing the most similarities with other members of the ERM family; 2) the C-terminal domain where the phosphorylation on T567 happens, $\sim$ 100 amino acids, has the ability to bind the FERM domain or actin filaments; 3) the central α-helical domain, $\sim$ 200 amino acids, links the FERM domain and the C terminal domain [11, 12, 13].

The X-ray structure analysis of the FERM domain from the three proteins are quite similar with the FERM domain arranged like a clover leaf-like structure that comprises three lobes (F1, F2 and F3) as shown in Figure 2.2B. The lobe F1 is very similar to ubiquitin, lobe F2 adopting structure like acy1-CoA binding protein, and lobe F3 folding into PTB (phosphotyrosine-binding) like structure [14]. The FERM domain of activated Ezrin can bind to cell membrane directly via the cytoplasmic tails of membrane proteins, such as CD44 [15], CD43 [16] and ICAM2 (intracellular adhesion molecule2) [17], or indirectly via other scaffolding proteins

which have PDZ (PSD-95/Drosophila discs large/ZO-1) domains, such as EBP50 (ERM-binding phosphoprotein 50) [18] and E3KARP. The sodium-hydrogen exchanger regulatory factors, EBP50 and E3KARP (NHE3 kinase A regulatory protein) are a family of adaptor proteins characterized by two tandem PDZ protein interaction domains which have the ability to bind to multiple different membrane proteins, and a C-terminal domain that can bind to the ERM family proteins [19]. In this way, Ezrin can work with and regulate more membrane proteins.

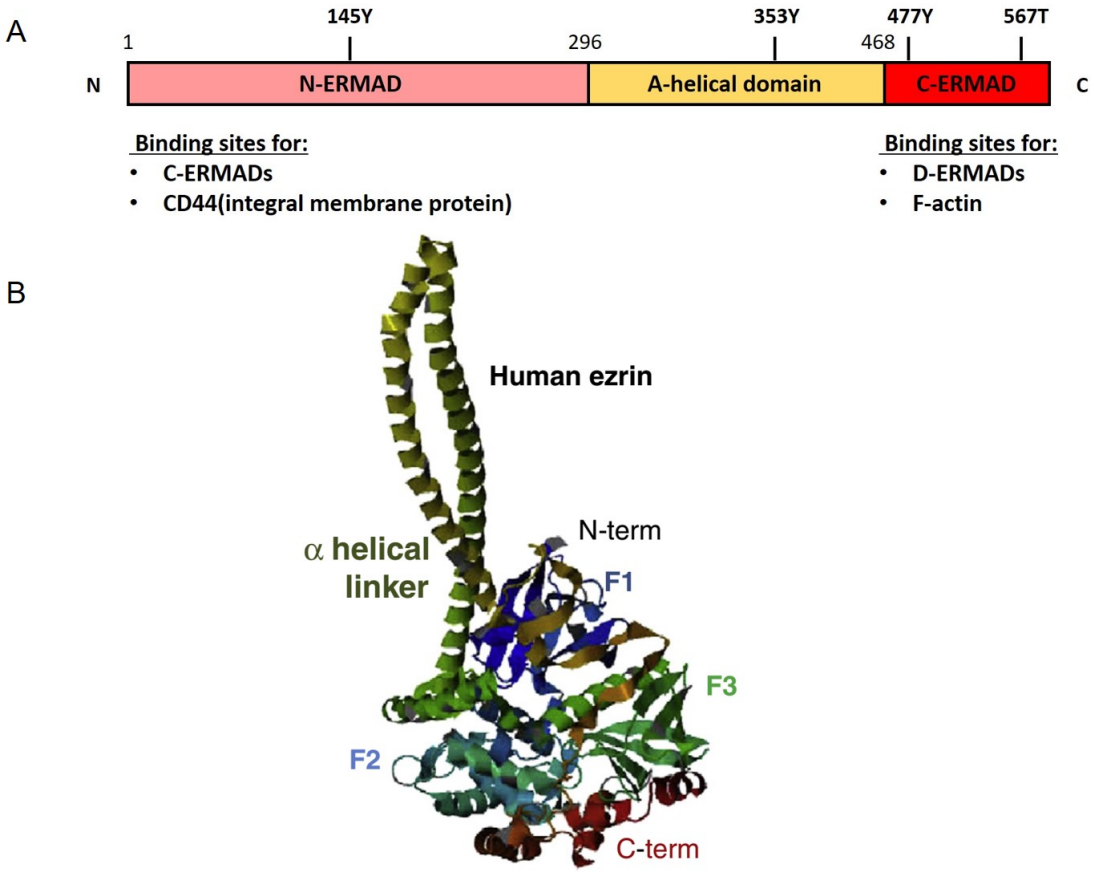

Figure 2.2: Domain structure of Ezrin. A. Domain organization of human ezrin: FERM domain, the C-terminal domain and α-helical domain. Major phosphorylation sites: 145Y, 353Y, 477Y, and 567T; B. Ribbon structure of dormant human Ezrin. F1 (dark blue), F2 (light blue) and F3 (green) are the three lobes of the FERM domain. The central α-helical region (green) links the FERM domain to the C-terminal domain (red). Image taken from Maniti et al, BBA-Biomembranes, 2012 [20].

Another important domain of Ezrin is the C-terminal domain, only 100 amino acids, which involves in regulation of Ezrin activity, and binding to actin filament and FERM domain. The phosphorylation state of amino acid threonine at 567 within the C-terminal domain is important in Ezrin activity. The last 34 residues of Ezrin were identified as actin filament binding site, which correspond to the last

three helices (αB, αC and αD) and are strongly conserved in the ERM proteins [13]. While among the 34 residues, R579 was reported to be the main actin-binding residue, which is also involved in the interaction with FERM domain [21]. While about 80 residues of 100 residue-C-terminal were found to bind tightly to the FERM domain, by which the actin filament site was masked [11].

For a long time, the central α-helical domain was thought to simply link the FERM domain and C-terminal domain until the full-length of insect Spodoptera frugiperda Moesin was successfully crystallized [22]. There were three α-helices, with the first α-helices folding back along lobe F1 and F2, the second helix in contact with lobe F1 in a hydrophobic way and extending as an anti-parallel coiled-coil with the third helix which lands on the back of lobe F1 and connects via a linker region to the C-terminal domain (Figure 2.2B).

2.1.2 The regulation of Ezrin activity

The structure of Ezrin and ability to interact between FERM domain and C-terminal domain determines the way how its activity is regulated. Instead of regulation at DNA transcription level and mRNA translation level, Ezrin activity is negatively regulated at protein level by intramolecular or extramolecular interaction between the FERM and C-terminal domains from the same molecule or other molecule [11], forming a monomer or homo-dimer. In its inactive state, the C-terminal domain adopts an extended structure, binding and covering a large region of F2 and F3 domains on the FERM domain [14] (Figure 2.2B). Therefore, the FERM-C terminal interaction masks both the cell membrane and actin filament binding sites, leading to a closed conformation. As a result, inactive Ezrin stays in the cell cytoplasm, forming a pool waiting to be activated.

The activation of Ezrin has been proposed to follow a two-step mechanism. The first step occurs when the FERM domain binds to phosphatidylinositol-4,5-bisphosphate (PIP2) at the membrane and at the same time, Ezrin translocates from cytoplasm to cell membrane [23]. FERM domain of Ezrin (amino acids 1–300) was necessary and sufficient for interaction with PIP2-containing liposomes [24]. Amino acids that are involved in binding to PIP2-containing liposomes have been identified. They are in two distinct regions of this domain. Amino acids 12–115 and 233–310 of Ezrin were reported to be involved in binding to PIP2, both regions containing a KK(X)$_n$K/RK motif conserved in the ERM family [25]. PIP2 is an important regulator during Ezrin activation. It has been reported that PIP2 was required in the association of Ezrin with the cytoplasmic tail of membrane protein, CD44 in vitro and in vivo, which suggested that the

binding of PIP2 with Ezrin leads to conformational changes, releasing the binding sites for the membrane proteins [23]. An in vitro system demonstrated that Ezrin bound via PIP2 to a solid-supported membrane (SSM) is capable of binding actin filaments, while Ezrin bound via a His-tag to a lipid bilayer displaying nickel nitrilotriacetic acid (NTA-Ni) headgroups does not significantly interact with F-actin, which may indicate that activation of ezrin can occur as a consequence of PIP2 binding and does not require additional cofactors [26].

The second step is that the threonine 567 within the C-terminal domain is phosphorylated by a number of kinases. Based on the first discovery that Moesin was phosphorylated on threonine 558 during platelet activation [27], the threonine 567 of Ezrin was found to be related with protein activation by replacing the threonine with aspartate [28]. Therefore the second regulator during Ezrin activation is kinases. Several kinases have been reported to be involved in the phosphorylation of the threonine 567. For example, Rho-kinase has the ability to phosphorylate the C-terminal threonine of Ezrin, regulating the head-to-tail interaction [28]. And protein kinase C (PKC) α has been shown to interact with Ezrin and phosphorylate Ezrin at T567, promoting cell migration at the wound edge [29]. Also Akt2 can phosphorylate the threonine 567 of Ezrin, triggering sodium–hydrogen exchanger 3 (NHE3) translocating to the membrane and activation [30]. Phosphorylation of the threonine residue within the C-terminal domain of Ezrin is considered a hallmark of Ezrin activation which can stabilize the active open conformation of Ezrin and prevent the interaction between FERM domain and C-terminal domain. This activation results in linking between plasma membrane and actin cytoskeleton through the FERM domain binding to plasma membrane proteins directly or scaffolding proteins indirectly and the C-terminal domain binding to the actin filament.

It is crucial for proper Ezrin activation that the binding of PIP2 and phosphorylation at threonine 567 act sequentially, as impairing one of these steps alters the correct localization and functions of Ezrin in epithelial cells [31]. The replacement of a threonine by an aspartic acid at 567 of Ezrin does not fully mimic a phosphorylated threonine, as for example, it lacks one of the negative charges at pH 7.4 [32], even though this mutation has been frequently used [33]. Also it has been reported that wild type Ezrin and Ezrin T567D adopt a closed conformation in solution, where F-actin binding site on C-terminal domain is not accessible. Only after binding to PIP2-containing bilayers, Ezrin T567D was able to undergo a remarkable conformational change, which attributing to an opening of the conformation resulting in monomeric protein on the lipid bilayer [34]. All these suggest that the process of Ezrin activation could not bypass the binding of PIP2.

Apart from phosphorylation at T567 of Ezrin for conformational activation, there

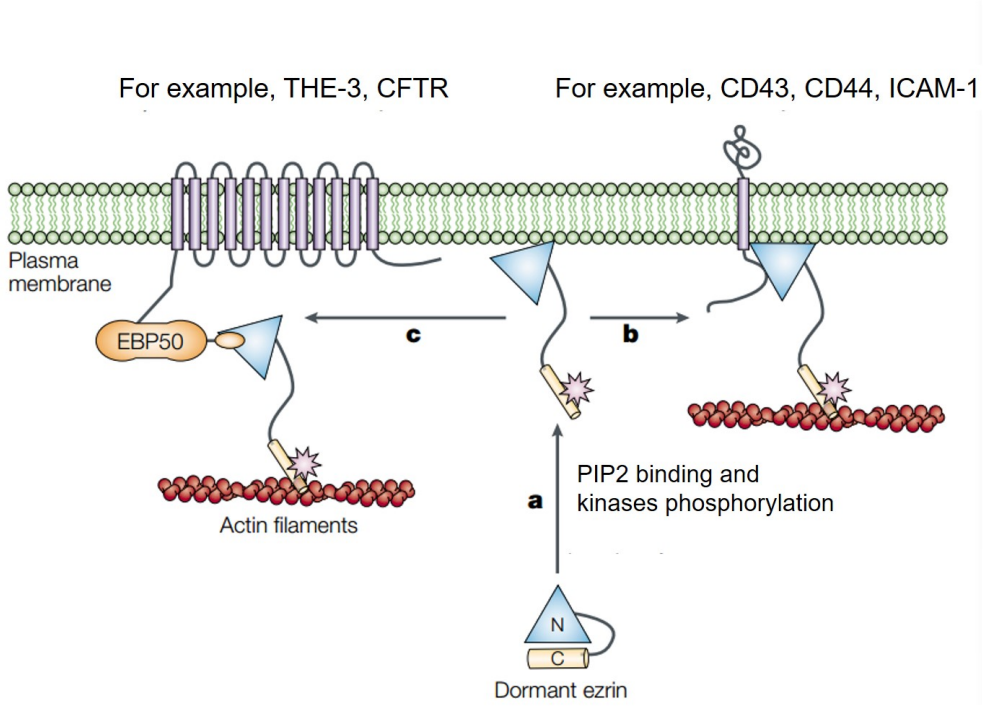

Figure 2.3: The process of Ezrin activation. Ezrin exists in an inactive state by its FERM domain associated with the C-terminal domain. Binding to PIP2 leads Ezrin translocating to the plasma membrane, then phosphorylated by kinases like Rho kinases. Activated Ezrin can participate in actin filament and membrane linkage either by direct association with transmembrane proteins like CD43, CD44 and ICAM-1, or indirectly through scaffolding proteins like EBP50 to bind to transmembrane proteins like THE-3, CFTR. Image taken from Bretscher et al, Nat Rev Mol Cell Biol, 2002 [35].

are other phosphorylation sites which are involved for signaling to downstream events (Figure 2.2 A). Residues of Y145 and Y353 were detected as the sites of phosphorylation after EGF treatment of A431 cells [36]. Y145F and Y353F, the phosphodeficient mutant, have been further reported to perturb morphogenic response to HGF [37]. Phosphorylation of Ezrin at Y353 has been reported to be important in signal survival during epithelial cell differentiation via the phosphatidylinositol 3-kinase [38]. Lck was reported to phosphorylate Ezrin at Y145 in T cells [39]. Ezrin T477 can be phosphorylated in a Src-dependent manner [40], which is important for HGF-induced cell scattering [41]. It has been further reported that interaction of Fes kinase with phosphorylated Ezrin at Y477 promotes HGF-induced scattering of epithelial cells [42]. Moreover, phosphorylation of Y477 Ezrin has been reported to be required for growth and invasion of Src-transformed fibroblasts in 3 dimensional (3D) matrix cultures. As well as invasion and metastasis of breast cancer cells, AC2M2 [43]. These phosphorylation sites may affect each other if one of them is mutated. For example, Y145 which locates in FERM domain, may be blocked by the constitutively interaction of FERM

domain and C-terminal domain in Ezrin T567A mutant.

2.1.3 The function of Ezrin

Ezrin has the ability to regulate interactions between cell membrane and actin cytoskeleton underneath. Regulated attachment of membrane proteins to actin filament is essential for many fundamental processes, including cell morphology, cell-cell adhesion, cell development and cell migration, as well as providing structural support to strengthen the cell cortex. At the same time, Ezrin participates in regulating cell signal pathways, through formation of specialized membrane domains which brings receptors and downstream signalling molecules together.

Ezrin functions as organizer of cell-cell adhesion and cell-matrix adhesion. Interaction with the cytoplasmic domains of adhesion membrane proteins can recruit these proteins to a specific membrane domain and facilitate adhesion. The localization of Ezrin in adherent junctions is regulated by Rac in a manner involving PIPK. The F-actin binding capacity of Ezrin is also needed [44]. Ezrin regulates the adhesion junction assembly, controlling the localization of E-cadherin in cells. Dysregulation of Ezrin expression in cells would result in poor maintenance of adhesive junctions. As it has been reported that experimental inhibition of Ezrin expression using antisense oligonucleotides generated a phenotype which formed loose cell-cell adhesions [45]. In addition, expression of T567 phosphorylated Ezrin decreased the connection, transferring the E-cadherin from the plasma membrane to the intracellular compartments [46].

Ezrin can regulate cell migration in different ways. Polarization of the cell is required for the first step of migration. It has been reported that phosphorylated Ezrin, activated by Mst4, was involved in the induction of brush border formation downstream of polarization complex [47]. Migration speed control is another step of Ezrin regulation. It is shown that PKCα enhanced cell migration at the wound edge by phosphorylation of Ezrin at T567 and mutant Ezrin T567A impairs PKCα mediated motility [29]. Ezrin promotes cell migration in response to hepatocyte growth factor (HGF) treatment, measured by wound healing experiment of epithelial cell line, LLC-PK1 cells [48]. Apart from that, Ezrin takes part in regulation of direction of migration. It has been reported that active Ezrin recruits Cdc42 and Rho-specific GEF Dbl to the lipid raft microdomains at the leading edge of the membrane and facilitates directed migration [49]. Furthermore, Ezrin is an important participant in bleb-based migration as asymmetries in the degree of membrane cortex attachment resulting from the asymmetric distribution of Ezrin. The site where Ezrin distribution level is reduced determines the initial place of

bleb formation, which is the direction of cell migration [50].

Ezrin is also involved in signal transduction pathways by associating with signalling proteins. The best example is the relationship between Ezrin and Rho family, which is complex. As Ezrin has the ability to act either as effectors of Rho GTPases or as regulators of their activity, suggesting that there is a positive feedback loop between the two type of proteins. Rho family GTPases are small GTP-binding proteins and, have a well-recognized role in the regulation of migration by acting on the cytoskeleton. The most extensively investigated and best characterized subfamilies are RhoA, Rac and Cdc42 subfamilies. Typically, Rho family GTPases act as molecular switches cycling between inactive (GDP-bound) and active (GTP-bound) forms. This cycling regulation is influenced by the activity of guanine nucleotide exchange factors (GEFs), GTPase-activating proteins (GAPs), and GDP dissociation inhibitors (GDIs) [51, 52, 53] (Figure 2.4). GEFs activate the Rho GTPases by catalyzing the exchange of GDP to GTP. While GAPs simulate the the intrinsic GTPases activity, leading to the inactivation. GDIs contributes to sequester Rho GTPases from the plasma membrane and keep them in an inactive form.

On one hand, as described above, Ezrin activity is regulated by a combination of PIP2 binding and phosphorylation at T567, both acting downstream of signals mediated by Rho [55]. On the other hand, recent studies show that Ezrin also can regulate Rho-pathway activity through direct interaction with proteins that regulate Rho functions as shown in Figure 2.4. ERM family was reported to directly interact with Rho GDI, promoting the activation of the Rho subfamily members by reducing the Rho GDI activity [56]. Ezrin was found to be able to form complex with Rho GDI under normal condition and phosphorylation of Ezrin at T235 was found to induce the release of Rho GDI from the complex to inhibit Rac1 activity in senescent cells [57]. Also it shows that Ezrin works like scaffolds associating with both GDP-bound Ras and its GEF SOS (son of sevenless) to form a complex, to enhance the catalytic activity of SOS and thereby Ras activation [58]. Ezrin recruits PLEKHG6 to the apical pole of epithelial cells where PLEKHG6 (pleckstrin homology domain containing family G with RhoGef domain member 6), induces the formation of microvilli and membrane ruffles [59]. Active Ezrin associates with Gem at the plasma membrane to organize actin cytoskeleton by regulating the activity of Rho pathway [60]. All suggest that Ezrin regulates Rho activity in a positive way.

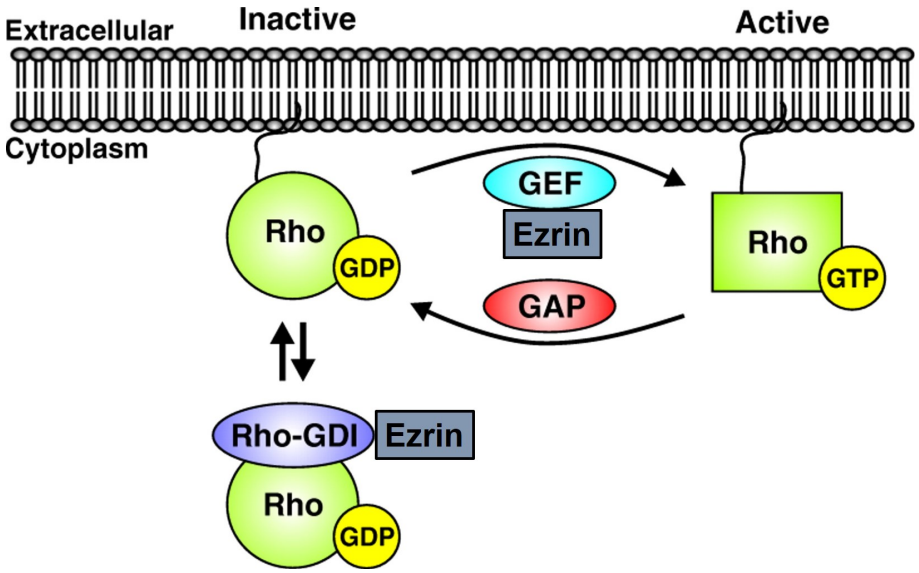

Figure 2.4: Interaction between Ezrin and Rho GTPases. In unstimulated cells which doesn't have enough activated protein to make cells react, Rho GTPases remain inactive bound with RhoGDI in the cytoplasm. Dissociation from RhoGDI activated Rho GTPases and Rho GTPases are targeted to the plasma membrane. Membrane recruitment and interaction with RhoGEFs induces the exchange of GDP for GTP on Rho GTPases, resulting in Rho GTPases activating the downstream effectors. RhoGAPs inactivate RhoGTPases by increasing their intrinsic GTPase activity, accelerating hydrolysis of GTP to GDP. RhoGDIs are able to extract GDP-bound Rho GTPases from the membrane. Ezrin could interact with GDI and GEF to regulate the activity of Rho GTPases. Image adapted from Huveneers et al, J Cell Sci, 2009 [54].

2.1.4 Ezrin and cancer progression

Deregulation of cell-cell contacts and increasing cell migration are both important steps during cancer metastasis, which make Ezrin crucial in cancer development. Furthermore, an increasing number of evidences have suggested that Ezrin has been involved in tumour progression, especially metastasis. Proteomic profiling and immunohistochemical analyses have demonstrated that not only the level of Ezrin expression, but also its activation state and its subcellular localization of Ezrin are vital factors in tumour progression. A table of references describing the role of Ezrin in cancer progression is shown in table 2.1.

Many studies have compared the expression level of Ezrin between cancer samples and healthy samples to figure out how Ezrin affects cancer progression. High Ezrin expression is associated with large tumour size, early development of metastasis, advanced clinical stage and lower overall survival rate in cancers, such as pancreatic ductal adenocarcinomas [61], uterine cervical cancer [62], colorectal cancer [63], osteosarcoma [64]. Inhibition of Ezrin expression in cancer

cells resulted in reduced proliferation ability and decreased migration and invasion [65]. Altogether, it suggests that high Ezrin expression is closely related to cancer progression.

Apart from changes in Ezrin expression level, it is found that changes in Ezrin phosphorylation level at T567 also associate with cancer progression. Many clinical studies have linked high expression of phosphorylated T567-Ezrin with poor outcome in patients that suffer from a wide variety of cancers. T567 hyperphosphorylation of Ezrin was reported to be tightly correlated to an invasive phenotype of clinical hepatocellular carcinomas and to poor outcomes in tumour xenograft assays [66] (Figure 2.5). Phosphorylation of Ezrin at T567, regulated by hormonal androgen through PKCα, was shown to induce Matrigel invasion of prostate cancer cells [67]. In addition, it has been reported that the regulation of Ezrin phosphorylation at T567 was a dynamic process during metastatic progression. Metastatic osteosarcoma cells expressed phosphorylated T567 Ezrin early after their arrival in the lung. There was a loss of phosphorylated T567 Ezrin during the metastatic lesion growing. Then re-expression of phosphorylated Ezrin was found at the invasive front of larger metastatic lesions [68].

The distribution pattern of Ezrin inside cells is another factor that affects cell behaviours. As a cross-linker between actin filament and plasma membrane, the localization of Ezrin determines the position of proteins that it interacts with. Many studies have found a relationship between Ezrin distribution and cancer progression. In some cancers, like breast carcinomas [69], lung cancer [65], the switch of Ezrin localization from the apical membrane to the cytoplasm or to the membrane in a non-polarized manner is correlated with significant lymph node metastasis and adverse clinical features. Moreover, Ezrin was widely distributed in the cytoplasm and membrane, while some cancers showing a cell membrane staining pattern like pancreatic ductal adenocarcinomas cells [61], some cancers showing a polarized distribution concentrated at the protrusion site, like gastric cancer cells [70]. Strong perinuclear staining of Ezrin has also been observed in cervical cancer, with some showing cytoplasmic and diffuse localization [62]. However, other studies showed contradictory results that cervical cancer patients with the perinuclear Ezrin expression pattern had longer survival time than those with the cytoplasmic Ezrin expression pattern [71].

Through modification of expression level, phosphorylation level and distribution pattern, Ezrin is involved in cancer progression. Its downstream effector, E-cadherin, is a major player in epithelial-mesenchymal transition (EMT). EMT is an imperative process during cancer progress that allows a polarized epithelial cell to undergo multiple biochemical changes acquiring mesenchymal, fibroblast-

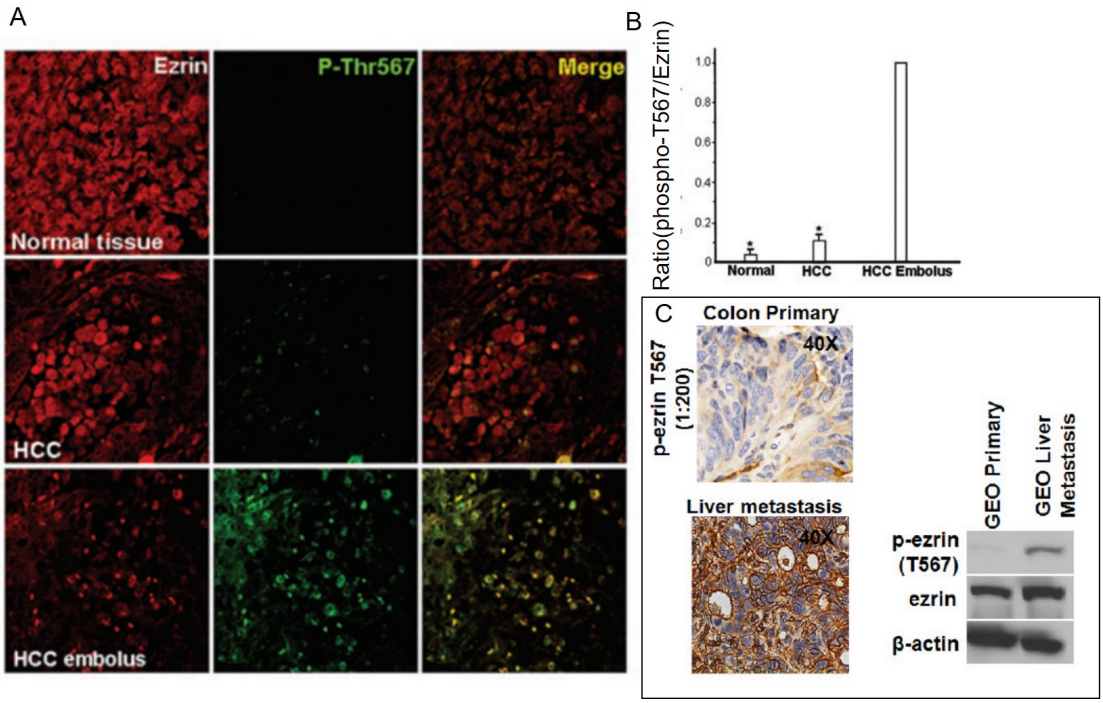

Figure 2.5: Phosphorylated Ezrin is involved in tumour progression, especially metastasis. A. Confocal images of double immunofluorescence of P-T567 Ezrin (green) versus Ezrin (red) in normal and hepatocellular carcinoma cells (HCC). Image taken from Chen et al, Cancer research, 2011 [66]. P-T567 Ezrin is highly expressed in metastatic HCC; B. Quantitation of P-T567 Ezrin levels in normal liver and HCC tissues; C. Immunohistochemical and western blot analysis of the GEO primary colon and liver metastatic tumors shows increased P-T567 Ezrin staining in the liver metastasis. Image taken from Leiphrakpam et al, Cellular signalling, 2014 [63].

like properties, showing reduced cell-cell adhesion and increased motility [72]. Ezrin, involved in organizing adherence junctions of cell-cell communications, is able to deregulate E-cadherin function. Recent study showed that Ezrin acted co-operatively with activated c-Src in deregulating cadherin-based cell-cell contacts, scattering of SP1 cells and preventing cell aggregation [73]. Silencing of Ezrin by small hairpin RNA showed reduced motility and invasion ability, increased E-cadherin expression and decreased phosphorylated β-catenin, reversing the metastatic behaviour of human breast cancer cells [74]. What's more, recent evidences suggest that Ezrin regulates cancer progression not only by controlling the E-cadherin expression, but also controlling E-cadherin localization. Ezrin expression was negatively correlated with E-cadherin expression in breast cancer with a high expression of Ezrin and a low expression of E-cadherin concentrated in the plasma membrane [75].

Table 2.1: Ezrin and cancer progression

Cancer type	Cell type	Model	Key findings
astrocytoma	patient samples	2D	Ezrin expression was positively correlated with tumor grade and increased malignancy[76]
breast cancer	AC2M2 (metastatic)	3D in vivo	overexpression of ezrin induced lung metastases [77]
	MCF10A (invasive) and patient samples	2D	ezrin relocalises to motile projections in invasive cell lines and the cytoplasm of breast tumours [78]
	MDA-MB-231 (invasive)	3D in vitro [79], 3D in vivo [80]	Silencing of Ezrin inhibited cell motility and invasion and induced an increased E-cadherin expression
	AC2M2 (metastatic)	3D in vitro and in vivo	Overexpression of Ezrin Y477F inhibits cell migration and invasion [43]
	MDA-MB-231 and AC2M2	3D in vitro and in vivo	silencing of ezrin reduced angio/lymphangiogenesis, cell migration, tube formation, and permeability [81]
	patient samples	2D	Ezrin expression was negatively correlated with E-cadherin expression [82]; High expression of Ezrin promotes migration, invasion, and angiogenesis [83]
	MDA-MB-231	3D in vitro and in vivo	ezrin regulates cancer cell invasion and metastasis by promoting FA and invadopodia turnover [84]
	SP1	2D	Ezrin works with c-Src in deregulation of cell-cell contacts and enhancing scattering [85]

	patient samples and EO771 (metastatic)	3D in vitro and in vivo	high expression of ezrin in lymph node metastases; high ezrin level is associated with increased relapse [86]
cervical cancer	HeLa, SiHa, C33A, and CaSki and patient samples	2D	Ezrin works as a regulator of epithelial-mesenchymal transition (EMT) and metastasis; perinuclear Ezrin expression pattern had longer survival time [87]
	patient samples	2D	expression of ezrin is associated with cancer grade [88]
colorectal cancer	patient samples	2D	Higher expression of the Ezrin correlates with tumor aggressiveness and worse prognosis [89, 90], tumor size, serosal invasion, lymph node metastasis [90], poor survival [91], ezrin expression was cytoplasmic [90]
	GEO	3D in vitro	increased expression of ezrin and phosphorylated ezrin at T567 is associated with liver metastasis [63]
endometrioid carcinomas	patient samples	2D	high ezrin expression correlated with poor overall survival [92]
esophageal squamous carcinoma	EC109, EC8712, EC171 and SHEEC	3D in vitro and in vivo	silencing ezrin suppresses the growth, adhesion and invasiveness of cells in vitro and tumour growth in vivo [93]
	patient samples	2D	ezrin expression was related to poor overall survival of ESCC patients [94]
	ESCC-DR (metastatic)	2D	Phosphorylated ERM (ezrin, radixin, moesin) was expressed at the leading edge, or invasive front [95]

Tongue Squamous Cell Carcinoma	patient samples and HSC-3	2D	Ezrin is overexpressed and silencing of Ezrin reduced cell migration, and invasiveness [96]
gastric cancer	patient samples	2D	ezrin is overexpressed [97, 98]; high expression of Ezrin is associated with lymph node and distant metastasis, and poor prognosis[98]
	SGC-7901 (metastatic)	2D	inhibition of ezrin expression inhibited cell migration and invasion [99]
gastrointestinal cancer	patient samples	2D	high ezrin expression was related with worse 5-year disease-specific survival [100] and poor disease-free survival [100, 101]
glioblastoma	LN18, LN229, LN308, U373, U251-MG, D54, and A172	2D	high ezrin expression inhibited NF2 activity by intermolecular association and aberrant intracellular recruitment [102]
Hepatocellular Carcinoma	HepG2	3D in vitro and in vivo	hyperphosphorylation of ezrin t567 was correlated to an invasive phenotype and poor outcomes in tumor xenograft assays [103]
	MHCC-1, MHCC97-H, SF7721, SMMC7721, Hep3B, and HepG2	2D	high ezrin expression was associated with high metastatic potetial [104]

	LNM-HCC(high metastasis) Hca-P (low metastasis)	2D	Ezrin expression was higher in high LNM-HCC than low LNM-HCC [105]
intraepithelial neoplasia	patient samples	2D	ezrin is overexpressed [106]
laryngeal squamous cell carcinoma	patient samples	2D	high ezrin expression was related to clinical stage, T stage, and cervical lymph node metastasis [107]
lung cancer	LTE, BE1, H446, and H460	2D	silencing of ezrin reduced cell migration and invasion; ezrin expression correlated with lymphatic metastasis [108]
	patient samples	3D in vivo	Ezrin was up-regulated at sites of bone metastasis [109]
Soft Tissue Sarcomas	patient samples	2D	expressions of ezrin is associated with distant metastasis, death and overall survival [110]
myxofibrosarcomas	patient samples	2D	high Ezrin expression was associated with tumor necrosis, increased histological grades, advanced Cancer stages, and higher mitotic rate [111]
nasopharyngeal carcinoma	patient samples	2D	high ezrin expression was related to high lymph node metastatic rate [112]
non-small cell lung cancer	patient samples	2D	high expression of ezrin, p-ezrinT567, and p-ezrinT353 were correlated with late stage and poor differentiation; p-ezrinT567 was correlated with lymph node metastasis [113]

	patient samples	2D	The expression of ezrin were correlated with pleural invasion, pathologic stage and shorter survival [114]; high-level ezrin expression contributed to increased tumor stage and lymph node metastasis [115]
osteosarcoma	K7M2 (metastatic)	3D in vivo	ezrin expression provided a survival advantage reaching the lung, expression of ezrin t567a inhibited experimental metastases [116]
	MG63 (poorly metastatic)	3D in vivo	overexpression of ezrin in MG63 cells promoted tumor cell invasion and migration [117]
	patient samples	2D	expression or high expression of ezrin was related with metastase, recurrence and poor survival [118, 119**?** , 120]
	MNNG/HOS (metastatic)	2D	Ezrin phosphorylation at T567 was dynamically regulated during metastatic progression [121]
	non-metastatic patient samples	2D	cytoplasmic and membranous immunostaining of ezrin was related with lower 3-year probability of disease-free survival [122]
ovarian carcinoma	patient samples and SKOV-3 (metastatic)	3D in vitro	High expression of Ezrin was related with reduced overall survival. silencing of ezrin inhibited skov-3 in vitro invasion [123]
pancreatic cancer	MiaPaCa-2 (metastatic)	3D in vitro and in vivo	Ezrin overexpression promoted cell motility and invasion, and increased the number of metastatic foci [124]
	PaCa3	2D	Podosome and podosomal rosette formation is ezrin dependent and associated with cancer invasion [125]
salivary gland adenoid cystic carcinoma	patient samples	2D	overexpression of Ezrin was related to tumor size, clinical stage, perineural and vascular invasion, and recurrence [112]

Pancreatic Ductal Adenocarcinoma	patient samples	2D	overexpression of pEzrin-T353 was associated with lymph node metastasis, less differentiation, pAkt overexpression, and shorter survival times [126]
	patient samples	2D	Overexpression of ezrin was related with larger tumor size, lymph node metastasis and advanced clinical stage [127]
prostate cancer	LNCaP-FGC, LNCaP-R and PC3	2D	ezrin works as a mediator of c-Myc-induced tumorigenesis [128]
rectal cancer	patient samples	2D	high ezrin expressin was related with short local recurrence [129]
urothelial bladder cancer	patient samples	2D	reduced membranous ezrin expression or ezrin expression was associated with more advanced T-stage, impaired survival [130]
uterine cervical cancer	patient samples	2D	Ezrin overexpression was related with poor differentiation, late stage, and lymph node metastasis [131]
melanomas	patient samples	2D	expression of ezrin is associated with higher mortality [132]
rhabdomyosarcoma	patient samples	2D	Ezrin expression was enhanced and correlating with clinical stage [133]

2.1.5 Summary

In summary, Ezrin, a member of ERM family, is a linker between cell membrane and actin cortex, which is involved in regulating of cell morphology, migration and development. The phosphorylation of the amino acid T567 locating at C-terminal domain is crucial for Ezrin activation. In addition, Ezrin has been reported to participate in cancer metastasis, through increased expression of Ezrin or phosphorylated Ezrin at T567, or Ezrin intracellular distribution.

2.2 Cell migration and cancer metastasis

Cell migration is a complex and highly coordinated process by which cells move from one location to another. Cell motility plays a critical role in a variety of normal physiological events, such as morphogenesis, immune defense and repair, as well as in many diseases like cancer invasion and metastasis. This section includes the process and mechanics of two main types of single cell migrating modes, lamellipodia based migration and bleb based migration, and the introduction of cancer metastasis.

2.2.1 Lamellipodia based migration

Cells migrating in lamellipodia based migration, also known as mesenchymal migration, typically adopt an elongated, spindle-like shape and exert traction on their substrates via focal adhesions associated with actin rich protrusions, e.g. lamellipodia or filopodia. Sheet-like membrane protrusions found at the leading edge, are a hallmark of lamellipodia based mode of cell migration [134].

2.2.1.1 Cyclical process of lamellipodia based migration

Lamellipodia based migration can be thought of as a cyclical process, including four steps as shown in Figure 2.6.

1. **Protrusion formation**: In response to the directional cue in the extracellular environment, cells polarize to form a defined cell front and a rear. The leading edge is usually characterized by intense actin polymerization that generates leading pseudopod protrusions. There are two forms of protrusions, lamellipodia and filopodia. Lamellipodia are thin projection containing densely packed branched actin filaments. Filopodia project from the cell

surface as tiny micrometer-long finger-like structures composed of a bundle of 10-30 parallel linear actin filaments. These two forms of protrusion are thought to serve different roles: filopodia act as antennas to sense chemical or mechanical cues as filopodia contain several types of receptors [135]. Whereas lamellipodia provide wide surfaces that generate traction for forward movement.

2. **Adhesion formation**: New focal adhesion attaches the protrusion to the substrate on which the cell is migrating. Cell adhesion serves as traction points for migration mainly via integrin receptors. Integrins, transmembrane proteins, are a major family of migrating-promoting receptors. These receptors bind adhesion to different extracellular matrix ligands, and mediate the linkage between the substratum and actin cytoskeleton. The shape, size and functional role of the adhesions vary with their subcellular localization and cell type. Smaller adhesion close to the leading edge tends to actively promote actin filament assembly and disassembly rapidly. while larger and stable adhesion near the cell rear anchors large actin filament bundles.

3. **Cell body translocation**: Contractile force is needed to move the cell body forward. The force is generated by a coordinated contraction of the actomyosin cytoskeleton. Myosin II and microtubule motors are involved in controlling translocation of the nucleus.

4. **Cell rear retraction**: Old adhesion at the cell rear disassembles as the trailing edge retracts. The rates of protrusion formation and rear retraction both contribute to the migration speed. Several mechanisms converge to promote adhesion disassembly, including microtubule-dependent targeting of dynamin, integrin endocytosis and actomyosin contraction ripping the adhesion. Rear retraction requires the coordinated contraction of the actin cytoskeleton.

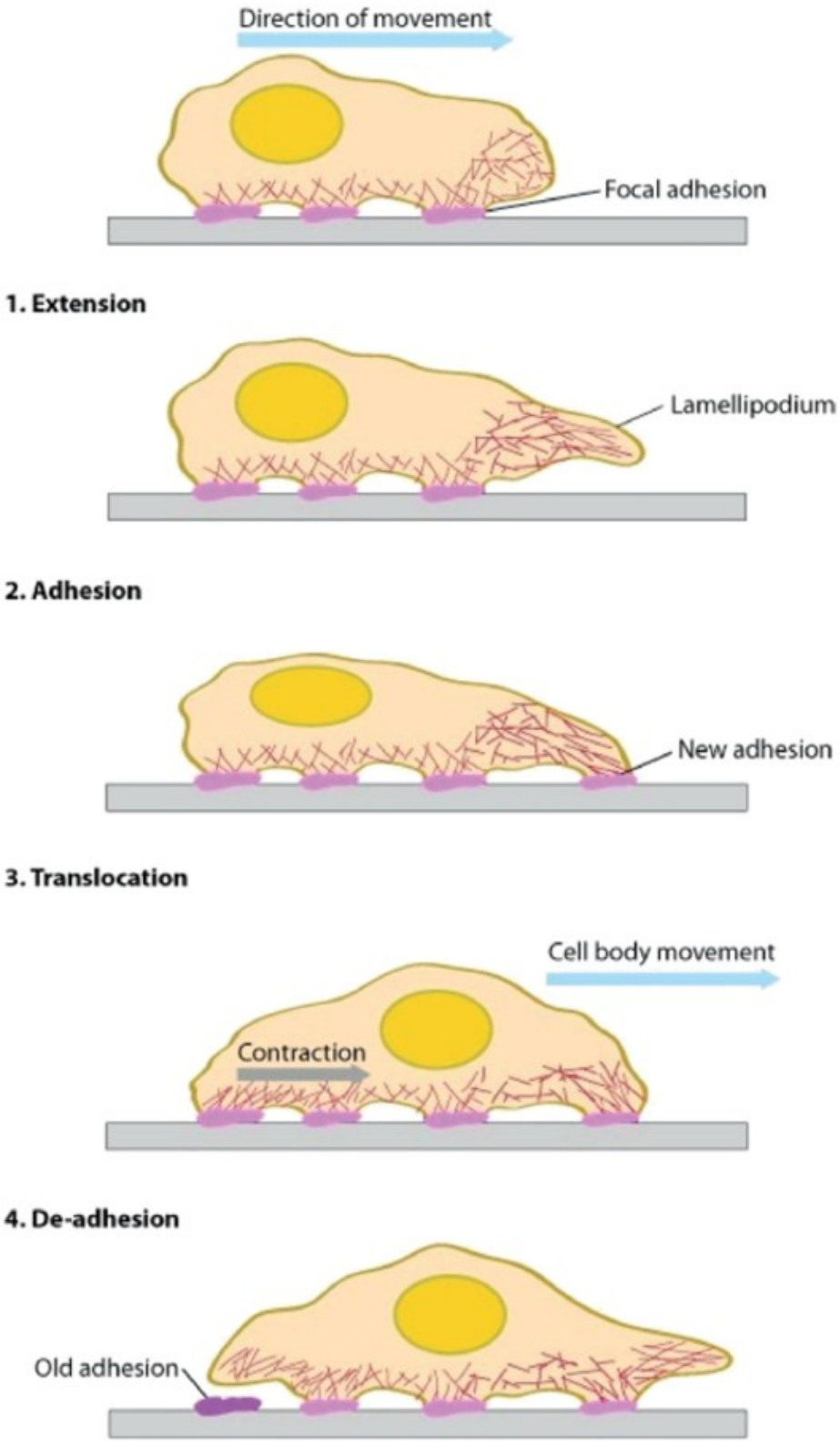

Figure 2.6: Schematic representation of the different steps in mesenchymal cell migration on 2D substrates. The migration process includes extension of a lamellipodium, formation of a new adhesion, translocation of the cell body, and de-adhesion and retraction at the trailing edge. Image taken from Ladoux and Nicolas, Rep Prog Phys, 2012 [136].

2.2.1.2 Mechanics in lamellipodia based migration

To migrate, cells must exert forces on their substrate to propel the cell forward. Classical models of cell migration is based on lamellipodia based migration on two dimensional surfaces exhibited by fibroblasts, keratocytes and epithelial cells. At the cell size scale, the weight of the cell is not sufficient to maintain surface contact with the substrate. Therefore, cells on 2D substrate need matrix binding adhesion receptors to help them anchor to the surface. Lamellipodia and filopodia at the leading edge are stabilized by the focal adhesion complexes formed between matrix binding adhesion receptors and ECM proteins. Stable attachment to the ECM is crucial for lamellipodia based migration [137].

Lamellipodia drive cell motility by assembly of actin network below the leading plasma membrane generating the pushing force required for protrusion formation. As the tension of the plasma membrane opposes the free anterograde expansion of the actin network, the filaments are pushed back into the cell body, which is visible as retrograde actin flow. Through integrin-mediated adhesion complexes that couple the cytoskeleton to the substrate, these retrograde-directed forces, which are enforced by actomyosin contraction, are translated into forward locomotion of the cell body [138].

The actual displacement of cells occurs when the intracellular pulling forces from the cytoskeleton are transmitted to the substrate through focal adhesion. Results from traction force microscopy showed that forces transmitted by single focal adhesion can be tens of nanonewtons [139]. Disassembly of the focal adhesion at the cell rear allows the cell to detach from the substrate as myosin II bound to the actin filaments contracts. Contractility of actomyosin is maintained by the small GTPase Rho and its downstream effector ROCK.

2.2.2 Bleb and bleb based migration

Blebs are spherical cellular protrusions that occur at the cell surface, which have been observed in many cell types like fibroblast, human melanoma and endothelial cells [140]. Bleb based migration, also known as amoeboid migration, in which protrusions of blebs contribute to the migratory behaviour, happens in dictyostelium, zebrafish primordial germ cells [141] and cancer cells [142].

2.2.2.1 Life cycle of bleb

Driven by hydrostatic pressure and cytoplasmic flow, plasma membrane forms protrusions that appear like spherical expansions, which is bleb. Bleb expansion occurs quickly, which last around 30 s, while the retraction occurs much more slowly, taking about 2 min [143]. Almost all of our understanding of bleb formation comes from non-migratory cells, although blebbing is related with cell migration. Recent studies suggest that both migratory cells and non-migratory cells utilize the same mechanisms during blebbing cycle, including bleb initiation, bleb expansion, and bleb retraction as shown in Figure 2.7. The difference is the last step, migratory cell moving forward as a result of contraction of the rear instead of bleb retraction [144]. The following part will discuss what happens in bleb life cycle.

1. **Bleb initiation** (Figure 2.7 A): Under normal situation, the plasma membrane and the cell cortex are bound tightly, which contributes to one type of tether forces. The close association is maintained by interaction between membrane and actin filament, myosin and other related proteins like ERM proteins [145]. Non-equilibration of hydrostatic pressure generated by myosin contraction is exerted on the plasma membrane via cortical tension, leading to actin cortex detaching from plasma membrane [146]. According to the actin cortex morphology, the process can be divided into local decrease in membrane cortex attachment and local rupture of the cortex [143]. Also bleb initiation can be induced artificially by affecting each factors, like local breakage of connection between cortex and membrane by micropipette aspiration or local disruption of the actin cortex by laser ablation [147].

2. **Bleb expansion** (Figure 2.7 B,C): During this process, the forward movement of cell cytosol into the bleb occurs [94], through the bleb neck. Bleb expansion driven by actomyosin contraction lasts about 5 to 30 seconds following bleb initiation. The expansion of a bleb is thought to be a direct mechanical consequence of intracellular pressure pushing against the plasma membrane. There is a critical threshold of cortical tension for bleb expansion, and below the threshold, bleb expansion cannot occur [147]. As the lipid membrane can't be stretched, the bleb volume is increased by the tearing of plasma membrane from the actin cortex. Abundant cortical actin remains at the site of membrane detachment, both in non-migratory cells and migratory cells. The newly formed bleb is devoid of actin or other cytoskeletal structures. Bleb expansion eventually slows down as actomyosin contraction cannot force sufficient cytosol into the bleb. The maximal bleb

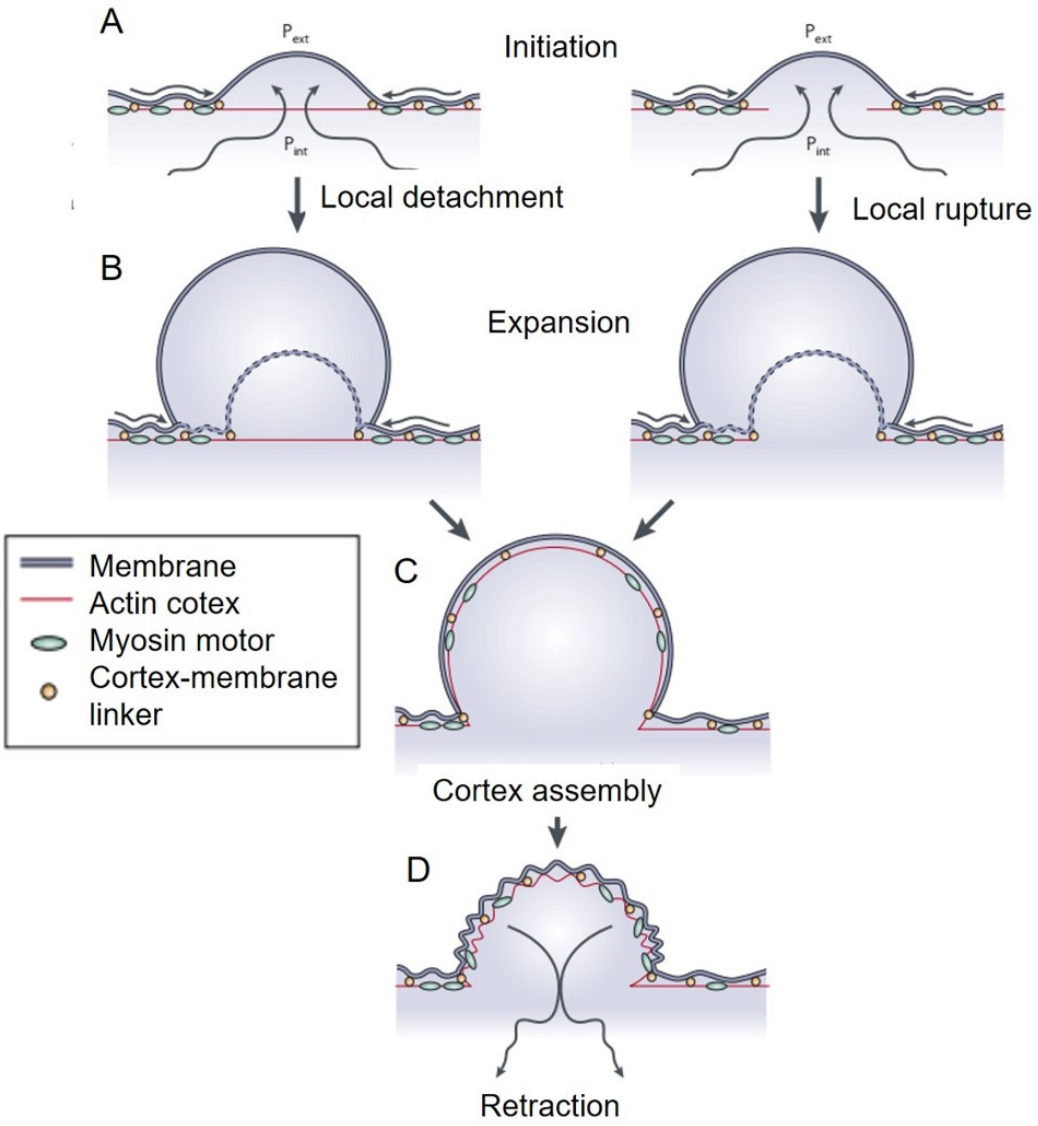

Figure 2.7: The bleb life cycle. The bleb life cycle can be divided into three phases: bleb initiation, expansion and retraction. A. Bleb initiation can result from a local detachment from the membrane (left) or a local rupture (right); B. Hydrostatic pressure drives the cytosol into the bleb. C. New actin cortex reforms under the bleb membrane by recruiting cytoskeleton elements; D. Recruitment of myosin to the new cortex is followed by bleb retraction. Image taken from Charras and Paluch, Nat Rev Mol Cell Biol, 2008 [144].

size is determined by the initial growth rate of the bleb and the time needed for the cortex to repolymerize at the bleb membranes.

3. **Bleb retraction** (Figure 2.7D): As the expansion slows, bleb membrane undergoes a transition from a lipid bilayer to the one linked with actin cortex. Ezrin, is reported to be the first one to be recruited to the bleb membrane, followed by actin, actin bundling proteins and finally proteins involved in the retraction such as myosin II [148] (Figure 2.8). All the proteins recruited

in the bleb form a continuous rim under the bleb. During the process of repolymerization, actin cortex at the base of the bleb neck disassembles due to rapid actin turnover and redistribution. As the bleb will become more unstable with the size getting bigger, retraction powered by myosin happens, which generally lasts 1 to 2 minutes. Myosin-driven contraction mediates bleb retraction which also involves GTPase Rho and its effectors ROCK. Activated ROCK by Rho directly phosphorylates myosin light chain and then generates actomyosin contraction [149].

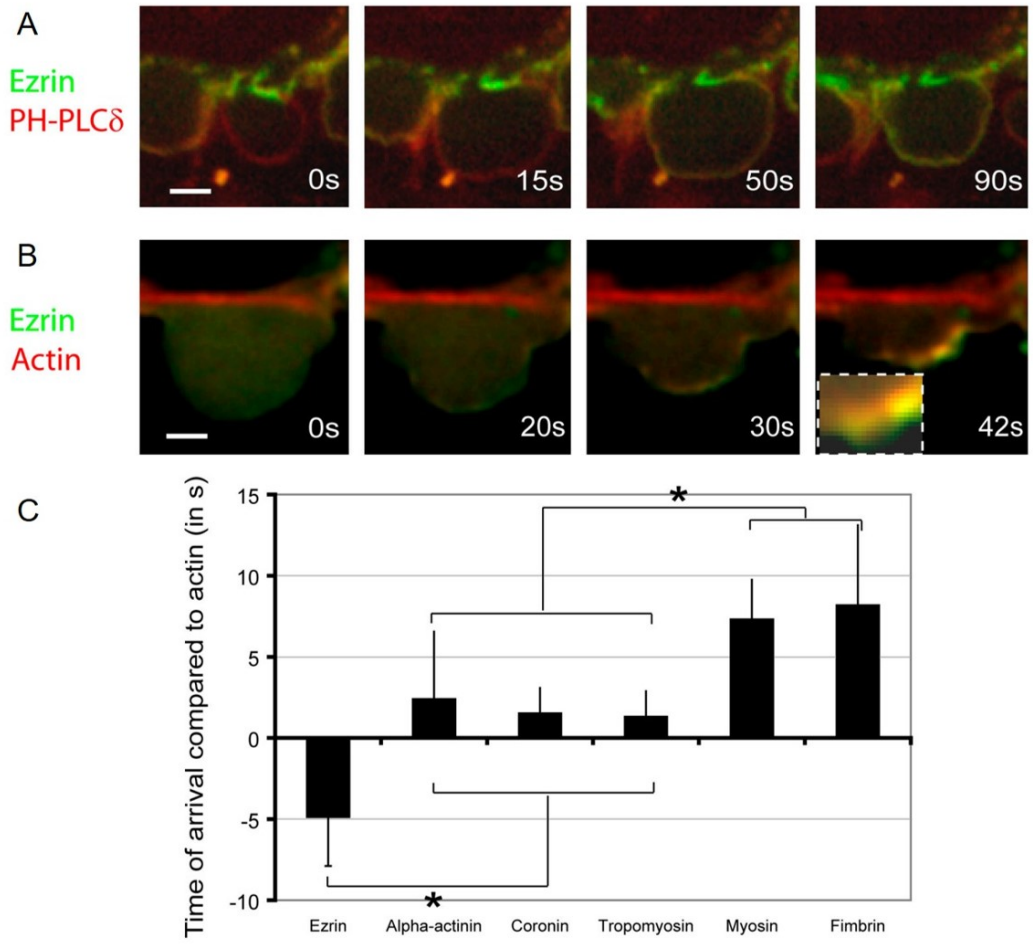

Figure 2.8: Recruitment of proteins into the bleb. A. Ezrin (green) is recruited to the membrane (red) to form a continuous rim. B. Ezrin (green) appears before actin (red) and forms a continuous rim external to the actin shell (red, inset). C. Timing of arrival of the different actin-binding proteins in relationship to actin (t = 0 s). Image taken from Charras, J Cell Biol, 2006 [148].

2.2.2.2 Mechanics in bleb based migration

Research into lamellipodia based migration has led to new treatment strategies for cell migration associated disorders, like blocking integrins in inflammatory dis-

order or inhibition of protease in cancer [150]. However cells are able to adapt to the change and switch into bleb based mode of migration [151]. It is because in the body cells live confined in a 3D environment much more complex than 2D environment. The behaviours of cells in the body are different from those on the plastic or glass. So it happens that drugs showing good efficiency in the lab don't work when administered to patients. Bleb based migration, originated from the first observation of the unicellular protozoa, Amoeba proteus [152], is characterized by constantly changing shapes by rapidly protruding and retracting extensions. Recent studies suggest that bleb based migration is also commonly found in multicellular organisms. Cells form round bleb-like protrusions and change their shape rapidly which allows them to squeeze through pre-existing gaps without adhesion and proteases in 3D environment.

Our understanding of bleb based migration in multicellular organism is based on the migration of leukocytes, such as neutrophils, lymphocytes and dendritic cells in 3D environment. Leukocyte trafficking is required for the arrival to the destination quickly and independently. Leukocytes devoid of receptors have to cross the tissue barriers like the endothelial layer of blood vessels, whose diameter is smaller than the diameter of cell [153]. Therefore they can change their shape to confine in the channel and anchor themselves mechanically without connections and proteases. Bleb based migration utilizes mechanisms of repeated adaptation of cell shape to overcome geometric obstacles. It has been reported that bleb based cell migration occurs in a poorly adhesive mode and does not have interactions between specific molecular and the ECM. However intracellular forces can only deform the cell body, they can drive locomotion only if they are transmitted to the environment [154]. Recent study suggested that cells perform integrin independent 'chimneying' migration between two closely adjacent glass slides. 'Chimneying' is used to describe the confined migration of pushing off the surrounding surfaces for propulsion, because of its resemblance of a technique used by alpinists to climb up rock clefts [155]. Recent studies show that actin cortex flows drive the cell movement through nonspecific substrate friction, and the magnitude of the propelling forces are several orders of magnitude lower than that of lamellipodia based migration. The intracellular actin network expands, rather than contracts, the substrate in the direction of motion [156]. Moreover, it has been reported that the forces generated by cells on two surfaces increases while the gaps between two surfaces decreases, predicting the enhancing the cell membrane to actin cortex adhesion [157].

Bleb based migration is driven by the protrusive forces generated by actin polymerization and myosin contraction [158]. While other cytoskeletal elements play

barely regulatory or supportive roles. Also different levels of actomyosin contraction in the front and the rear of the cell, which leads to hydrostatic pressure gradients, generates cytoplasmic flow that protrude blebs at the leading edge. Rho/ROCK signalling is very crucial for controlling these processes.

2.2.3 Cancer metastasis

There are two types of cancer cells: 1) benign tumours [159] which have the features of slow growth, no spreading to other parts of the body and covered by normal cells which separate them from the surrounding tissues by a capsule of connective tissue [160] and 2) malignant tumours with fast growth which can metastasize and form secondary tumours. Benign tumours can be cured by surgical resection and adjuvant therapy, while malignant tumours are largely incurable because of the systemic nature and the resistance of disseminated tumour cells to existing therapeutic agents. That is why metastasis is the leading cause of cancer mortality, accounting more than 90 $\%$ of death [161]

2.2.3.1 Process of cancer metastasis

Metastasis occurs when cancer cells adapt to a tissue microenvironment that is distant from the primary tumour due to genetically unstable, the process termed metastatic cascade. The steps involved in the metastatic cascade can be summarized as followings (Figure 2.9): (1) tumour angiogenesis and invasion of local tissue, (2) intravasation into blood vessels, (3) survival in vasculature circulation, (4) extravasation into the parenchyma of distant tissue, (5) initially survive in the foreign microenvironment and outgrowth of secondary tumours.

a. Tumour angiogenesis and invasion of local tissue Angiogenesis, the formation of new blood vessels from pre-existing vasculature, occurs during development [163], wound healing [164], and pregnancy [165], as a series of controlled physiological processes leading to neovascularization which supports changing tissue requirements. This process is strictly regulated by a delicate balance of proangiogenic and antiangiogenic factors. Loss control of this balance will cause inappropriate angiogenesis, occurring in many diseases including diabetic retinopathy [166], age-related macular degeneration [167] as well as cancer [168].

Angiogenesis is an important factor in the progression of cancer. Without the oxygen and nutrient supply, tumours are unable to grow beyond 2 mm in diameter [169, 170]. To get rid of hypoxia and nutrient deprivation situation, tumour cells

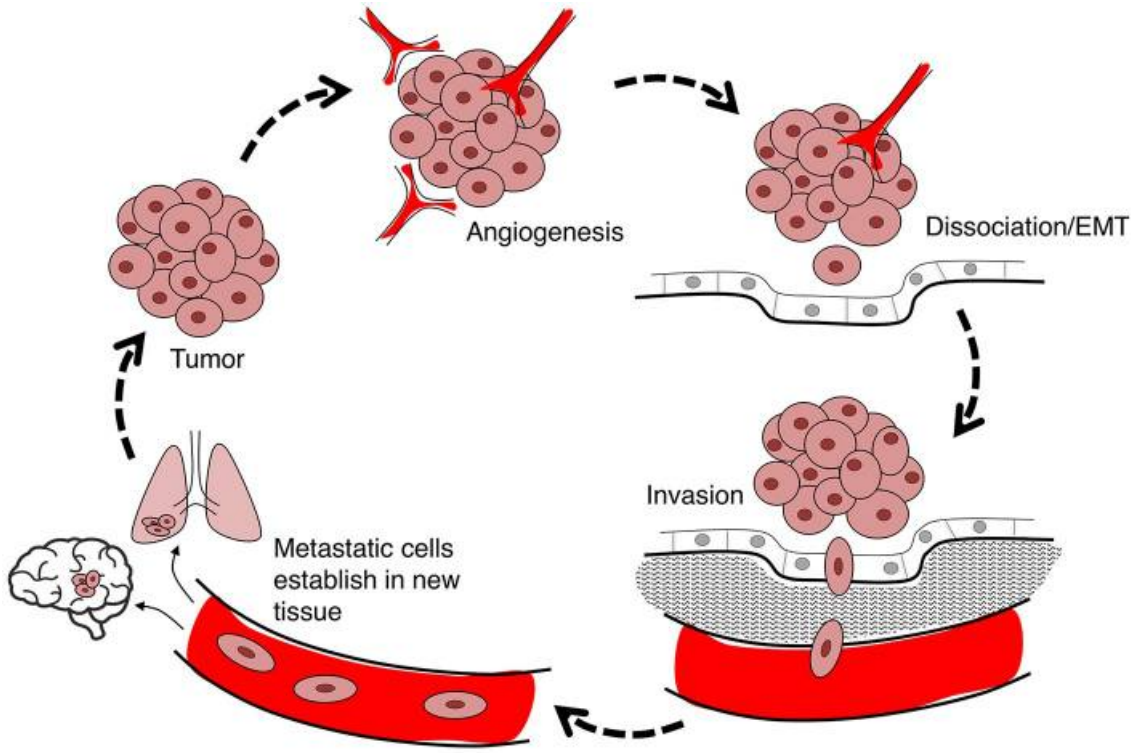

Figure 2.9: The illustration of the steps in metastasis cascade. Primary cancer cells exit initial sites (angiogenesis, local invasion, and intravasation), translocate systemically (survival in the circulation, arrest at distant site and extravasation), and survive in distant tissue (micrometastasis and colonization). Image taken from De Ieso and Yool, Front Chem, 2018 [162].

can exploit their microenvironment by secreting cytokines and growth factors to activate normal, quiescent cells around them and drive the vascular growth. Tumour angiogenesis (Figure 2.10) is a four-step process. Firstly, hypoxia resulting from the increasing distance between the growing tumour cells and the capillaries can induce tumour cells secreting proangiogenic factors, such as vascular endothelial growth factor (VEGF) [171], platelet derived growth factor (PDGF) [172] and interleukin 8 (IL-8) [173]. These proangiogenic factors diffuse into the surrounding tissues, leading to a concentration gradient which drives angiogenesis. Secondly, proangiogenic factors like VEGF bind to the receptors on endothelial cells nearby, components of the interior surface of blood vessels, activating proteins that transmit signals into the endothelia cell nucleus. The nuclear signals promote a group of gene expression to secret proteins needed for new endothelial cell growth and proliferation. At the same time, tumour cells can produce adhesion molecules including integrins, and proteases such as matrix metalloproteinases (MMPs), to adhere and degrade the ECM to migrate [174]. With the aid of proteases, the extracellular matrix which fills the spaces between cells can be degraded. Therefore, new endothelial cells migrate through degraded area to

the chemoattractant gradient provided by tumour cells. Subsequently endothelial cells organize into hollow tubes that evolve gradually into a mature network of blood vessels with the help of an adhesion factor, such as integrinα [175]. Angiotensin-1,-2 and their receptor tie-2 which are required for newly formed blood vessels stabilization and maturation [176]. Finally, tumour cells can get oxygen and nutrients from newly formed vessels. Whereas perivascular coverage typically provides vascular stability and maturation, it does not lead to mature vessels with proper function, as the vessels are exposed to persistent stimulatory signals within the tumour microenvironment. They are often incompletely formed with abnormal architecture characterized by increased fenestration and leakiness [177]. Permeability of the vessel walls serves as an outlet for the cancer cells to enter the systemic circulation [178].

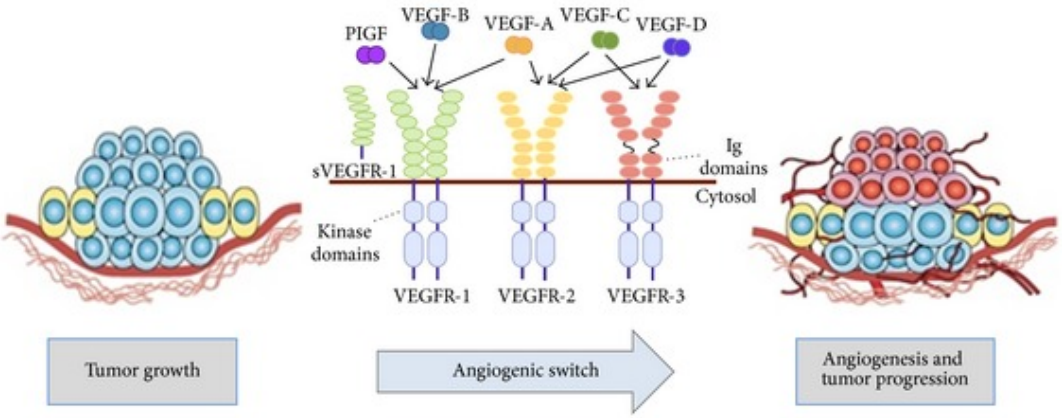

Figure 2.10: Tumour angiogenesis. One of the most important properties of cancer is their ability to generation blood vessels, promoting cancer growth and metastasis. Image taken from Giordano et al, Gastroent Res Pract, 2014 [179].

Local invasion means the entry of cancer cells that have resided within a well-confined primary tumour into the surrounding stroma and thereafter into the adjacent normal tissue parenchyma. Epithelial tissues, representing the origins of most solid tumours, are highly organized by lateral belts of cell-cell adhesion complexes and are separated from the stroma by a basement membrane (BM). During the progression from a tumour to an invasive carcinoma, tumour cells have to escape from the primary tumour mass first and then breach the basement membrane. And one of the key events is epithelial-mesenchymal transition (EMT) [180].

EMT is a process by which epithelial cells lose their polarity and cell-cell adhesion, and gain migratory and invasive properties. Loss of cell-cell adhesion permits disaggregation of tumour cells and it has been reported that cancer cells

show diminished cell-cell adhesiveness compared to normal epithelial cells [180]. Cadherins are a family of cell surface glycoproteins that play a prominent role of cell-cell adhesion [181]. E-cadherin, a type I classical cadherin, is a key component in the formation of cell-cell adhesions type junctions in epithelial tissues. Studies in variety of cancers show that E-cadherin plays an important role in metastasis. In vitro, suppression of E-cadherin function or expression leads to mesenchymal morphology and increased migration [182, 183]. And loss or down-regulation of E-cadherin has also reported in vivo in many cancer types like breast cancer [184], stomach [185], lung, kidney et al. What's more, cadherin-catenin complexes are also involved in intracellular signal transduction pathways. Catenin released from the dissolved E-cadherin complex affects the activity of small GTPases, the regulators of cell migration [186].

The loss of cell-cell adhesion promotes further events of invasion and migration of tumour cells through the epithelial BM and surrounding ECM. BM, a specialized ECM with the thickness of about 50-100 nm, plays vital roles in organizing epithelial tissues, including separating their epithelial and stromal compartments. BM is a complex structure comprising mainly laminin, entactin, nidogen and type IV collagen [187]. Invasion BM by tumour cells involves some participants like integrin and proteases. Tumour cells initially bind to the BM and ECM via interactions mainly between the integrin family and a variety of components, such as collagen or laminin. Integrin also stabilize the interaction as well as maintain the architecture of the structure. Altered expression of integrin is a common feature of cancers [188]. Following attachment, cancer cells can traverse the BM and ECM through secreting proteases like urokinase, cathepsins and MMPs, helping them through the barriers [189]. In normal tissues, the activity of proteases is tightly controlled at transcriptional and posttranslational level. However, in cancer cells, control mechanism is lost. For example, MMPs are often overexpressed in tumours, especially in the tumour stroma, which can remodel the ECM within the tumour microenvironment and stimulate cell migration and angiogenesis [190].

b. Intravasation into vasculature circulation After invading through the epithelial BM, surrounding ECM and the stromal compartment, tumour cells come into contact with tumour-associated microvasculature. Then tumour cells have to cross the pericyte and endothelial cell barriers into blood or lymphatic vessel, which is called intravasation. The process of intravasation is likely to be strongly influenced by the structural features of tumour-associated blood vessel. Compared to normal blood vessel, tumour-associated vessel is characterized by defective architecture, weak cell-cell conjunction and continuous reconfiguration [191]. High resolution electron microscopy showed that tumour cells adhere to the

vascular endothelial cells and protrude membrane extensions through gaps in the endothelial wall when endothelial cells retract. What's more, tumour-associated macrophages play a crucial role in intravasation. In xenograft and transgenic breast cancer models, macrophages are shown to guide tumour cells to blood vessels and sites of intravasation [192].

c. Survival in vasculature circulation Once tumour cells are in the blood stream, their survival is threatened by several events such as shear forces generated by the flow of blood, immune response attack, and anoikis resulting from loss of anchorage to substratum [193]. It has been reported that tumour cells prevent themselves from immune destruction through interactions with platelets, leukocytes and the vascular endothelium [194]. Another question is how long tumour cells can circulate in the vasculature. Some studies suggest that they are trapped in the first or second capillary bed that they encounter, given the large diameters of tumour cells and the vessel diameter of capillaries [195]. While other studies claim that a large fraction of cell injected into the vasculature gets rapidly lost due to cell death. Therefore, only a small proportion of tumour cells entering the vasculature will eventually form a full size metastasis. For a long time, the blood system has been considered the main route of the metastatic spread. However, there is increasing evidence that the lymphatic system might play the same important role in cancer metastasis [196]. The lymphatic system is a network of tubes and nodes in the body that filter body fluid and fights infection. Compared with blood capillaries, the lymphatic capillaries only consist of single layer of endothelial cells lacking tight cell-cell junction. Besides there is no smooth muscle cells and basement membrane covered the capillaries. Therefore macromolecules, even bacteria can easily enter the lymphatic. What's more, the slow flow of lymph has little stress to harm cancer cells. If cancer cells go into the small lymph vessels near the primary tumour, they may end up in lymph nodes. Most cancer cells may be destroyed before they can start growing but some may survive and settle, finally grow to form second tumour in lymph nodes.

d. Extravastion into the parenchyma of distant tissue Extravasation is a vital step in cancer metastasis, which involves arrest in the capillary and transmigration across the endothelial monolayer of the vessel. Circulating tumour cells reach the capillaries of a similar diameter to the tumour cell and get physically restricted. Then the tumour cells adhere to the endothelium by specific cell surface receptors to form stable attachment. For example, integrin supports breast cancer cell attachment under blood flow conditions in an activation-dependent manner [197]. After adhering to the endothelium, tumour cells have to traverse the wall of blood vessel. However, compared with the neovasculature formed by primary tumour

which is tortuous and leaky, microvessels in distant normal tissue are likely to be highly functional and with low intrinsic permeability. In order to overcome physical barriers, tumour cells are able to secret factors that induce vascular hyperpermeability and degrade the basement membrane. For example, the secreted protein pleiotropically acting factors EREG, COX-2, MMP1 and MMP2 disrupt endothelia cell-cell junctions for tumour cells transmigration [198].

e. Survival in the foreign microenvironment Once tumour cells reach the secondary site, they may be destroyed-most undergoing apoptosis within 24 hours, may become dormant without proliferation, or may proliferate to form secondary tumours. The new environment in the distant tissue, also called microenvironment, usually differs greatly from that present in the site of primary tumour formation, like the types of stromal cells, ECM constituents and even the microarchitecture of the tissue itself. It does not provide the same survival and growth factors as the original tissue, which promotes tumour growth. Therefore, the vast majority of tumour cells are not able to effectively metastasize in the new site. Solitary tumour cells can be found in the bone marrow many years before the development of overt metastasis [199]. However, most of these cells will fail to convert into metastasis.

Recently, it is reported that distant tissue may be pre-conditioned to become fertile ground for the tumour cell proliferation. Bone marrow-derived haematopoietic progenitor cells that express vascular endothelial growth factor receptor 1 (VEGFR1) home to tumour-specific premetastatic sites and form cellular clusters before the arrival of tumour [200]. What is more, cancers from different primary sites show distinct and typical patterns of metastatic dissemination. For example, breast cancer cells specifically metastasize to either lung, brain or bone. Through these observation, Stephen Paget described the formulation of the seed and soil hypothesis, which stated that metastatic spread was a choice of particular tumour cells (seeds) to a suitable environment (soil), where the tumour can develop the second metastasis [201]. Therefore, a secondary tumour can form only if the seed can grow in the soil. There are some evidence to explain the hypothesis. First, the endothelia of vessels in different tissues have different adhesion molecule expression, which suggest tumour cell-endothelia cell coherence is a specific event and is a necessary step for the completion of the metastatic cascade. Only tumour cells expressing the corresponding receptors can bind to the endothelium of the vessel. For example, $\alpha 3 \beta 1$ integrins on circulating cancer cells bind to laminin-5 expressing blood vessels during metastasis to lungs [202]. Then, evidence from a number of work suggested that specific organ microenvironments are indeed intrinsically more or less suitable for the survival and growth of certain types of

tumour cells.

2.2.3.2 Mechanics in cancer metastasis

Apart from the role of biological and biomedical signals in cancer metastasis, mechanical properties of cancer environment have been recognized as also being functionally important during tumor progression (Figure 2.11). Cancer cells sense the changes in their surroundings and transduce physical to biochemical signals, which helps them to control the function, biochemical changes and gene expression [203]. For example, the high interstitial pressure, increased ECM stiffness, as well as flow shear stress, all could contribute to cancer progress.

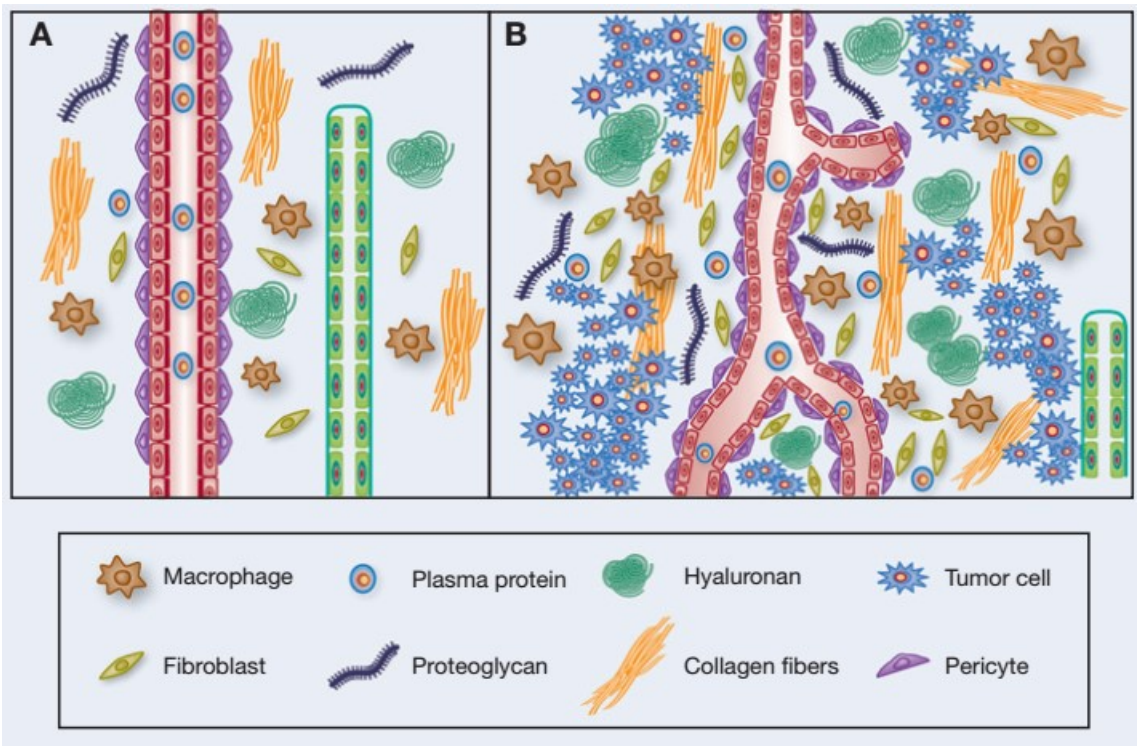

Figure 2.11: Interstitium in normal tissue versus tumor tissue. A. normal tissue interstitium containing blood vessel, lymphatic vessel, hyaluronan, macrophages, fibroblasts, proteoglycans, and collagen fibers; B. tumor tissue interstitium containing leaky and tortuous tumor vasculature, lacking in lymphatic vessel, higher amount of extravasated plasma proteins, macrophages, fibroblasts, proteoglycans, hyaluronans and collagen fibers, and proliferating tumor cells. Image taken from Ariffin et al, Cancer Research, 2014 [204].

The growth of solid tumour requires existing vasculature as well as new formed blood vessels inside the tumour which is leaky, highly irregular and tortuous [205]. Compression of these blood vessels by the increasing cell number generates high microvascular pressure. In addition, the lack of functional lymphatic system limits drainage of excess fluid and thus reduces fluid movement through the interstitum.

Together, these factors, including abnormal tumor vasculature and lymphatic, and proliferating tumor cells within a confined space lead to an increased interstitial fluid pressure, reducing perfusion rates and creating hypoxia [206]. In turn, hypoxia induced is proposed to promote malignant progression by selecting for cells that can survive in a harsh microenvironment, which enhances the invasive and metastatic potential of cancer cells [207]. Also, hypoxia also promote cells to produce growth factors like VEGF and TGF-β (transforming growth factor β) that suppress the activity of macrophages and have the potential to convert macrophages to protumorigenic (tumor-friendly) cells [205]. In addition to indirectly amplifying tumorigenesis through hypoxia, high interstitial fluid pressure induces vessel closing that limits curative drug delivery. Because many drugs used for treatment of patients with cancer, which are high-molecular-weight compounds in particular, are transported from the circulatory system through the interstitial space by convection rather than by diffusion [208].

What's more, matrix rigidity, the most remarkable mechanical and physical feature of solid tumour, is suggested to directly influence tumor progression through the mechanotransductive regulation of tumorigenic biochemical pathways [209]. The increased tissue stiffness is due to ECM remodeling, deposition, and crosslinking [210]. This mechanical stiffness may break the balance of cellular surface force, promote integrin clustering and focal adhesion formation which transmit exogenous matrix force signals into cells, and ultimately affect their biological phenotypes and characteristics such as cell morphology, cell growth, and differentiation, as well as the synthesis and secretion of cytokines and metabolism [211]. One of the process that matrix stiffness affects is EMT, modulating cell migration through cytoskeleton remodeling [212], .

EMT frequently occurs in the initiation of tumor invasion and metastasis. Apart from factors like ECM components and hypoxia, matrix stiffness is also involved in inducing a transition of tumor cells from epithelial state to mesenchymal state [213]. By comparing tumor and nontumor human epithelial cell lines, it has been reported that an increase of the substrate stiffness mechanotransductively increases adherent junctions with the substrate and favors the epithelial cell-ECM interaction rather than cell-cell interactions, thereby physically triggering EMT phenotypes [214]. Others reported that high matrix stiffness causes an activation of integrins which in turn leading to the phosphorylation of Twist at Tyr 107, in mouse and human breast cancer cells [215]. Phosphorylated Twist is then released and translocated into the nucleus where it can activate the transcriptional events of EMT, causing invasion and metastasis. Increased matrix stiffness has been reported to be associated with mesenchymal shift where cells develop

prominent actin stress fibers and mature focal adhesions [216], or enhance TGF-β1-induced Smad signaling in HCC cells [217]. Furthermore, it has been reported that higher matrix stiffness acts as an initiator triggers EMT in HCC cells independently converging on Snail expression [218]. This indicates that matrix stiffness could potentially regulate EMT to facilitate tumor dissemination, or this mechanical cues could induce the biochemical signals to regulate EMT.

Once tumour cells escape its primary tissue and arrives in the circulation, cancer cells are exposed to a new set of conditions in the vascular microenvironment. In addition to immunological stress and blood cell collisions, they must be able to withstand mechanical forces associated with fluid and shear [219]. Such shear stresses and rates can affect cancer cells' survival and thus the chances of metastasis. For example, B16 melanoma cell exposure to fluid shear stress in a cone-plate viscometer caused a significant loss of cell viability [220]. On the other hand, fluid shear stress is an important component to induce cancer metastasis, as it is critical for cancer cell adhesion to the endothelial cell wall and subsequent extravasation into tissues. Exposure to shear forces has been reported to activate specific signaling pathways in tumor cells which is involved in the reorganization of the cytoskeleton and adhesive machinery and ultimately facilitating reinforcement of cell structure and attachment to the vascular wall [221]. Also it has been reported that shear forces can enhance adhesion to collagen-based ECM substrates in vitro through a process that involves activation of Src and subsequent assembly of the actin cytoskeleton and formation of focal adhesions [222]. Similarly, Haier et al showed that shear can enhance FAK phosphorylation in colon carcinoma cells, thereby strengthening adhesion to collagen-based ECMs. Correspondingly, parallel in vivo studies demonstrated that overexpression of dominant-negative FAK significantly reduced the ability of tumor cells to adhere to vasculature within the hepatic microcirculation [223].

The force journey of a tumour cell during metastasis involves not only its ability to withstand these mechanical forces that arise from the growth of the tumour, tissue homeostasis and transport in the vascular microenvironment, but also taking advantages to promote the metastasis through mechanotransduction.

2.2.4 Summary

To conclude, two modes of single cell migration, lamellipodia based migration and bleb based migration, and cancer metastasis were described in this section. Many cells are able to switch between blebbing-driven and polymerization-driven motility according to the environmental conditions or in response to genetic or

pharmacological manipulation. This study focuses on the effect of Ezrin on lamellipodia based migration. At the same time, a sandwich model is constructed to study bleb based migration.

2.3 Cell cytoskeleton

The cytoskeleton is a complex structure that helps cells maintain their shape and organizes the internal contents, and it also provides mechanical support that enables cells to carry out essential functions like division and migration. Moreover, it connects the cell to the external environment physically and biochemically through interacting proteins.

The cytoskeleton of eukaryotic cells is composed of three major types of filamentous proteins as shown in Figure 2.12: actin filaments, microtubules, and intermediate filaments, which differ in size and protein composition. Actin filaments, the smallest type, are thin, solid rods, with a diameter of only about 6 nm. They are made of contractile protein actin and particularly prevalent in muscle cells. Microtubules, the largest type of filament, are hollow rods with a diameter of about 25 nm. They are composed of a protein called tubulin. Intermediate filaments, as their name suggests, are mid-sized, with a diameter of about 10 nm. They provide support for actin filaments and microtubules by holding them in place. Unlike actin filaments and microtubules, intermediate filaments are constructed from a variety of different subunit proteins.

These three types of cytoskeletal polymers with different structural and physical properties, enable them with specific cellular functions. The cytoskeleton is not a fixed structure that stays stationary all the time. Rather, it is a dynamic network where the three major filaments are under the control of proteins that regulate their nucleation and elongation, state of polymerization, and level of cross-linking. Proteins of the myosin family migrate with vesicles along actin filament with specific directionality, whereas proteins of the kinesin/KRP and dynein families move cargoes along microtubule tracks and play an important role in the formation and function of the mitotic spindle. All forms of migration require ATP hydrolysis to provide essential energy. The architecture and function of the networks between the three main cytoskeletons can be distinguished by the size and protein composition, the dynamics of their assembly, the mechanical properties, and the type of molecular motors they interact with.

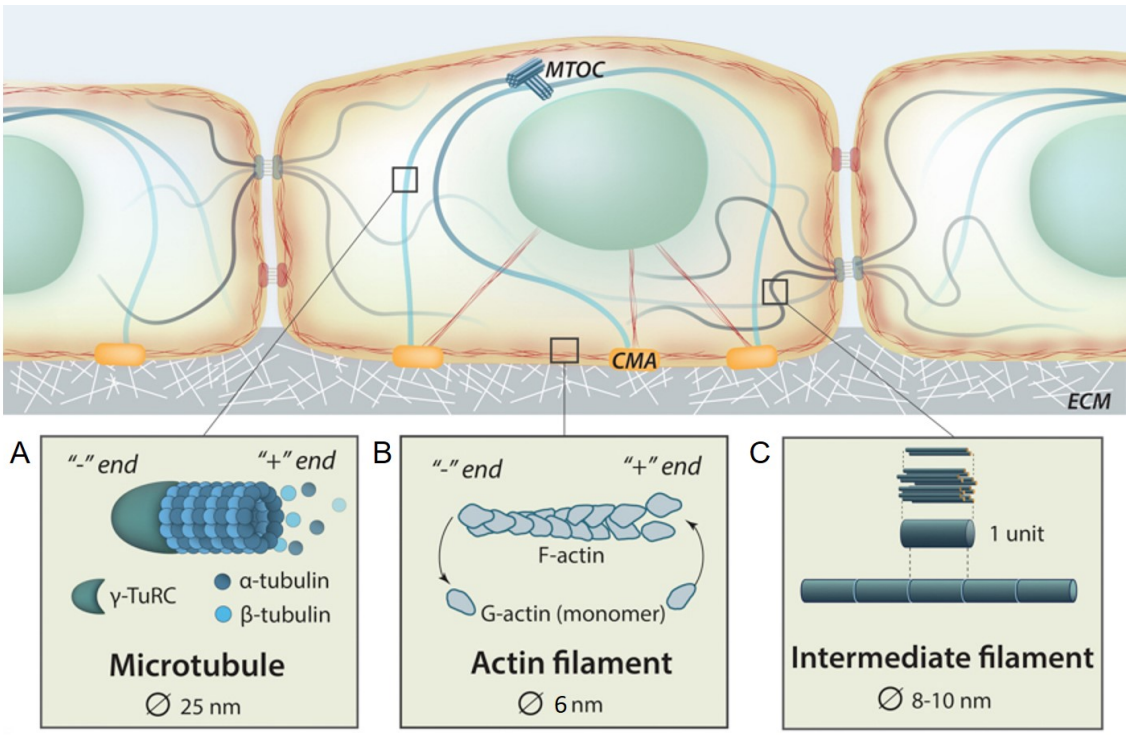

Figure 2.12: Three main components of the cytoskeleton. A. Microtubules; B. Actin filaments; C. Intermediate filaments. They have distinct structural compositions and exhibit slightly different interdependent functions. Adapted from MBInfo (https://www.mechanobio.info/cytoskeleton-dynamics/what-is-the-cytoskeleton/).

2.3.1 Actin cytoskeleton

Actin is the most abundant protein, which is highly conserved, in most eukaryotic cells. The eukaryotic actin cytoskeleton has an essential role in various cell processes, ranging from cell motility, cell adhesion, vesicle trafficking, endocytosis and exocytosis to the maintenance of cell shape and polarity. The main component of the actin cytoskeleton is monomeric actin (G-actin) [224], a 43 kDa ATPase which can self-assemble into actin filaments. Actin filament is asymmetric with a fast growing barbed end and a slower growing pointed end [225]. Based on the importance of its function, the precise regulation of the dynamics of polymerization and depolymerization, and the structure of actin cytoskeleton is crucial for many developmental and physiological processes in multicellular organisms. A large number of actin binding proteins (ABPs) have been identified to control the transition between G-actin and actin filament in time and space. ABPs have multiple roles, including actin filament nucleation, elongation, severing, capping, and crosslinking, stabilizing and actin monomer sequestration [226].

2.3.1.1 Actin filament assembly

Firstly, the spontaneous initiation of actin filament assembly requires the formation of a stable oligomer of actin monomers which is called nucleation [227] (Figure 2.13A). Nevertheless, because the formation of small oligomers of two to four actin subunits is kinetically unfavorable. Moreover, actin monomers are controlled by associating with actin-monomer-binding proteins such profilin, which suppress spontaneous nucleation of new filaments. Therefore, spontaneous nucleation becomes the rate limiting step and needs the assistance of actin nucleating proteins [228]. So far, three main families of actin nucleating proteins have been identified as shown in Figure 2.13, actin-related protein 2/3 (Arp2/3) complex and its nucleation promoting factors (NPFs), formins, and tandem-monomer-binding nucleators, each promoting actin nucleation by distinct mechanisms [229]. The first two nucleators will be discussed in more details as follows.

The Arp2/3 complex is a stable complex of seven subunits consisting of two actin-related proteins, Arp2 and Arp3, and subunits ARPC1 to ARPC5 [230]. Arp2/3 complex itself has very low nucleation activity [231], and its activation function requires NPFs which can recruit one to three G-actin and promote a conformational change within the Arp2/3 complex [232]. NPFs are characterized by WCA domains consisting of G-actin binding WH2 (W) domain and Arp2/3-binding central/acidic (CA) sequences [227]. The best known NPFs includes Wiskott-Aldrich Syndrome protein (WASP), neuronal WASP (N-WASP), and verprolin homologs (WAVEs) [233]. Once activated, the actin monomer bound to the W domain, together with Arp2 and Arp3, are thought to form a trimetric seed to mimic an actin dimer or trimer and to function as a template for the initiation of a new actin filament that extend from the sides of preexisting filaments at a 70° angle to form a Y branched network [229] (Figure 2.13C). The free barbed end of the new filament elongates until a capping protein terminates its growth.

The second class of actin nucleators, formins, which are conserved in most eukaryotes, promote the assembly of unbranched actin filaments [235]. Formins are multi-domain proteins defined by strongly conserved FH1 domains and FH2 domains. The FH2 dimer, which is necessary and sufficient for nucleation and elongation, consists of two rod-shaped domains being connected in head-to-tail fashion. These structural determination suggested that the FH2 dimer “stair-steps” to mediate the sequential incorporation of actin monomers at the barbed end during processive filament elongation [236] as shown in Figure 2.13B. Dimerization of the FH2 domain is regarded as a nucleation as each FH2 domain binds an actin monomer where the ring-like dimer helps stabilize a short-pitch actin dimer

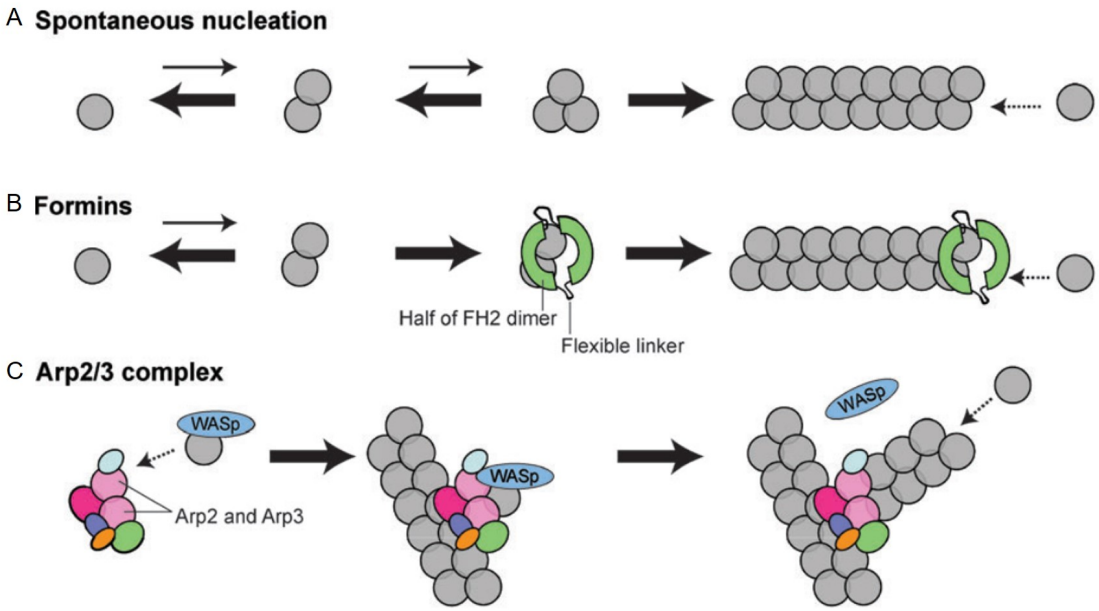

Figure 2.13: Mechanisms of actin polymerization by formins, the Arp2/3 complex compared with spontaneous actin assembly. A. Spontaneous actin assembly from actin monomers is shown for comparison. Actin dimers and trimers are highly unstable species that rapidly dissociate; B. Formins stabilize actin polymerization intermediates, like short-pitch dimers. The two halves of the formin FH2 dimer are green, connected by flexible linkers (black); C. The Arp2/3 complex, associated with NFPs which is connected with monomer actin, mimic actin trimer to polymerize. The two actin-like subunits of Arp2/3 complex (Arp2 and Arp3) are pink. Image taken from Goode et al, Curr Opin Cell Biol, 2004 [234].

[236]. While FH1 domain is responsible for increasing the local concentration of profilin-bound G-actin [237]. Then one side of the FH2 dimer could dissociate and incorporate a third actin monomer while the other side remains bound with the dimer actin. In contrast to Arp2/3 complex, formins remain associated with the growing barbed end of actin filaments which allows the continuous addition of G-actins and at the same time, protects it from other capping proteins which stops growing by capping the barbed end [234].

2.3.1.2 Structure and function of actin cytoskeleton

In order to perform biological functions efficiently, individual actin filaments are assembled into two different types of structures, actin bundles and actin networks, and they play distinct roles in cell. In bundles, actin filaments are crosslinked into closely packed parallel arrays; whereas in networks, actin filaments are loosely crosslinked into orthogonal arrays that form three dimensional meshwork with the properties of semisolid gels [238]. Within these structures, actin filaments

function as force generating polymer motors, structural scaffolds and tracks for motor proteins.

It is well known that cell migration is driven by the continuous reorganization and turnover of the actin cytoskeleton. In order to migrate, cells must have two abilities, the ability to push forward by polymerization of actin filaments and the ability to retract by interacting with myosin. Actin polymerization generates most of the driving forces for the membrane protrusion during cell migration. In normal condition, actin filaments are assembled at a steady state and turnover by the association of actin monomers at the barbed end balanced by the dissociation of filament subunits at the pointed end, a process called treadmilling [239]. In migrating cells, treadmilling is accelerated by 2 orders of magnitude due to the activity of ABPs. Many studies indicate that polarized filament barbed end growth, at specific sites on the plasma membrane, generates the forces to form extension of sheet-like and rod-like protrusions at the cell front, named respectively lamellipodia and filopodia (Figure 2.14). Lamellipodia contain a network of short, branched actin filaments, which is promoted by the Arp2/3 complex from the sides of preexisting filament at the leading edge [240]. While filopodia contain long parallel actin filaments arranged into tight bundles which is promoted by formins with needle-like protrusions at the leading edge [241]. Another important structure that plays important role in cell migration is actin stress fiber. Because actin filaments cooperate with myosin to form contractile stress fibers at the cell rear that drive the cell body moving forward.

Actin filaments can provide mechanical support to modulate cell shape and cell stiffness. The use of disruptive pharmacological agents which dissolve the actin filaments, like cytochalasin D and latrunculin A, resulted in a significant decrease in cell stiffness [243]. There are two types of actin filament structures that are pivotal in the determination of cell mechanical properties, stress fibers and actin cortex, as shown in Figure 2.15A.

Stress fibers are composed of bundles of approximately 10-30 actin filaments, which are crosslinked together by α-actinin [245]. The well-organized stress fibers are much stiffer, which increases the whole cell mechanical properties. These contractile actomyosin bundles are often anchored to focal adhesions, which connect the extracellular matrix (ECM) to the actin cytoskeleton. Based on their morphology and subcellular location, stress fibers can be divided into four different categories: dorsal and ventral stress fibers, transverse arcs and the perinuclear actin cap (Figure 2.15).

1. **Ventral stress fibers**: As the most commonly observed structures, ventral

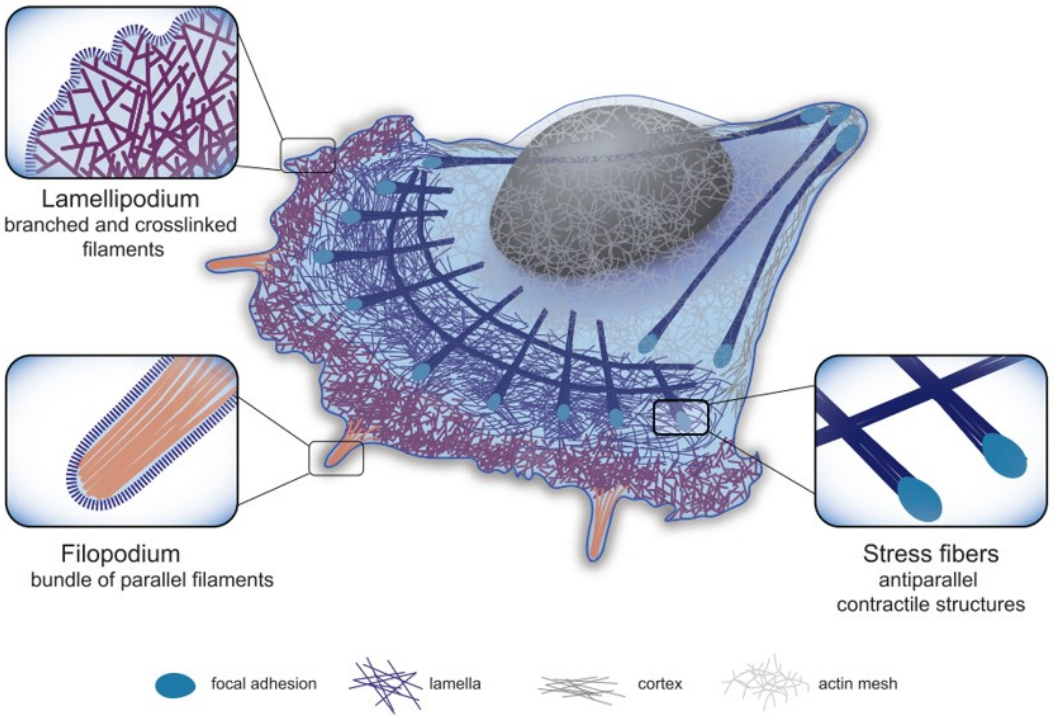

Figure 2.14: Cellular actin organization during cell migration. Schematic representation of the three main actin structures found in migrating cells: 1. Lamellipodium: dense, branched network involved in cell protrusion; 2. Filopodium: a finger-like structure located at the leading edge of the motile cell composed of aligned filaments; 3. Contractile structure: dynamic structure made of antiparallel and/or mixed-polarity actin filaments associated with myosin. Zoomed regions highlight the specific actin organization of the different cellular actin structures. Image taken from Letort et al, F1000 Research, 2015 [242].

stress fibers represent the major contractile machinery. Ventral stress fibers are contractile actomyosin bundles that lie along the base of the cell, attaching to focal adhesions at both ends. Ventral stress fibers are often located at the posterior parts of the cell, where they are responsible for tail retraction and cell shape changes during cell migration. Furthermore, their location determines where they can structure cell borders against inward pressure of the membrane [246].

2. **Dorsal stress fibers**: Dorsal stress fibers anchor to focal adhesions at their distal ends, which tethers them to the base of the cells. The rest of the structures rise towards the dorsal surface, forming a loose matrix of actin filaments. It has been reported that dorsal stress fibers don't exhibit periodic distribution of α-actinin and myosin [247]. Therefore, they may serve as a platform for the assembly of other types of stress fibers, as well as to link them to focal adhesions.

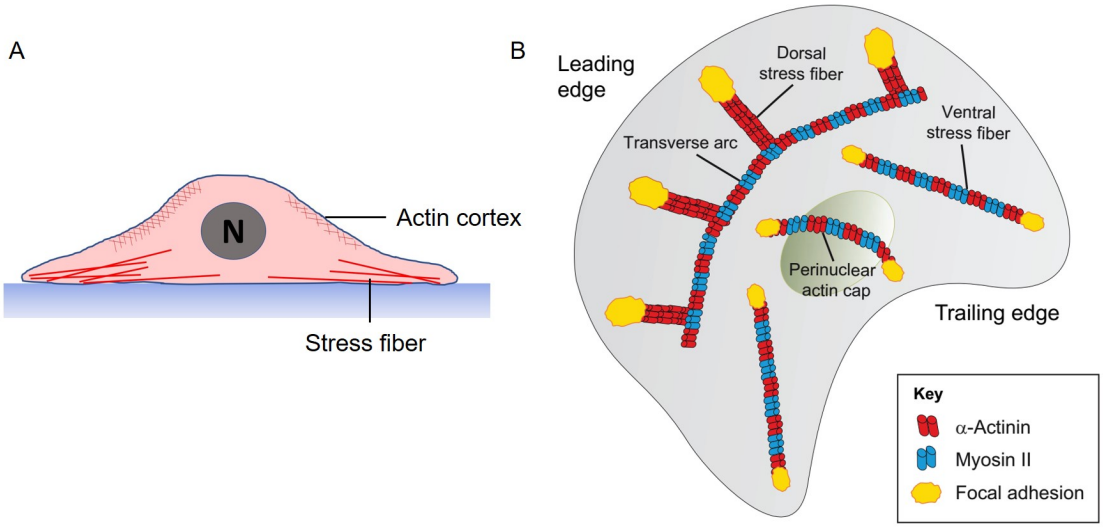

Figure 2.15: Actin cortex and Stress fiber. A. Cellular distribution of actin cortex and stress fiber. Actin cortex is at the cell perimeter under the plasma membrane, while the stress fibers at the cell attachment interface. B. Schematic presentation of the stress fiber network of motile mesenchymal cells. These cells can contain at least four discrete categories of stress fibers; (i) dorsal stress fibers, which are anchored to focal adhesions at their distal end, (ii) transverse arcs, which are curved actomyosin bundles that flow towards the cell center and are typically connected to focal adhesions through interactions with dorsal stress fibers; (iii) ventral stress fibers, which are actomyosin bundles anchored to focal adhesions at both ends, and (iv) perinuclear actin cap bundles, which resemble ventral stress fibers but their central parts are located above the nucleus. Image taken from Tojkander et al, J Cell Sci, 2012 [244].

3. **Transverse arcs**: Transverse arcs (TAs) appear as curved actin filament bundles, which display a periodic α-actinin myosin pattern that is typical for contractile actomyosin bundles. Unlike the ventral fibers, TAs do not interact directly with focal adhesions [248].

4. **The perinuclear actin cap**: The perinuclear cap consists of stress fibers positioning above the nucleus. The key function of the perinuclear actin cap is to regulate the shape of the nucleus as well as to act as mechanotransducers to convey force from the cell environment to the nucleus [249].

Stress fibers have critical roles in regulating cell adhesion, migration and mechanotransdoction. Focal adhesions are complex structures that ensure the proper communication between the cell and the ECM through the interaction of the transmembrane proteins, integrins, with their extracellular ligands during adhesion and migration. As discussed above, focal adhesions are often connected to the actin fibers and stress fiber tension or contractility can convert mechanical signals into biochemical cues, and therefore have an important role in focal adhesion matura-

tion and dynamics. In addition, the detachment of cell rear from the stiff substrate requires the contractility of stress fibers to drive the cell move forward. Nevertheless, for cells growing in their native tissue environment or 3D systems, stress fibers were reported to be less necessary [250]. Moreover, stress fibers are involved in mechanosensing through focal adhesions, by sensing the mechanical environment and converting the mechanical stimuli into biochemical signals. Mechanosensing is therefore considered to be critical for cell differentiation and cell fate determination.

Another structure of actin filament, actin cortex, approximately 50-200 nm thick, is a thin, crosslinked actin network that lies under and is tethered to the plasma membrane (Figure 2.15A). Most of the classical ABPs localize to the cell cortex, including actin bundling and crosslinking proteins e.g. α-actinin and filamin, proteins involved in contractility, e.g. myosins which generate contractile stresses in the network, and linker proteins e.g. the ERM proteins. Cell shape is mainly determined by cell cortex, which is defined by cellular mechanical properties and by cell's physical interactions with its environment. Mechanically, the cortical actin mesh plays a role like the cell wall in bacteria or plant cells. It is the main determinant of stiffness of the cell surface in the mechanical test, resisting external mechanical stress and internal osmotic pressure. At the same time, the cell cortex plays a critical role in cell shape changes which is important for cell survival in a changing extracellular environment. The cell cortex undergoes dynamic remodeling on timescales of seconds by turnover of its protein components and network reorganization through myosin-mediated contractions to allow the cell to rapidly change shape, migrate or exert forces. Moreover, for cells growing in their native tissue environment or 3D systems, actin cortex also participates in bleb based migration, as blebs form at the locations of reduced attachment between actin cortex and plasma membrane.

Apart from promoting cell mobility, providing support for the cell structure, and transmitting force signals, actin filaments also act as a network of tracks existing as single filament, branched networks or actin bundles where motor proteins can move along to directly deliver vesicles or cargoes. This process is essential to ensure an adequate concentration of required components at sites undergoing rapid modulation. Specific members of the Myosin superfamily of motor proteins are known to transport cargo along actin filaments, for example Myosin-V (Figure 2.16).

Myosin-V is composed of three domains (Figure 2.16A). The first domain is a two-head motor located at the carboxyl terminus, which can bind to actin filaments [251]. Myosin-V is able to walk on single filament by binding two heads

simultaneously to two actin monomers, with a step size of 36 nm [252]. The second domain contains an extended α-helical 'neck', which connects the head and the tail domain. The globular tail domains (GTDs) following the coiled-coil region mediate the binding of different cargoes, such as RNA, vesicles, organelles and mitochondria. Myosin-V is capable to move along actin filament without detaching in a processive manner (Figure 2.16B). Processive movement means that one molecule can undergo multiple productive catalytic cycles and associated mechanical steps before it detaches from its track.

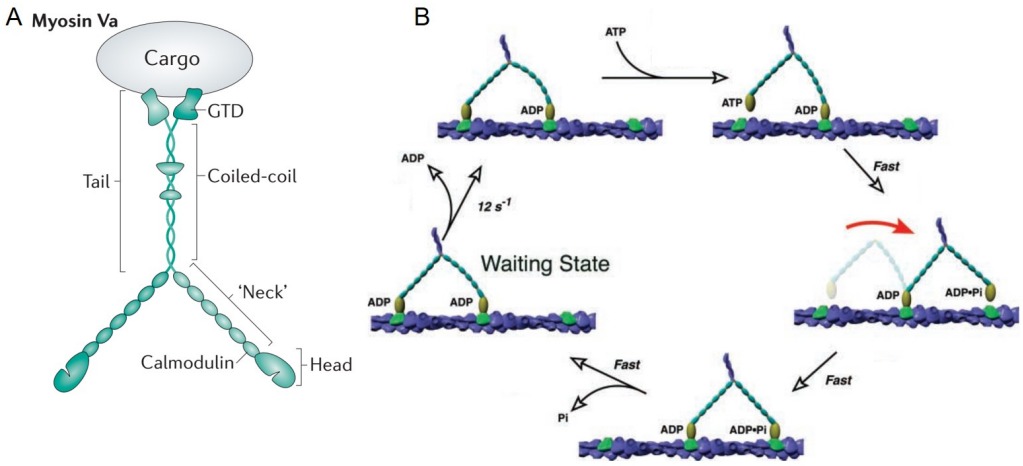

Figure 2.16: Actin filament motor protein, Myosin V. A. Domain structure of myosin Va. The head domain or motor domain contains the nucleotide-binding and actin-binding sites. The 'neck' domain consists of an α-helical segment of the heavy chain. The tail domain consists of a coiled-coil forming domain with periodic interruptions, which dimerizes the heavy chains, and two globular tail domains (GTDs), which bind cargo. Image taken from Hammer and Sellers, Nat Rev Mol Cell Bio, 2012 [251]; B. Model for the processive movement of myosin V along actin filament. In waiting state, both heads bind to ADP. Then ADP from the trailing head is first released. The head then binds to ATP and rapidly dissociates from actin filaments. The attached head undergoes a power stroke, positioning the new leading head to find a forward binding site via a thermally driven search. Upon binding to actin, the leading head rapidly releases Pi and establishes a strong binding conformation, which brings myosin V to the same state as in waiting state but translated forward by 36 nm. Image taken from Mehta et al, Nature, 1999 [252].

2.3.2 Microtubule cytoskeleton

Microtubules are essential cytoskeletal polymers, existing in all eukaryotic cells. They provide a skeletal framework that supports the cell body, establishes cell po-

larity and provides tracks on which motor proteins transport vesicles throughout the cell during interphase. While cells are in mitosis, microtubules get remodeled into the mitotic spindle on which the chromosomes are segregated into two daughter cells.

2.3.2.1 Microtubule assembly

Microtubules contain two polypeptide subunits, α-tubulin and β-tubulin, which interact with each other in a head-to-tail fashion to make long strands called protofilaments (Figure 2.17A left). 11-15 protofilaments, depending on the species and cell types, interact with each other laterally to form a hollow, straw-shaped filaments of microtubules [253, 254] (Figure 2.17A middle). Like the dynamics of actin filaments, microtubules are changing all the time with reactions constantly adding and subtracting tubulin dimers at both ends of the filaments. The β-tubulin exposed end that grows faster is called the plus end, whereas the α-tubulin exposed end which is more stable is known as the minus end (Figure 2.17A right). In cells, the minus ends of microtubules are anchored in structures called microtubule organizing centers (MTOCs), which contain γ-tubulin and other protein components [255]. The primary MTOC in a cell is called the centrosome, and it is usually located adjacent to the nucleus. Microtubules tend to grow out from the centrosome to extend towards the cell periphery as shown in Figure 2.19A.

Microtubules have the ability to control the polymerization and depolymerization from their plus ends, which can switch between phases of growth and shortening, a behavior termed dynamic instability [258]. A transition from a state of growth to shrinkage is called 'catastrophe', whereas a transition from a state of shrinkage back to growth is termed as 'rescue'. Dynamic instability is fundamentally linked to the binding and hydrolysis of GTP by tubulin subunits [259] (Figure 2.18B). Both α-tubulin and β-tubulin have GTP binding sites, i.e. nonexchangeable N site on α-tubulin and exchangeable E site on β-tubulin. After polymerization, GTP binding with β-tubulin is hydrolyzed and becomes unchangeable. As a result, the β-tubulin binding with GTP at the plus end of microtubules forms a cap. The cap helps stabilize the microtubule structure and promotes its growth. When the GTP within the cap is hydrolyzed, the microtubule rapidly depolymerized (catastrophe). Whenever the depolymerizing microtubules bind to GTP bound β-tubulin again, the microtubules switch from depolymerization to growth (rescue).

This dynamic instability enables the microtubule cytoskeleton to disassemble and assemble into different arrangement rapidly. The plus ends can display phases of rapid growth and shortening which enable the microtubules to explore the whole

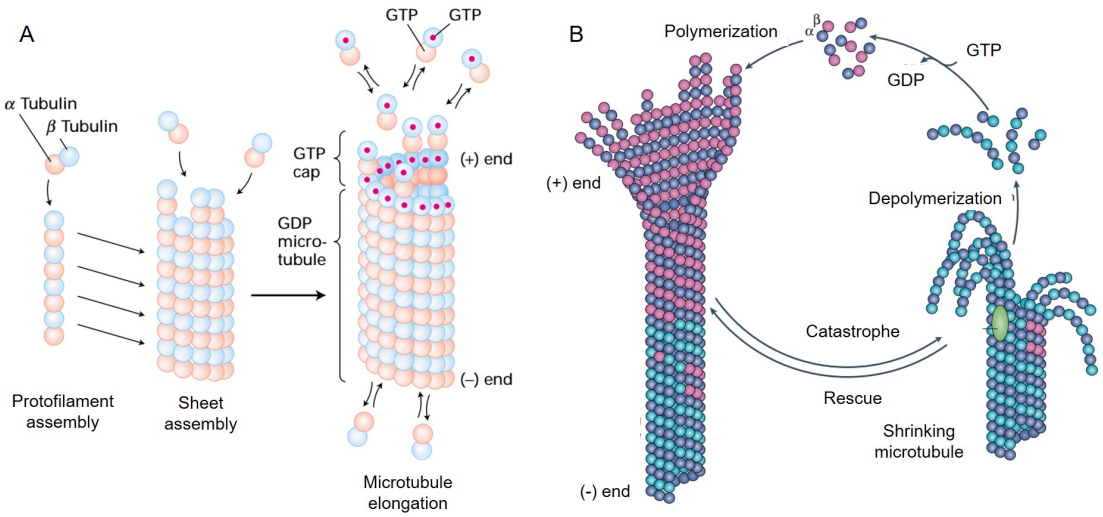

Figure 2.17: Microtubule assembly and dynamics. A. Stages in assembly of microtubules. Free α and β tubulin dimers associate longitudinally to form short protofilaments. These protofilaments quickly associate laterally into more stable curved sheets. Eventually, a sheet wraps around into a microtubule with 13 protofilaments. The microtubule then grows by the addition of subunits to the ends of protofilaments composing the microtubule wall. The free tubulin dimers have GTP (red dot) bound to the exchangeable nucleotide-binding site on the β-tubulin monomer. Image taken from Lodish et al, Molecular cell biology, 2013 [256]; B. Microtubule dynamics stability. The cycle of tubulin polymerization and depolymerization is powered by hydrolysis of the GTP bound to β-tubulin, which enables microtubules to switch between catastrophes and rescues. GTP-bound tubulin dimers are incorporated into growing microtubules. GTP hydrolysis occurs, with a delay, after a GTP-tubulin dimer incorporates into the sheet-like structure of growing microtubule tips. Growing microtubule ends thus maintain a stabilizing GTP cap, the loss of which leads to a catastrophe and rapid depolymerization. Image taken from Akhmanova and Steinmetz, Nat Rev Mol Cell Bio, 2015 [257].

cellular space from the nucleus [260]. Otherwise, the plus end can be stabilized by their dynamics as reduced by interacting with different cellular structures. While the minus ends are more stabilized, being concentrated in central regions of the cell, where they attach the nucleation sites, such as the centrosome. The significance of intracellular functions of microtubule polymerization dynamics determines that all phases of microtubule growth dynamics are highly regulated by a number of proteins [261]. Proteins that regulate microtubule dynamics fall into two main classes: proteins that stabilize microtubules and those destabilize microtubules. The former class of proteins is exemplified by the classic microtubule-associated proteins (MAPs), which are considered to bind along the length of the microtubule polymer and enhance their stability.

2.3.2.2 Function of microtubules

Microtubules are the stiffest of the three polymers and their hallmark behavior, i.e. dynamic instability, is key to their cellular functions. Microtubules participate in the regulation of intracellular transport, chromosome segregation, cellular internal organization as well as cell motility.

There are three classes of molecular motors that can transport organelles and cargoes inside cells, apart from myosins, dyneins and kinesins walking along microtubules instead of actin filaments. Microtubules, much longer than actin filaments, act as highways throughout the cell. The motor proteins kinesin and dynein associate with cargoes and transport them along microtubules by taking the energy form ATP hydrolysis. Kinesins move towards the microtubule plus-end along only one protofilament with a step size of 8 nm [262, 263]. While dynein moves towards the minus-end with variable sized steps [264] (Figure 2.18). Both kinesins and dynein are capable of binding to most cargoes, and they work like a team to transport in both directions. Robust control of intracellular transport is required to maintain proper signalling and degradative pathways, and defects result in developmental and neurodegenerative disease. Many studies revealed that rather than simply acting as passive tracks, microtubules contain signals that regulate the activities of kinesin and dynein to target cargoes to specific locations in the cell [265]. These signals include the organization of the microtubule network, post translational modifications that alter the microtubule surface properties and mechanics, and microtubule associated proteins that modulate the motility of motor proteins and microtubule polymerization.

Equally, microtubules are crucial for cell division. As accurate mitosis, where genetic material is divided equally between two daughter cells, is essential to eukaryotic life. To achieve chromosome segregation, a self-assembled mitotic spindle, which is a dynamic and highly complex structure comprising microtubules, associates with motor proteins and non-motor proteins [266]. Mitotic spindle extends from two opposing MTOCs located in two poles of the cell, with the less dynamic minus end anchoring at the MTOCs and the more dynamic plus end pointing into the center of the cell (Figure 2.19B). A part of microtubules plus ends attaches to kinetochore of sister chromatids, forming bundles of 20-40 microtubules called K fibers [267]. K fibers are responsible for maintenance of attachment of chromosomes to the spindle and allow them to align and segregate. The rest microtubules form astral microtubules [268], which help maintain the position of the spindle through the interaction with cell cortex, and interpolar microtubules [269], which makes antiparallel overlaps in the center part of the spin-

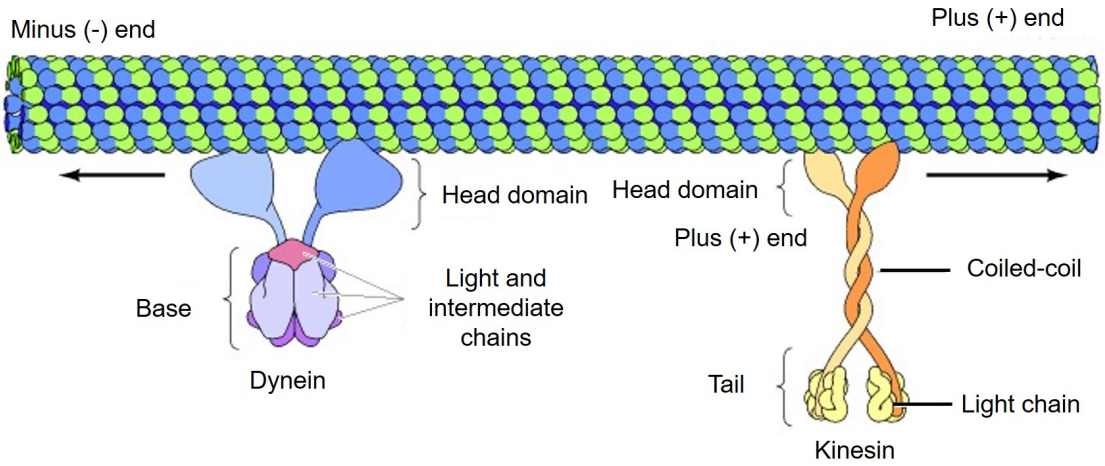

Figure 2.18: Microtubule motor proteins: kinesin and dynein. Kinesin and dynein move in opposite directions along microtubules, toward the plus and minus ends, respectively. Kinesin consists of two heavy chains, wound around each other in a coiled-coil structure, and two light chains. The globular head domains of the heavy chains bind microtubules and are the motor domains of the molecule. Dynein consists of two or three heavy chains (two are shown here) in association with multiple light and intermediate chains. The globular head domains of the heavy chains are the motor domains. Image taken from Cooper and Hausman, The cell, 2000 [238].

dle involved in pushing the spindle apart during mitosis (Figure 2.19C). During anaphase, spindle plays a vital role in the migration of duplicated chromosomes into two identical daughter cells.

The cellular regulation of microtubule dynamic instability helps throughout the whole cell division process, for example, transforming from the interphase array into a mitotic spindle. It has been reported that mitotic microtubules turn over 5 to 10 fold faster than interphase microtubules [271]. In addition, the pushing and pulling forces generated by the assembly and disassembly of microtubules, together with motor proteins, contribute to the correct positioning of chromosomes, mitotic spindles, and segregation of chromosomes [272].

Microtubules are key organizers of the cell interior. Because microtubule networks grow out from the centrosome near the nucleus, radiating out to the plasma membrane, providing the basic organization of the cytoplasm. Within this network, microtubules can move and position organelles by pushing, pulling or sliding. Pushing forces can be generated by microtubule polymerization towards the organelle [273]; while pulling involves in microtubule depolymerization or motors and sliding is powered by motor proteins between one microtubule and another microtubule. It is essential for cell to organize the interior organelles efficiently in response to the change of the extracellular environment.

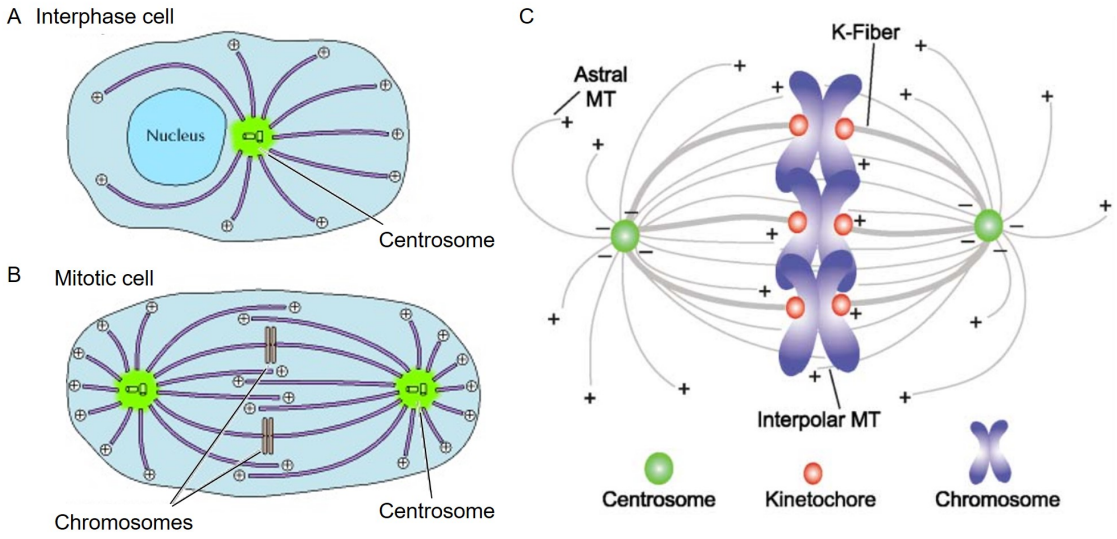

Figure 2.19: Organization of microtubule in interphase cell and mitotic cell. A. Organization of microtubules in interphase cell; B. Organization of microtubules in mitotic cells, in metaphase. Image taken from Cooper and Hausman, The cell, 2000 [238]; C. Mitotic spindle components: the basic components of the mitotic spindle in somatic cells. Three different organizations of microtubules: K-fiber, astral microtubule and interpolar microtubule. Image taken from Kline-Smith and Walczak, Molecular cell, 2004 [270].

Another major function of microtubules is the control of polarized cell motility. In order to support the asymmetry of cellular activities, asymmetric microtubule distribution and dynamics are needed. As actin filaments are the dominant regulator of cell motility, i.e. the supporting roles of microtubules in cell migration include the following three parts. The first part is that microtubules affect the formation of actin filament containing leading edge protrusions by interacting with the small Rho GTPase proteins, like Rac1, Cdc42, which is reported to be involved in regulation of actin polymerization [274]. The second part is that microtubules facilitate the turnover of focal adhesions. Microtubules, which grow directionally towards focal adhesions, are able to promote the disassembly of focal adhesions [275]. For the third part, efficient cell migration requires microtubule-dependent transport of membrane vesicles, post-Golgi carriers and other functional entities to the leading cell edge [276]. Apart from those, recent studies show that cells failed to retract their rear by partially suppressing microtubule dynamics and migrate more randomly at normal speed in the absence of microtubules, which indicates that microtubules can also restrain cell motility and control the migration direction [277].

2.3.3 Intermediate filaments

Intermediate filaments have a diameter of 10 nm, which is intermediate between the diameters of actin filaments and microtubule. Unlike actin filaments and microtubules, intermediate filaments are composed of a large family of cytoskeletal proteins, whose expression is cell and tissue specific. The proteins, encoded by over 70 genes, are divided into 5 major types based on their structure, assembly properties, sequence homology and their developmentally regulated tissue-specific expression patterns. The first four types (I-IV) are cytoplasmic, while type V exists in the nucleus. Types I and II are the acidic and neutral-basic keratins, which assemble into heteropolymeric filaments, typically in epithelial cells. By contrast, type III intermediate filaments, which are composed of vimentin, desmin, peripherin, and glial fibrillary acidic protein (GFAP), form homopolymer filaments. Type IV intermediate filaments include the neurofilament triplet proteins (NF-L, NF-M and NF-H), α-internexin, nestin and syncoilin, which are expressed in the nervous system. The nucleoskeletal proteins, lamin A, lamin C, together with lamin B1 and lamin B2, comprise the type V intermediate filaments [278].

2.3.3.1 Intermediate filament assembly

All intermediate filament proteins share a common secondary structure: a tripartite organization, which consists of a structurally conserved central α-helical rod domain flunked by distal head and tail regions at the N- and C-terminus (Figure 2.20A). The central rod domain contains three coil domains that are separated by linker domains. The rod domains of two intermediate filament polypeptide chains align in parallel to form coiled-coil dimers, which are stabilized by a hydrophobic left-hand stripe [279]. Two dimers associate laterally in an anti-parallel and approximately half-staggered fashion to form tetramers [280] (Figure 2.20A). The variability observed among the N-terminus and C-terminus, unique in length and amino acid sequences, leads to striking differences in assembly pathway, dynamics and speed, persistence length, and structure formation, representing different characters of each intermediate filaments for tissue and cell type specific [281]. Unlike the assembly of actin filaments and microtubules by monomer or dimer adding at one end, intermediate filaments are formed by end-to-end fusion of unit-length filaments (ULFs) [282]. There are three steps involved in the intermediate filament assembly. Firstly, typical eight of tetramers rapidly associate laterally to assemble into unit-length filaments (Figure 2.20B), which are approximately 16 nm in diameter and 60 nm in length. It is a fast process that the formation of ULFs only happens within seconds. ULF2 are precursors of the formation of long

intermediate filaments. This is followed by the ULFs annealing end-to-end to yield loosely packed filaments, i.e. the elongation step forming filaments containing two or more ULFs. Finally, at certain length, the growing filaments start to compact to reduce their diameter and to reorganize the structure, yielding mature intermediate filaments with diameter of about 11 nm [282] (Figure 2.20 C). While in living cells, intermediate filaments exist in filamentous form or as detergent soluble filament precursors of various short filamentous, such as tetramers, ULFs, particle and squiggles. Unlike actin filaments and microtubules, intermediate filaments are not polarized, which implies that they do not act as tracks for the movement of molecular motors.

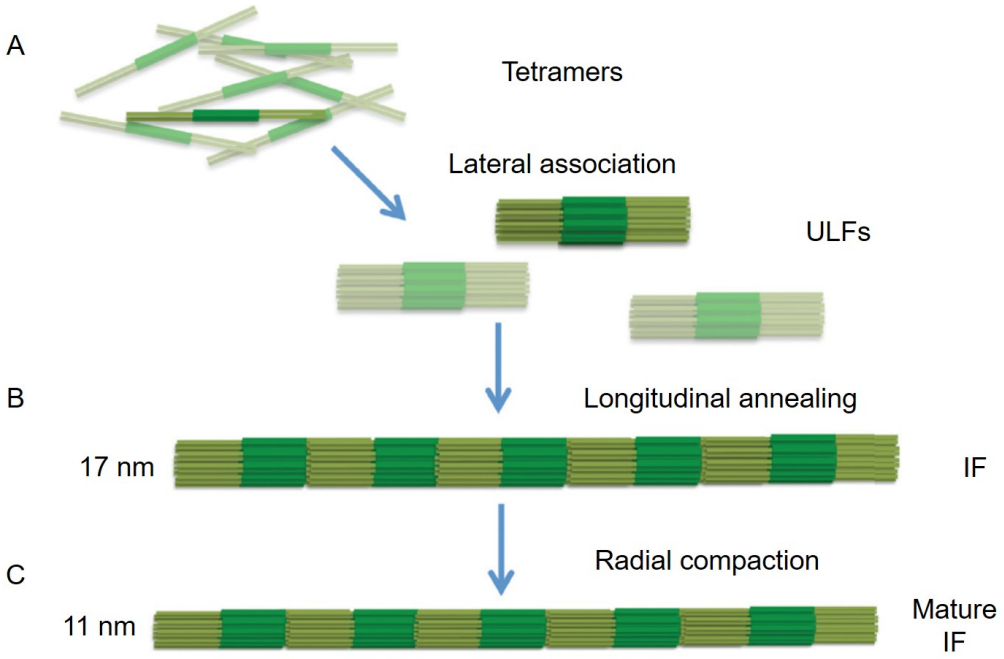

Figure 2.20: Assembly of intermediate filaments. Schematic representation of the three-phase assembly model for cytoplasmic intermediate filaments: A. Tetramers lateral associate to form unit-length filaments (ULFs); B. Intermediate filaments elongate by end-to-end annealing to form loose filament with diameter of 17 nm; C. Last, the filaments are radially compacted to form mature intermediate filaments with diameter of 11 nm. Image taken from Herrmann and Aebi, CSH Perspect Biol, 2016 [278].

2.3.3.2 Function of intermediate filaments

Intermediate filaments are major building materials for cellular architecture and involved in the maintenance of the integrity and mechanical properties of the cy-

toplasm, organelle anchorage distribution and stability of the other cytoskeleton.

Intermediate filaments are capable to form extensive networks within the cytoplasm. These networks point to all directions to form a central cage-like structure that encapsulates the nucleus and further radiates toward the cell periphery. The presence of the extensive and well-organized structure in all areas of the cytoplasm offers an obvious advantage for intermediate filaments to support the whole cell shape and integrity, and at the same time, coordinate activities of other cytoskeleton. What's more, the type V intermediate filaments, like lamins, provide structural support for the nuclear membrane, helping space out the nuclear pore complexes and organize genetic materials [283].

Cells are facing mechanical strain all the time throughout the whole development. Intermediate filaments have unique features that not only distinguish them from the other cytoskeleton polymers, e.g. actin filaments and microtubules, but also make them major contributors in providing mechanical resistance to the cells. The length of intermediate filaments is much shorter and more various than that of actin filaments and microtubules. Cross-sectional diameter, i.e. the basic structure and various length, provides intermediate filaments with superior elasticity and much better flexible and extensible properties, which makes them main factors in regulating the mechanical properties of cells [284] (Figure 2.21). Furthermore, intermediate filaments exhibit strain-induced strengthening without catastrophic failure, which makes them very suitable as intracellular load bearing springs [285]. In conclusion, intermediate filaments contribute to both cells' elasticity and tensile strength [284].

Although the three cytoskeletons are often considered as three separate networks, these filamentous arrays cooperatively interact with each other in many ways [286] (Figure 2.22). Intermediate filaments can be crosslinked to each other, as well as to actin filaments and microtubules physically by proteins called plectins [287]. Even some intermediate filament structures may be organized mainly through interactions with microtubules or actin filaments. Microtubules are responsible for intermediate filament subunit exchange and turnover. There are many studies on microtubule-based intermediate filament motility showing that intermediate filament movements are bidirectional, with around 65-70$\%$ towards the cell periphery via candidate motor protein, kinesin [288], around 30-35$\%$ moving towards the cell center via the regulation of microtubule motor, dynein [289]. Actin filaments is also involved in the interaction with intermediate filaments. For example, keratin bundles are closely associated with actin stress fiber. The disruption of stress fiber with drugs also resulted in the disruption of the organization of keratin intermediate filament networks [290]. Actin filament motor protein, myosin

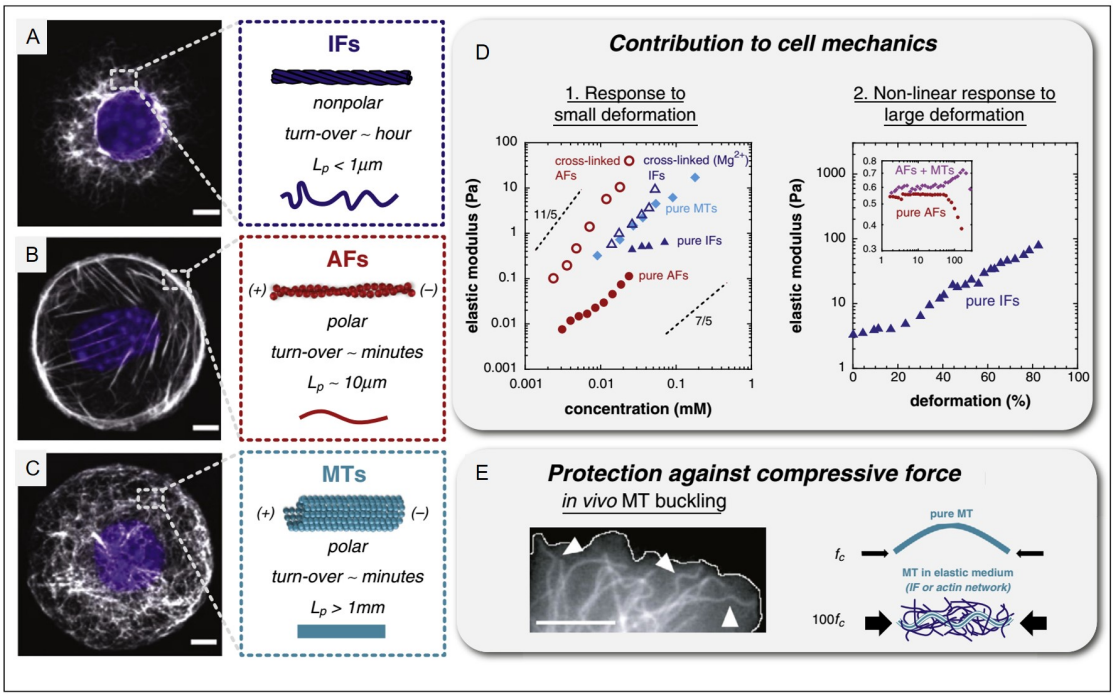

Figure 2.21: Contribution of the cytoskeleton to the mechanical properties of cells. The polarity, turnover dynamics and persistence length (Lp) of intermediated filaments (A) , actin filaments (B) and microtubules (C) are different; D. Cytoskeletal networks display a wide range of elastic moduli at small deformations, spanning about five orders of magnitude, depending on their concentration and on the extent of cross-linking. A particularity of intermediate filament network is their nonlinear response to large strain. Microtubules promote strain-stiffening of actin networks by suppressing inhomogeneous actin filaments deformations; E. Actin filaments and intermediate filaments networks provide an elastic background network that reinforces microtubules against compressive forces, increasing the critical buckling force fc. All scale bars shown are 5 mm. Image taken from Huber et al, Curr Opin Cell Biol, 2015 [286].

Va, is reported in the regulation of the distribution of intermediate filaments in neurons [291].

2.3.3.3 Brief introduction of vimentin

Among the large protein family of intermediate filaments, vimentin is one of the most familiar members, which is a fine mesh network loosely arranged in a parallel or crisscross fashion. Vimentin, a highly conserved 57 kD protein, is typically expressed in cells of mesenchymal origin, like fibroblasts, endothelial cells and leukocytes [292].

Except serving a stabilizing role as intracellular scaffold, vimentin network also plays a critical role in regulation the distribution and organization of organelles

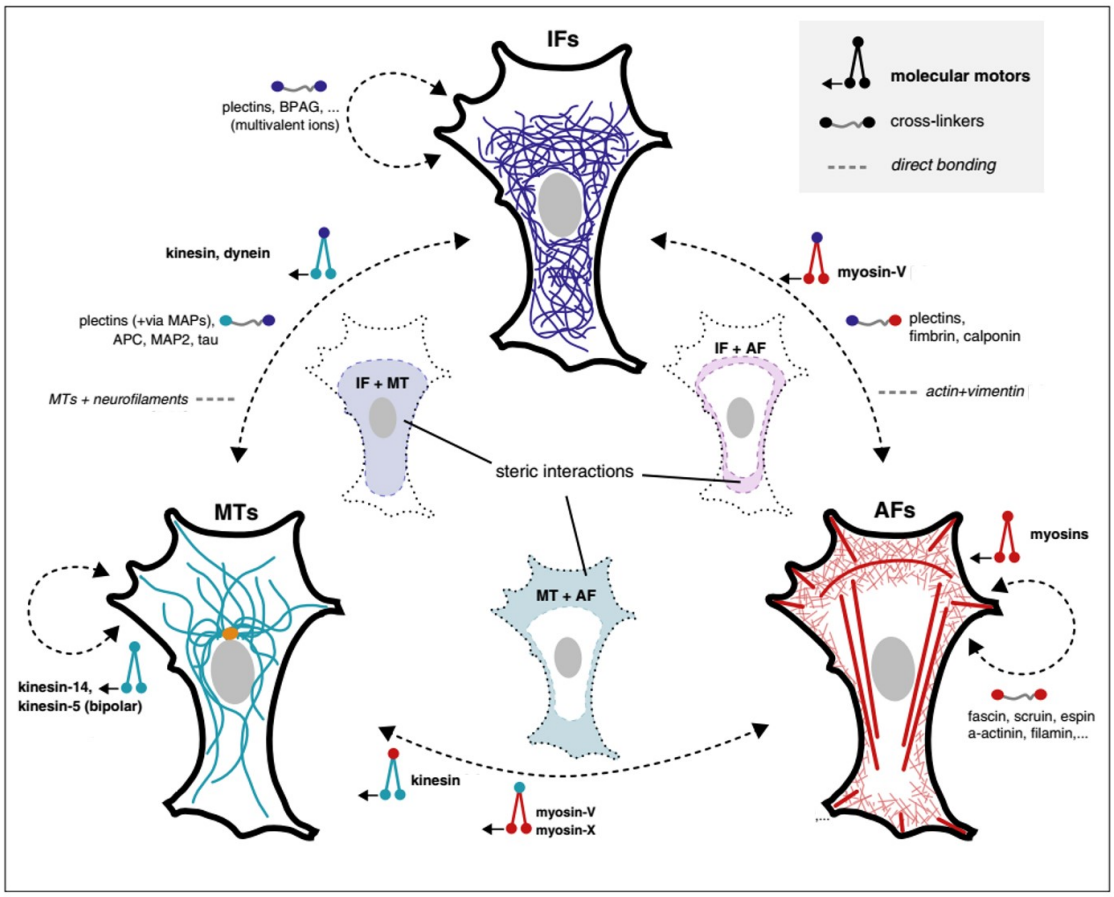

Figure 2.22: Cross talk between three cytoskeletons. Multiple physical interactions exist within and in between the three cytoskeletal subsystems: intermediate filaments (IFs), microtubules (MTs) and actin filaments (AFs). In the center, the subsystems interact via steric effects: intermediate filaments and microtubules interact mainly in the cell interior; microtubules and actin filaments interact mainly in the cell periphery; intermediate filaments and actin filaments interact mainly at the periphery of the intermediate filament network. Crosstalk between actin filaments and intermediate filaments, microtubules and intermediate, are facilitated by cross-linkers and motors and by direct binding in certain cases. Crosstalk between actin filaments and microtubules is mediated by numerous cross-linkers as well as actin filament-based and microtubule-based motors. Image taken from Huber et al, Curr Opin Cell Biol, 2015 [286]

within the cytoplasm, cell migration and adhesion, and cell signalling. By stabilizing the positions of organelles, vimentin network determines the intracellular mechanical properties, such as cell cytoplasm stiffness. By preventing the organelles displacement by random fluctuating cytoplasmic forces, vimentin is responsible for cell cytoplasm stiffness [293]. On the other hand, vimentin network regulates the organelles distribution, such as mitochondria and Golgi. It has been reported that the motility, distribution and anchorage of mitochondria is modulated by interactions with vimentin [294]. Vimentin is involved in associating with the residents of Golgi proteins to position the Golgi apparatus [295].

Also, vimentin around the nucleus has an influence on position and modulate the movement of nucleus [296], by interacting with nucleus cytoskeleton proteins, with major component of the type V intermediate filaments. What's more, cell migration and adhesion require the function of vimentin. Primary fibroblast derived from vimentin-deficient mouse embryos displayed reduced motility and directional migration, and impaired spatial organization of focal contact proteins [293]. Finally, vimentin network interacts with signalling proteins, such as Phospholipases A2 (PLA2) and 14-3-3 protiens [297].

2.3.4 Summary

To conclude, the cytoskeleton, including actin filaments, intermediate filaments and microtubules, works together to maintain cell shape and internal organization, as well as provide mechanical support cellular essential functions. Even though the sizes, structures, the way of assembly are different, changes in one particular cytoskeletal network would appear alongside changes in other networks. What's more, changes of cytoskeleton are the reasons for other cellular changes, like migration, and mechanical properties.

2.4 Cell mechanical properties

The study of cell mechanics has attracted blooming interest from the cell biology and biomedical communities in the last decade. The mechanical properties of cells, such as stiffness and viscosity have been extensively studied, providing more insight into the biological characteristics of cells. Recent studies have revealed that changes in cell mechanics are hallmarks of many diseases. Especially, the property of cell stiffness, has been well studied in recent years, with a focus on its correlation with cancers. Cancer cells with different degrees of malignancy exhibit different stiffness, different states of cytoskeletal tension and organization, as well as other mechanical alterations. The comparison of mechanical properties of cancer cells with normal cells could provide a better understanding of the physical nature of cancer and an alternative way in cancer diagnosis. It has been reported that cancerous (MCF-7) human breast epithelial cells has apparently lower stiffness compared with its benign (MCF-10A) cells. In addition, a reduction in the presence of well-organized actin stress fibers, a key constituent of the cytoskeleton system which greatly determines mechanical cell elasticity, is observed in these breast cells [298]. Similar results have also been reported

in ovarian cancer cells [299, 300], thyroid cancer cells [301]. To conclude, there is an increasing demand for such in-depth research to further investigate on the correlation between cell mechanical properties and disease, which will make a great impact to human health. The following part will introduce cell mechanical properties and techniques used to measure cell mechanical properties.

2.4.1 Introduction of cell mechanical properties

Cells are continuously subjected to mechanical forces from the surrounding environment, including shear, compressive and extensional forces. Crowded with a range of proteins, subcellular structures, organelles, as well as cytoskeleton network, cells are able to detect mechanical stimulation in the environment by the activation of mechanosensitive signaling pathways and respond to physical cues. The ability of cells to deform and actively respond to mechanical forces is critical for cellular function maintenance, such as shape, motility, differentiation, division and adhesion to surrounding environment.

The ability of cells in response to applied forces depends on the composition and organization of subcellular structures, like the cytoskeleton, cell membrane and nuclear, to act as a whole (Figure 2.23). As the most important cellular component for mechanical behavior, cytoskeleton includes (1) actin filaments, (2) intermediate filaments and (3) microtubules. (1) Actin filaments withstand tension in the cell and provide overall resistance to deformation from external stimuli. (2) Intermediate filaments are responsible for forming a network in the cytoplasm, extending from cell nuclear to cell membrane, as well as other cytoskeleton. (3) Microtubules resist compression, as opposed to actin filaments and intermediate filaments [302]. Through reorganizing the cytoskeleton by controlling polymerization and depolymerization of the filaments, cross-linking between single cytoskeleton or different cytoskeleton, cells are able to adapt to the changing environment. The cell membrane is an integral contributor to cell mechanical behavior, through connecting to the underlying cytoskeleton. Even though cell membrane alone has weak mechanical properties [303], it is connected to the rest of the intracellular environment transmitting external forces to the intracellular tensile. Through nucleocytoskeletal proteins, such as lamin A, B1, B2 and C, nucleus is connected to the cytoskeleton and able to influence both local and whole cell mechanical properties.

Like all complex materials, cells are viscoelastic materials, as they are able to maintain their shape under mechanical stresses like solids, and at the same time exhibit time-dependent responses to deformation. Depending on the time scale,

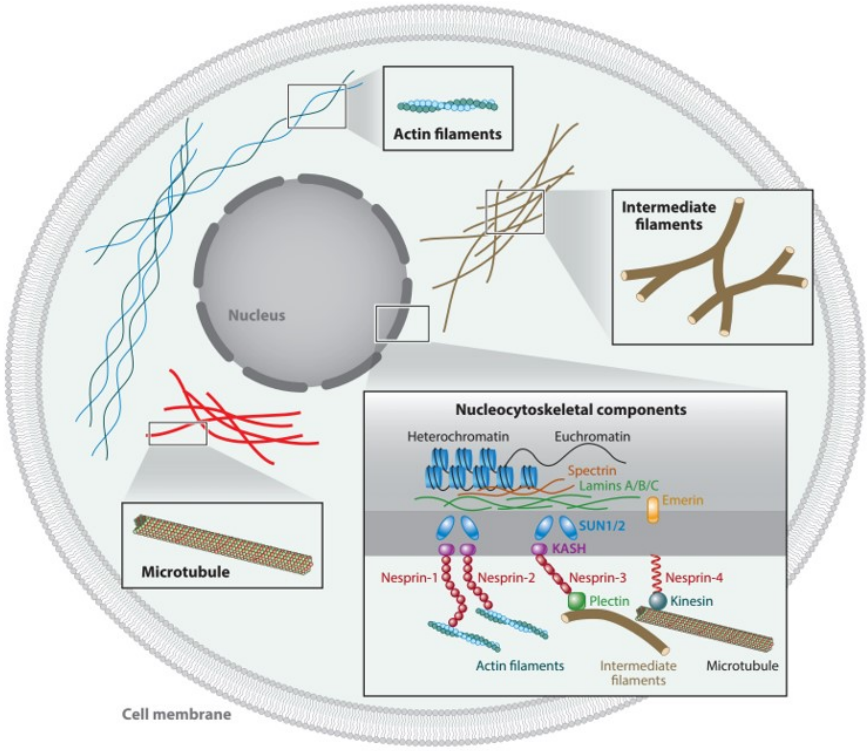

Figure 2.23: Schematic of intracellular components contributing to cellular mechanical properties. Cell cytoskeleton including actin filaments, intermediate filaments, and microtubules, cell membrane and nucleus are main contributors to cell mechanical properties. Image taken from Darling and Carlo, Annu Rev Biomed Eng, 2015 [302].

the elastic or viscous-like behaviour dominate the response of viscoelastic materials. Simple mechanical terms elasticity and viscosity can be used as comparative quantities in cell mechanics. Elasticity, the most commonly assessed mechanical properties of cells, requires the deformation resulting from a force. This provides the structural stiffness that can be used for estimation of the elastic modulus. Another parameter, the apparent viscosity, describes how cell deforms over time, revealing the mechanical deformability of cells. The mechanical properties of cells are studied using different techniques each with a different method to apply a mechanical deformation and measure the corresponding force.

2.4.2 Techniques to measure cell mechanical properties

Cells are soft biological materials with an elastic modulus that varies from a few hundred pascals to tens of kilo-pascals, together with a small size in the order of tens of microns. As a result, the mechanical measurement requires the capability of monitoring deformations and forces in the range of micro to nano meters

and nano to pico newtons respectively. With the rapid development of precision instrument, various testing methods have been developed to quantify the mechanical properties of living cells. Till now, there are a wide array of experimental techniques that are able to study the mechanical behavior of cells, including cell poker, compression, optical tweezers, magnetic technique, micropipette aspiration, atomic force microscope and particle tracking microrheology. Generally, to chose the right experimental techniques is determined by two factors, (1) the size or type of biological structure that is being investigated, and (2) what specific information that is desired regarding that structure and must be identified.

2.4.2.1 Atomic force microscopy

AFM, also known as scanning force microscope (SFM), is part of a large family of instruments termed as scanning probe microscopes (SPMs). The invention of the AFM by Binning, Quate and Gerber in 1986 created new hope for biological studies [304]. Originally, AFM systems were developed to characterize the atomic and surface properties of materials for electronic devices. As a high resolution surface characterization technique, now AFM is widely used for imaging and measurement of cell mechanical properties [305]. In order to investigate the complexity of biological systems, such as liquid condition and certain temperature, various technological developments have been made to meet these requirements. AFM has now become a powerful, multi-functional imaging platform that allows biological samples, from single molecules to living cells, to be visualized and manipulated [306].

AFM consists of four major parts as shown in Figure 2.24A, including a laser diode, a photo-detector, which works as a scanner, a cantilever with a tip mounted underneath it, and a piezo-scanner that drives the cantilever in x, y and z directions. Cantilevers are commonly made in V-shaped or rectangular shaped. The tips are most commonly in the form of a squared-based pyramid or a cylindrical cone. The most common materials used for AFM cantilever and tip are silicon and silicon nitride (Figure 2.24B), with a wide variety of cantilevers ranging from 100-200 μmm in length, 10-40 μm in width and 0.3-2 μm in thickness [309].

A sharp tip probes the surface features by raster scanning, which means that the tip is scanning back and forth along a series of parallel lines. During AFM scanning, the cantilever probes the surface by sensing the force between AFM tip and sample surface. The systems are built based on the atomic interaction between the tip and sample surface at different distances, which can be either short-range repulsive interaction or longer-range attractive interaction. As the tip approaches

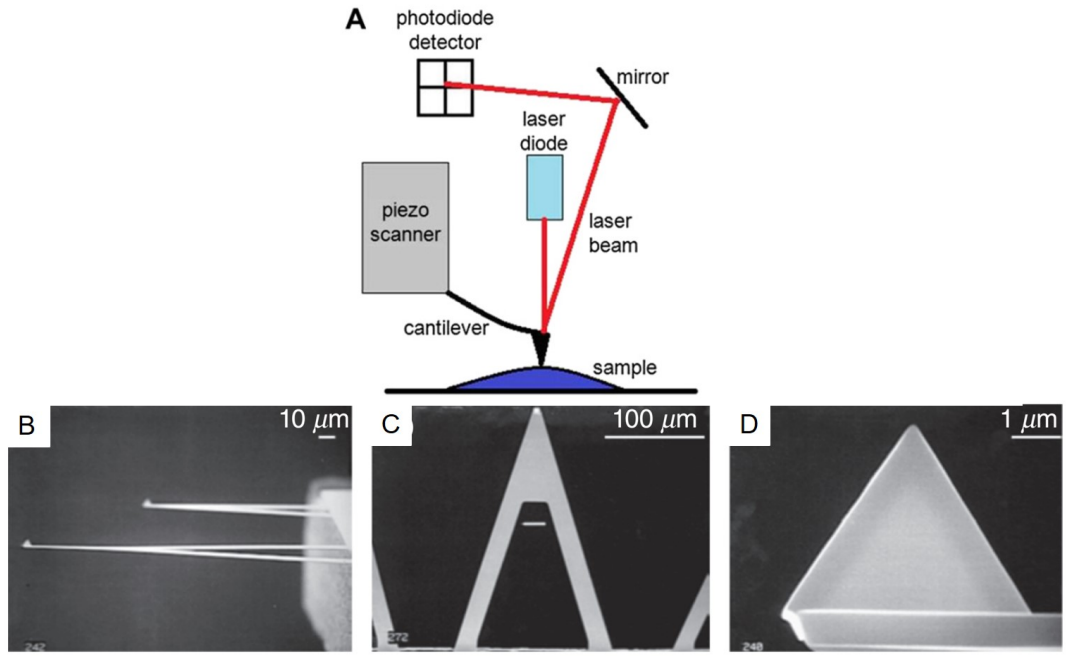

Figure 2.24: Typical AFM setup and SEM images of cantilever. A. Main elements in AFM setup, including cantilever, laser diode, photodiode detector and piezo-scanner, Image taken from Chang et al, Tzu Chi Med J, 2012 [307]; B. Side view of a cantilever with a tip attached to it; C. Top view of triangular shape of the cantilever; D. View of the pyramid shaped tip. Image taken from Rao and Costa, Biomedical Imaging, 2014 [308].

the surface, the attractive forces between the cantilever tip and sample, such as Van der Waals force, deflects the cantilever toward the sample surface. While as the cantilever tip is brought in contact with the sample surface, the repulsive forces, such as Pauli-exclusion interaction [310], deflects the cantilever in the opposite direction (Figure 2.26). Then the quadrant photodiode detector detects the deflections of the cantilever by a laser beam which could reflect off the back of the cantilever. The photodiode detector could pick up the vertical and lateral motion of the tip while the tip is continuously moving along the surface of the sample. In this way, the topographic images of the sample surface are generated by plotting the deflection once the tip completes the scanning over the sample surface.

Apart from the topography of the sample surface, the amount of force between the tip and sample can also be obtained depending on the spring constant of the cantilever and the distance between the tip and sample surface by using Hook's Law as $F = kx$. F is the force exerted on the cantilever during scanning, while k is the spring constant of the cantilever, and x is the cantilever deflection. By tracking how the sample deforms in response to applied force, the mechanical properties of the sample are obtained. During AFM scanning, force curves are recorded dur-

ing approaching the AFM tip to the sample surface and retracting (Figure 2.25). A force curve can be divided into approach force curve and retracting force curve. From the approach force curve, topography of the surface, indentation forces, deformation as well as the stiffness of the sample can be quantified. While from the retraction force curve, adhesion forces and viscosity can be calculated.

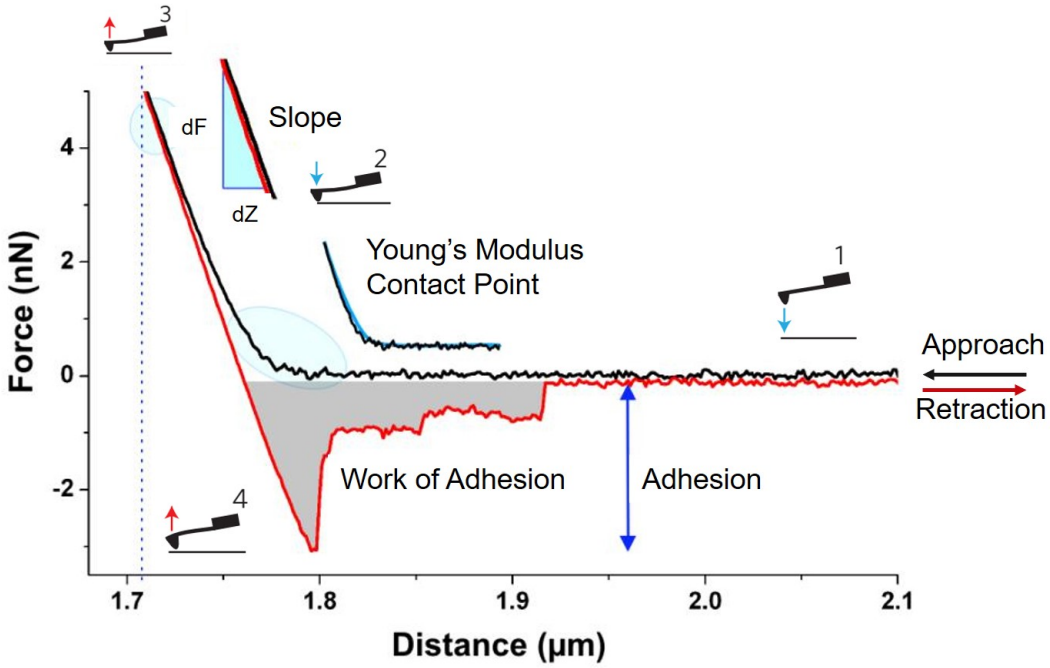

Figure 2.25: Force curve of AFM. Principle of force curve by approaching (black) and retracting (red) the AFM tip. The tip of the cantilever is initially away from the sample (1) to which it is brought into contact (2). During retraction (3) of the AFM tip, adhesive event (4) may occur [311]. Adapted from JPK handbook.

There are several imaging modes available for AFM measurement that could generate a wide range of useful information. The most commonly used modes are contact mode, non-contact mode and tapping mode, depending on the applied force and the distance from the tip to the sample (Figure 2.26A).

a. Contact mode: The AFM tip moves directly across sample surface (Figure 2.26B). As a result, the tip-sample interaction occurs in the repulsive region as shown in Figure 2.26A. This mode is preferred when the sample surface is not substantially stiffer than the tip. Contact mode can be divided into constant force mode where a feedback loop is used to keep the deflection of cantilever constant, and constant height mode which is suitable for scanning samples with small height differences. Since the tip is constantly in contact with the sample surface, the applied force and its created frictional forces would gradually cause undesirable damage to both the vulnerable soft samples and tips. Damaged or blunted tips would lead to a decrease in the resolution of obtained topography images.

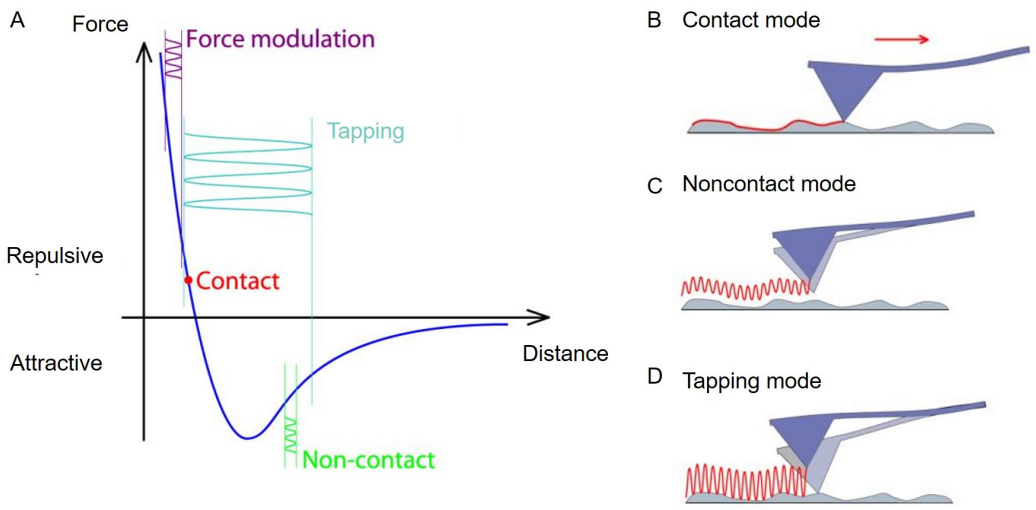

Figure 2.26: Force as a function of probe-sample separation. A. Tip-sample separation curve illustrating the main interaction during AFM scanning; Schematic representation of contact mode (B), noncontact mode (C) and tapping mode (D) [312]. Adapted from JPK handbook.

b. Non-contact mode: The AFM tip and sample surface remains non-contact with a certain distance (Figure 2.26C), so that the tip-sample interaction only occurs in the attractive region as shown in Figure 2.26A. In non-contact mode, the cantilever vibrates near the sample surface at a frequency higher than its resonant frequency. The benefit of using non-contact mode, is that it effectively avoids frictional forces, making it possible to measure soft samples without any damage to their surface. The disadvantage is, however, that non-contact mode generates images with lower lateral and z-resolution when compared to contact mode,

c. Tapping mode: In order to overcome the limitations of both contact mode and non-contact mode, tapping mode was developed [313]. An AFM tip makes intermittent contact with sample surface at a resonant frequency (Figure 2.26D). Unlike contact mode, the tip just touches the sample surface at the bottom of its swing, which takes very short time. In this way, during the tip scanning across the sample surface, frictional forces are greatly reduced. At the same time, the resolution of the surface topography is not affected. Therefore, tapping mode is the most often used AFM mode for soft materials like biological samples due to its high resolution, and the nearly non-destructive nature of the imaging.

AFM is a sophisticated tool that can reveal nano-scale structures of a cell within pico-newton forces. One of the advantages by using AFM is that the forces applied can be controlled precisely, and the accessible range of forces is large. In

addition, there are many choices for tips from the stiffness to shapes such as pyramid shape and core shape. On the other hand, the experiments taken by the AFM are typically on the cellular surface, not intracellular properties. Furthermore, the shape of the AFM tip, as well as the location of tip attachment, affect the nature of the force-deformation curves and biases the results of the test; therefore results are not easily transferable and comparable between experiments employing different AFMs.

2.4.2.2 Cell poker

In cell poker experiment, a glass needle is used to poke a cell or one of its subcellular structures [314]. The needle is made thin enough to apply small but meaningful forces to deform the cell without damaging it (Figure 2.27). Working as a spring, the bending stiffness of the glass microneedle has to be calibrated before the experiment. The force applied on the cell can be calculated by the deflection of the needle [315]. Elasticity of the cell can be determined from the slope of these experimental force-displacement curves by monitoring force and deformation of the cell. However, this approach is time-consuming and data-limited.

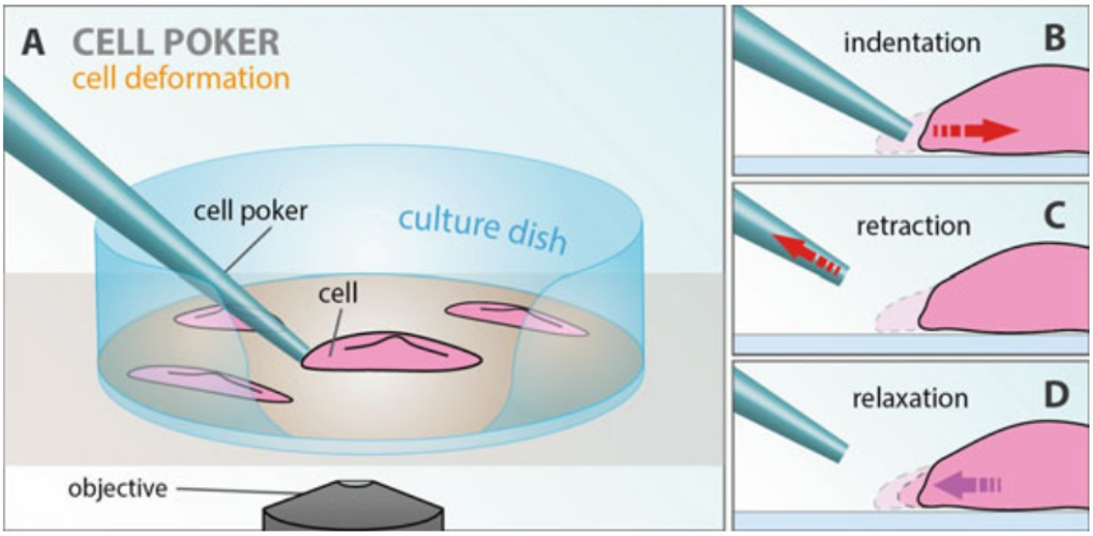

Figure 2.27: Cell poker. A. Schematic representation of the cell poking device and detection by microscope; A. The adherent cell is indented by a glass stylus that is coated with BSA to prevent its attachment to the cell; B and C. Images of the cell edge are taken after poking and immediate retraction of the glass stylus; D. The relaxation of the cell membrane after deformation is recorded by a high-speed video camera. The rate of relaxation is determined from the analysis of video frames using an elastic response theory. Image taken from Tanishita and Yamamoto, Springer, 2016 [316]

2.4.2.3 Compression

The compression technique is used to measure the mechanical responses of cells to unidirectional compression. The experiment is performed on a single cell or a population of cells growing on a flat plate, with another plate coming into contact with these cells. The force applied to the cells is strictly monitored and the deformation of the cells is recorded by a light microscope (Figure 2.28A). With this concept, many new compression techniques have been developed and used in cell mechanics-related research. For example, cells are seeded inside a gel to mimic the 3D environment, and the gel is compressed to check the response of the cells [317] (Figure 2.28B). Alternatively, cells seeded on the top of a gel with different topographies are compressed laterally by the compression of the substrate [318] (Figure 2.28C). Advantages of compression are wide force range, possibility to study cells in 2D or 3D.

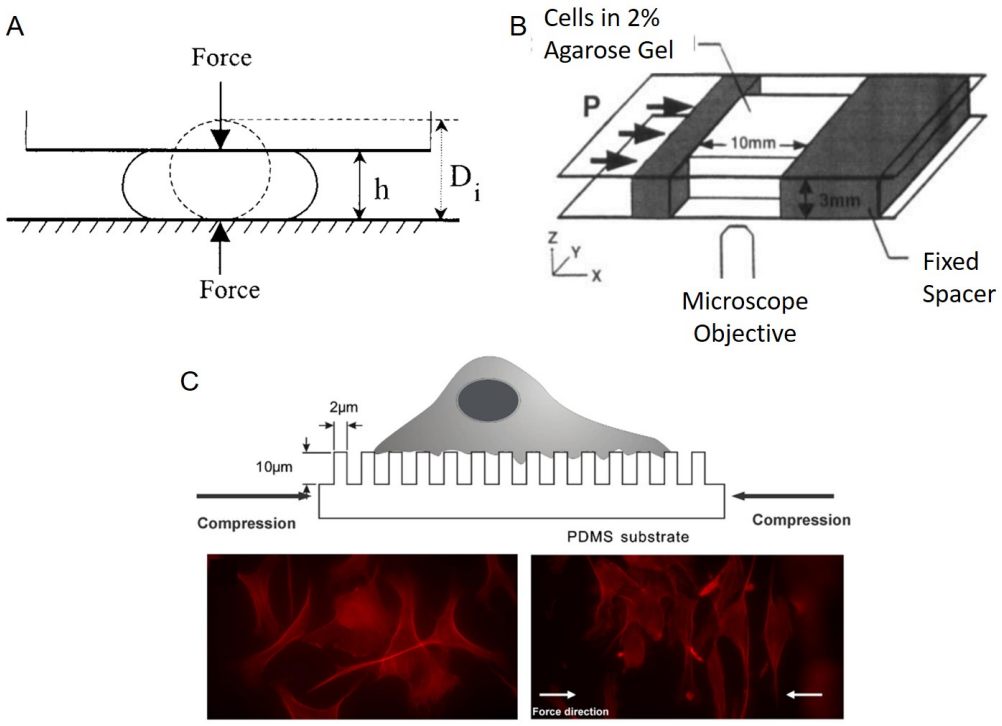

Figure 2.28: Schematic of the compression experiment. A. An optic fibre probe positioned above a single cell, is automatically moved by a motor controller at constant velocity to compress the cell. The force is measured as a function of time. Di and h represent the height before and after compression. Image taken from Smith et al, PNAS, 2000 [319]; B. Chondrocytes embedded in agarose gel were uniaxially compressed from one side. The changes of cell shape is monitored under constant strain. Image taken from Jalili and Laxminarayana, Mechatronics, 2004 [317]; C. Schematic of the cellular microdomain compression device with polydimethylsiloxane (PDMS) microchannels. Image taken from Cheng, J Biomech, 2009 [318].

2.4.2.4 Optical tweezers

Optical tweezers also called optical trapping, relies on the concept that as light enters a medium of a different refractive index, the direction of light path changes. A restoring force is created by the passing light due to conservation of momentum. Therefore, a particle can be trapped or deformed optically and manipulated with a collimated light source [320]. Optical tweezers use the gradient forces to trap a bead and control its movements with a highly focused laser beam (Figure 2.29A). The beads are coated with ECM proteins to allow the binding of the beads to cell membrane. The trapping force can be calculated, by knowing the intensity of gradient of the laser, the refractive index of the beads and cell medium.

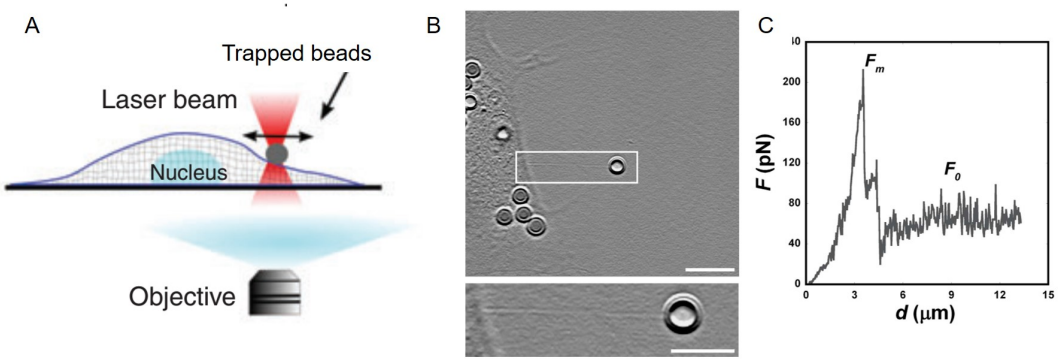

Figure 2.29: Optical tweezers. A. A small particle is stably trapped by a highly focused laser beam. The position of the particle can be controlled by the movement of trap and small forces can be estimated from the changes in the displacement of the particle from the center of trap. Image taken from Moeendarbary and Harris, WIREs Systems Biology and Medicine, 2014 [321]; B. Up: the tether extraction experiment involves pulling of an optically trapped bead attached to a cell membrane away from the cell. Scale bar: 10 m; Down: zoom of the white rectangle, scale bar: 5 m; C. The force-distance curve of tether extraction experiments on microglial cell. Image taken from Pontes et al, PLoS One, 2013 [322].

Due to the advantages of noninvasiveness and sterility, optical tweezers are more desirable tools for cellular manipulations during biology research. In addition, the high sensitivity and high accuracy of bead systems allow us to perturb particular subcellular structures, such as the pulling of membrane tethers [322] (Figure 2.29B and C). Nevertheless, due to limitations on the number of lasers that can be simultaneously used to trap different particles, the amount of force is limited. Moreover, increasing the laser power in order to increase the optical forces could induce local heating of the cell, which would result in damage of cell structures and changes in cell mechanical properties [323].

2.4.2.5 Magnetic technique

The working principle of magnetic tweezers is similar to that of optical tweezers, which is pulling on cells or subcellular structures [324]. The difference is that the beads, which are ferromagnetic, are controlled by a magnetic field gradient produced by electromagnetic coil. The magnitude of the force applied to the beads can be regulated by the intensity of the magnetic field (Figure 2.30A). Another choice is magnetic twisting cytometry, which utilizes oscillating magnetic fields to create a torque on magnetic beads [325] (Figure 2.30B), which are attached to the surface of the cells by specific receptors.

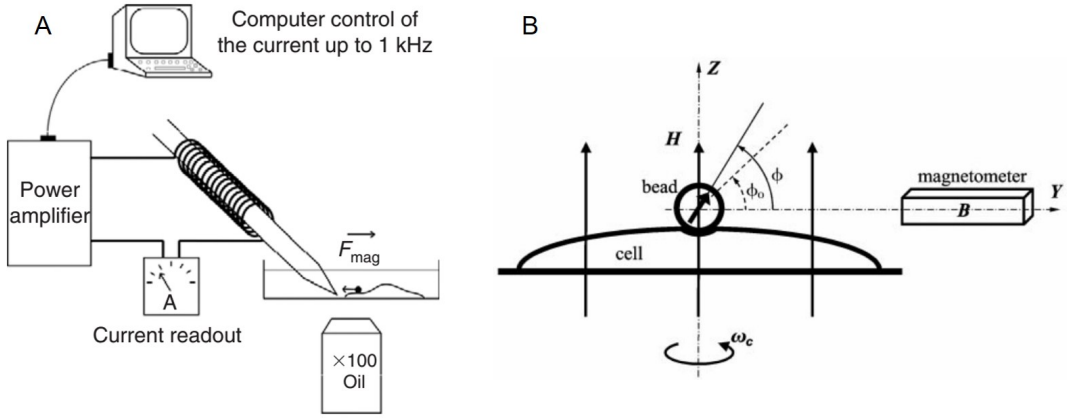

Figure 2.30: Magnetic technique. A. Schematic representation of the magnetic tweezers and imaging system. An electromagnet with a ferromagnetic core sharpened at the sample side was built to concentrate the magnetic field and allow generation of high-amplitude forces on micrometer-sized particles. The current in the solenoid is controlled via computer through a power amplifier. Image taken from Tanase et al, Method Cell Biol, 2007 [326]; B. Schematic of the magnetic twisting cytometry measurements. Ferromagnetic microbeads attached to the cell membrane are magnetized in the (ϕ_0) direction. The bead is twisted (ϕ) by applying a vertical magnetic field (H). The bead rotation is computed from the change in the magnetic field recorded with a magnetometer. Image taken from Puig-De-Morales et al, J Appl Physiol, 2001 [327].

Magnetic tweezers and magnetic twisting cytometry have the advantage of large force range, which require a strong magnetic gradient that can be generated a variety of coil alignments. Moreover, compared with optical tweezers, magnetic techniques produce little heat or photodamage to the cells during long term experiment [328]. However, this requires cumbersome feedback control in addition to sophisticated custom-machined pole pieces [329].

2.4.2.6 Micropipette aspiration

Micropipette aspiration techniques measure the whole cell mechanical properties by examining how much cellular material is pulled into a glass pipette in response to negative pressure. Generally a micropipette aspiration system as shown in Figure 2.31, is composed of: 1) a set of micro-manipulators, 2) a pressure generator, 3) a pressure gauge, and 4) an optical microscope [330]. This technique is mainly performed on cells in suspension. Videos taken by the microscope are used to monitor the cell deformation, like the radius and length of cellular material within the glass pipette at varying known negative pressures.

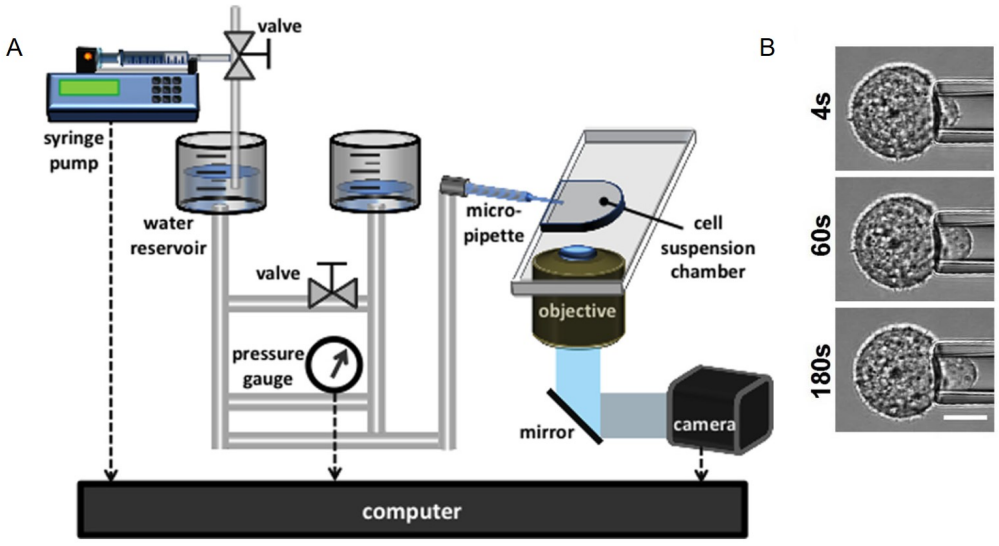

Figure 2.31: Micropipette aspiration. A. Experimental setup of a traditional micropipette aspiration system. The pressure is generated by the differential water level between columns of reservoirs. The cell is aspirated by a negative pressure into the micropipette and the deformation is recorded by the optical microscope. Image taken from Lee and Liu, J Nanotechnol Eng Med, 2014 [330].; B. Representative images showing cell aspiration inside the pipette at 4 s, 60 s and 180 s after applying 0.755 kPa pressure. Scale bar: 10 mm. Image taken from Sliogeryte et al, Sci Rep, 2014 [331].

The relative simplicity and low cost make micropipette aspiration still a widely adopted technique to study cell mechanics. It can provide force resolution down to piconewtons, and can be applied to a large range of cell types [332]. However, the glass capillary micropipette has to be manufactured by the operator, requiring both time and expertise. Moreover, only a single cell can be aspirated at one time, which is time consuming. The long-term experiment will affect measurement accuracy due to changing cell condition and environment. What's more, the experiment is operated on cells in suspension instead of attaching to the surface. The results may not reflect the real physiology state of the cells.

2.4.2.7 Particle-tracking microrheology

This technique focuses on the measurement of cytoplasm mechanical properties. Fluorescent beads of less than 1 μm in diameter are injected into the cytoplasm of live cells (Figure 2.32C). The paths of the beads are tracked by fluorescence microscope (Figure 2.32D). The local mechanical properties of living cells can be quantified by monitoring the non-Brownian motion of individual micro-injected fluorescent particles. Interaction of trapped beads inside the cell with elastic cellular network could be one of the sources of non-Brownian movement [333]. Multiple particle tracking analysis can be broken down into four processing stages: 1) correcting imperfections in individual images, 2) accurately locating particle positions, 3) eliminating false or unwanted particles, and 4) linking these positions in time to create a trajectory [334] (Figure 2.32 E and F).

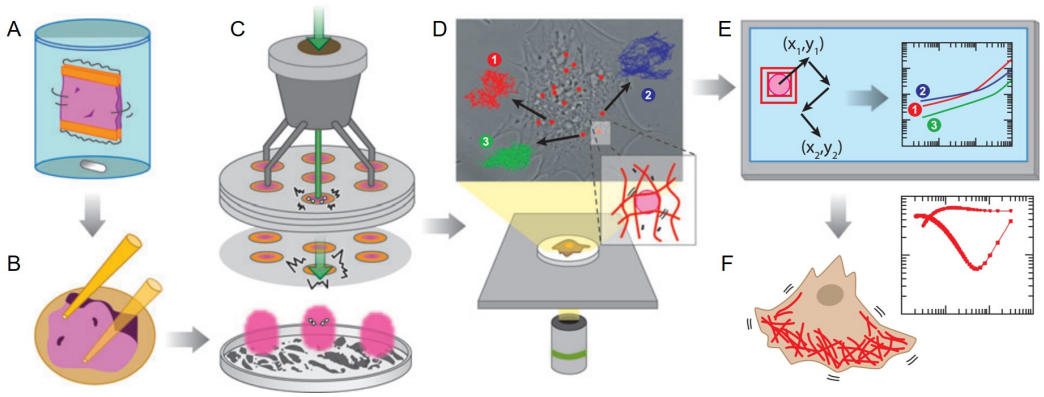

Figure 2.32: Particle-tracking microrheology. A. Submicron fluorescent beads are dialyzed; B. The beads are spread on a grid placed inside a ballistic injection machine; C. Beads are injected and dispersing within the cytoplasm; D. The random spontaneous movements of the beads are monitored with high spatial and temporal resolution a high-magnification fluorescence microscopy; E. Using the appropriate software, the time-dependent (x, y) coordinates of the beads are mathematically transformed into mean squared displacements (MSDs); F. The time lag-dependent MSDs of the beads are subsequently transformed into local values of either the frequency dependent viscoelastic moduli. Image taken from Wirtz, Annu Rev Biophys, 2009 [333].

One of the advantages is that particle tracking microrheology can measure directly the mechanical properties of the cytoplasm because of the intimate contact between the fluorescent beads and subcellular structures. Also it is quite efficient that the measurement requires short time of data collection, typically 10-20s. By tracking multiple beads at one time, it can give results of mechanical responses of various parts of the cells [335]. Furthermore, particle tracking microrheology could be used to study mechanics of cells embedded in a 3D matrix. However, It is computationally intensive to analyse the measurements[336].

2.4.3 Summary

In summary, cell mechanical properties are essential for cellular and subcellular functions and changes in these mechanical properties could reveal healthy states of cells, like cancer cells with soft stiffness. The techniques introduced above can be used to measure the mechanical properties on a population of cells, a single cell, or subcellular structures of a range of cell types. Although not every method is perfect, each of these techniques has its technical advantages and limitations. Among these techniques, AFM attracts more and more attention in measuring mechanical properties in biological studies. The AFM system employed in this thesis will be discussed in more details in chapter 3 and chapter 5.

2.5 Hypothesis and Aims

Previous studies have shown that cells with higher motility are usually softer than the counterparts, which is applicable to both for cancer cells and normal cells. It is therefore believed that being soft is an advantage for cell deformation and would improve its capability for migration and invasion. On the other hand, previous literature has also clearly shown that increasing phosphorylated T567 Ezrin is related with cancer progression, as well as cell migration. The hypothesis of this thesis is that phosphorylated Ezrin at T567 could promote cell migration by making the cell softer. Also all the changes in cell migration and mechanical properties will be explained by changes in cytoskeleton organization.

In order to test the hypothesis, several aims were listed as followings:

1. Investigate the effects of phosphorylated Ezrin on cell migration and protein distribution patterns by long-term live cell imaging;
2. Investigate the effects of phosphorylated Ezrin on cell mechanical properties by AFM measurement;
3. Investigate the effects of phosphorylated Ezrin on cell morphology and three cell cytoskeleton: actin filaments, microtubules, vimentin by image quantification approaches;
4. Build up a sandwich model to confine cells between two gels in order to study bleb-based migration.

Chapter 3

Materials and methods

3.1 Cell culture medium, buffers and reagents

Information about cell culture medium, buffers and reagents are summarized in Table 3.1. Information about antibodies are summarized in Table 3.2.

Table 3.1: Information about cell culture medium, buffers, reagents and chemical formulations

No.	Product	Source	Composition or stock	Storage condition
1	DMEM (Dulbecco's Modified Eagle Medium)	Gibco UK	1x	4°C
2	RPMI 1640 medium (Roswell Park Memorial Institute medium)	ThermoFisher, UK	1X	4°C
3	Opti-MEM Medium	Gibco UK	1X	4°C
4	Flurobrite-DMEM	Thermo Fisher Scientific, UK	1X	4°C
5	PS (penicillin/streptomycin)	Sigma-Aldrich, UK	10X	-20°C
6	Trypsin-EDTA	Sigma-Aldrich, UK	1x	-20°C
7	BSA	Sigma-Aldrich, UK	1 g of powder per 10 ml of di water	4°C

8	type 1 collagen from calf skin	Sigma-Aldrich, UK	1mg/ml in 0.1M acetic acid	4°C
9	PBS (Dulbecco's Phosphate Buffered Saline)	Sigma-Aldrich, UK	9.6 g of powder per liter of di water	4°C
10	DMSO (Dimethyl sulfoxide)	Invitrogen, UK	N/A	RT
11	kanamycin	Sigma-Aldrich, UK	50 g/ml	-20°C
12	ampicillin	Sigma-Aldrich, UK	100g/ml	-20°C
13	toluene	Sigma-Aldrich, UK	neat	RT
14	3-(Trimethoxysilyl) propyl methacrylate)	Sigma-Aldrich, UK	N/A	4°C
15	40% acrylamide	Bio-Rad, UK	N/A	4°C
16	2% bis-acrylamide	Bio-Rad, UK	N/A	4°C
17	TEMED (Tetramethylethylenediamine)	Sigma-Aldrich UK	N/A	RT
18	APS (Ammonium Persulfate)	Sigma-Aldrich UK	10X	-20°C
19	PDMS (Polydimethylsiloxane)	Sigma-Aldrich UK	N/A	RT
20	PFA (formaldehyde)	Sigma-Aldrich UK	8% (w/v) in PBS	RT
21	Triton x-100	Sigma-Aldrich UK		RT
22	LB (Luria Broth)	Invitrogen, UK	1:500	RT
23	agar	Invitrogen, UK	1:500	RT
24	Phalloidin	SantaCruz sc301530, sc363791, US	1;500	-20°C
25	Prolong gold antifade mountant	ThermoFishers,UK	N/A	RT
26	Lipofectamine LTX Plus	ThermoFisher Scientific, UK	N/A	4°C

Table 3.2: Information about the antibodies used in the experiment

No.	Antibody	Catalog No.	Dilution ratio
1	Tubulin (anti-rabbit)	Abcam ab4074	1:200
2	Vimentin(anti-mouse)	SantaCruz sc373717	1:500
3	Ezrin (anti-mouse)	SantaCruz sc58758	1:500
4	Goat anti-rabbit (TRITC)	Abcam ab6718	1:500
5	anti-mouse(TRITC)	Invitrogen a21202	1:500
6	anti-rabbit(FITC)	Invitrogen a21206	1:500
7	anti-mouse(FITC)	Invitrogen a31570	1:500

3.2 Cells and cell culture

3.2.1 NIH 3T3 cells

NIH 3T3 fibroblast cells were derived from Swiss albino mouse embryo tissue. NIH 3T3 cells were cultured in Dulbecco′s Modified Eagle Medium (DMEM, GibcoUK) supplemented with 10$\%$ Fetal Bovine Serum (FBS, Sigma-Aldrich, UK). A humidified incubator with 5$\%$ CO_2 at 37°C was used for cell growth and storage. 3T3 cells, which have high growth rate, were passaged every two days to prevent full confluence. Adherent 3T3 cells were washed with Phosphate-Buffered Saline (PBS) solution once before detachment by incubation with 500 μL trypsin solution (Sigma-Aldrich, UK) at 37°C for 5 min. As soon as cells detached, fresh culture medium was added to stop the reaction with trypsin and the mixture was then centrifuged at 1000 rpm for 5 min. The waste medium was then pipetted out without disturbing the cell pellet, followed by resuspending in fresh medium. Lastly, cells were pipetted into new flasks at a split ratio of 1:5 before putting back into the incubator. Cells were stored in complete growth medium supplemented with 10 $\%$ Dimethyl sulfoxide (DMSO, Invitrogen, UK) in liquid nitrogen.

This study was carried out in fibroblasts, which is due to their mesenchymal nature. When cultured in sparse conditions, they become well spread and display a strong migratory phenotype. This makes them a suitable model to study the relationship between cell migration direction and cytoskeletal organization or intracellular distribution of proteins.

3.2.2 U937 cells

U937 cells (a kind gift from Dr Jing Xu, Queen Mary University of London) are of the myeloid lineage isolated from the histiocytic lymphoma of a 37-year-old male. Growth medium, RPMI 1640 medium (Roswell Park Memorial Institute medium) (ThermoFisher, UK), was supplemented with 10% FBS (Sigma-Aldrich, UK), 1% penicillin/streptomycin (PS). U937 cells were suspensively cultured in a humidified atmosphere with 5% CO_2 at 37°C. Passage the cells every 3-4 days by centrifuging at 1000 rpm for 5 min. After discarding the supernatant, the cells were resuspended and reseeded in T25 flask at 1-2 x 10^5 cells/ml. For direct cell imaging experiment, resuspended cells were seeded into a petri dish containing a gel with low cell density to get single cell for imaging. Cells were stored in complete growth medium supplemented with 5% DMSO at liquid nitrogen.

3.3 Transient cells transfection

3.3.1 Plasmids for Ezrin and its mutants

To analyze the role of Ezrin phosphorylation state, NIH 3T3 cells were transfected with different mutants of Ezrin as illustrated in Figure 3.1: (1) wild type Ezrin, which can switch between active and inactive modes; (2) the phosphomimetic mutant, Ezrin T567D, which acts as a constitutively activated Ezrin; (3) the phosphodeficient mutant, Ezrin T567A, which is constitutively inactive. Apart from those, cells were also transfected with truncated Ezrin, FERM domain, which only contains the plasma membrane binding domain, acts as a competitive inhibitor of endogenous ERM proteins [35]. Plasmids were a kind gift from Prof Guilluame Charras (University College London, UK). The Ezrin, Ezrin T567D and Ezrin T567A were tagged with EGFP, while FERM domain was tagged with RFP. Therefore, the transfected cells could be visualized by fluorescent microscope.

3.3.2 Plasmid mini preparation

Prepare Luria Broth liquid medium: Firstly, 12.5 g Luria Broth base and 500 ml distilled water were mixed evenly. Then the cap was loosely closed on the bottle and the medium was autoclaved. After autoclaving, the cap was screwed tightly on the bottle after the medium cooling to room temperature. The medium was stored in a fridge at 4°C. Before use, antibiotics were added.

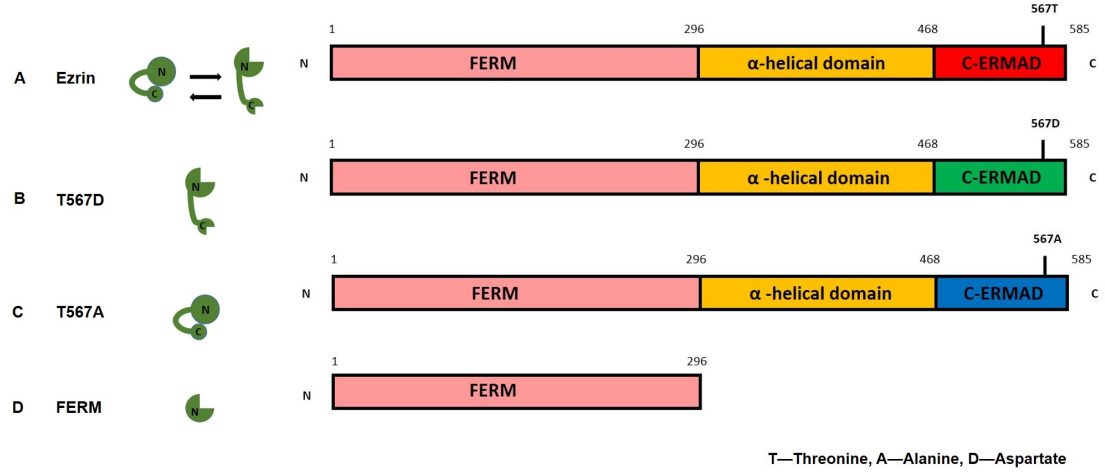

Figure 3.1: Ezrin mutant used in this study. On the left: schematic depicts the domain structure of Ezrin and its mutant; on the right: domain organization of Ezrin and its mutant. A. Wild type Ezrin, which can switch between active and inactive mode; B.The phosphomimetic mutant, Ezrin T567D, in which the 567 threonine was replaced by aspartate, mimicking constitutively activated Ezrin; C. The phosphodeficient mutant, Ezrin T567A, in which the 567 threonine was replaced by alanine, which is constitutively inactive; D. Truncated Ezrin, FERM domain, which only contains the plasma membrane binding domain.

Prepare LB agar plates: 12.5 g Luria Broth base, 7.5g agar and 500 ml distilled water were mixed evenly. The medium was autoclaved and allowed to cool to below 50°C. Then antibiotics were added before pouring the medium into plates (about 10 ml per plate) on a clean bench next to a Bunsen burner to sterilize the surrounding environment. Plates were left overnight in room temperature for solidification. Plates were stored inverted at 4°C for future use. Before use, plates were incubated at 37°C for at least 10 minutes.

Obtain single colony: The surface of frozen bacterial glycerol stock was lightly scratched with a sterilized wire loop or pipette tip. The loop with bacteria was streaked slightly across the agar plate. Then the plate was inverted and incubated overnight at 37°C to get single colony.

Culture bacterial within plasmids: Suspension culture of E.coli in LB liquid medium supplemented with antibiotic (kanamycin 50 g/ml; ampicillin 100g/ml). Using a sterilized tip, single colonies were selected from the LB agar plate. Then the tip was dropped into the liquid medium. Tubes were loosely closed to allow its contact with air and the colonies were incubated at 37°C for 12-18 h in a shaking incubator at 225 rpm. Plasmids were extracted from the bacterial culture using Spin Miniprep kit (Qiagen Ltd, Germany).

3.3.3 Cell transfection

NIH 3T3 cells were seeded the day before transfection so they could reach 80-90$\%$ confluence at the time of transfection. All transfections were carried out with Lipofectamine LTX Plus (ThermoFisher Scientific, UK). For 1x10^5 cells, 250 ng of plasmid was used. The transfection was conducted according the protocol in table 3.3. After 6 h, transfection medium was replaced with normal growth medium. Transfection efficiency was approximately 60 $\%$ for NIH 3T3 cells. All the experiment was performed on visible transfected cells only.

Table 3.3: Transfection protocol with Lipofectamin LTX

No.	Step	Component	
1	Seed cells be to 80-90$\%$ confluent at transfection	Adherent cells	1x10^5
2	Dilute Lipofectamine LTX Reagent in Opti-MEM Medium	Opti-MEM Medium Lipofectamine LTX Reagent	25 μ l 2 μ l
3	Dilute DNA in Opti-MEM Medium with PLUS regent	Opti-MEM Medium Plasmid PLUS regent	25 μ l 250 ng 2 μ l
4	Mix the diluted DNA and Lipofectamine LTX	Diluted DNA Diluted Lipofectamine LTX	25 μ l 25 μ l
5	Incubation	Time	5 min
6	Add DNA-lipid mix to cells	Mix	50 μ l

3.4 Cell staining

3.4.1 Actin staining

Staining was performed next day after reseeding transfected cells. Firstly, cells were washed with PBS twice to remove medium components before fixing by incubation with cold 3.7$\%$ formaldehyde (PFA) (Sigma-Aldrich UK) solution at room temperature for 10 min. Then the cells were washed with PBS three times. Secondly, cells were permeabilized by incubation with 0.25$\%$ Triton x-100 (Sigma-Aldrich, UK) for 5 min before washing cells with PBS three times. Lastly, cells were incubated with Phalloidin (SantaCruz sc301530, sc363791, US) diluted at the ratio of 1:500 in PBS at room temperature for 1.5 h without light, followed by washing three times with PBS. Finally, coverslips were mounted for microscope

imaging using Prolong gold antifade mountant (ThermoFishers,UK) on the slides.

3.4.2 Tubulin, vimentin and Ezrin staining

Transfected cells were fixed with 3.7% PFA for 10 min followed by washing with PBS three times. Then the cells were permeabilized with 0.25% Triton X-100 for 5 mins in order to create holes on the cell membrane for the entry of large molecules, followed by washing with PBS three times. Next the permeabilized cells were blocked with 10% BSA (Sigma-Aldrich, UK) for 1h at room temperature in order to reduce nonspecific background noise and improve the sensitivity of the experiment. After that, samples were incubated overnight at 4 °C with primary antibodies including tubulin, vimentin and ezrin, diluted with 1% BSA. The next day, samples were washed three times with PBS to get rid of unbinding antibody before subsequently incubated with secondary antibodies for 1h at room temperature in the dark. After staining, coverslips were mounted onto glass slides using ProLong Gold Antifade Mountant containing DAPI. The information and usage of primary antibodies and secondary antibodies are listed in Table 3.2.

3.5 Statistical analysis

Statistical analysis was performed with OriginLab analysis software. Results of Ezrin and its mutants were statistically analyzed by one-way analysis of variance followed by Dunnett test against control (Ezrin transfection). Statistical significance was reported at p, 0.05 (*), p, 0.01 (**) and p, 0.001 (***) unless otherwise stated. Data was displayed by box plots, which is a graphical representation of key values from summary statistics. The box plot used here extends from the 10th to the 90th percentile covering 25th and 75th percentile, whiskers from the 5th to the 95th as shown in Figure 3.2.

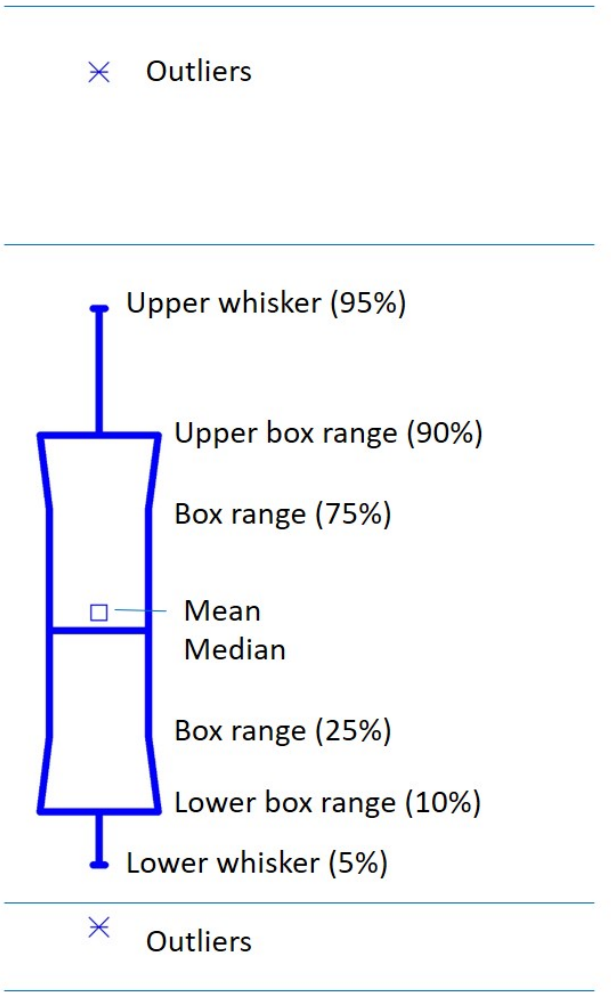

Figure 3.2: Example of box plot used in this study. Image adapted from OriginLab website: https://www.originlab.com/doc/Origin-Help/PD-Dialog-Box-Tab.

3.6 Long-term live-cell imaging

Long-term live-cell imaging is a powerful technique that enables the observation of biological process over extended periods of time. The advantage of live-cell imaging over fixed-cell imaging is to allow direct visualization and temporal quantitation of dynamic cellular events. One of the biggest challenges is to main both temperature and 5% humidified CO_2 atmosphere in order to keep cells healthy and live. Another challenge is to acquire long-term videos encompassing multiple fields of view with several fluorescence channels together as the experiment is always time-consuming. Ultimately, manually tracking cell dynamics is also highly laborious to analyze the generated massive data files. The microscope used in this study, lumascopy-720 microscope, together with the image quantification

pipeline developed by our group have well solved these challenges.

3.6.1 Lumascopy-720 microscope

LS720 microscope (Etaluma, US) is a highly versatile, compact inverted fluorescence microscope. The biggest advantage of this microscope is that LS720 microscope is highly compact that it could be placed in an incubator (Figure 3.3). In this way, the imaging environment, e.g. the concentration of CO_2, the temperature and humidity, can be well maintained during long term imaging. Cells can also be well protected from outside interference. LS720 microscope can detect blue, green and red fluorophores, such as BFP, DAPI, FITC, Fluo-4, GFP and mCherry. It enables the examination of samples with different fluorescent labels simultaneously. What's more, the microscope is equipped with exquisite X-Y stage with auto-focusing in Z-axis, which ensures the stability of the imaging process to avoid drifting. Furthermore, LS720 microscope allows multiple field imaging in the flasks or multi-well plates, offering the benefits to obtain sufficient data to be selected for analysis during one single experiment. This automation system becomes especially useful when an experiment takes hours or even days. In this thesis, Lumascopy-720 was used to track cells expressing fluorescent proteins, EGFP or RFP, for the migration and protein dynamics.

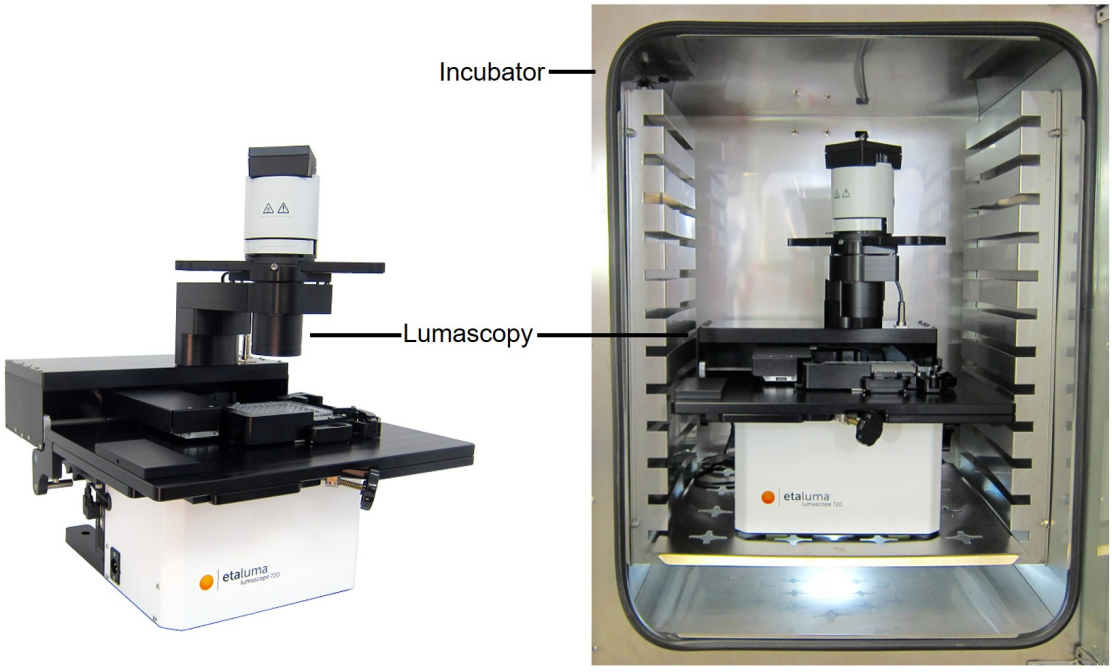

Figure 3.3: Lumascopy-720 microscope in an incubator for long-term live-cell imaging.

3.6.2 Cell migration experiment

Transfected cells were seeded onto 6-well plate at low density. Prior to imaging, cell culture medium was replaced with FBS supplemented Flurobrite-DMEM imaging specific medium (Thermo Fisher Scientific, UK) to reduce background fluorescence and protect fluorescent protein from photo-bleaching. The software used for imaging can divide a well in 6-well plate into 1356 fields as shown in Figure 3.4. Fields with single transfected cells were selected and multiple fields within the same well were imaged at the same time. Time-lapse recordings of single cell dynamics were acquired with a 20x objective by LS720 microscope with a frame rate of 5 min for at least 12 h. Videos were analyzed to measure the migration speed as well as the protein distribution pattern during migration. All the work was performed across independent experiments, which were repeated at least three times.

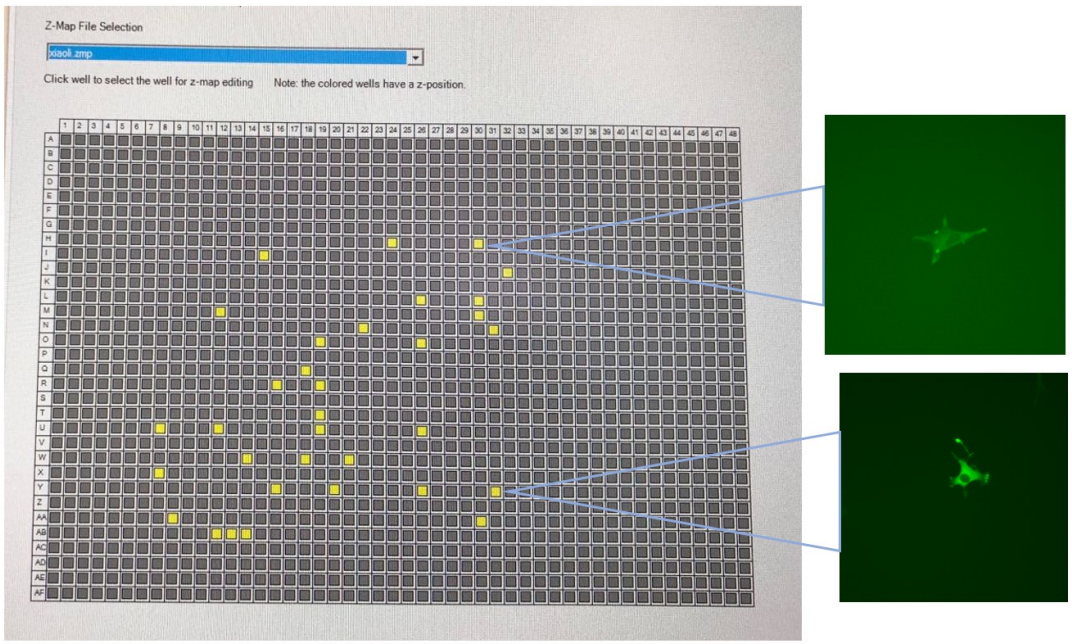

Figure 3.4: Example of multiple well selection in the imaging. Each well of 6-well plate was divided into 1356 fields. The yellow square represents the selected view. Each selected view has its own z-position. Images on the right represent views of the selected fields.

3.6.3 Image analysis

Single fluorescent images were generated from the microscope. The algorithm written by Matlab was used to analyze the images, which was based on grey-

scale fluorescent channel. Only these images showing that cells had been healthy during the imaging process were selected and then converted from RGB type into 8-bit type. Detailed process to analyze the stack are described as follows, which could be divided into three main steps:

(1) Determination of the cell outlines for every frame:

Based on the contrast between pixels with and without fluorescent signal, the algorithm could recognize all the pixels with signals and put them together, which then became the outline of a migrating cell as shown in Figure 3.5.

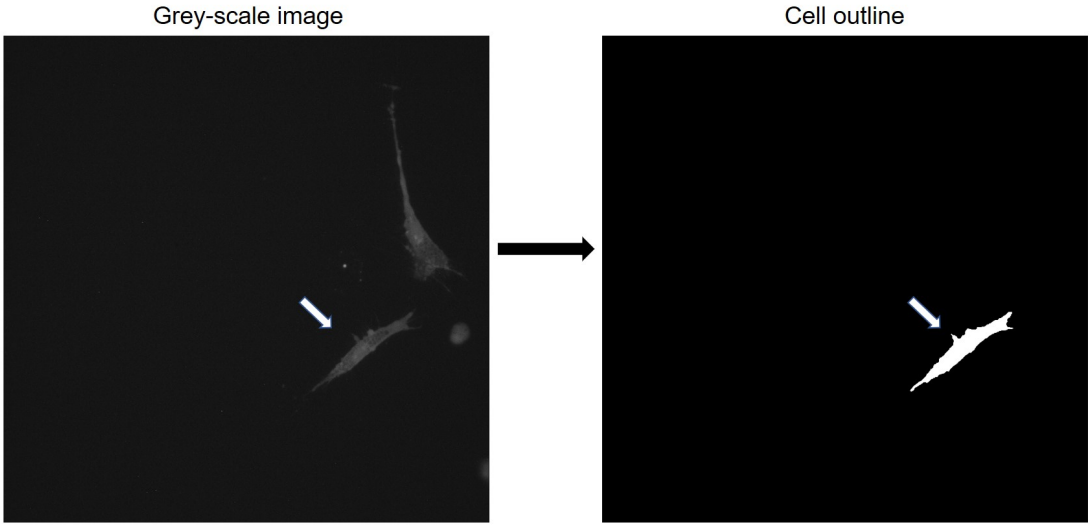

Figure 3.5: Determination of the cell outlines. The white arrow points to the outline of a migrating cell.

(2) Calculation of the positions of cell centroids:

After cell outlines were identified, the positions of cell centroids inside the field were calculated as x and y-coordinates in pixels (Figure 3.6). By comparing one frame with the next one, the migration direction could be obtained. Cell rear and cell front can also be distinguished. At the same time, instantaneous velocity at each point was calculated using the xy-coordinates as obtained from each frame.

(3) Output results:

Fluorescent signal was analyzed for every frame. The algorithm for analyzing fluorescent cells will be described in detail in the section of image quantification approaches. Quantification results of protein intensity, protein distribution parameters, such as polarization ratio and peak front-to-back ratio were generated.

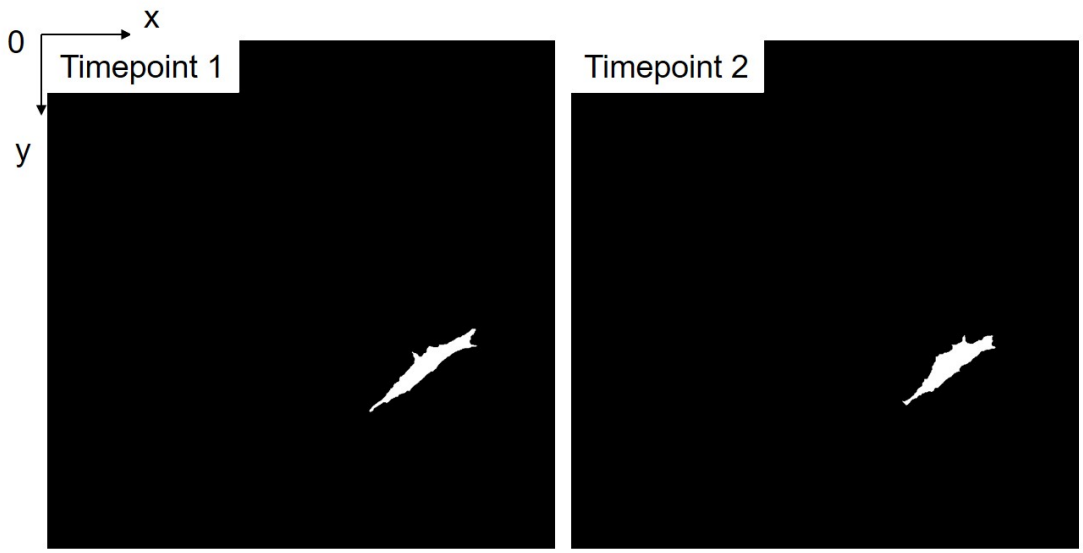

XY coordinate of the centroids (pixel)

	X	Y
Timepoint 1	284.844	243.463
Timepoint 2	285.687	242.609

Figure 3.6: Calculation of the positions of cell centroids. After finding all migrating cells' outlines, the code could output the x-y coordinate of the centroids.

3.7 Measurement of cell mechanical properties

3.7.1 NanoWizard 4 AFM for biological studies

Originally invented to measure topography of materials, AFM has now become a powerful tool in biological studies, through continuous improvement and adjustment. Nanowizard 4 AFM (Figure3.7) used in this study was developed to meet most requirements for biological research. The key breakthrough that led to the application of AFM in biology was the development of an optical detection system [337]. The system is compatible with optical microscope for viewing samples in bright field or fluorescent channels, even to make optical and AFM images overlays. In addition, the introduction of a fluid chamber and precise temperature control, mimicking the native state of the biological system, has made it possible to perform long term experiment on biological samples, like cells. More importantly, fast scanning combined with atomic resolution allows to observe cell and tissue dynamics in real time and also protect cells from long term disturbance. The high resolution in atomic scale makes it capable of revealing specific cellular structures such as cytoskeleton, filopodia, lamellipodia and microvilli.

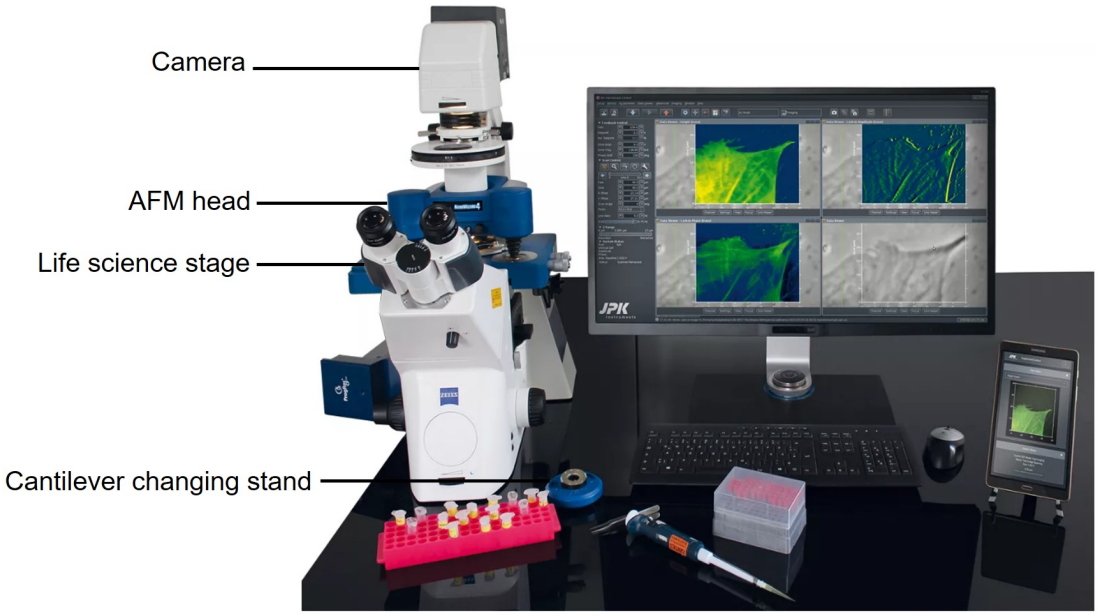

Figure 3.7: NnanoWizard4 AFM used in this study. Adapted from JPK handbook.

3.7.2 Cell preparation

3T3 cell culture and transfection have been described in the previous chapter. Next step after transfection was to reseed the transfected cells in a petri dish with a diameter of 35 mm. Before seeding, the surface of the petri dish was coated with collagen by incubation with collagen at 37°C for one hour. After incubation, the petri dish was rinsed with PBS and transfected cells were seeded at low cell density in order to get single cell. Two hours prior to the AFM experiment, cell culture medium was replaced by imaging medium supplied with 4-(2-hydroxyethyl)-1-piperazineethanesulfonic acid (HEPES), which could maintain the right PH value during the experiment. Also the medium does not contain phenol red, which could reduce the background when the cells express fluorescent proteins. For the transfection of FERM domain, cells were seeded at the petri dish at low density before transfection. Transfection was conducted in the same petri dish to skip the step of detaching cells with trypsin.

3.7.3 AFM experiment

Cells transfected with one of the plasmids were plated on the petri dish in FBS supplemented medium (ThermoFisher, UK). All the experiments were conducted on a Nanowizard 4 AFM (JPK, Germany) with a petri dish heater to maintain the samples at 37°C. Rectangular gold-coated silicon nitride cantilevers with four-sided pyramidal tips (0.06 N/m spring constant, BudgetSensors, Germany) were

used as probes. Before each experiment, the spring constant of the cantilever was calibrated using the thermal fluctuations method. Briefly, cantilever sensitivity was calculated based on a force curve on a bare region of the petri dish in contact mode. Then after the cantilever was lifted a minimum of 500 μm above the surface, the force constant was calibrated by thermal fluctuations. Fluorescent images of transfected cells were acquired by using an Axio Observer Z.1 epifluorescence microscope with Plan-Apochromat lenses (20x) equipped with a cooled CMOS camera (Orca Flash 4). Mechanical measurement was performed by JPK's QI mode, which rapidly acquires force-curves generating a detailed image of the topography and mechanical properties of the sample. For each measurement, a matrix (32 x 32 force curves) that could cover the cell nuclear and cell periphery was selected. For stiffness measurement, single transfected cell was firstly selected by the epifluorescence camera as demonstrated in Figure 3.8. Then not only the area above the nucleus, nearly the whole cell was scanned by the tip where 1024 force curves were taken during the measurement. All the work was performed across independent experiments, which were repeated at least three times.

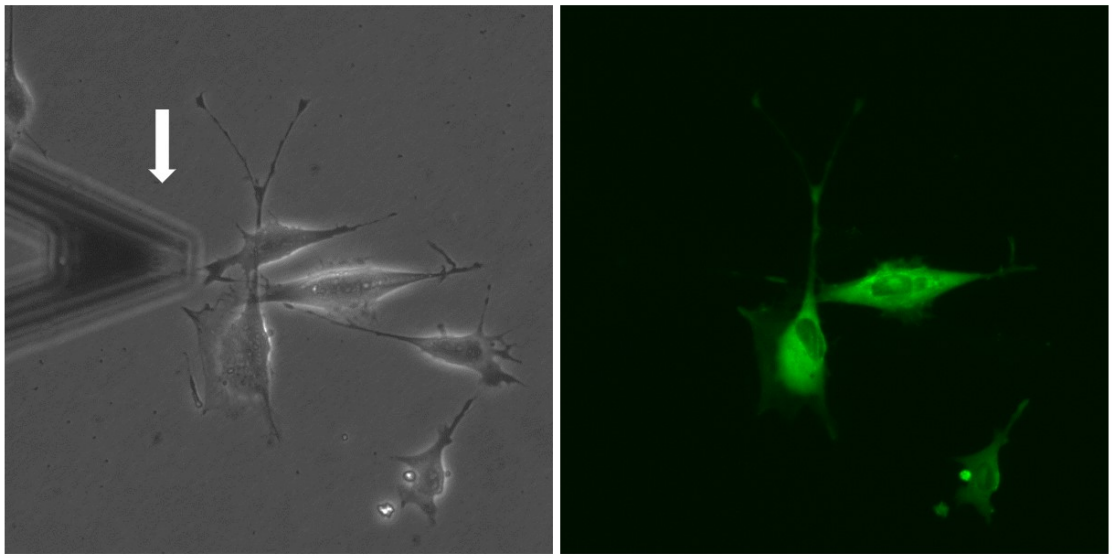

Figure 3.8: Example images for AFM measurement. Left: bright field images of cells, arrow indicates the cantilever; right: fluorescent image of cells transfected with inactive Ezrin T567A.

3.7.4 Data analysis

BECC model: Data analysis of the force curves was carried out using the BECC model for thin adherent cells on a stiff substrate using a pipeline written in MAT-

LAB as previously described [338, 339]. Briefly,

$$F = \frac{8E \tan\theta\delta^2}{3\pi} \times \left\{1 + 1.7795\frac{2\tan\theta}{\pi^2}\frac{\delta}{h} + 16(1.7795)^2\tan^2\theta\frac{\delta^2}{h^2}\right\} \quad (3.1)$$

where F is the applied force, δ is indentation, θ is the half-opening angle of the cone, and Poisson's ratio is assumed to be 0.5. At the same time, the applied force could be expressed in another way where the deflection of the cantilever (d) multiple the spring constant of the cantilever (k) as:

$$F = kd \quad (3.2)$$

The indentation can be expressed as:

$$\delta = (Z - Z_{CP}) - d \quad (3.3)$$

where Z is the displacement of the piezo and Z_{CP} represents the piezo-position at the contact point. The contact point was identified using a sequential search algorithm as the point that maximized the goodness of the fit (r^2) to the contact part of the indentation curve using Eq. 3.1.

Finally, sample height can be computed as:

$$h = Z_{CP} - Z_{glass} \quad (3.4)$$

where Z_{glass} is the piezo-position at the contact point obtained on a region of bare glass.

Depth-sensing analysis: Cell stiffness is determined on the basis of force curve that is usually obtained by subtraction of cantilever deflections measured on rigid and soft surfaces at a given relative sample position (Figure 3.9A). For cells, which are soft, cantilever deflections are much smaller and the resulting force curves are non-linear in character. The difference between these curves represents the deformation of the sample surface. Depending on the magnitude of the indentation depth, distinct properties of cells can be calculated, revealing the heterogeneity of the cell structure. Figure 3.9B presents the idea of the Young's modulus determination at different indentation depths. After choosing the contact point position, the fit was performed at different indentation depths [340]. With this method, the stiffness of both cell cortex (indentation depth at 200 nm) and cell cytoskeleton (indentation depth at 1200 nm) can be calculated from a single force curve .

Viscosity analysis: As cells are complex viscoelastic materials, their viscous response plays an important role during AFM indentation process. In this method,

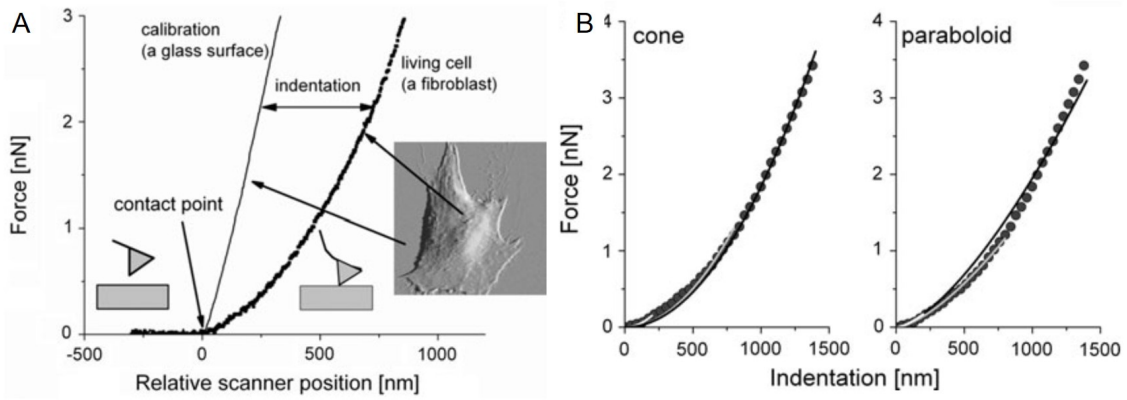

Figure 3.9: Depth-sensing analysis. A. Young's modulus is determined by subtraction of curves recorded on hard (in our case glass coverslip) and soft (fibroblasts) surfaces; B. Comparison between fits obtained for models using conical or parabolic shape AFM tip (lines correspond to the fit performed for indentations of 200, 800, and 1400 nm; black points are experimental data). Image taken from Pogoda et al, Eur Biophys J, 2012 [340].

conventional AFM force curves are used to estimate the apparent viscosity of non-adhesive soft samples. Perfectly elastic samples recover their original shape instantaneously after the load is removed. The work done by AFM indentation of cells is stored in the form of elastic energy in the cantilever deflection and cell indentation. After the load is removed, the elastic energy is to restore to the original undeformed state of cantilever and cell. Thus, the work done by the elastic force is equal during cantilever approach and retract. If viscous effects are present, the cell response to the cantilever force is composed of an elastic and a viscous component, so that the work done by the cantilever is partially lost by internal friction, generating an hysteresis in the approach/retraction cycle [341] (Figure 3.10). Accordingly, cellular viscosity can be computed using the same force curves.

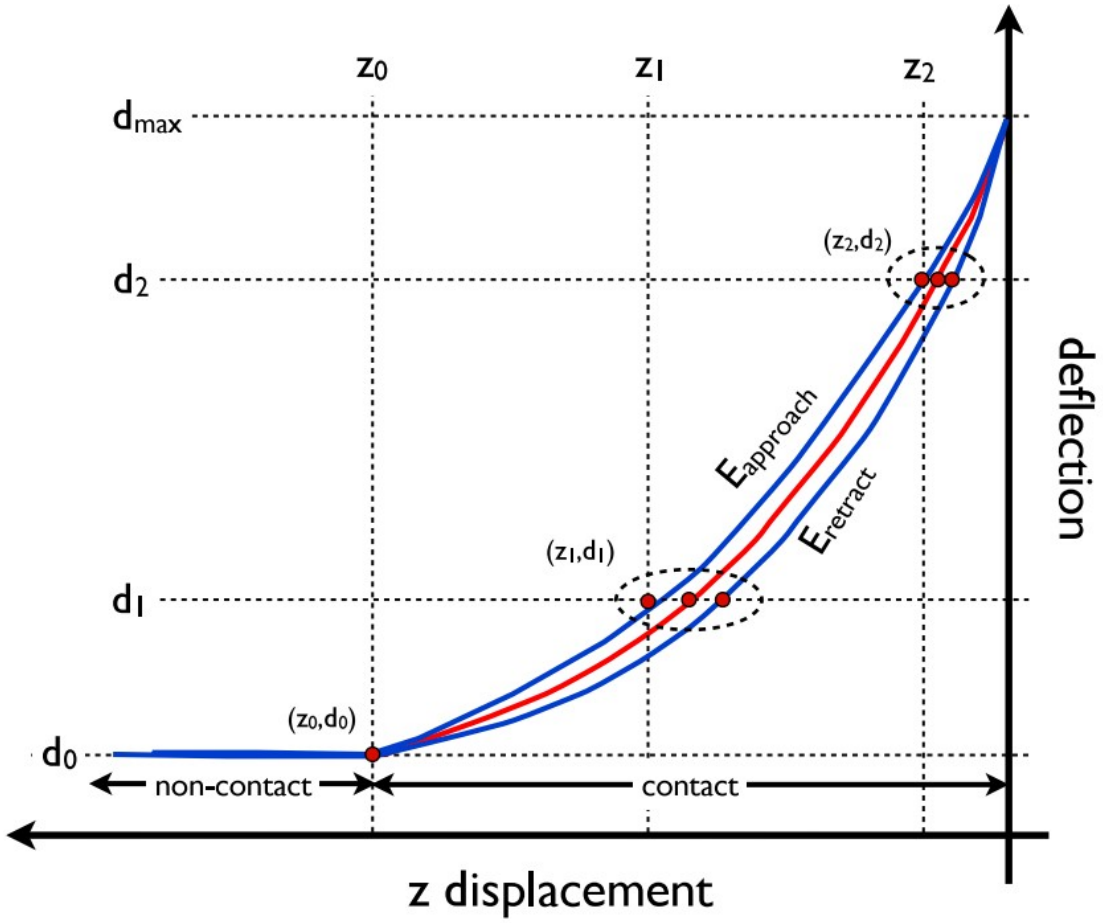

Figure 3.10: Schematics of a typical AFM force curve for soft samples exhibiting hysteresis between approach and retract curves. The difference between $E_{approach}$ and $E_{retract}$ is an indirect measure of the apparent viscosity η of the sample. The red curve represents the average between approach and retract curves, which can be used to determine $E_{average}$. Image taken from Rebelo et al, Nanotechnology, 2013 [341].

3.8 Image quantification approach

Gene transcription level and protein translation level are normally calculated and understood in terms of a cell population because all the information was generated from samples containing millions of cells, like PCR and western blot experiments [342]. However, the diversity of cells among the members of the population is large and thus it is important to group the population based on the differences between individual cells. For example, the transfection ratio can not reach 100 $\%$ so cells used in the experiment contains transfected cells as well as non-transfected cells. The results, such as western blot, are therefore also affected by the non-transfected cells. Single cell analysis emerges in recent years with advantages in studying of cell-to-cell variation within a cell population, like organ, tissue and cell culture, providing useful information for researches like drug development and stem cell differentiation [343, 344]. Singe cells can be isolated with greater accuracy and specificity with the well-established methods, such as micro-manipulation and cells expressing fluorescent markers.

3.8.1 Cell preparation

After 3T3 cell culture and transfection as described in previous chapters, transfected cells were reseeded onto coverslips with a diameter of 22 mm. The coverslips were coated with collagen by incubation with collagen solution at 37°C for one hour. Then the coverslips were rinsed with PBS and placed inside the 6 well plate with the treated face up. After that, transfected cells were seeded onto the coverslips with a low cell density to obtain singe cell for imaging. For the transfection of FERM domain, NIH 3T3 cells were seeded onto collagen treated coverslips at a low density. Transfection was carried out on the cells attached to the coverslips so that the step of detaching cells with trypsin can be skipped.

3.8.2 Epifluorescence microscope imaging

Leica DMI4000B, an inverted epifluorescence microscope, was used for images acquiring. Leica DMI4000B is suitable for bright field (BF), phase contrast (PH) acquisition and epifluorescence imaging with DAPI, FITC (fluorescein isothiocyanate), TRITC (tetramethyl rhodamin isothiocyanate), and Texas Red filters on fixed cell and tissue samples (¡20m thickness). The internal filter wheel with motorized excitation manager and FIM (Fluorescence Intensity Manager) enables

excitation of fluorochromes in less than 20 milliseconds. FIM regulates light intensity at five fixed levels and remembers the setting for each filter cube.

Fluorescent images of cell cytoskeleton, Ezrin and nuclear on fixed samples were acquired by using an inverted epifluorescence microscope (Leica DMI4000B, Germany) with a x20/0.5 NA objective lens and a CCD (Charged Coupled Device) camera (Leica DFC300FX). The x20 objective was chosen for maximizing the imaging depth, and at the same time, capturing high resolution of cytoskeleton and nuclear images. Isolated cells that remained neither damaged nor mitotic were chosen for imaging. Cells were sequentially imaged on TRITC, FITC and DAPI channels with adjusted gain and exposure time. The values of gain and exposure time were stored in matadata files used for later imaging processing. All the work was performed across independent experiments, which were repeated at least three times.

3.8.3 Procedure of single cell analysis

Based on fluorescent images of single cells by staining or transfection, our group has developed a specialized image processing pipeline for the analysis of single cell cytoskeleton and nuclear, as described in previous publications [338, 345, 346]. With the help of epifluorescence microscope, images of single cells are taken at different channels. Then the pipeline is used to convert large collection of single cell images into quantitative data. The pipeline was written in Matlab (Mathworks) and the procedure how it works is briefly described as follows.

The pipeline uses grey-scale immunostaining-based images and it follows five independent steps:

(1) Determination of the cell outlines for every singe cell: Because images were taken with 20x objective and cell sizes are small so there are normally many cells in one single frame. The first step is that single cells, which were not attached with other cells, were selected and cropped by a rectangular area. Figure 3.11 A-C show examples of cropped images with different channels. The outline of the cell was identified by detecting the difference between signals inside and outside the cells. In order to obtain accurate cell boundary, an outline around the cell perimeter was drawn manually on the image. Then a cell mask was automatically generated by using the algorithm (Figure 3.11D);

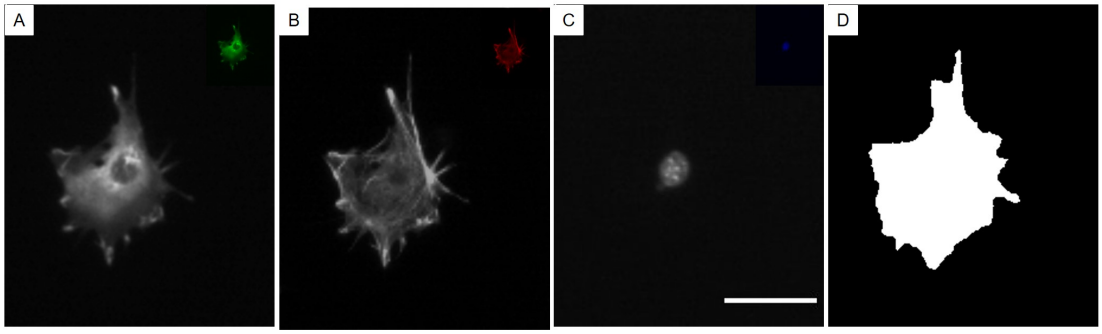

Figure 3.11: Example inputs and outputs of the image analysis pipeline. Images of cells transfected with Ezrin (A) stained with actin filaments (B) and DAPI (C) are used as inputs to calculate Ezrin properties, cytoskeleton morphometric parameters and nuclear properties, respectively; D. Outline of the cell is generated from these images to identify the perimeter of a single cell. Scale bar:30 μm

(2) Initial fiber segmentation: After identification of cell outline, cytoskeleton fibers were determined by convolution of the cell image with elongated Laplace of Gaussian (eLoG) kernels [347]. A small window with a size of 21x21 pixel working as a fiber template filter is applied at each pixel location within the cell. The window was rotated 180° with a step size of 6° gradually and a map of putative fibers was generated by the maximization of image cross correlation signals;

(3) Fiber refinement: Fiber refinement was then carried out using a coherence-enhancing diffusion filter. The fiber map identified in step two was refined by extension and interconnection of interrupted fibers. Then the values of newly inserted pixels were examined by comparing with the average orientation of neighbouring pixels within the same fiber, using a 9 x 9 pixel window. The pixel was discarded if the difference was larger than pre-defined threshold. Also this step would correct artifacts like bright dots. These fiber enhancement and trimming steps were iterated until convergence of the algorithm.

(4) Subtraction of background: Lastly, fluorescent signals of non-specific binding that did not belong to the fibers were determined and removed by the pipeline. A background fluorescence map is generated by computing median signal intensity within a 21 x 21 window surrounding each non-fibre pixel near fibre edges. The result was a smoothly changing intensity map with fiber pixels replaced by the median of non-fiber pixels. This background map was then subtracted from the original image and the pixels that obtained negative values belonging to a fiber map were removed and the process was iterated until convergence was reached. This process ensured that only pixels truly belonging to a fiber were included in the resulting fiber map.

(5) Parameter calculations: 18 parameters were calculated characterizing the

cytoskeleton and nuclear properties. Figure 3.12 shows an example of analyzed actin fibers using this pipeline method and outputs of the actin fiber maps.

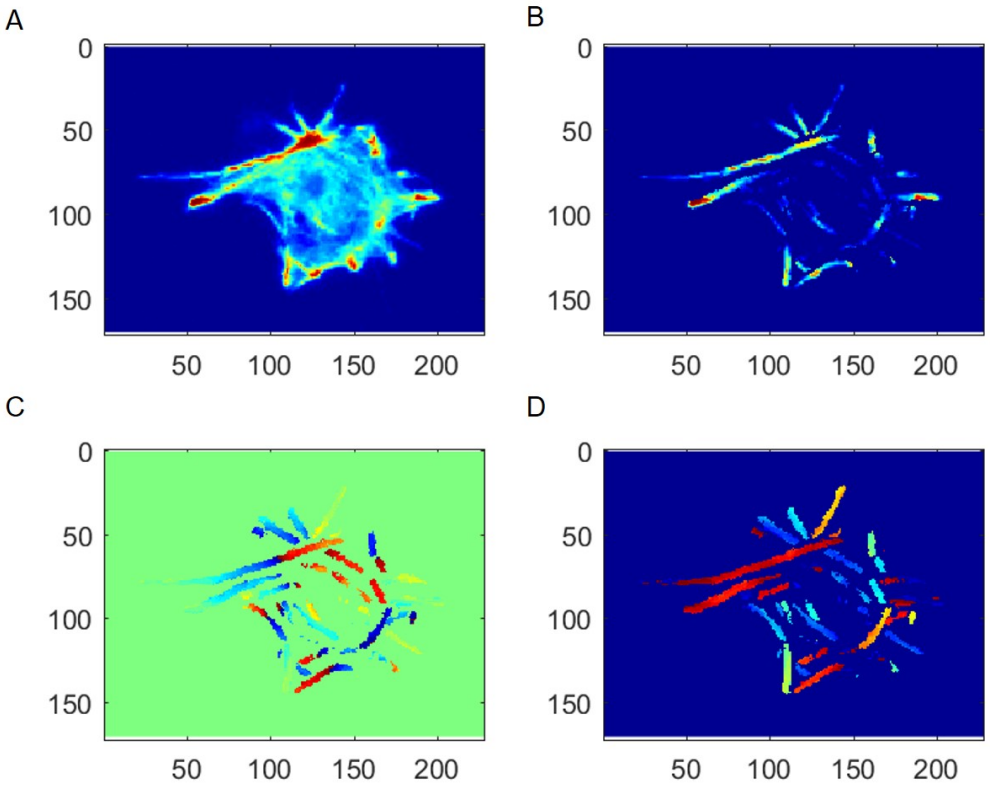

Figure 3.12: Example outputs of the actin fiber maps using the pipeline method. A and B represent the hot map and actin fibers identified by the pipeline; while C and D represent map angular orientation of actin fibers. More detailed information can be found in references [338, 345, 346]

3.8.4 Output parameters

The pipeline could output 18 parameters, including parameters for cell morphology, cytoskeleton properties, cytoskeleton micro-organization and nuclear state.

a. Morphology parameters

- **Cell area**: Sum of pixels covered by the mask of cell shape;
- **Aspect ratio**: Ratio between major and minor axis of cell shape, excluding filopodia;
- **Stellate factor**: Determines the smooth level of the cell boundary. Larger values indicate the presence of filopodia or a more stellate shape, whereas lower values indicate a more solid shape;

b. Cytoskeleton fiber parameters

- **Total fiber intensity**: Sum of pixel intensities for all pixels identified as fibers;
- **Fiber thickness**: Average of pixel intensities for all pixels that were identified as fibers. The value was calculated by summing up intensities of all pixels belonging to a fibre bundle normalized by its length. This process was repeated for each fibre bundle and their median value was recorded.
- **Variability in thickness**: Variability in the distribution of all pixel intensities for all pixels identified as fibers;
- **Alignment**: Dispersion of fibers within a cell by using the previously computed orientations for all pixels identified as fibers. Values close to 0 indicate that the majority of fibers were oriented in the same direction, whereas values close to 1 indicate random orientations of fibers;
- **Curvature**: Determine the curvature of fibre bundles in reference to the centre of the cell. Values close to 1 indicate fibers that were very curvy, whereas values close to 0 indicate straight fibers;
- **Location of fiber peak**: Radial position where fibers of maximum intensity was found in the cell. Value of 1 corresponds to cell edge and 0 to the cell center;
- **Fiber spread**: Represent the level of the diffusion or concentration of fibers across the cell. Large values indicate that fibers were well spread through the cell, whereas small values indicate that fibers were preferentially localized in a single radial position;
- **Length**: Average length of the fibers weighted by average pixel intensity;
- **Variability in fiber length**: Variance associated with the length of the fibers in a cell;
- **Chirality**: Once the center of the cell was identified, the fiber orientation map was converted to compute the relative orientation of each fiber with respect to the cell's center. Values close 0° indicate that fibers were preferentially pointing to the center of the cell, whereas values to 90° indicate that fibers were preferentially pointing to the cell edge;
- **Variability in chirality** : Variance associated with chirality measurements;

c. Nuclear parameters

- **Brightness**: Sum of pixel intensities identified as the nuclear which had DAPI signals;
- **Chromatin condensation**: A measure of the local changes in nuclear DAPI fluorescence intensity. Increased amount of nuclear speckles surrounded by regions of dimmer intensity reflects increased chromatin condensation;
- **Relative nuclear volume**: Relative nuclear volume was estimated by measuring 2D nuclear images and extrapolating a fluorescence intensity gradient in 2D nuclear images to approximate the nuclear height profile. Relative volumes were calculated through the equation of a 3D ellipse;
- **Poisson's ratio**: Ratio determined with the boundary condition that the cell nuclear assumed perfectly spherical shape in the absence of external forces. For each nucleus, Poisson's ratio was described through the relationship between volumetric changes and length changes in stretched materials. Negative Poisson's ratio means that the material expands in the perpendicular direction of stretching forces and shrinks in the perpendicular direction of compressive forces;
- **Apparent nuclear stiffness**: An apparent measure of nuclear stiffness, as reflected by the amount of nuclear 3D deformation induced by the cell's intracellular tension.

3.9 Construction of sandwich model

3.9.1 Preparation of polyacrylamide gel

In order to facilitate binding of the polyacrylamide gel to the coverslip, the coverslips need to be activated at the very beginning. Briefly, coverslips with diameter of 22 mm were placed on plasma oxidizer tray with one face up and oxidized with oxygen plasma for 15 min. In the following experiment, the oxidized side was kept face up. Then the coverslips were transferred to a glass petri dish and incubated with activation solution (dry toluene and 3-(Trimethoxysilyl) propyl methacrylate) in a fume hood overnight at room temperature. After washing coverslips three times with water and once with ethanol, the coverslips were put in an oven for 1h to dry and stored at room temperature afterwards.

Stock solutions of acrylamide/bis-acrylamide mix were prepared from 40% acrylamide and 2% bis-acrylamide following table 3.4. Next, stock solutions were degassed with nitrogen for 30 min to reduce oxygen within the solutions which prevents polyacrylamide polymerization. Subsequently, the working solutions were prepared following table 3.5 and mixed as fast as possible. A 40 μL drop of the working solution was placed onto the hydrophobic slide and gently overlaid with an activated coverslip with oxidized face side down. The gel solution was left for several minutes to polymerize according to the stiffness. It is worth noting that once the polymerized gel moves away from the coverslip edge resulting air gap at the edge of the coverslip, it indicates the completion of polymerization. To avoid drying of the hydrogel, after completion of polymerization was observed, the coverslip with gel was separated immediately from the glass slide by tweezers. The coverslips with gels were stored in PBS in a fridge.

Table 3.4: Stock polyacrylamide solutions

Gel	E(kPa)	40 %AAm [ml]	2%Bis [μl]	UPW [ml]	Total vol. [ml]
1	0.5	0.625	25	4.35	5
2	2	0.625	50	4.325	5

Table 3.5: Working polyacrylamide solutions

Gel	Vol. stock solution [μl]	TEMED [μl]	10%APS [μl]	Total vol. [μl]
1	500	4	0.75	509.75

3.9.2 Mechanical characterisation of polyacrylamide gel

The AFM measurements were performed on a Nanowizard 4 AFM (JPK, Germany), integrated with an Axio Observer Z.1 epifluorescence microscope with Plan-Apochromat lenses (x20) equipped with a cooled CMOS camera (Orca Flash 4). Before each experiment, the spring constant of the cantilever was calibrated using the thermal fluctuations method. Coverslip with polyacrylamide gel on the top was fixed in a petri dish and submerged in PBS. Mechanical measurement was performed by JPK's QI mode for rapid acquisition of force-curves and topography mapping. Regions with a dimension of 100 by 100 μm were randomly selected and measured in each sample. Data analysis of the force-displacement curves was carried out by JPK analysis software.

3.9.3 Sandwich model construction

Coverslips with gel on the top were fixed at the bottom of a petri dish with superglue. Then the petri dish was washed with PBS several times and sterilized under UV lamp in tissue culture hood for 30 min along with another gel and spacer. The sterilized spacer was placed on the top of the gel, at the same time the prepared cells were seeded on the gel. Cells were allowed to settle onto the gel for several minutes. Then a second gel, attached to a coverslip, was overlaid onto the spacer with tweezers. To minimize drifting of the top gel during image acquisition, a PDMS block was placed above the top coverslip as a weight. Then growth medium was added and the petri dish was put in the incubator to settle down.

3.9.4 Time lapse imaging

Cells were seeded onto gel at low density in order to obtain single cell dynamics. Time-lapse recordings of single cell dynamics were acquired with 20x objective by LS720 microscope (Lumascope, Etaluma, US) with a frame rate of 5 s for about 30 min. The microscope was placed inside the incubator so the temperature and CO_2 concentration of the imaging condition was maintained.

3.9.5 Images processing

Analysis of cell migration was performed using CellTracker, implemented in Matlab (R2013b, MathWorks) as previously described in literature [348]. It is an image processing software for automated, semi-automated, and manual cell migration detection (http://www.celltracker.website). All tracks were examined excluding those cells that were not isolated. The output data of average speed, x-,y-coordinate, and distance from the original point, were chosen for further analysis.

3.9.6 Statistical analysis

Statistical analysis was performed with OriginLab analysis software. Results were statistically analyzed by one-way analysis of variance followed by t-test. Statistical significance was reported at p, 0.05 (*), p, 0.01 (**) and p, 0.001 (***) unless otherwise stated.

Chapter 4

Effects of Ezrin and its mutants on cell migration

4.1 Introduction

Cell migration is a fundamental process in the development and maintenance of multi-cellular organisms during embryonic development, wound healing and immune responses. The most extensively investigated migration mode is lamellipodia based migration, which is often characterized by cell polarization to form a leading edge that extends actin filament rich protrusions, like lamellipodia and filopodia, via focalized cell matrix adhesions and proteolytic ECM remodeling. Cellular movement is achieved by retraction of cell rear by actomyosin [349].

Ezrin, as the linker between plasma membrane and actin cortex, is involved in the regulation of cell morphology and cell migration. Its direct interaction with actin filaments provides a regulatory link between the cytoskeleton and the cell membrane. Its FERM domain can bind to multiple membrane proteins via direct binding or indirect binding. With the aid of its interacting proteins, Ezrin is able to control cell migration along with other signals. For example, Ezrin promotes cell migration in response to HGF stimulation as measured by the ability of epithelial cells to close a wound [48]. 14-3-3 proteins are able to regulate the actin cytoskeleton remodeling, cell adhesion and migration. It was found that Ezrin is required by 14-3-3 ζ for direct physical interaction in the regulation of cell migration and membrane ruffling [350]. CD44, the main transmembrane receptor which transduces environment cues to morphological changes controlled by actin cytoskeleton, interacts with Ezrin to direct cell motility [351].

The aim of this chapter is to investigate the role of Ezrin and its mutant, which

have altered phosphorylation state at amino acid 567, in regulation of cell migration by long-term live-cell imaging. In addition, the protein distribution pattern during migration at single cell level is studied as the location of Ezrin determines the local intensity of the connection between plasma membrane and actin cortex.

4.2 Results

4.2.1 Optimum condition for cell transfection

Because the amount of Lipofectamine LTX regent required for successful transfection varies depending on the cell types, the first step was to test the recommended four concentrations of Lipofectamine LTX reagent to determine an optimum amount from 2 μl, 3 μl, 4 μl and 5 μl. 2 μl of Lipofectamine was found to be able to get about 60 $\%$ transfection ratio (Figure 4.1). Increasing the amount of Lipofectamin LTX had similar transfection ratio but caused more cell death. Even the transfection ratio varies between different plasmids, the results were considered to be good enough to carry out the following experiments.

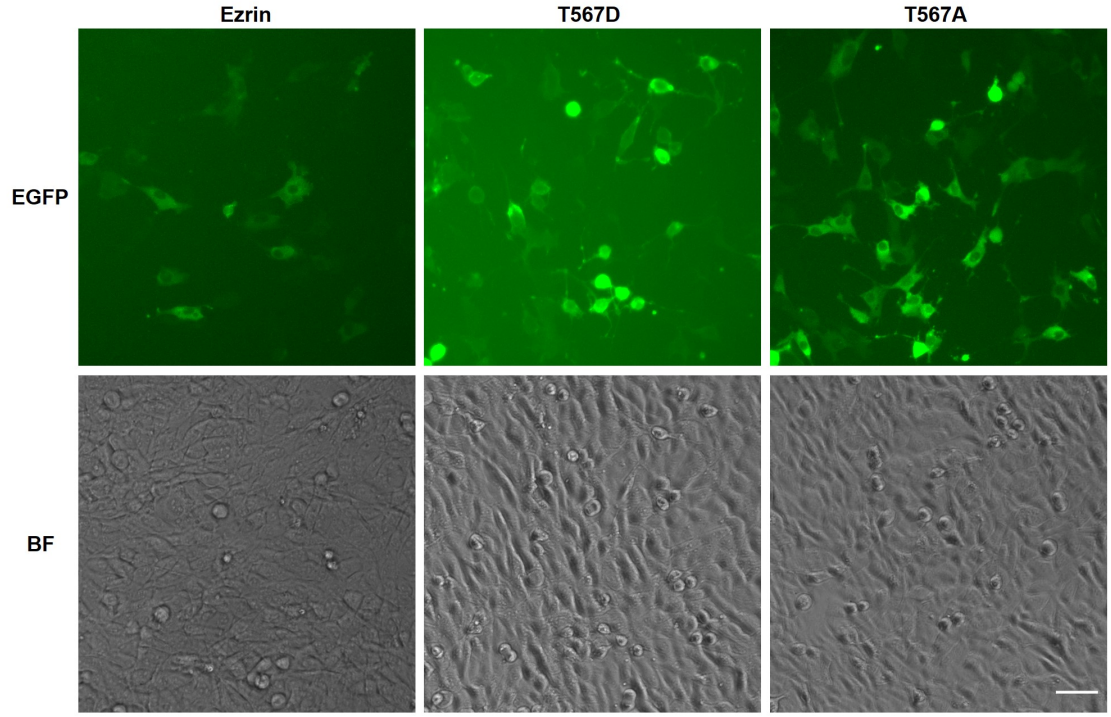

Figure 4.1: Transfection efficiency of NIH 3T3 cells with Ezrin and its mutant. Up panel: fluorescent images of 3T3 cells transfected with Ezrin, T567D, T567A; Bottom panel: bright field images of the transfected cells. Scale bar: 50 μm

Next step was to reseed the transfected cells in 6-well plate for the observation of each individual cell. However, it was found that after reseeding the cells transfected with FERM domain, the intensity of RFP signal dropped sharply in comparison to those cells without trypsin treatment (Figure 4.2). It means that, the fluorescent protein tagged with FERM domain was RFP, which made the results different from GFP. It is possible that the RFP is not as stable as GFP when they are exposed to chemicals. The protocol used in this study was then optimized for FERM transfection, where 3T3 cells were transfected directly in 6-well plate and subjected to no treatment before imaging. Also the Flurobrite-DMEM imaging specific medium was used to reduce the fluorescent background and at the same time protect the fluorescent proteins from photo-bleaching.

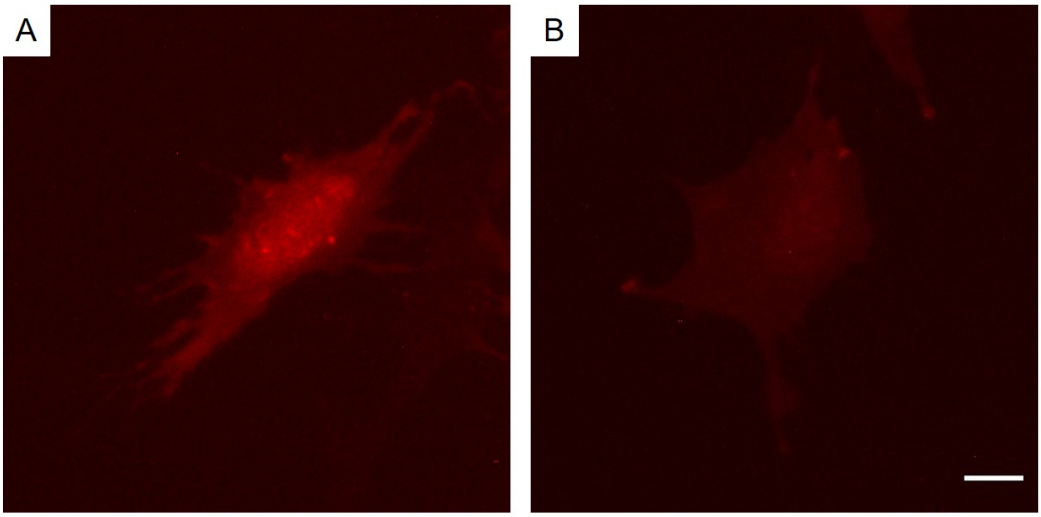

Figure 4.2: Comparison of 3T3 cells transfected with FERM domain treated with or without trypsin. A. Fluorescent image of 3T3 cells transfected with FERM domain was taken two days after transfection; B. 3T3 cells transfected with FERM domain was digested with trypsin and reseeded next day after transfection. Fluorescent image was taken two days after transfection. The exposure time for the two images was the same. Scale bar: 20 μm.

In this study, cells transfected with Ezrin was chosen as control because exogenous Ezrin is considered to be regulated as endogenous Ezrin through characteristic signalling pathways. To further verify that, cells were transfected with plasmid encoding EGFP and Ezrin-GFP and the results showed that neither Ezrin-GFP nor EGFP altered 3T3 cells' motility (Figure 4.3). Therefore in the following study, wild type Ezrin was used as control group as compared to other Ezrin mutant.

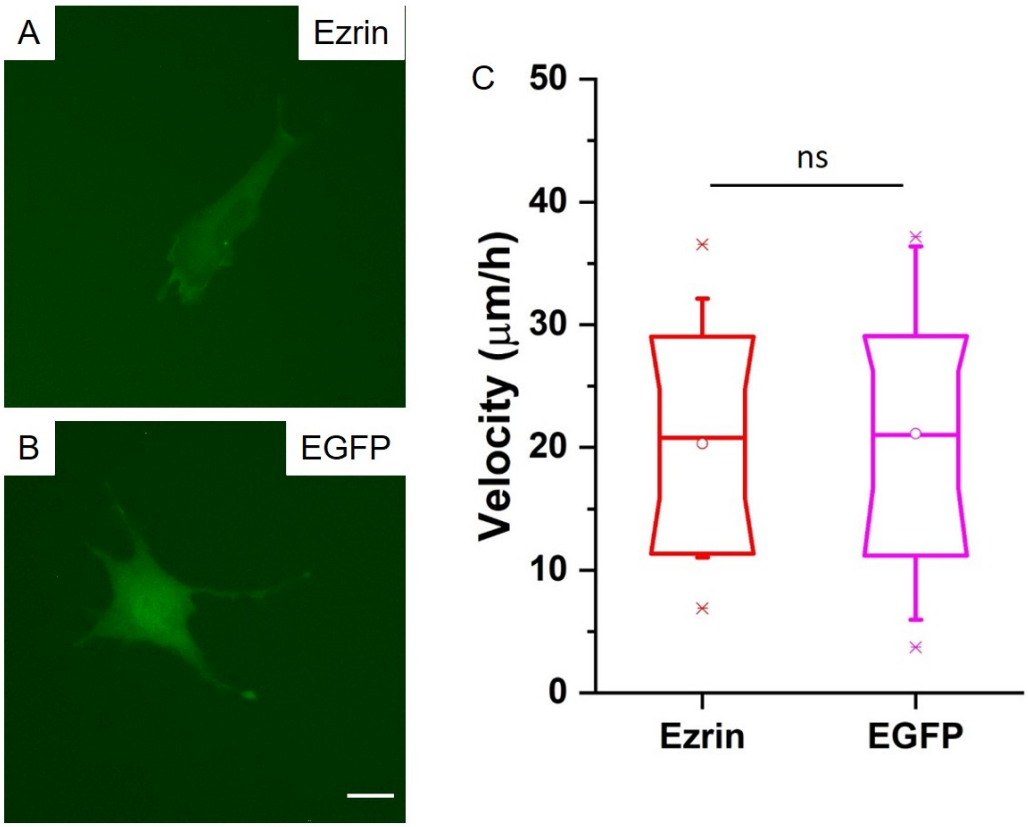

Figure 4.3: Transfection of Ezrin had no significant effect on cell migration compared with cells transfected with EGFP. Fluorescent images of cells transfected with Ezrin (A) or EGFP (B). Scale bar: 20 μm.; C. Box plots shows the results of migration velocity of these two types of cells, n=21 (Ezrin), n=34 (EGFP). ns indicated no significant difference, Dunnett test.

4.2.2 The effect of Ezrin and its mutant on cell migration

Migration videos of cells transfected with Ezrin mutant were taken and analyzed. The time lapse in Figure 4.4 shows representative images of four types of cells from 0 h to 16 h (14 h for Ezrin) during migration. Cells transfected with Ezrin T567D have the largest displacement during these 16 hours. While other cells appear to stay at the same place, moving back and forth. Also quantification of parameters obtained from the algorithm shows that transfection with active Ezrin T567D promotes cell migratory capacity, with a speed of 30 μm per hour, compared with transfection with other plasmids. In contrast, expression of inactive Ezrin T567A and dominant negative FERM domain had no significant effect on cell migration as compared to Ezrin plasmid (Figure 4.5). These results demonstrate that phosphorylated Ezrin at T567 has the ability to promote cell motility.

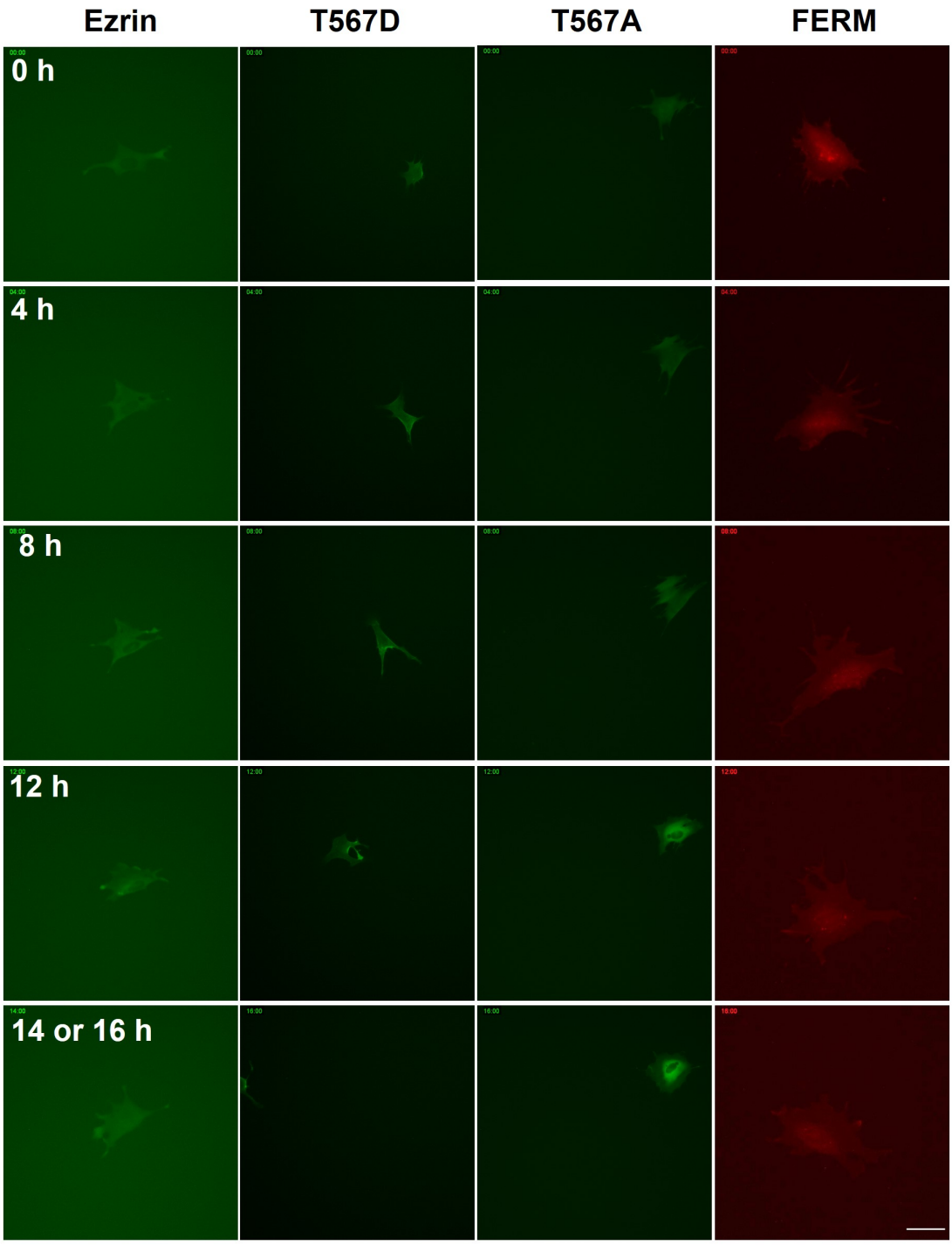

Figure 4.4: Time-lapse sequences of cells transfected with Ezrin, Ezrin T567D, Ezrin T567A, or FERM domain. Fluorescent images were taken at 0 h, 4 h, 8 h, 12 h, 16 h (14 h for Ezrin transfection). Scale bar: 50 μm.

The migrating directionality of the transfected cells was also assessed. Figure 4.6 shows that the representative migrating path of about 10 cells for each transfection over 12 hours of imaging. In agreement with Figure 4.4, transfection of Ezrin T567D promotes cells migrating for longer distance with more persistence. Two methods were used to calculate the straightness: one was Euclidean dis-

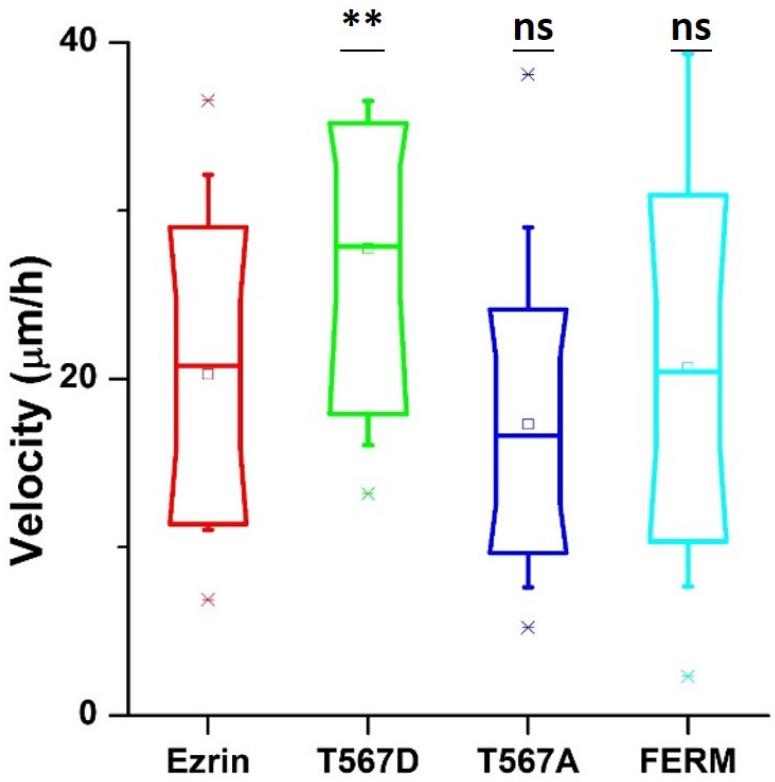

Figure 4.5: The effect of Ezrin mutant on cell migration. NIH 3T3 cells were transfected with wild type Ezrin (red), Ezrin T567D (green), Ezrin T567A (blue) or FERM domain (cyan). Transfected cells were used for migration experiment. Box plots show the results of migration velocity. Box plots extend from the 10th to the 90th percentage, whiskers from the 5th to the 95th. For migration experiments, n=21 (Ezrin), n=45 (Ezrin T567D), n=52 (Ezrin T567A), n=60 (FERM) cells were analyzed. Asterisks indicate a statistical difference (* $p<0.05$, ** $p<0.01$, *** $p<0.001$, obtained using Dunnett test against wild type Ezrin).

tance (e.g. line OA in Figure4.6 B) divided by total displacement; another one was maximum distance from origin divided (e.g. line OB in Figure4.6 B) by total displacement. It suggests that from both methods that cells transfected with Ezrin T567D migrated with larger directionality (Figure 4.6 E and F). While other plasmids, Ezrin T567A and FERM domain had no effect on the directionality.

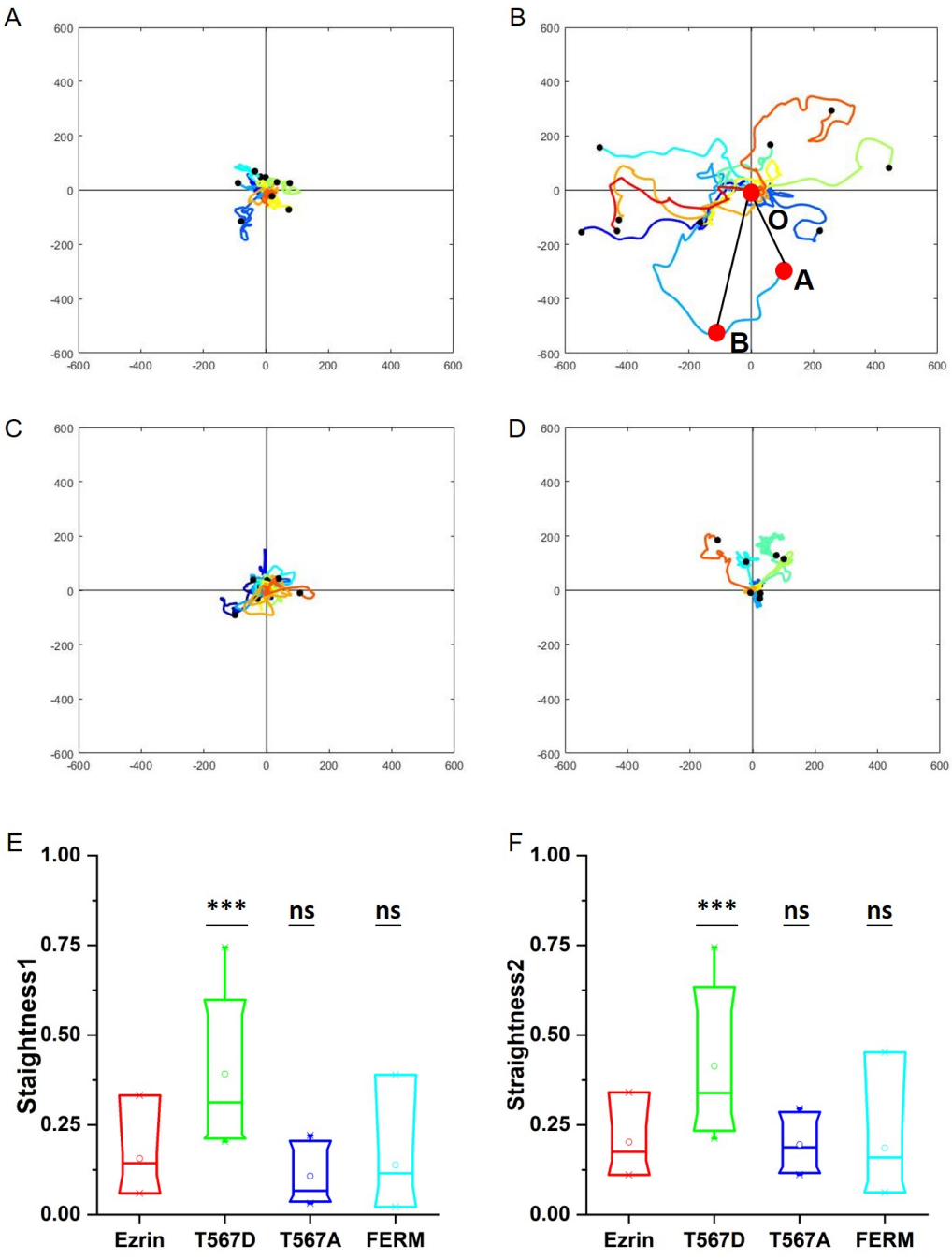

Figure 4.6: Migration efficiency of transfected cells. A-D. Representative trajectories of around 10 cells for each transfection, Ezrin (A), Ezrin T567D (B), Ezrin T567A (C) and FERM domain (D) over 12 hours imaging. The starting position of each cell were registered to the center of the plot. Box plot shows the migration straightness of the transfected cells by two methods, method one (E) and method two (F), n=9 (Ezrin), n=11 (Ezrin T567D), n=10 (Ezrin T567A), n=9 (FERM) cells were analyzed.** $p<0.01$, ns indicated no significant difference, obtained using Dunnett test against wild type Ezrin.

4.2.3 Sub-cellular distribution of Ezrin mutant

The protein intracellular distribution patterns of Ezrin mutant were found to be different during migration (Figure 4.7). The next step was to identify the relationship between Ezrin mutant distribution patterns and its biophysical properties. Two parameters were created separately, polarization ratio and peak front-back ratio, to describe intracellular distribution. Polarization ratio describes the level of signal spread, with the value of 1 meaning fully spread and 0 concentrated at one point as shown in Figure 4.8 left. Peak front-back ratio identifies the place where protein is predominantly located with respect to the direction of cell movement, with 1 at cell front and 0 at cell rear (Figure 4.9 left). The majority of active Ezrin T567D is localized in cell periphery with polarization ratio of 0.51 (Figure 4.8). Also, the polarized Ezrin T567D is localized at the cell rear during migration, with a peak front-to-back ratio of 0.48 (Figure 4.9). Conversely, inactive Ezrin T567A forms a ring around the nucleus (Figure 4.7), which also has a lower polarization ratio of 0.52, even though no statistically significant difference compared with wild type Ezrin. Wild type Ezrin and dominant negative FERM domain is distributed all around the cells with the highest polarization ratio of 0.54 (Figure 4.8). These results indicate that the distribution of protein is related to its function.

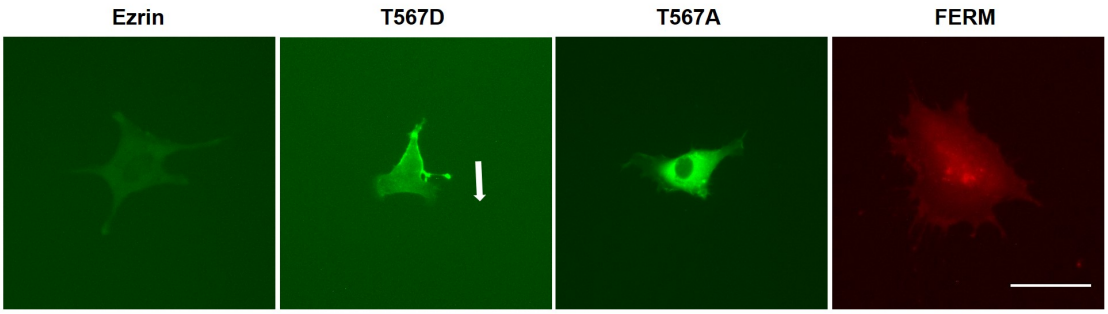

Figure 4.7: The subcellular distribution of Ezrin and its mutations during migration. Example fluorescent images of transfected cells obtained from the time-lapse videos. The example cell for Ezrin T567D showed clear persistent directional migration, indicated by the arrow. The other example cells showed no clear directional migration. Scale bar 50 μm.

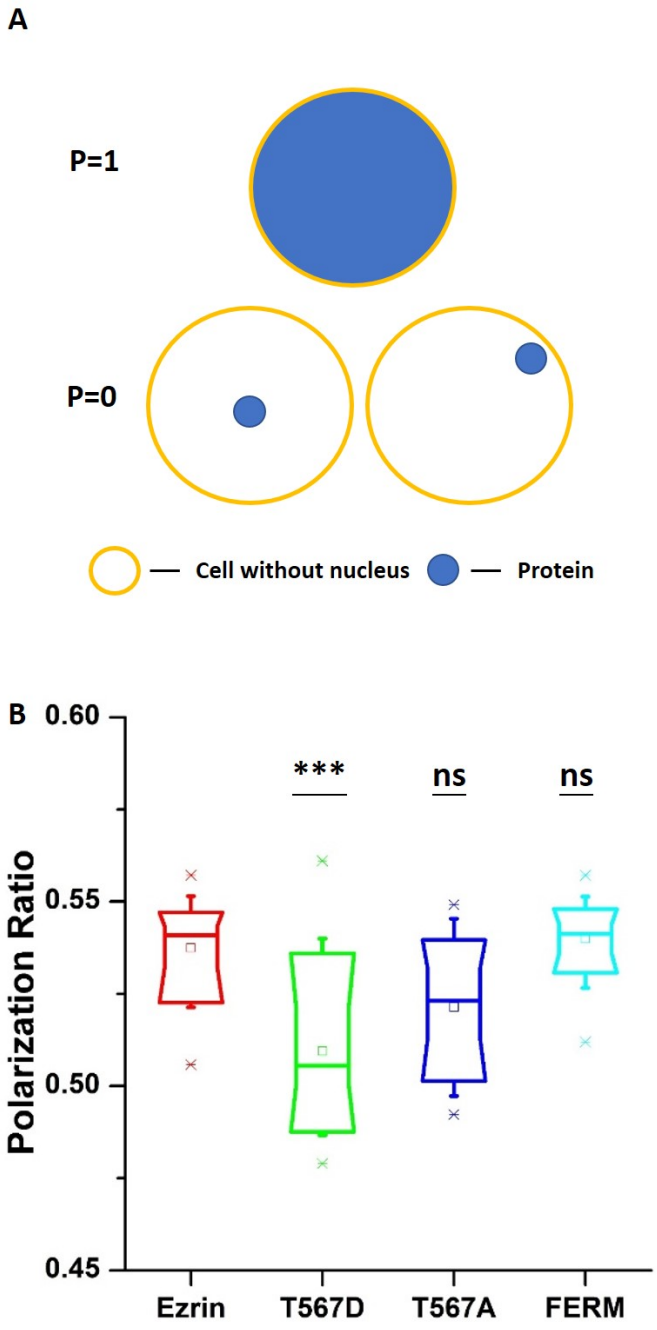

Figure 4.8: Transfected proteins have different polarization ratios. A. Schematic images represent how blue signal distributes when polarization ratio equals 1 and 0. When p=0, blue signal could concentrate at any point inside the cell, for example, cell center and periphery ; B. Box plot of the result of polarization ratio. n=21 (Ezrin), n=45 (Ezrin T567D), n=52 (Ezrin T567A), n=60 (FERM) cells were analyzed. Asterisks indicate a statistical difference (* $p<0.05$, ** $p<0.01$, *** $p<0.001$, obtained using Dunnett test against wild type Ezrin).

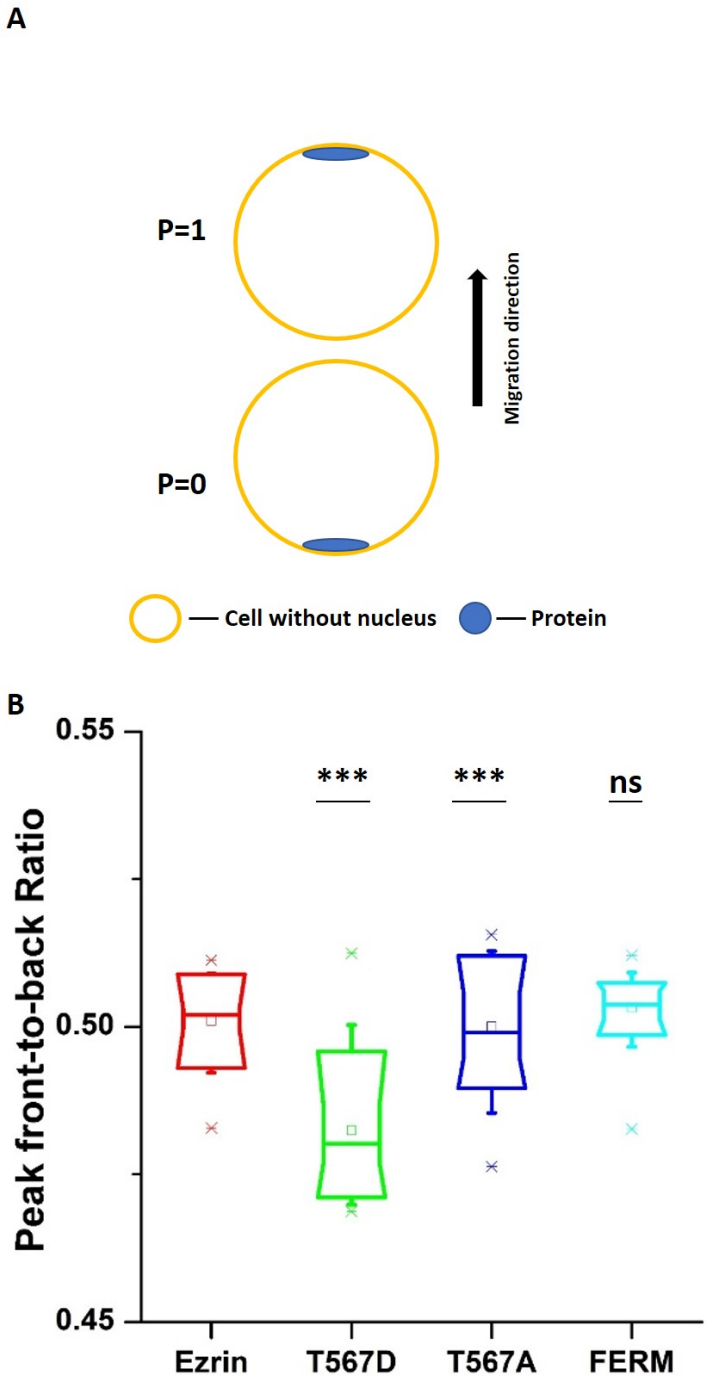

Figure 4.9: Transfected proteins have different peak front-to-back ratio. A. Schematic images represent how blue signal distributes when peak front-to-back ratio equals 1 and 0; B. Box plot of the results of peak front-back ratio. n=21 (Ezrin), n=45 (Ezrin T567D), n=52 (Ezrin T567A), n=60 (FERM) cells were analyzed. Asterisks indicate a statistical difference (* $p<.05$, ** $p<0.01$, *** $p<0.001$, obtained using Dunnett test against wild type Ezrin).

4.2.4 The relationship between distribution parameters and cell migration

Since cell migration is a dynamic process, the values of cell migration speed, polarization ratio and peak front-to-back ratio for each individual cell change during the course of a time lapse experiment. Therefore, it would be useful to find out whether there is a relationship between cell instantaneous migration speed and protein distribution patterns. All the parameters from each video were put together and the relationship between migration speed and protein distribution parameters were plotted. By this means, a linear relationship between migration speed and these two parameters, polarization ratio and peak front-back ratio, was found for active Ezrin T567D. It means when active Ezrin T567D accumulates at the cell rear, cells migrate faster (Figure 4.10 A and B). More importantly, it also shows that when inactive Ezrin T567A accumulates at the back of the nucleus according to the migrating direction, the cells migrate faster.

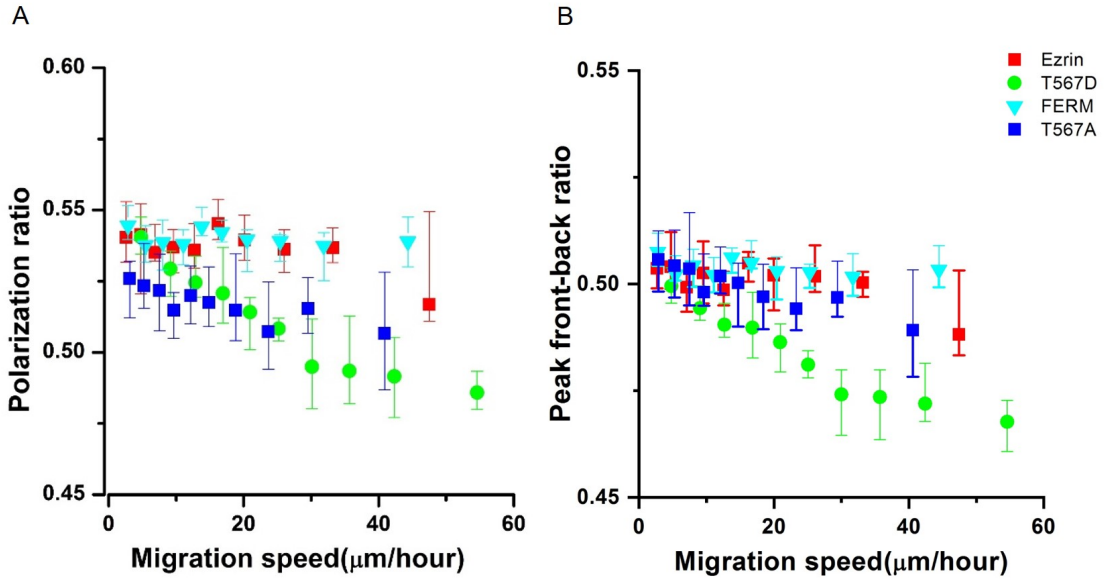

Figure 4.10: The relationship between cell migration speed and the two parameters, polarization ratio and peak front-back ratio. Plot shows how polarization ratio (A) and peak front-to-back ratio (B) change with the velocity increasing. n=21 (Ezrin), n=45 (Ezrin T567D), n=52 (Ezrin T567A), n=60 (FERM) cells were analyzed.

In summary, these results suggest that active Ezrin T567D enhance cell migration by preferentially localizing at the cell rear and, other mutant have no effect on cell migration but have their own distribution patterns during migration.

4.3 Discussion

4.3.1 Ezrin T567D promotes cell migration by polarized distribution

In this chapter, the role of Ezrin, a linking protein between plasma membrane and actin cortex, in the regulation of cell migration was investigated. As Ezrin was reported to be involved in cancer metastasis, by promoting cell migration. Some studies showed that the increased expression level of Ezrin promoted cell migration. Meng et al reported that Ezrin over-expression promoted cell protrusion and cell motility in a pancreatic cancer cell line, MiaPaCa-2 [352]. Zhang et al transfected osteosarcoma cell line MG63 with Ezrin and found that over-expression of Ezrin promoted tumor cell invasion and migration [117]. On the contrary, the results here showed that over-expression wild type Ezrin had failed to increase cell migration speed by comparing the migratory ability with cells transfected with EGFP. This is because the amount of activated Ezrin instead of wild type Ezrin is related to cell migration. It has been reported that transfection of phosphorylated states of Ezrin, Ezrin T567D, promoted cell migration [49]. Agree with their results, the expression of phosphorylated Ezrin at T567 was found to have the ability to enhance cell motility significantly. Other mutants, similar to wild type Ezrin, inactive Ezrin T567A and dominant negative FERM domain had no significant effect on cell migration. It has been reported that T-lymphoblasts cultured from transgenic mice expressing phosphomimetic Ezrin T567E showed attenuated in vitro migration and chemotaxis and in vivo homing and transmigration, as well as reduced lamellipodia extension, as compared to cells overexpressing wild type Ezrin [353]. In contrast to their results, expression of T567D Ezrin increased in vitro migration with increased cell polarization and protrusion formation in T cells [354]. The discrepancy may be due to differences in extent of over-expression and cell types.

Not only the expression level of Ezrin T567D, but also distribution pattern inside the cell, could affect cell migration. The results revealed that Ezrin T567D, the one enhanced cell migration, was concentrated at the cell rear during cell migration. Polarization is the preliminary step during cell migration, which determines the leading edge and retracting rear [355]. This includes the actin filaments, myosin and microtubules [356]. Now Ezrin is added to the list of components for cell polarization. Ezrin may act as a role to recruit actin filaments as Ezrin has been reported as the first one to be recruited to the bleb membrane, followed by actin in blebbing reassembly [148]. How Ezrin is involved in cell polarization and mainte-

nance of polarization is worth exploring. Furthermore, the more Ezrin T567D was localized at the cell rear, the faster the cell migrated. These findings suggest that the polarized Ezrin T567D distribution at the cell rear could be associated with accelerated migration speed, by assisting the retraction of the cell body. Contractility driven by the action of non-muscle myosin II (NMII) on actin filaments is key for the generation of force required to actively retract the rear, and RhoGTPase signaling is critical in determining NMII activity. Strong connection between actin filaments and membrane at the cell back caused by Ezrin T567D could increase the cortical tension, powering the cell body retraction [357]. At the same time, in the front of cell, the connection between plasma membrane and actin cortex is weak, which may be helpful for the formation of protrusions, such as lamellipodium and filopodium. Because the loose connection between plasma membrane and actin cortex may make it easier to push the membrane forward by polymerization of actin filaments [357].

Additionally, the cell rear accumulation of active Ezrin T567D may inhibit the formation of cell extensions at the cell back to maintain the front-back polarity, increasing in migration persistence. Persistence characterizes the average time between significant changes in the direction of a cell's translocation. Processes involving directional cell migration are essential for many fundamental biological processes including the innate and adaptive immune systems [358], embryonic development [359], cancer metastasis [360]. The results here showed that the expression of active Ezrin T567D enhances the directionality of migrating cells compared with those of other mutants. It has been reported that mouse embryonic fibroblasts which displayed multiple unstable and disorganized protrusions had defects in the directional stability of migration [361]. Agree with results obtained here, phosphorylated Moesin, another member of ERM protein, was reported to provide a directional memory to migrating cells by preferentially accumulating at the cell rear in chemotaxis experiments and remaining polarized even after the removal of the chemoattractant [362].

What's more, the way how Ezrin distributes inside the cell is also related with cancer progression as reported by Piao et al [61] that a cell membrane staining pattern is correlated with significant cancer metastasis. Here the results suggest that polarized membrane staining at the cell rear with high migratory ability may explain how Ezrin is involved in cancer metastasis.

4.3.2 The distribution of Ezrin T567A inside the cell

Transfection with inactive ezrin T567A, which binds to the membrane but cannot bind to actin, showed a trend to decrease the cell migration speed as compared with wild type Ezrin, even though there was no statistically significant difference. Transfection of Ezrin T567A in 2C4 fibrosarcoma cells was reported to show a decrease in cell migration and a significant loss of persistence of the wound closure response [29]. It is possible that the effect of Ezrin T567A on cell migration differs in cell types.

Interestingly, the results showed that inactive Ezrin T567A accumulated around the cell nucleus, forming a ring. As Ezrin T567A has an impaired ability to bind to cell membrane and actin filament, it was supposed to stay in the cytoplasm evenly. The nuclear-surrounding distribution suggests that Ezrin has other functions as inactive state in the cytoplasm, such as connecting the nucleus. It has been reported that the lack of nucleus deformability limits migration speed through 3D tissues [363]. The surrounding Ezrin T567A may work as a supporter of the nuclear during cell migration, resulting in reduced migration speed. It has also been reported that expression of Ezrin T567A in C2C12 cells results in a decrease in nuclear translocation of β-DG (β-Dystroglycan) which is an integral plasma membrane receptor, concomitant with a reduction of actin-rich cell surface protrusions [364]. In addition, it has been revealed that cervical cancer patients displaying perinuclear Ezrin localization patterns have longer survival time than those with a more diffuse cytoplasmic Ezrin localization [71]. Therefore, it is possible that the role played by inactive Ezrin T567A during cell migration could be associated with the nucleus, by limiting the movement of nuclear to slow down the whole cell migration. Similar to results of Ezrin T567D, cells migrated faster when inactive Ezrin T56A was preferentially localized behind the nucleus near the cell rear.

Another possible explanation of these observations is that transfected Ezrin T567A distributes uniformly in the cytoplasm but with a higher thickness. Due to the limitations of epifluorescence microscope used in this experiment, the images display the sum of all the signals in the cell instead one layer of the cell. A laser scanning confocal microscope might be used to obtain a stack of images to identify how Ezrin T567A distributes inside.

Ezrin T567A, where the threonine residue at 567 is mutated to alanine, is phosphodeficient, which is thought to be constitutively inactive. As Ezrin T567A was reported to be poorly associated with the cytoskeleton, forming oligomers in vivo [365]. It also has been reported that Ezrin T567A inhibited RhoA-mediated contractility and focal adhesion formation in NIH 3T3 cells [366]. However, Yonemura

et al reported that Ezrin T567A was recruited to microvilli and ruffling membrane after EGF (epidermal growth factor) stimulation in serum-starved A431 cells [367]. Ezrin in the closed conformation was reported to be able to localize to membrane by an exposed N-terminal binding site. However the opened phosphorylated form of Ezrin is more readily cosediments with actin filaments and bind more tightly to membrane than the closed formsa [368]. This may be because phosphorylation is not required for activation of Ezrin but required for the rapid turnover of activated and inactivated Ezrin in normal biological functions. Ezrin T567D, the phosphomimetic mutant, is more dynamic, so that a small fraction of the mutants is in the "open" conformation for a long enough time period to be competent to bind to other proteins. This is why cells expressing Ezrin T567D migrate faster than cells expressing wild type Ezrin and Ezrin T567A.

4.3.3 FERM domain had no effect on migration

Truncated Ezrin, FERM domain, which only comprises N-terminal of the protein, has been used to generated dominant negative effects [369]. It has been assumed that expression of FERM domain could inhibit the functions of all ERM proteins in connecting to plasma membrane because of the high degree of conservation of this domain between the ERM proteins. However, it remains unclear whether the inhibition effect would spread to all functions [35], such as cell morphology, cellular distribution and cell migration.

The signal of FERM domain is found to distribute all around the cells, even in the nucleus, which is agreed with other report that transfection with a cDNA encoding approximately 55 kDa of the ezrin N-terminus (N-ezrin) showed that it can translocate to the nucleus [369]. Analysis of FERM domains using web-based software reveals that the majority of these contain potential nuclear export signals (NESs) and some also contain nuclear localization signals (NLSs), which could explain the nuclear distribution of FERM domain [370]. This also suggests that FERM domains may be involved in the transfer of information between the cell cortex and the nucleus. The effects of FERM domain on cell migration has been investigated by other researchers. Transfection of FERM domain was reported to decrease cell migration in MDA-MB-232 breast cancer cells [49] and LLC-PK1 epithelial cells [371]. However the results here showed that the expression of FERM domain had little impact on cell migration in NIH 3T3 fibroblast cells. The different inhibition effects may be to the cell type used.

4.4 Summary

Together, this chapter demonstrated that transfection of active Ezrin T567D enhanced cell migration, with more proteins concentrated at the cell rear. Other Ezrin mutants, Ezrin T567A and FERM domain, had negligible effect on cell migration but they had their own distribution patterns inside the cells. Main changes due to different Ezrin mutations during cell migration are summarized in Table 4.1.

Table 4.1: Summary of main changes due to different Ezrin mutations during cell migration in this study. (+) indicates significant increase, (-) indicates significant decrease and (=) indicates no significant changes.

Biophysical parameter	T567D	T567A	FERM
Migration velocity	+	=	=
Migration directionality	+	=	=
Rear localization	+	=	=
Polarized distribution	+	+	=

Chapter 5

Effects of Ezrin and its mutants on cell mechanical properties

5.1 Introduction

In the previous chapter, the effects of Ezrin and its mutants on cell migration were compared, revealing that transfection of active Ezrin T567D increased cell migration speed. The promotion effect was correlated with its localization inside the cell during migration. While the other two mutants, inactive Ezrin T567A and FERM domain had negligible influence on cell migration. During migration, cells not only undergo molecular changes but also mechanical modulation. This latter process is regulated by cell cytoskeleton serving as backbone of intracellular force and converts external mechanical signal via focal adhesion complex into the cell [372]. Cell mechanical properties are closely related to many important biological behaviors of cells. In particular, cell stiffness, one of the mechanical properties, has been reported to be related with the motility of cells. For example, MGF-C25E, a synthetic mechano-growth factor, is reported to promote rate tenocyte migration by lessening cell stiffness and increasing pseudopodia formation via focal adhesion kinase (FAK)-extracellular signal regulated kinase1/2 (ERK1\2) signaling pathway [373]. Inhibition of phosphatase and tensin homolog deleted on chromosome 10(PTEN), a dual phosphatase, also promotes cell migration in the wound healing assay by decreasing cell stiffness near the wound edge [374]. More importantly, cell stiffness has been found to be associated with the migration capability of cancer cells, especially cancer metastasis. Most studies showed that cancer cells with higher metastatic ability are usually softer than the counterparts [375, 376]. Based on the distinctions between cancer cells and healthy cells, cell stiffness is suggested to be a diagnostic marker for cancer progression in

the clinic. The aim of this chapter is to determine the mechanical changes (i.e. stiffness, adhesion, and viscosity) of cells transfected with different Ezrin mutants by using AFM.

5.2 Results

5.2.1 Comparison of stiffness

Surface topography and stiffness map of the scanned area were analyzed by JPK data processing software (Figure 5.1). From Figure 5.1B, it shows that area around the nucleus are taller than the periphery. Also Figure 5.1C shows that area around the nucleus are much softer than the periphery. This is consistent with other reports that the Young's moduli of the areas over the nucleus were much smaller than those of the cell peripheries [377].

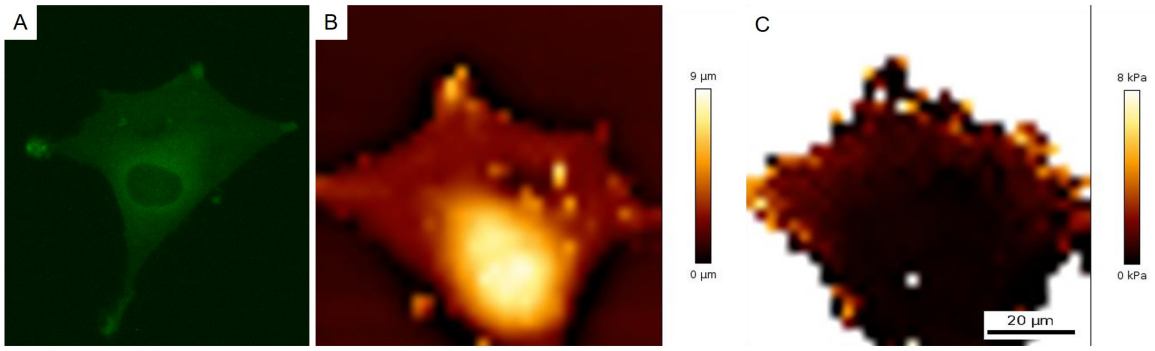

Figure 5.1: AFM measurements of a cell transfected with Ezrin T567A. A. Fluorescent image of a cell transfected with Ezrin T567A; B. Height image of the cell; C. Elasticity map of the cell. B and C are specular images of A

Next, the algorithms written in Matlab were used to analyze all the force curves got from the experiment. The force curves include the force curves indented on the bare surface of petri dish which could be used to calculate the sensitivity, and force curves indented on the cells. The output results contained the whole cell stiffness, as well as the stiffness of the cell cortex and the underlying cytoskeleton. When assessing the whole cell stiffness, only inactive Ezrin T567A was found to have the ability to stiffen the cell compared with wild type Ezrin (Figure 5.2A). During the AFM experiment, as the tip indented on the cell, the first organization it contacted with was the actin cortex, which is just underneath the plasma membrane with a thickness of about 200 nm [378]. With the tip approaching further down, the cytoskeleton under the cortex was indented (Figure 5.2B). According to

the depth sensing analysis of the force curve, cortical stiffness and cytoskeleton stiffness could be obtained from the same force curve [340]. When comparing

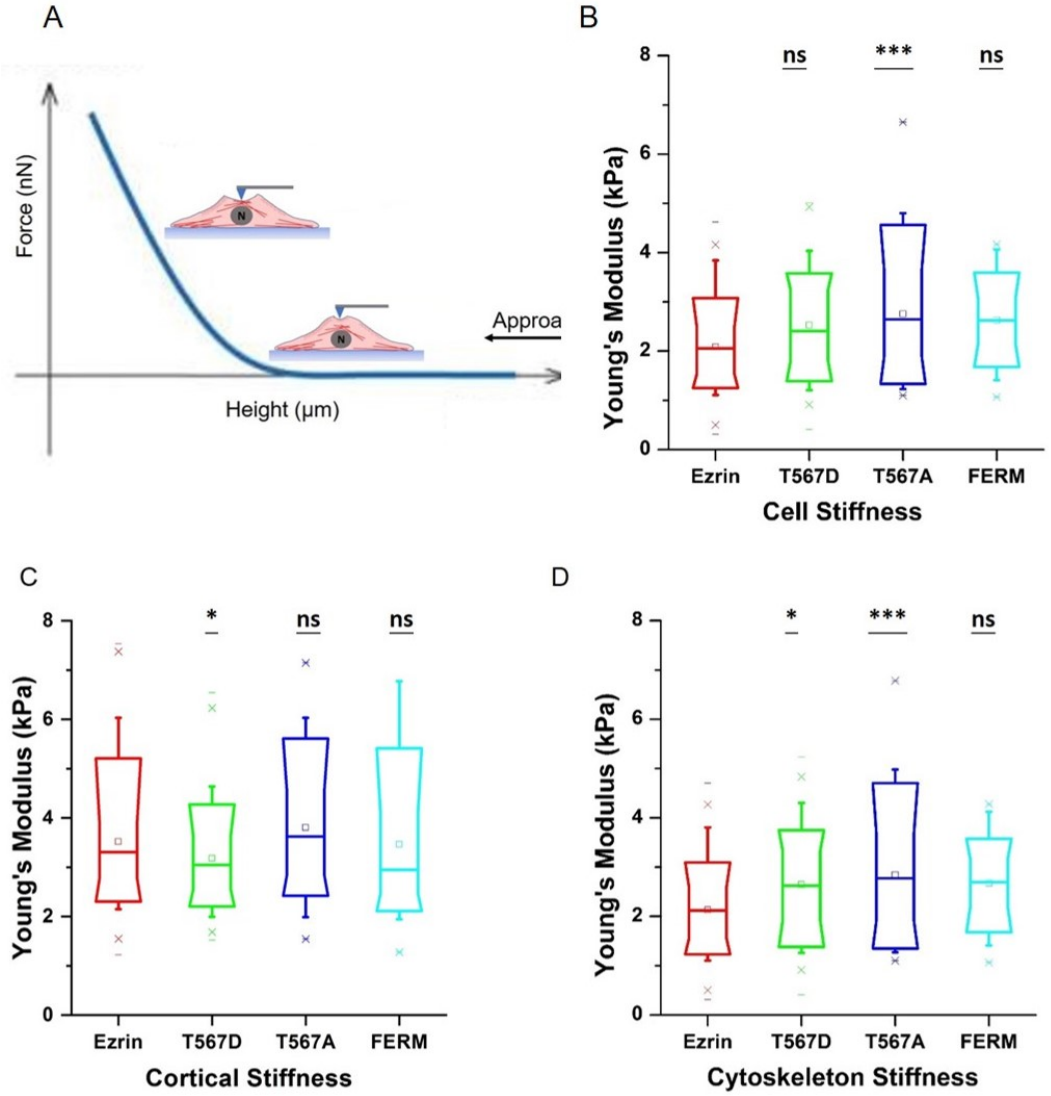

Figure 5.2: The effect of Ezrin mutants on cell stiffness. NIH 3T3 cells were transfected with wild type Ezrin (red), Ezrin T567D (green), Ezrin T567A (blue) or FERM domain (cyan). Transfected cells were used for AFM experiment. A. Depth sensing analysis of the force curve according to the indentation depth. Box plots show the results of whole cell stiffness (B), cortical stiffness (C), cytoskeleton stiffness (D). Box plots extend from the 10th to the 90th percentile, whiskers from the 5th to the 95th. For AFM experiment, n=125 (Ezrin), n=115 (Ezrin T567D), n=89 (Ezrin T567A), n=74 (FERM) analyzed cells. Asterisks indicate a statistical difference (* $p<0.05$, ** $p<0.01$, *** $p<0.001$, obtained using Dunnett test against wild type Ezrin).

cortical and cytoskeleton stiffness, it shows that the expression of active Ezrin T567D leads to a decrease in cortical stiffness (Figure 5.2C). While both active Ezrin T567D and inactive Ezrin T567A have the ability to stiffen the cytoskeleton in comparison to wild type Ezrin (Figure 5.2D) with Ezrin T567A increasing the

stiffness more significantly. On the other hand, it shows that dominant negative FERM domain had no significant effect on cell stiffness, neither the whole cell stiffness nor the stiffness of cortex and cytoskeleton (Figure 5.2).

5.2.2 Comparison of adhesion force and adhesion work

The force–distance curves acquired in AFM indentations of live cells often contain tip-cell adhesion forces. Adhesion force can be directly visible on the retracting force curve as occurrence of negative values of externally applied force, which indicates an external force that acts to detach the tip from the cell. Tip-cell adhesive force appears in both approaching and retracting parts of the force–displacement curves measured in cell indentations, favoring tip displacement during approaching and opposing it during retracting. As a function of the nano-mechanical properties of the existing cellular surface adhesive molecules, adhesion force could be obtained from the measurement. After the AFM tip was brought into contact with and indented the cell surface, rupture events occurred during tip retraction from the cell surface, revealing the general tip-cell surface adhesion interactions special to each cell type. The analysis of the adhesion forces revealed that cells transiently transfected with inactive Ezrin T567A and dominant negative FERM domain have significantly lower adhesion force (Figure 5.3A). Adhesion work, which defined as the energy per unit of surface area required to separate two bodies, is also measured in this study. The results show that Ezrin T567A and FERM domain also have lower adhesion work (Figure 5.3B). However, transfection of active Ezrin T567D has little effect on adhesion force and adhesion work (Figure 5.3).

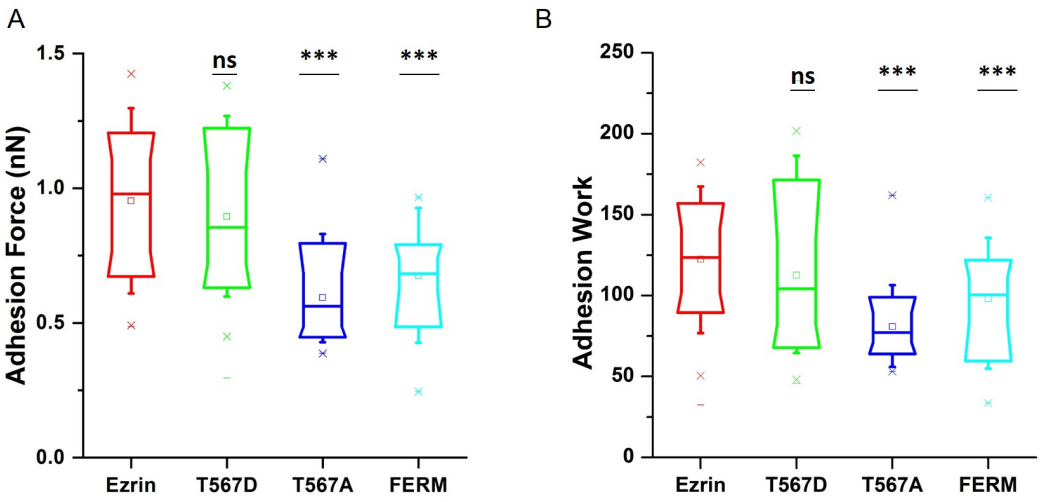

Figure 5.3: The effect of Ezrin mutants on adhesion force and adhesion work. Box plots show the results of adhesion force (A) and adhesion work (B). Box plots extend from the 10th to the 90th percentile, whiskers from the 5th to the 95th. For AFM experiment, n=125 (Ezrin), n=115 (Ezrin T567D), n=89 (Ezrin T567A), n=74 (FERM) analyzed cells. Asterisks indicate a statistical difference (*** $p<0.001$, ns, no significant difference, obtained using Dunnett test against wild type Ezrin).

5.2.3 Comparison of viscosity

Lastly, another parameter, viscosity, was compared, between cells with different transfection. Based on the hysteresis between the approach and retraction curves, the apparent viscosity of the cells was calculated. As cells are complex viscoelastic materials, their viscous response plays an important role during AFM indentation. The viscosity of cytoplasm is commonly related with the kinetics of actin filament network turnover which includes polymerization, depolymerization, crosslinking and bundling. Surprisingly, cells expressing inactive Ezrin T567A showed decreased viscosity compared with wild type Ezrin (Figure 5.4). On the other hand, active Ezrin T567D which displayed decreased cortical stiffness shows no significant effect on cell viscosity, as in the same case with dominant negative FERM domain.

In summary, the analysis from AFM measurements shows that transfection of active Ezrin T567D promotes cell motility, and at the same time, shows decreased cortical stiffness and increased cytoskeleton stiffness. Conversely, inactive Ezrin T567A and FERM domain have little effect on the migration and mechanical properties apart from Ezrin T567A increasing the cytoskeleton stiffness.

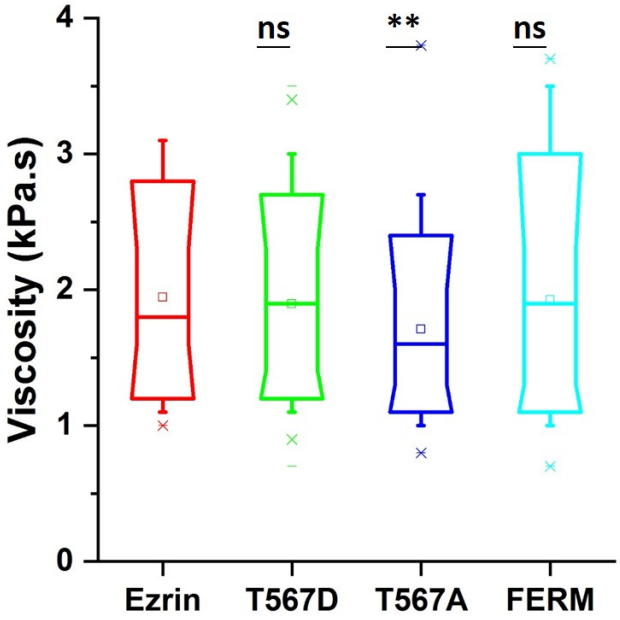

Figure 5.4: The effect of Ezrin mutant on viscosity. Box plots extend from the 10th to the 90th percentage, whiskers from the 5th to the 95th. For AFM experiment, n=125 (Ezrin), n=115 (Ezrin T567D), n=89 (Ezrin T567A), n=74 (FERM) analyzed cells. Asterisks indicate a statistical difference (** $p<0.01$, ns no significant difference, obtained using Dunnett test against wild type Ezrin).

5.3 Discussion

5.3.1 Ezrin T567D showed decreased cortical stiffness and increased cytoskeleton stiffness

In this chapter, the mechanical effects of transfection of Ezrin and its mutants were investigated by using AFM. Firstly, the whole cell was chosen to scan instead of area over the nucleus. Because the nucleus is the largest and stiffest organelle in cells. Most of the previous experiments performed by AFM were chosen to be located over nucleus [2]. However, as shown in the presented results, the peripheral regions were stiffer than the central regions of cells [379]. Even using common settings of AFM procedures with less than 5 nN contact forces and approximately 200-500 nm indentation depth will not stay in contact with the nucleus. As a result, the stiffness of around the nucleus only contributes part of the global stiffness since the cell is nonuniform in nature.

Given that the role of Ezrin is as linker between the membrane and the actin cortex, the stiffness of actin cortex and cytoskeleton of the transfected cells were

compared separately. Because actin cortex and cytoskeleton have their own biomechanical functions. Complete and comparative studies of cytoskeleton integrity have already demonstrated that two types of actin filaments are pivotal in the determination of cell mechanical properties, cortical actin filaments and stress fibers. Because increase microtubule polymerization by Paclitaxel or disruption of microtubule structures by Colchicine had little effect on cell stiffness [380, 381]. The cell cortex plays an important role in cell shape changes during movement [382]. On the other hand, cytoskeleton, mainly stress fibers which are bundles of actin filaments, provides force for cell migration [383]. The findings of this study demonstrated that cells transfected with active Ezrin T567D showed lower cortical stiffness but higher cytoskeleton stiffness. This result might be explained by the observation of last chapter, the polarized Ezrin T567D distribution pattern. Ezrin T567D was concentrated at the cell rear during migration, which indicated that the connection between the membrane and cell cortex is weakened at the cell front and strengthened at the cell back. This polarized distribution pattern may result locally enhanced rigidity of cell cortex but overall decreased cortical stiffness. It has been reported that T567E Ezrin expression in T-lymphoblasts resulted in increased membrane tension due to increased actin-membrane linkage measured by optical tweezers [353]. The different findings about cortical stiffness might be due to the techniques used because optical tweezers only measure subcellular mechanical properties instead of overall cell stiffness. Because Ezrin T567D displayed polarized distribution in transfected cells, which in turn may result in polarized cell functions and cell mechanical properties. The softness of actin cortex detected in the results may be responsible in determining the deformation capability of cells during migration. The formation of protrusions is suppressed in cell rear, which would allow or possibly even promote localized protrusion formation in the front where T567D Ezrin is lacking. On the other hand, the increased stiffness of cytoskeleton in Ezrin T567D transfected cells as shown in the results, might result from the polymerized stress fibers, which in turn promoted cell migration. Altogether, different effects of Ezrin T567D on cortical stiffness and cytoskeleton stiffness revealed distinct functions of actin cortex and cytoskeleton during cell migration.

Cancer is characterized by a malfunctional behavior of cells that undergo uncontrolled division, and disrupt healthy body tissues. Some important biomechanical characteristics of cancer cells are their enhanced softness compared to non-malignant ones [384, 385, 341]. Ward et al used the micropipette aspiration technique to investigate the deformation properties of transformed rat fibroblasts derived from non-tumorigenic cell lines [386]. They pointed out a direct correlation between an increase in deformability and progression of the transformed cells

from non-tumorigenic into tumorigenic metastatic cells. Lekka et al used AFM to quantify the elasticity of non-malignant and cancerous epithelial cells from the human bladder [387]. They showed that the stiffness of cancer cells is about one tenth that of normal cells. Even though NIH 3T3 cells are not cancer cell types, the results also show that cells expressing Ezrin T567D exhibiting high migratory ability have weaker membrane-actin cortex connection. Together, these suggest that their mechanical disorder and motility may be fundamental features of the architecture of cancer cells.

Compared with wild type Ezrin, Ezrin T567A showed the ability to increase the whole cell stiffness, which might result from increased cytoskeleton stiffness as there is no effect on cortical stiffness. While FERM domain had effect on neither on cortical stiffness nor cytoskeleton stiffness. Interestingly, it has been reported that suppression Ezrin expression by siRNA in confluent MDCK II cells showed dropped membrane tension by 40% [32]. The different effects on cortical stiffness may be explained as followings: firstly, single NIH 3T3 cells were measured instead of confluent MDCK II cells because neighbour cells would affect measured cell's mechanical properties [388]; secondly, unlike siRNA, Ezrin T567A and FERM domain also has some active fragments which may have other biological functions.

5.3.2 Ezrin T567A and FERM domain showed decreased adhesion values

The adhesion force is determined as the derivative of the adhesion energy of the tip-cell contact, as the adhesion energy and contact area are considered to be continuously varying during the indentation. From the retraction part, adhesion force can be measured directly. Many of the AFM studies of the adhesion refer to values of the adhesion force, which is measured as the external pulling force required to detach the tip from the sample [389, 390]. A number of studies have implicated ERM proteins in the regulation of cell-cell and cell-matrix adhesion. Ezrin T567D expression has been reported to inhibit E-cadherin–dependent cell-cell junction assembly, by translocating E-cadherin from the plasma membrane to cell cytoplasm in epithelial cells [46]. What's more, it has been reported that the non-specific cell-surface adhesion of metastatic tumor cells which showed decreased stiffness compared with the benign cells is significantly less than that of the normal cells [391]. Here, agreed with other reports, lower but not significant adhesion forces for T567D transfections were observed in this study. The less significance may be explained by our measurement methods which average the

mechanical properties. The adhesion forces is polarized distributed like Ezrin T567D. Another possibility is that fibroblast cells do not form much cell adhesion as they can migrate freely.

On the contrary, the results showed that inactive Ezrin T567A transfection which resulted in increased cell Young's modulus, showed decreased adhesion force instead. Furthermore, transfection of FERM domain which had no significant effect on cell stiffness also decreased adhesion force. It indicates a less strong relationship between cell stiffness and adhesion force. Regarding to the dominant negative FERM domain, the results showed that it had little effect on cell's mechanical properties, except reduced adhesion force and adhesion work.

Another parameter, adhesion work, was used in this study too, as it is very difficult to compare the results of adhesion force from different studies because the values of the adhesive force depend on the size and geometry of the tip. When the adhesion is generated by the interactions of large number of molecules at the region of contact between the tip and live cell, adhesion work becomes a more suitable parameter [392]. Again, similar effects of Ezrin T567D, Ezrin T567A and FERM domain on adhesion work were observed. Compared with wild type Ezrin, transfection of Ezrin T567D had lower but not significant adhesion work, while transfection of Ezrin T567A and FERM domain resulted in lower adhesion work.

5.3.3 Expression of Ezrin T567A reduces apparent viscosity

A previous report by Griffith and Pollard demonstrated that actin filaments have viscosity properties that are at least five times larger than those of microtubule, which means higher concentrations of actin will result in higher viscosity responses of the whole cell body [393]. Triggerred actin polymerization by high concentrations of colchicine have been reported to increase cell cortical tension as well as cellular viscosity in neutrophil cells [380]. What's more, the apparent viscosity of cells is used to determine the disease state of cells. It has been reported that cancer cells with high metastasis ability are tending to have lower elasticity modulus and apparent viscosity at the same time in comparison to normal cells [394]. Therefore, viscosity is also considered to be another hallmark for cancer progression. Different from other reports, results here demonstrated that Ezrin T567D which had decreased cortical stiffness and increased cytoskeleton stiffness showed little effect on apparent viscosity. Again these observation may rise from the polarized distribution of Ezrin T567D which result in polarized actin filament distribution in NIH 3T3 cells. Interestingly, Ezrin T567A expression had the ability to increase cell stiffness but at the same time decrease the apparent

viscosity. Organization of cell cytoskeleton affected by Ezrin mutant assessed in next chapter may explain these results. Otherwise, explore the effects of interruption of actin polymerization by drugs, like Cytochalasin D which binds to actin filaments or latrunculin A which binds to monomer actin, in transfected cells.

5.4 Summary

Together, mechanical properties were tested by AFM on cells expressing Ezrin and its mutants. It showed that Ezrin T567D had increased cytoskeleton stiffness and decreased cortical stiffness. Ezrin T567A is able to strengthen cytoskeleton but decrease viscosity and adhesion strength. At last, FERM domain had little effect. Mechanical changes due to different Ezrin mutations are summarized in Table 5.1.

Table 5.1: Summary of mechanical changes due to different Ezrin mutations in mechanical properties measured in this study. (+) indicates significant increase, (-) indicates significant decrease and (=) indicates no significant changes.

Biophysical parameter	T567D	T567A	FERM
Cortical stiffness	-	=	=
Cytoskeletal stiffness	+	+	=
Viscosity	=	-	=
Adhesion strength	=	-	-

Chapter 6

Effects of Ezrin and its mutants on cell cytoskeleton

6.1 Introduction

In the previous two chapters, the effects of transfection of Ezrin and its mutants on cell migration and cell mechanical properties were investigated. The results showed that active Ezrin T567D could enhance cell migration with its polarized cell rear distribution. In addition, AFM results demonstrated that transfection of Ezrin T567D softened the cell actin cortex but stiffened the cytoskeleton. As introduced before, Ezrin is a linking protein between cell membrane and actin cytoskeleton, changes in cell migratory capability and mechanical properties by Ezrin mutants should be related to actin conformation changes, which then affects cell migration and mechanical properties. Stella Hurtley pointed out in her 1998 editorial for Science that "Changes in the cytoskeleton are key, and even diagnostic, in the pathology of some diseases, including cancer" [395]. This means that all the changes observed in cell migration and cell mechanical properties could be explained by the changes in cell cytoskeleton. Because cytoskeleton not only spatially organizes the contents of the cell, but also connects the cell physically and biochemically to the external environment. What's more, it generates coordinated forces to enable the cell to move and change shapes [396]. Actin filaments, microtubules and intermediate filaments are three main types of cytoskeleton in cells. Among them, actin filaments have drawn the most attention due to their multiple cellular roles as well as their relationship with Ezrin. During cell migration, the formation of protrusions at the cell leading edge is driven by polymerization of actin filaments with two structures, filopodium and lamellipodium. Even though actin filaments are not the most rigid cytoskeleton, the

presence of high concentrations of actin binding proteins that bind actin filaments promotes the assembly of highly organized and stiff structures, which makes actin filament primarily responsible for cell stiffness. Ezrin is one of the actin binding proteins. Once activated, Ezrin is able to bind to actin filaments through its C-terminal domain. Through this connection, Ezrin regulates the formation of apical membrane structure. The whole cytoskeleton, actin filaments, microtubules and intermediate filaments work together to support normal cellular functions. So it was hypothesized that changes in the assembly of one particular cytoskeleton network will appear alongside with changes in assembly of all other networks [345]. As the three cytoskeleton could crosstalk through physical interaction or biological connection [286], it is thus of great significance to explore the changes of microtubules and intermediate filaments caused by Ezrin and its mutants. Therefore, the aim of this chapter is to investigate the effects of Ezrin and its mutants on cell cytoskeleton, including actin filaments, microtubules and vimentin, and find out how Ezrin regulates cell behaviours through the cytoskeleton. Vimentin, expressed mostly in normal fibroblast cells, was used in this study as intermediate filament. Moreover, nuclear properties were investigated at the same time.

6.2 Results

6.2.1 Ezrin antibody

Ezrin antibody was used to examine the distribution of the endogenous and exogenous Ezrin in transfected cells. Figure 6.1 shows that the signals of GFP and Ezrin antibody are overlapped. Also, Ezrin signal for non-transfected cells was found to be not strong enough to be visualized maybe due to the low exposure time and strong transfection signal. On the other hand, through the DAPI channel, the non-transfected cells near the transfected cells could be identified. A previous study using a similar transfection strategy but a different cell line stated that the expression levels of exogenous ezrin are at least an order of magnitude larger than those of endogenous ezrin, thus likely ruling out the fact that the endogenous protein may have a strong influence on the observed behavior after transfection [35]. Altogether, the results indicate that in transfected NIH 3T3 cells, the amount of exogenous Ezrin is much larger than that of endogenous Ezrin.

The Ezrin antibody bought from SantaCruz was raised against amino acids from 362 to 585. And FERM domain only contains the first 300 amino acids in the N-terminal domain. Therefore, in cells expressing FERM domain, this antibody

was not able to recognize the transfected FERM domain.

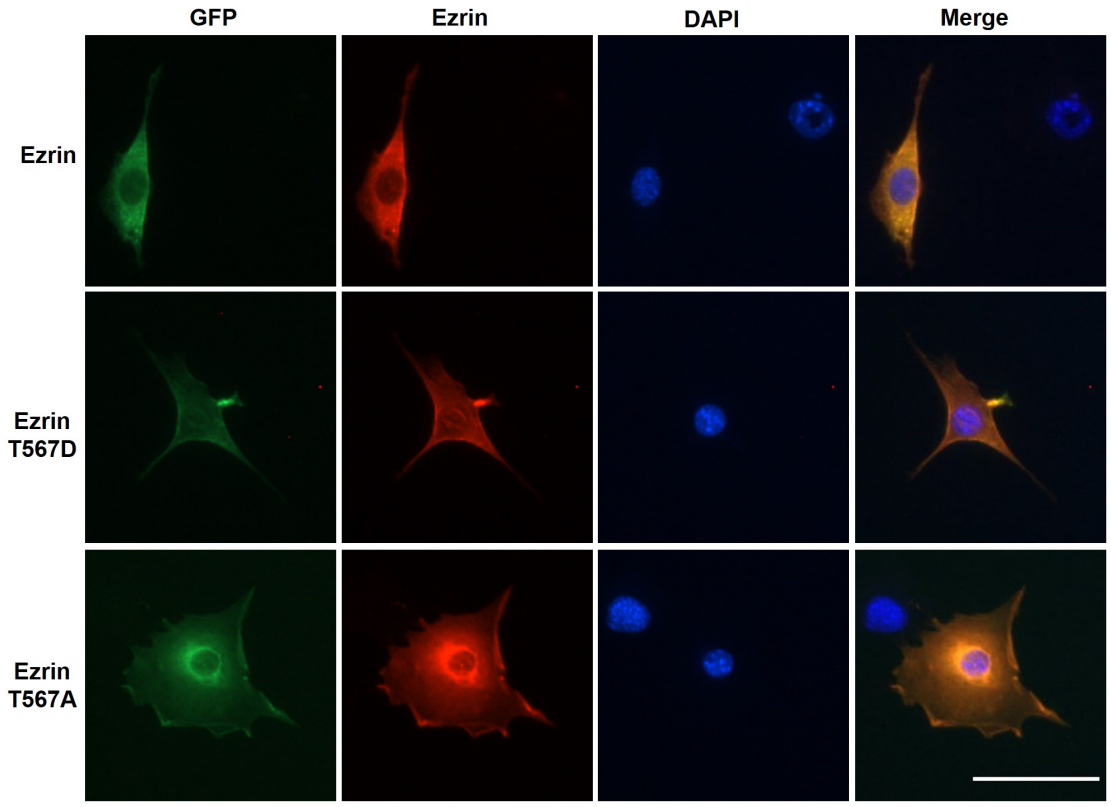

Figure 6.1: Fluorescent images of transfected cells co-stained with Ezrin antibody and DAPI. Left: transfected cells expressing Ezrin mutants coupled with GFP; 2nd column: Ezrin stained with Ezrin antibody; 3rd column: cell nuclear stained with DAPI; right: merged images for the three channels. Scale bar: 50 μm.

Next the fluorescent images of transfected cells for both GFP and Ezrin staining channels were analyzed for the quantification of the amount of exogenous Ezrin and total amount of Ezrin expressed inside the cells. Instead of comparing population averages, single-cells data according to exogenous Ezrin expression were pooled together. Total Ezrin expression as a function of Ezrin transfection was plotted (Figure 6.2). By fitting the plot, the amount of exogenous wild type Ezrin relative to endogenous Ezrin was estimated to be about 6-fold from the quantification, 8-fold for active Ezrin T567D relative to endogenous Ezrin and 18-fold for inactive Ezrin T567A. In agreement with the immunostaining results, cells expressed much larger amount of exogenous Ezrin than endogenous Ezrin.

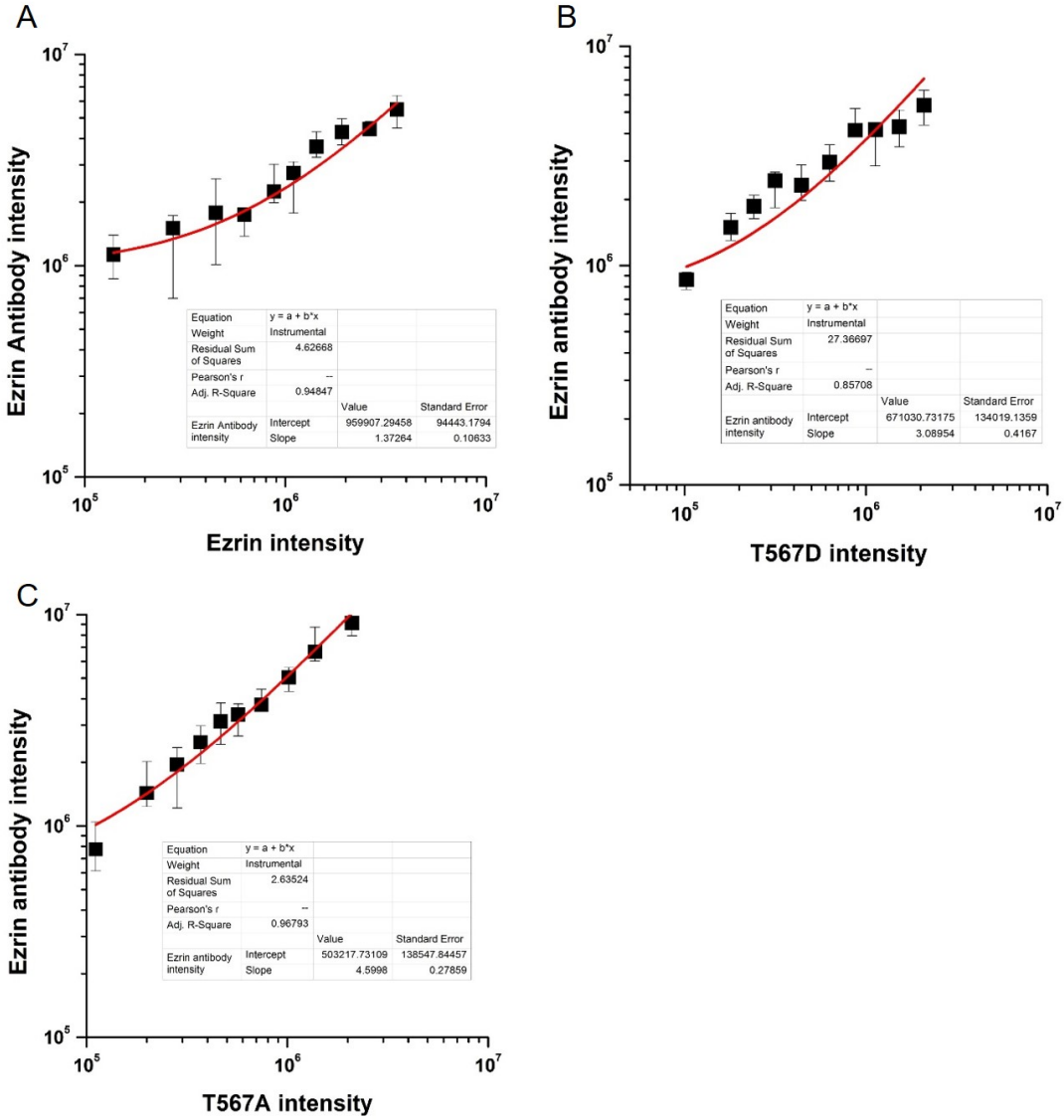

Figure 6.2: Comparison of transfected Ezrin with total Ezrin. Plots show the relationship between transfected wild type Ezrin (A), active Ezrin T567D (B) and inactive Ezrin T567A (C), and the total Ezrin including endogenous and exogenous Ezrin from antibody results. Values for more than 20 cells were pooled to compute each individual data point. Data is on a logarithmic scale with base 10 and presented as geometric mean, while error bars indicate interquartile range (Q1–Q3). Fit lines correspond to a linear model. Endogenous Ezrin intensity is intercept of the equation when exogenous Ezrin is not expressed. Exogenous Ezrin intensity is calculated by mean of total Ezrin intensity subtracted by endogenous Ezrin intensity.

6.2.2 The effect of Ezrin mutants on cell morphology

As shown previously that different Ezrin mutants were associated with different intracellular localization. Here the focus is to understand the effect of this local-

ization on cell morphology and actin cytoskeleton. To achieve that in this study, transfected NIH 3T3 cells were seeded at very low density in unrestricted spreading condition and then immunostained with phalloidin. Fluorescent images of channels for Ezrin mutants, the actin cytoskeleton and cell nucleus were taken by epifluorescence microscope as shown in Figure 6.3. The intracellular distribution patterns of Ezrin and its mutants are in line with those previously measured in the migration experiments (Figure 6.3). Active Ezrin T567D is polarized concentrated on the cell membrane, which appears to be at the cell rear. When moving to actin filament signal, the concentrated Ezrin T567D is found to be colocalized with actin filaments. Conversely, wild type Ezrin and inactive Ezrin T567A is found to be localized in the cytoplasm with some more wild type Ezrin and Ezrin T567A concentrated around the nucleus. It is possible when Ezrin is inactive, it has other functions related to nucleus. Or, the nuclear distribution may be due to the limitations of Epifluorescence microscope that the total signals of the cell are displayed. Interestingly, it is obvious that signals of actin filaments are quite weak at the places where wild type Ezrin and Ezrin T567A concentrate, which suggests that like inactive Ezrin T567A, wild type Ezrin in the cytoplasm was not activated. On the other hand, FERM domain is found to be distributed throughout the whole cytoplasm even inside the nucleus.

Next, the fluorescent images were analyzed by our quantification pipeline, which can output information about cell morphology and actin fiber organization. Figure 6.4 illustrates the comparison of three morphological parameters, cell area (Figure 6.4A), aspect ratio (Figure 6.4B) and stellate factor (Figure 6.4C), respectively, in cells transfected with Ezrin and its mutants. Firstly, it can be observed that transfection of active Ezrin T567D and FERM domain reduces the cell areas, while transfection of inactive Ezrin T567A has no significant effect on cell size (Figure 6.4A). Secondly, compared with wild type Ezrin, all the Ezrin mutants are able to increase cell aspect ratio, with FERM domain being the most significant one (Figure 6.4B). Furthermore, cells transfected with Ezrin T567D, Ezrin T567A and FERM domain all have larger stellate factor (Figure 6.4C) than the control, which reflects the tendency of cells to extend protrusions such as blebs, lamellipodia or filopodia. In summary, these results have clearly shown that transfection of all Ezrin mutants affects cell morphology but at various levels.

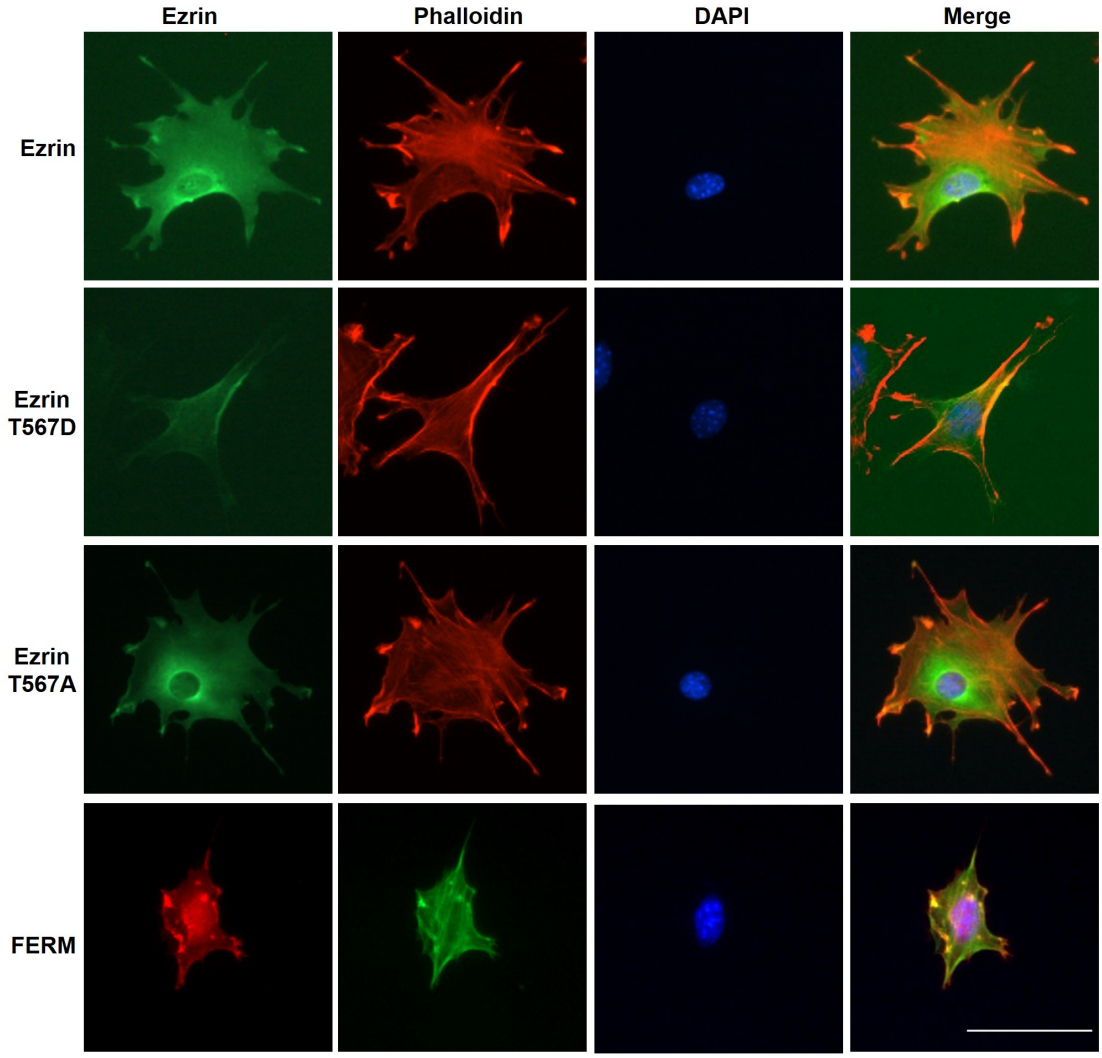

Figure 6.3: The effect of Ezrin and its mutants on cell morphology. Fluorescent images of transfected cells subsequently stained with phalloidin and DAPI. Left: transfected cells expressing Ezrin mutants coupled with GFP or RFP; 2nd column: actin filament stained with phalloidin; 3rd column: cell nucleus stained with DAPI; right: merged images for the three channels. Scale bar: 50 μm.

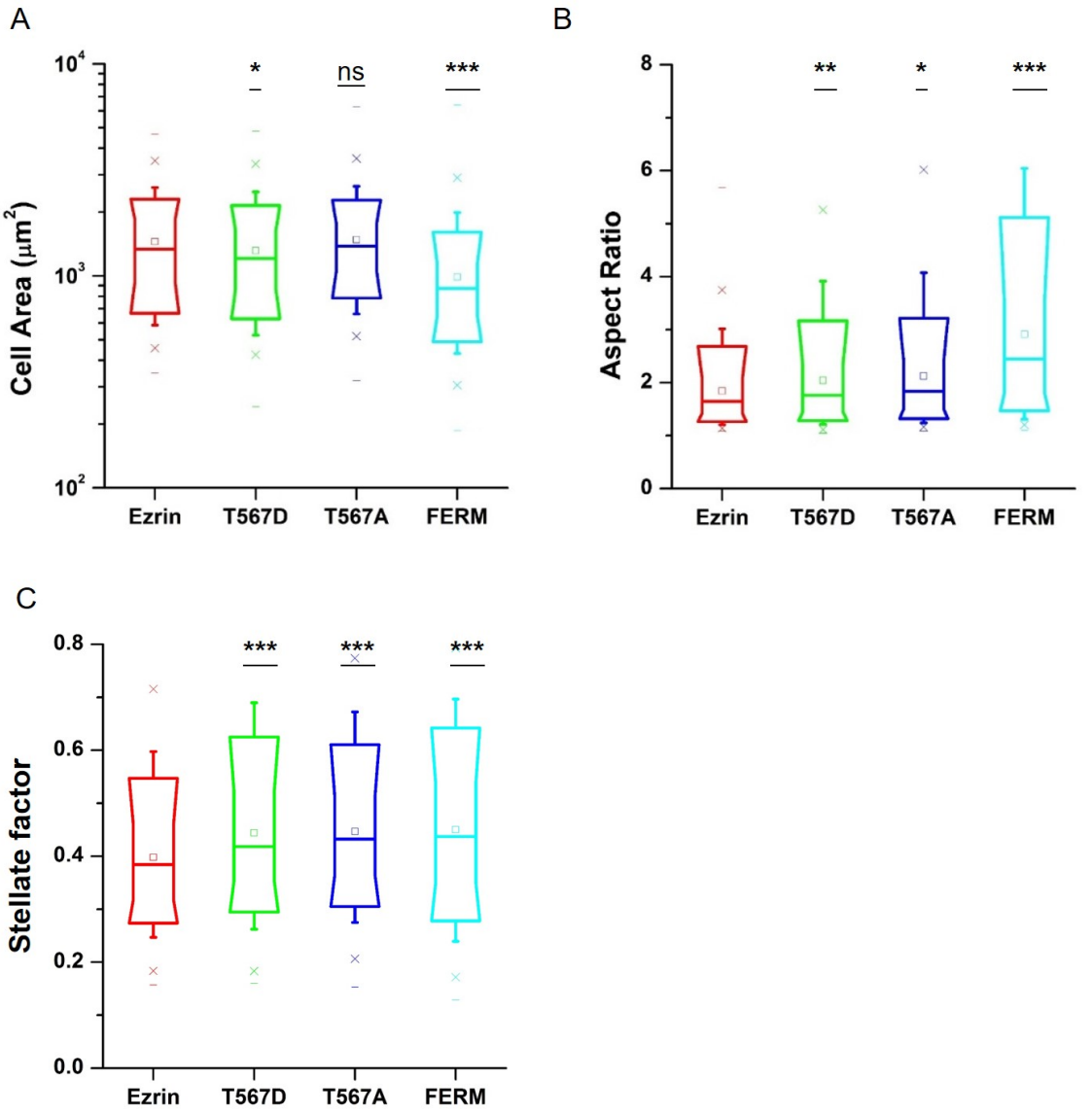

Figure 6.4: Effect of Ezrin and its mutants on cell morphology parameters. Box plots show the results of cell area (A), aspect ratio (B) and stellate factor (C). n=420 (Ezrin), n=496 (Ezrin T567D), n=1235 (Ezrin T567A), n=562 (FERM) cells were analyzed. Asterisks indicate a statistical difference (* $p<0.05$, ** $p<0.01$, *** $p<0.001$, as obtained using Dunnett test against wild type Ezrin).

6.2.3 The effect of Ezrin mutants on actin cytoskeleton

Single-cell data of different transfection was pooled together and the parameters related to actin cytoskeleton organization were compared at the population level. On the whole, the results clearly show that the Ezrin mutants not only affect the properties of actin filaments (Figure 6.5) which is related to fiber amount and shape, but also change the micro-organization of actin filaments (Figure 6.6) which is the relative positioning of the actin filaments within cells.

Transfection with active Ezrin T567D only induces thicker actin fibers (Figure 6.5D), but has no significant effect on other parameters. On the other hand, cells transfected with inactive Ezrin T567A promotes actin filament assembly (Figure 6.5A), and at the same time, elongates the fiber length (Figure 6.5B). It is worth noting that cells expressing FERM domain have larger impact on actin filaments compared with the results of cell migration and mechanical properties. Even though it did not change the amount of the assembled actin filaments, FERM domain promotes actin filaments organizing into longer and thicker fibers.

Then moving to the results for actin filament micro-organization, compared with wild type Ezrin, Ezrin mutants also have different effects. Firstly, actin fiber in active Ezrin T567D transfected cells is more spread (Figure 6.6A), with the fiber peak locating near the nucleus (Figure 6.6D). On the other hand, inactive Ezrin T567A has little effect on actin filament micro-organization except from fiber chirality. Figure 6.6E shows that the value of chirality measurement is close to 90°, meaning that actin filaments are oriented parallel to the cell edge. Similar with the actin filament properties results, transfection of FERM domain changes the actin filament micro-organization dramatically as well. Cells transfected with FERM domain have more spread actin fibers (Figure 6.6A), with the peak near the nucleus (Figure 6.6D). What's more, actin filaments are organized more aligned (Figure 6.6B) and oriented parallel to the cell edge (Figure 6.6E). In summary, this data evidences that transfection of Ezrin mutants has a great impact on both the properties and micro-organization of actin filaments.

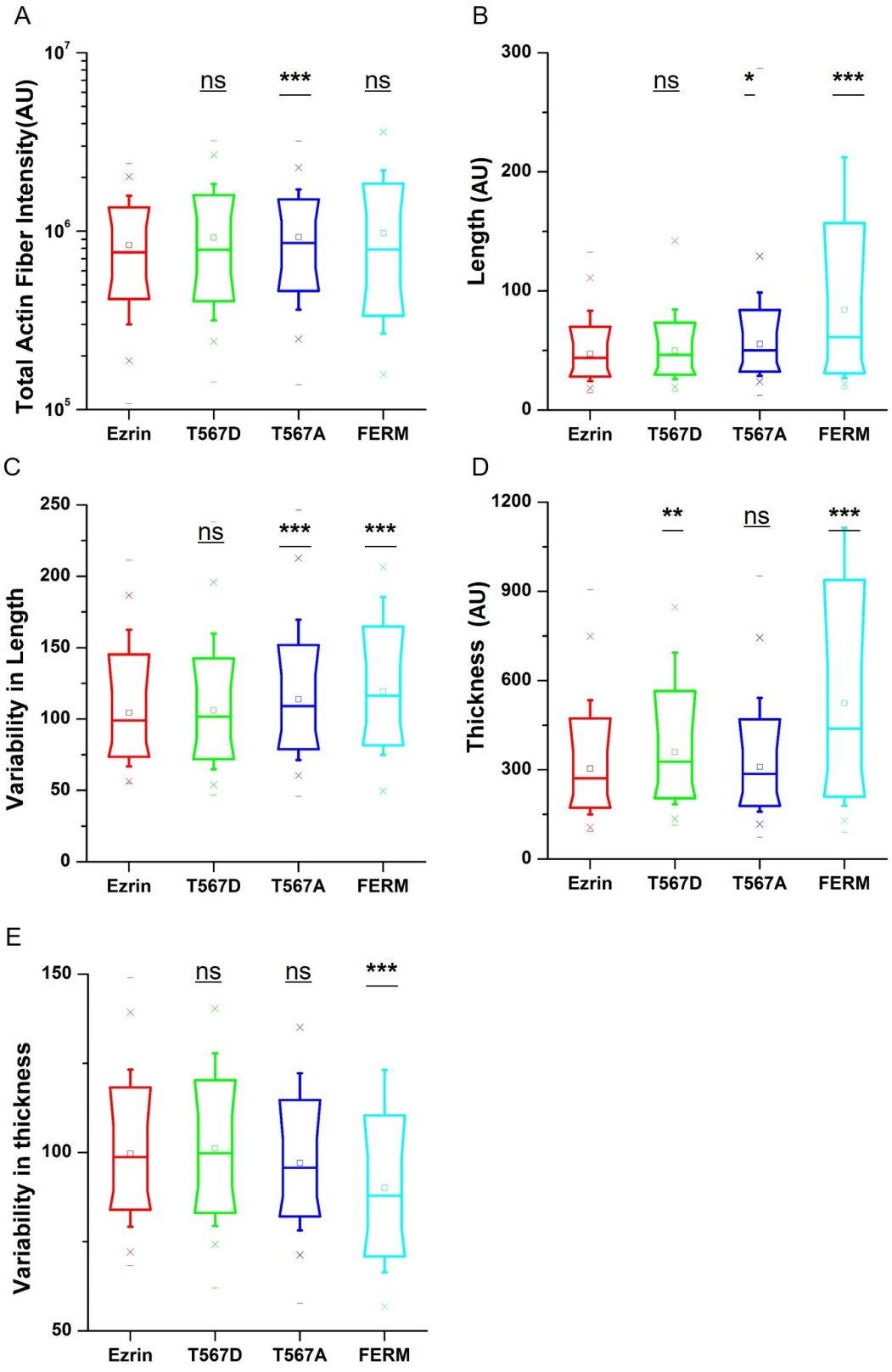

Figure 6.5: Effect of Ezrin and its mutants on actin filament properties. Box plots show the results of total actin fiber intensity (A), fiber length (B), variability in fiber length (C), fiber thickness (D) and variability in fiber thickness (E). n=420 (Ezrin), n=496 (Ezrin T567D), n=1235 (Ezrin T567A), n=562 (FERM) cells were analyzed. Asterisks indicate a statistical difference (* $p<0.05$, ** $p<0.01$, *** $p<0.001$, as obtained using Dunnett test against wild type Ezrin).

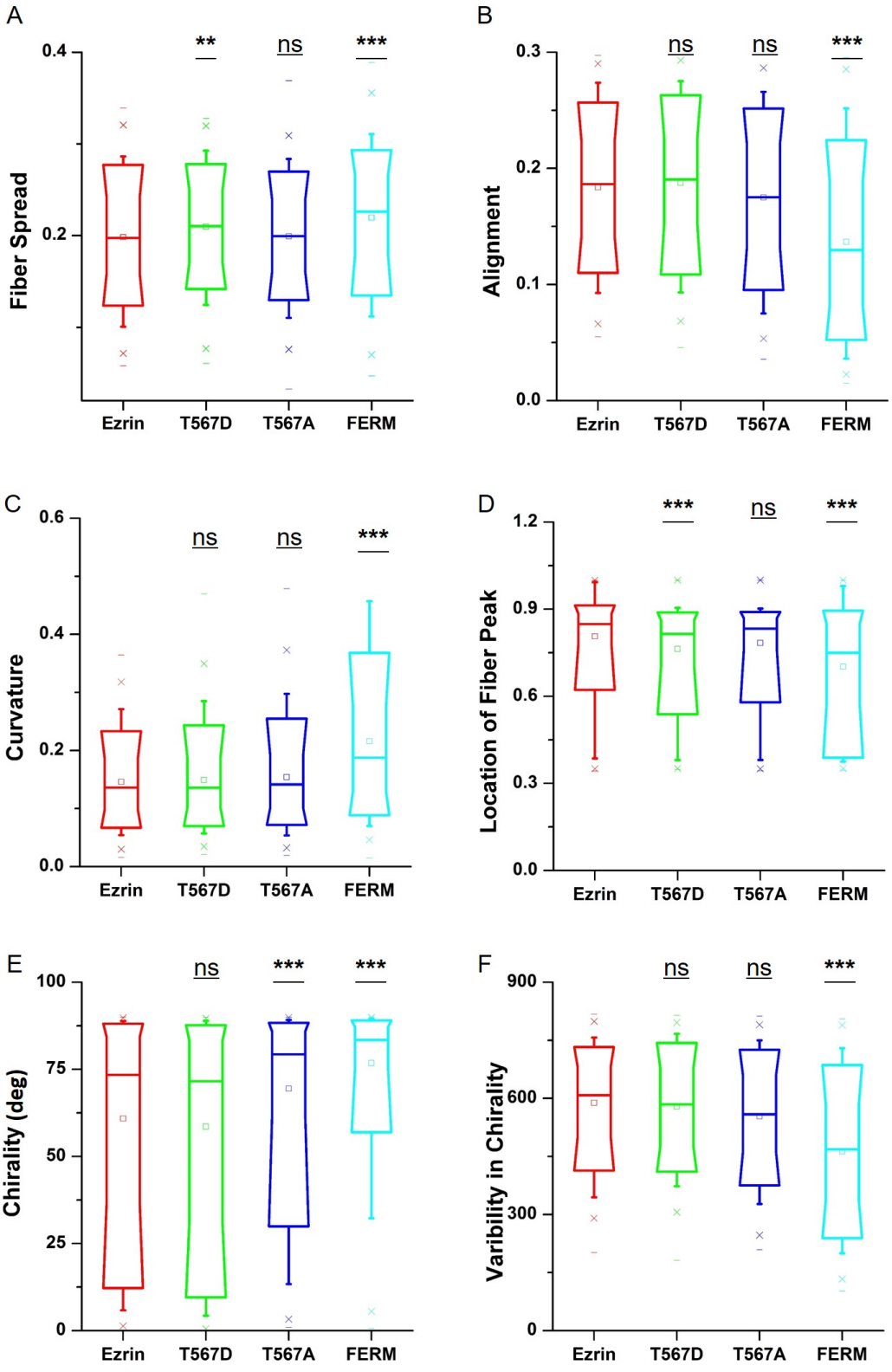

Figure 6.6: Effect of Ezrin and its mutants on actin filament organization. Box plots show the results of fiber spread (A), alignment (B), curvature (C), location of fiber peak (D), chirality (E) and variability in chirality (F) . n=420 (Ezrin), n=496 (Ezrin T567D), n=1235 (Ezrin T567A), n=562 (FERM) cells were analyzed. Asterisks indicate a statistical difference (* $p<0.05$, ** $p<0.01$, *** $p<0.001$, as obtained using Dunnett test against wild type Ezrin).

6.2.4 The effect of Ezrin mutants on tubulin cytoskeleton

Having estimated the detailed influence of Ezrin mutants on cell morphology and actin filaments, the role of Ezrin mutants on microtubule networks is then investigated. By replacing phalloidin staining with antibody against tubulin, transfected cells were stained with microtubules as shown in Figure 6.7. Unlike the effects on actin filaments that every Ezrin mutant has its own actin filament structure, microtubules were observed with similar structure regardless of different transfection. The microtubules form a dense network, starting from the nuclear vicinity, presumably the centrosome complex, and spreading randomly through the cytoplasm of the cell. Due to the overlap of microtubules running in different directions, microtubules of the center part are thicker and denser than those in the periphery where individual lines are easily seen at high magnifications.

Figure 6.8 shows that effect of Ezrin and its mutants on microtubule properties. Surprisingly, transfection of active Ezrin T567D and inactive Ezrin T567A have weak effect on tubulin fiber assembly, fiber length and fiber thickness (Figure 6.8A, B,and D), except that inactive Ezrin T567A increases the variability of fiber length and fiber thickness (Figure 6.8C and E). On the other hand, cells expressing FERM domain exhibit distinctively with other transfection. Transfection of FERM domain increases tubulin fiber assembly (Figure 6.8A), followed by longer and thicker tubulin fibers (Figure 6.8B and D) as well as increased variability of fiber length and fiber thickness (Figure 6.8C and E). These could be explained by the fact that huge changes of actin filaments caused by transfection of FERM domain are able to transfer to the microtubules via the crosstalk between them.

Next set of parameters describing the micro-organization of microtubules is shown in Figure 6.9. In cells expressing active Ezrin T567D, tubulin fibers are more spread across the cells (Figure 6.9A). Having similar effects on fiber spread with active Ezrin T567D, inactive Ezrin T567A also has the fiber peak more closely to the cell periphery (Figure 6.9D). Again, in consistent with the effect on microtubule properties, FERM domain changes the microtubule micro-organization significantly. Firstly, tubulin fibers in FERM domain transfected cells are more spread and the location of fiber peak is near the cell edge (Figure 6.9A and D). Furthermore, the fibers are more aligned and the orientation of the fiber is parallel to the cell edge with chirality value near 90° (Figure 6.9B and E).

In summary, these results suggest that Ezrin and its mutants also have marked effects on microtubule microstructure. It is possibly mainly because the effects of Ezrin and its mutants on actin filaments could extend to microtubules through the crosstalk between the actin filaments and microtubules.

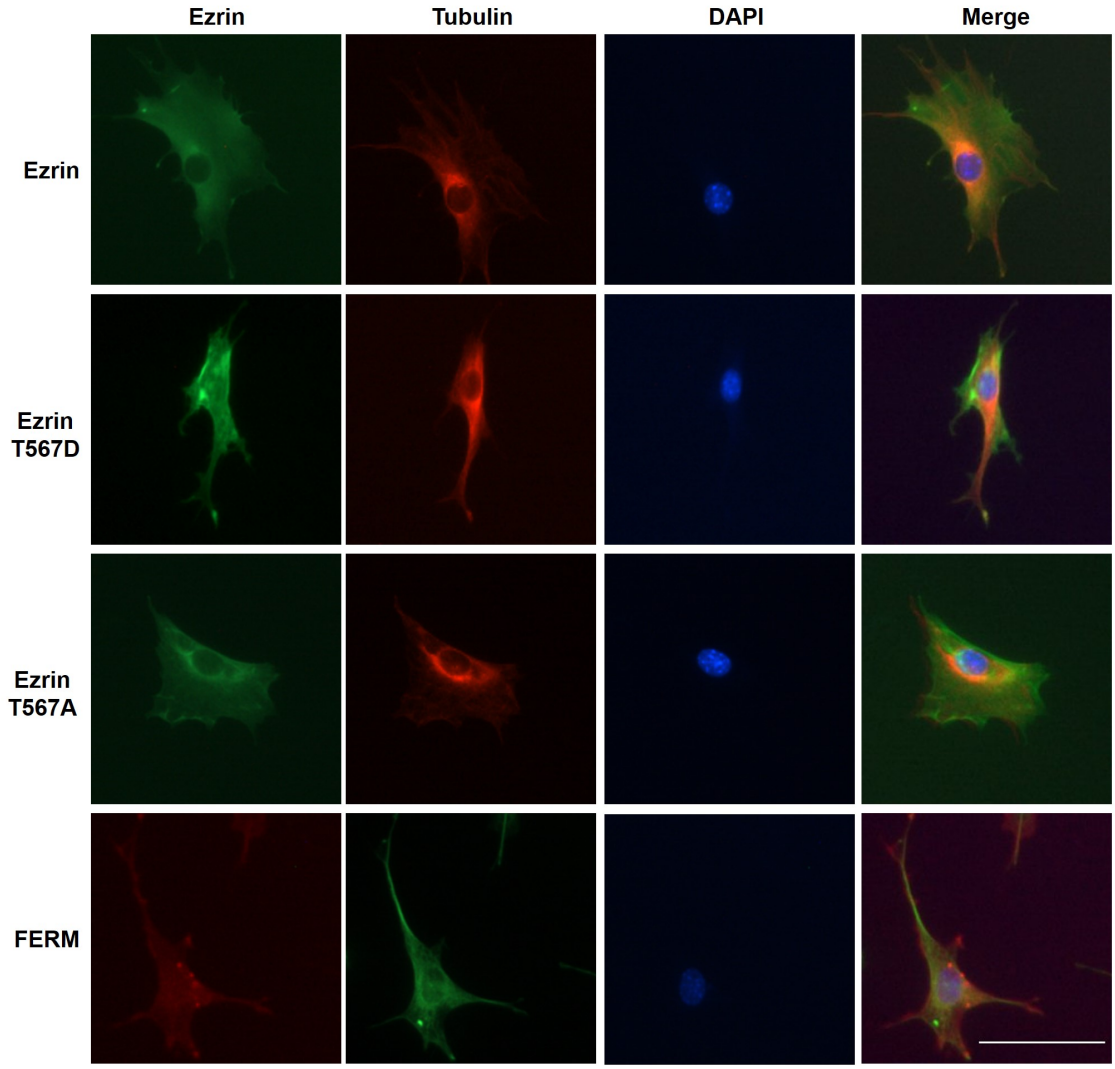

Figure 6.7: Example images of cells transfected with Ezrin and its mutants stained with tubulin. Left: transfected cells expressing Ezrin mutants coupled with GFP or RFP; 2nd column: microtubules stained with tubulin antibody; 3rd column: cell nucleus stained with DAPI; right: merged images for the three channels. Scale bar: 50 μm.

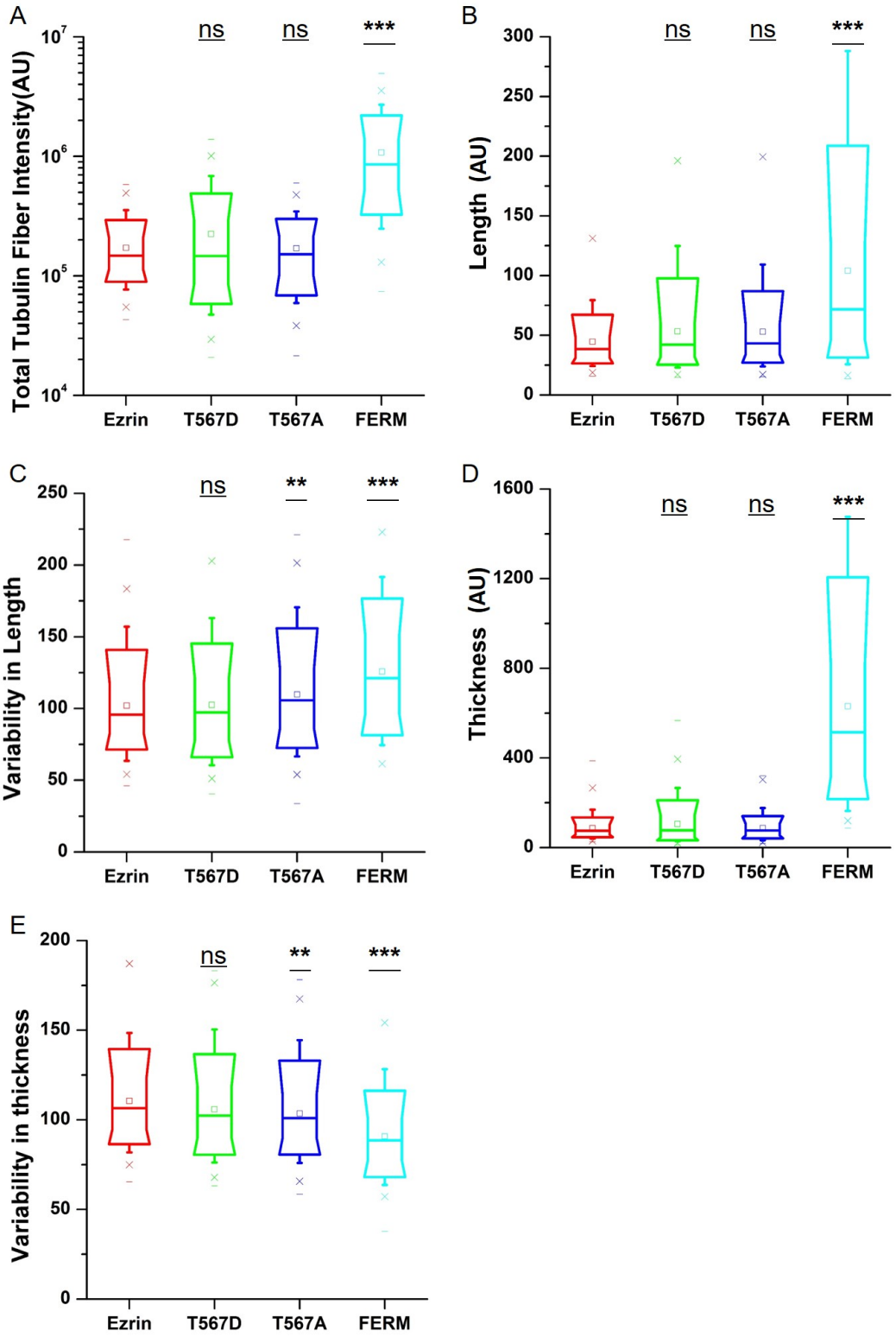

Figure 6.8: Effect of Ezrin and its mutants on microtubule properties. Box plots show the results of total tubulin intensity (A), fiber length (B), variability in fiber length (C), fiber thickness (D) and variability in fiber thickness (E). n=559 (Ezrin), n=578 (Ezrin T567D), n=526 (Ezrin T567A), n=408 (FERM) cells were analyzed. Asterisks indicate a statistical difference (* $p<0.05$, ** $p<0.01$, *** $p<0.001$, as obtained using Dunnett test against wild type Ezrin).

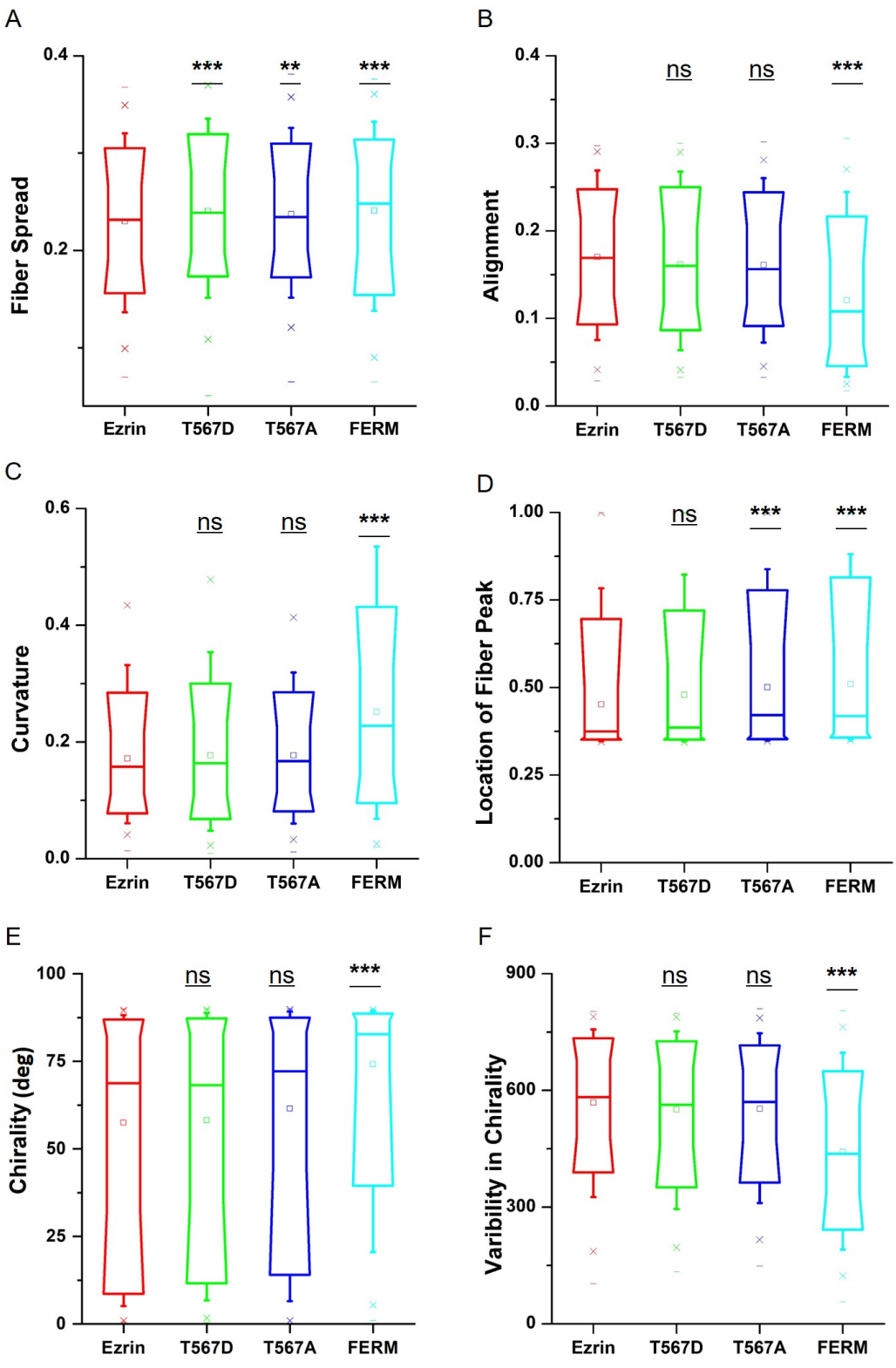

Figure 6.9: Effect of Ezrin and its mutants on microtubule organization. Box plots show the results of fiber spread (A), alignment (B), curvature (C), location of fiber peak (D), chirality (E) and variability in chirality (F) . n=559 (Ezrin), n=578 (Ezrin T567D), n=526 (Ezrin T567A), n=408 (FERM) cells were analyzed. Asterisks indicate a statistical difference (* $p<0.05$, ** $p<0.01$, *** $p<0.001$, as obtained using Dunnett test against wild type Ezrin).

6.2.5 The effect of Ezrin mutants on vimentin cytoskeleton

The effects of Ezrin mutants on one of intermediate filaments, which is vimentin, were also explored by replacing the antibody against tubulin by antibody against vimentin. The fluorescent images of cells transfected with Ezrin and its mutants stained with vimentin were taken by epifluorescence microscope as shown in Figure 6.10. Similar to the distribution of microtubules, it is obvious that vimentin is more concentrated near the cell center than cell periphery. Maybe it is because the 20x objective could reveal more detailed information.

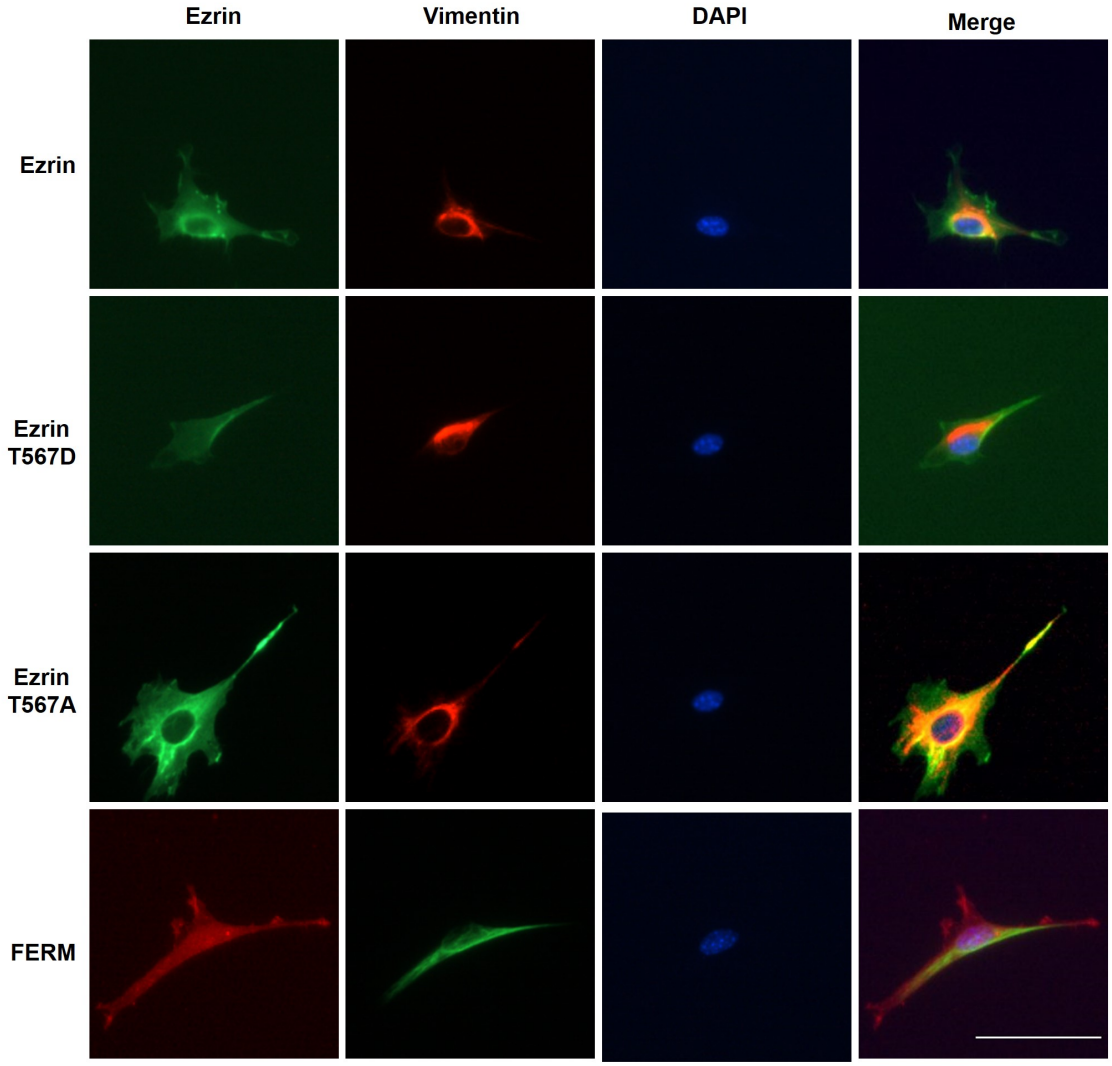

Figure 6.10: Example images of cells transfected with Ezrin and its mutants stained with vimentin. Left: transfected cells expressing Ezrin mutants coupled with GFP or RFP; 2nd column: vimentin stained with vimentin antibody; 3rd column: cell nucleus stained with DAPI; right: merged images for the three channels. Scale bar: 50 μm.

When assessing the vimentin fiber properties, active Ezrin T567D is found to be able to increase the vimentin fiber length and variability in fiber length (Figure

6.11B and C), but it has no significant effect on other parameters. Similar results are obtained for inactive Ezrin T567A (Figure 6.11). The strong influence of dominant negative FERM domain is applicable to vimentin as well. FERM domain promotes vimentin fiber assembly (Figure 6.11A), followed by increasing the fiber length (Figure 6.11B), fiber thickness (Figure 6.11D) as well as the variability of fiber length (Figure 6.11C). As predicated, with regard to the parameters for vimentin micro-organization, active Ezrin T567D and inactive T567A have no significant effects (Figure 6.12), except that Ezrin T567A promotes the assembly of more aligned vimentin fibers (Figure 6.12B) and increases the variability of chirality (Figure 6.12F). In contrast, cells expressing FERM domain have more spread vimentin fibers (Figure 6.12 D), with increased alignment (Figure 6.12 B).

In summary, Ezrin mutants have pronounced effects on actin, tubulin and vimentin structure, with paralleled effect, e.g. transfection of FERM domain increases the fiber intensity of actin filament, tubulin and vimentin at the same time. It is also suggested that all the three types of cytoskeleton have their own functions and are not independent as they could affect one another through crosstalk.

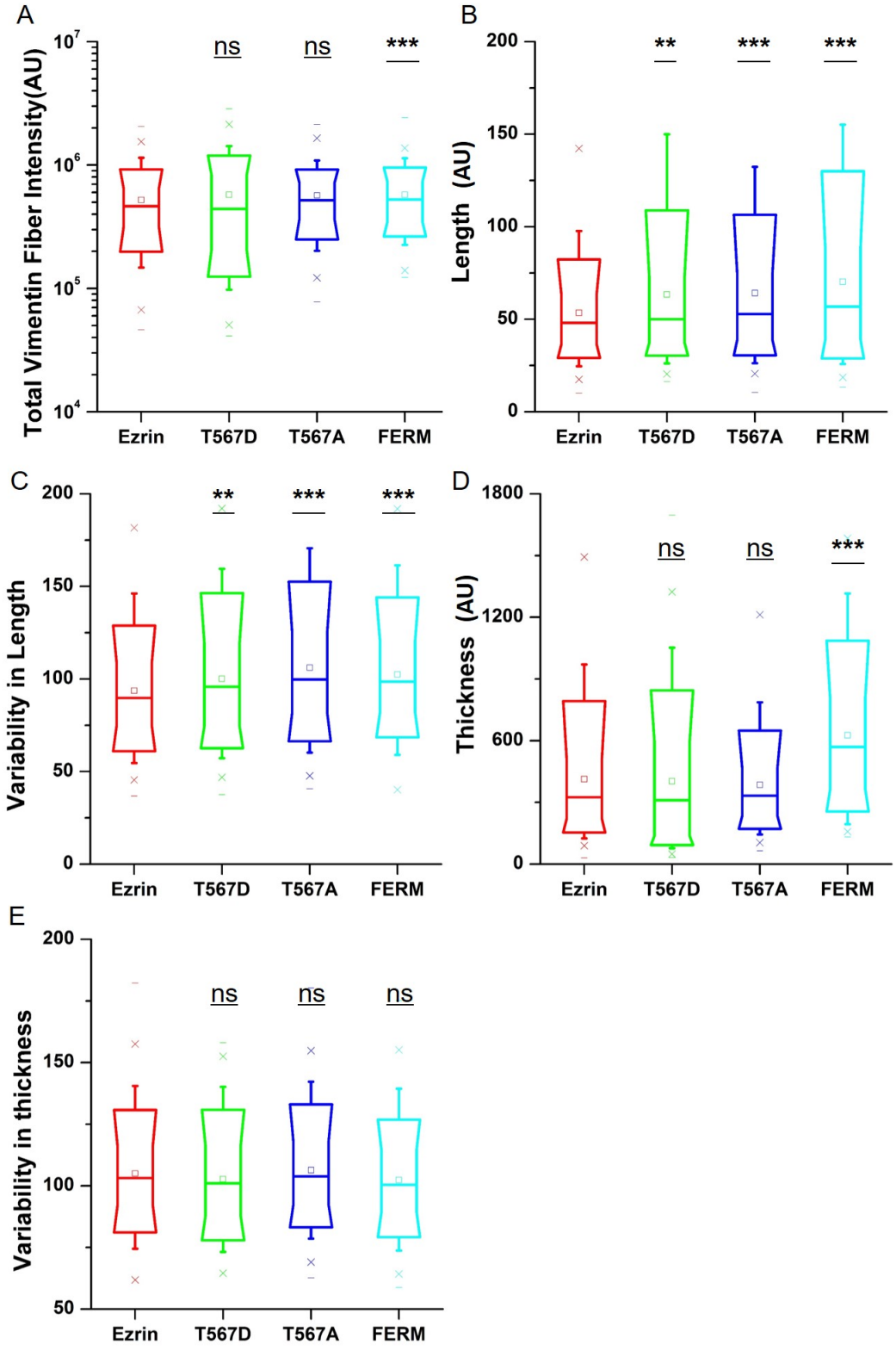

Figure 6.11: Effect of Ezrin and its mutants on vimentin properties. Box plots show the results of total vimentin intensity (A), fiber length (B), variability in fiber length (C), fiber thickness (D) and variability in fiber thickness (E). n=585 (Ezrin), n=424 (Ezrin T567D), n=768 (Ezrin T567A), n=425 (FERM) cells were analyzed. Asterisks indicate a statistical difference (* $p<0.05$, ** $p<0.01$, *** $p<0.001$, as obtained using Dunnett test against wild type Ezrin).

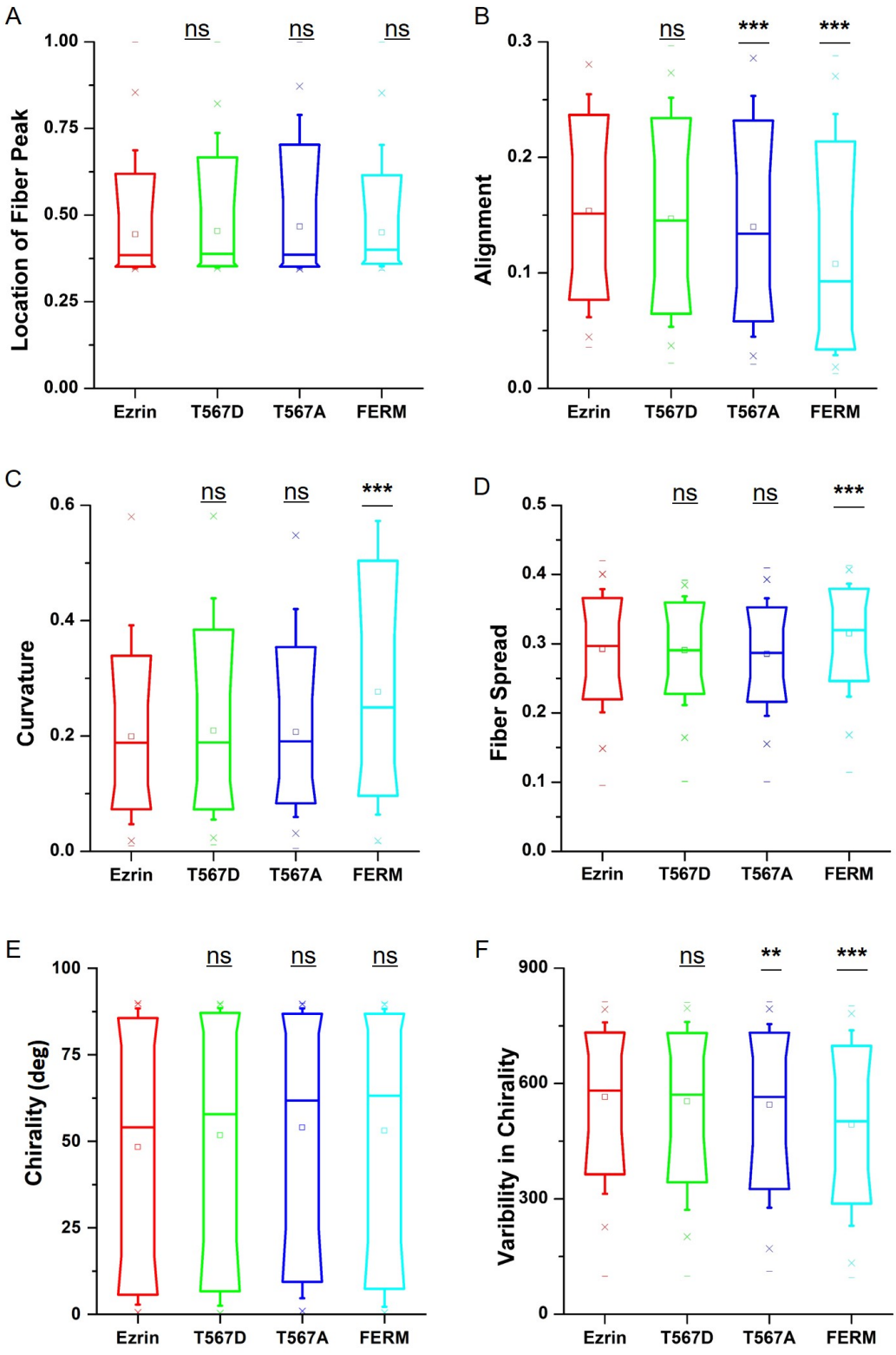

Figure 6.12: Effect of Ezrin and its mutants on vimentin organization. Box plots show the results of fiber spread (A), alignment (B), curvature (C), location of fiber peak (D), chirality (E) and variability in chirality (F) . n=585 (Ezrin), n=424 (Ezrin T567D), n=768 (Ezrin T567A), n=425 (FERM) cells were analyzed. Asterisks indicate a statistical difference (* $p<0.05$, ** $p<0.01$, *** $p<0.001$, as obtained using Dunnett test against wild type Ezrin).

6.2.6 The effect of Ezrin mutants on nucleus properties

The nucleus, as the largest and stiffest organelle in cells, is highly dynamic by biologically undertaking gene transcription and duplication and mechanically changing all the time to adapt to the external environment. It is assumed that all the changes observed outside the nucleus, such as motility ability, mechanical properties and cell cytoskeleton, could also result in changes of nuclear state. Parameters of nucleus have also been quantified to help understand the mechanical connection between the nucleus and the cytoskeleton.

Figure 6.13 shows that the effects of Ezrin and its mutants on nuclear state, including brightness, chromatin condensation, relative nuclear volume, Poisson's ratio and apparent nuclear stiffness. Firstly, there is no significant difference in nuclear brightness stained with DAPI (Figure 6.13A), suggesting that all the experiments were consistent regardless of different treatments. Both active Ezrin T567D and inactive Ezrin T567A increase the chromatin condensation (Figure 6.13B). In addition, nuclear volume is significantly increased for T567D transfection, which indicates a stronger transmission of intracellular tension to nucleus (Figure 6.13C). On the contrary, T567A and FERM transfection leads to significant reduction in nuclear volume. When assessing the Poisson's ratio of the nucleus, nucleus in all conditions are found to display auxetic properties, which was significantly enhanced for Ezrin T567D transfection and reduced in Ezrin T567A and FERM transfection (Figure 6.13D). In the end, nuclear stiffness is compared with T567D transfection increasing nuclear stiffness and FERM transfection decreasing the stiffness (Figure6.13E). Our previous work has shown that cell spread area modulates nuclear volume and nuclear mechanical properties [345]. However, the results obtained from this study did not follow the same trend. The reason is not known yet but one possible explanation is that the transfection of different Ezrin mutants has other effect that would affect nuclear state.

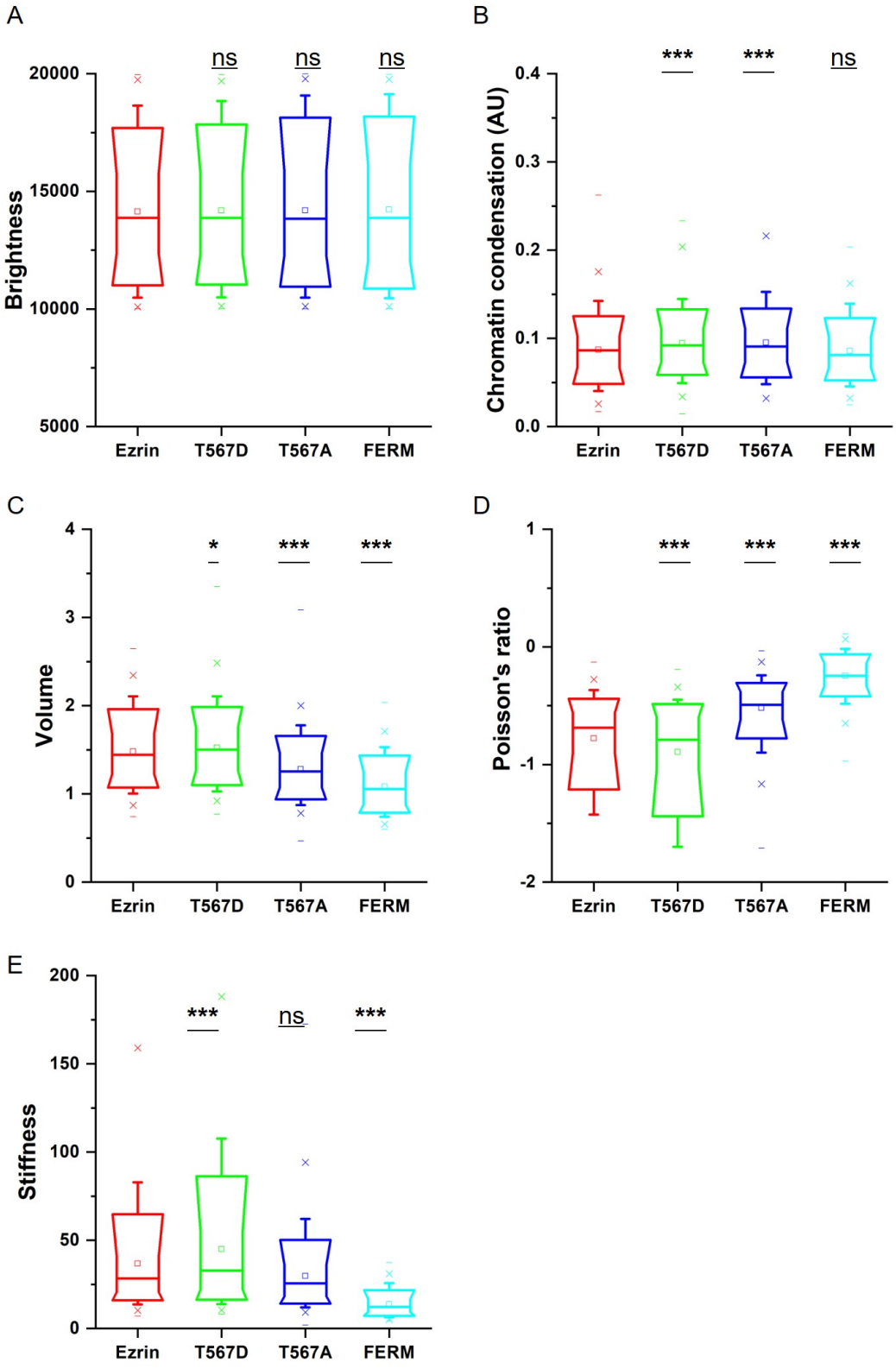

Figure 6.13: Effect of Ezrin and its mutants on nuclear properties. Box plots show the results of brightness (A), chromatin condensation (B), volume (C), poisson's ratio (D) and stiffness (E). n=803 (Ezrin), n=720 (Ezrin T567D), n=2153 (Ezrin T567A), n=562 (FERM) cells were analyzed. Asterisks indicate a statistical difference (* $p<0.05$, ** $p<0.01$, *** $p<0.001$, as obtained using Dunnett test against wild type Ezrin).

6.3 Discussion

In this chapter, the effects of Ezrin and its mutants on cell morphology, three cytoskeleton, including actin filament, microtubules and vimentin, and nuclear properties have been investigated.

6.3.1 Ezrin plasmids were confirmed by antibody

Firstly, antibody against endogeous and exogenous Ezrin was used to confirm the plasmids transfected in this study were correct. The results confirmed that signals of fluorescent staining against Ezrin and transfected Ezrin and its mutants were overlapped, which means the right plasmids were used. Also distribution patterns of transfected Ezrin and its mutant are different from each other, with Ezrin T567D accumulating at the cell rear, wild type Ezrin and Ezrin T567A in cell cytoplasm and FERM domain all over the cell. If funding and time permitted, it is better to do western blotting to ensure that all expression plasmids were not degraded when expressed in NIH 3T3 cells. Because western blotting can not only detect the studied protein specifically, but also output the molecular weight of proteins in case the degradation happens. Moreover it has been reported that cells transfected with full-length Ezrin expressing two GFP-tagged products corresponding to full-length and endogenously cleaved forms [369]. The signal of endogenously cleaved forms, which is the N-terminal Ezrin, is all over the cell even in the nuclear. Same results were seen in cells expressing FERM domain.

Moreover, the statistics Ezrin revealed that cells expressed much more exogenous than endogenous Ezrin. In order to exclude the effects of overexpression, lentivirus transfection could be used to generate stable cell lines expressing Ezrin and its mutants. Cells expressing certain amount of exogenous protein could be selected by fluorescence-activated cell sorting (FACS). Additionally, to rule out the possibility that endogenous Ezrin may have other effects on the experiments, siRNA could be used to knocked out the endogenous Ezrin. Cells without endogenous Ezrin are selected to transfect Ezrin and its mutants for all the tests.

6.3.2 Morphology effect of Ezrin mutant

Cell migration is fundamental to establishing and maintaining the proper organization of multicellular organisms. Morphogenesis can be viewed as a consequence, in part, of cell locomotion [397]. Corresponding to its high migratory ability, cells

transfected with active Ezrin T567D exhibited elongated cell shape, which means large aspect ratio. Also cells expressing Ezrin T567D formed more cell protrusions required for cell migration, like lamellipodium, which is reflected by larger stellate factor. Cell area changes for individual cells as they migrate, with membrane extensions at the leading edge and retraction of the rear cyclically increasing and decreasing the spreading area [398]. On the average, a decreased cell area was found in this study as compared with cell with less motility. Another reason for the decreased cell area is that phosphorylated Ezrin inhibit cell adhesion, reducing the spreading area [399]. On the contrary, even though cells transfected with inactive Ezrin T567A and FERM domain have larger aspect ratio and stellate factor, it is still an indication of global weakening of the cortex-membrane connection. Because cells expressing Ezrin T567A could form cell protrusions moving at same place as shown previously but they did not polarize to form leading edge for migration. Cells expressing FERM domain prefer to form filopodia instead of lamellipodium.

6.3.3 Ezrin T567D moderate strengthens the cytoskeleton

Alterations in the biomechanical properties and migrating ability of cells have been correlated with changes in their organization of cytoskeleton. Results of effects of Ezrin mutant on cytoskeleton closely paralleled the results of migration and mechanical properties. The main effects of Ezrin T567D and Ezrin T567A on cell migration, cell mechanical properties and cell cytoskeleton are summarized in Figure 6.14 and Figure 6.15.

Firstly, all the results suggest that active Ezrin T567D has moderate impact on cell cytoskeleton in comparison to wild type Ezrin, such as same total actin fiber intensity, increased actin fiber thickness, more spread actin and tubulin fibers, and increased vimentin fiber length. The hypothesis is that moderate strengthened the cytoskeleton would promote cell migration as cytoskeleton is needed in cell migration. However, like cells transfected with inactive Ezrin T567A and FERM domain, huge strengthened cytoskeleton would result in slow migration as the turnover speed would reduce for longer and thicker fibers. What's more, cells treated with Cytochalasin D or Jasplakinolide resulting in disassembled stress fibers or stabilized stress fibers are reported to display impaired migration ability [400, 401].

Our group has reported the relationship between cell stiffness and stress fiber amount, revealing that a strong correlation between stress fiber amount and stiffness of the cytoskeleton. The spatial distribution of stress fiber, such as fiber

location, alignment and fiber thickness, had weaker effect on cell stiffness [338]. Agreed with this report, the amount of actin stress fiber in cells expressing Ezrin T567A is significantly higher than that of wild type Ezrin, which corresponds to results of increased whole cell stiffness and cytoskeleton stiffness in last chapter. Even though Ezrin T567D and FERM domain has different effects on the organization of actin filaments, the influence on the cell stiffness is different, with increased cytoskeleton stiffness in Ezrin T567D expressing cells and no effect in FERM domain expressing cells. The transfection of Ezrin T567D resulted in actin fiber peak towards the cell center, which might be another explanation on the decreased cortical stiffness.

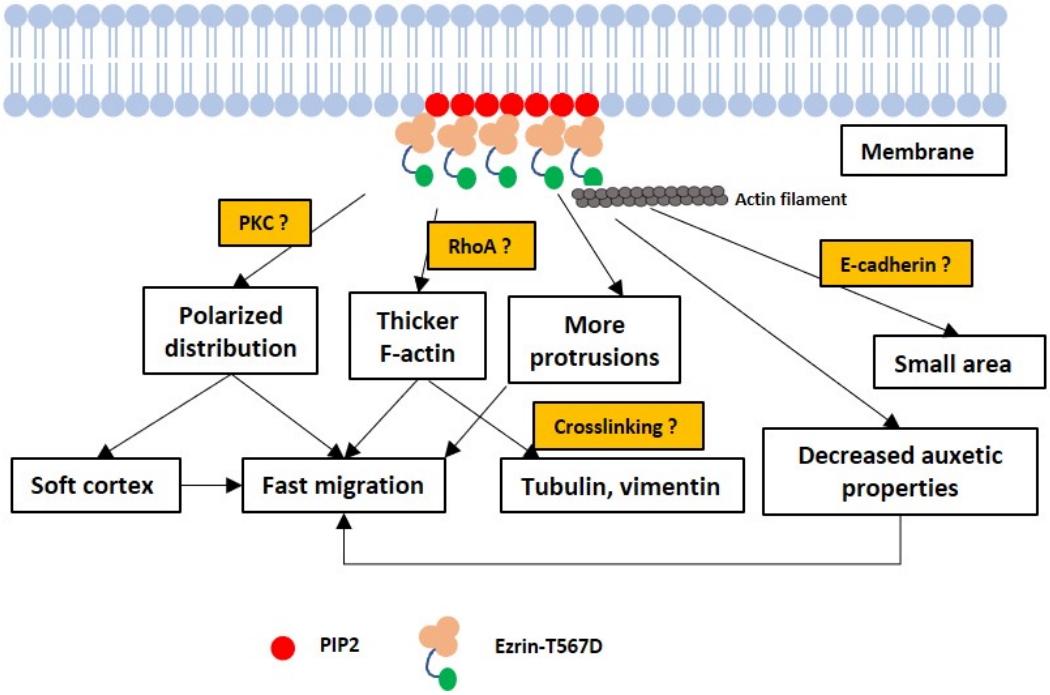

Figure 6.14: Effect of Ezrin T567D on cell's function. The main effects of Ezrin T567D on cell migration, cell mechanical properties and cell cytoskeleton are summarized and the potential molecular pathways are indicated in the orange boxes.

It has been reported that the amount of tubule fiber, or disruption or chemical stabilization of tubule fiber has no effect on cell elastic properties [338, 381]. The results in this study show that transfection of FERM domain increases the microtubule fiber intensity, makes the fiber longer, thicker and more aligned. However, these effects don't extend to cell mechanical properties, without changing cell stiffness.

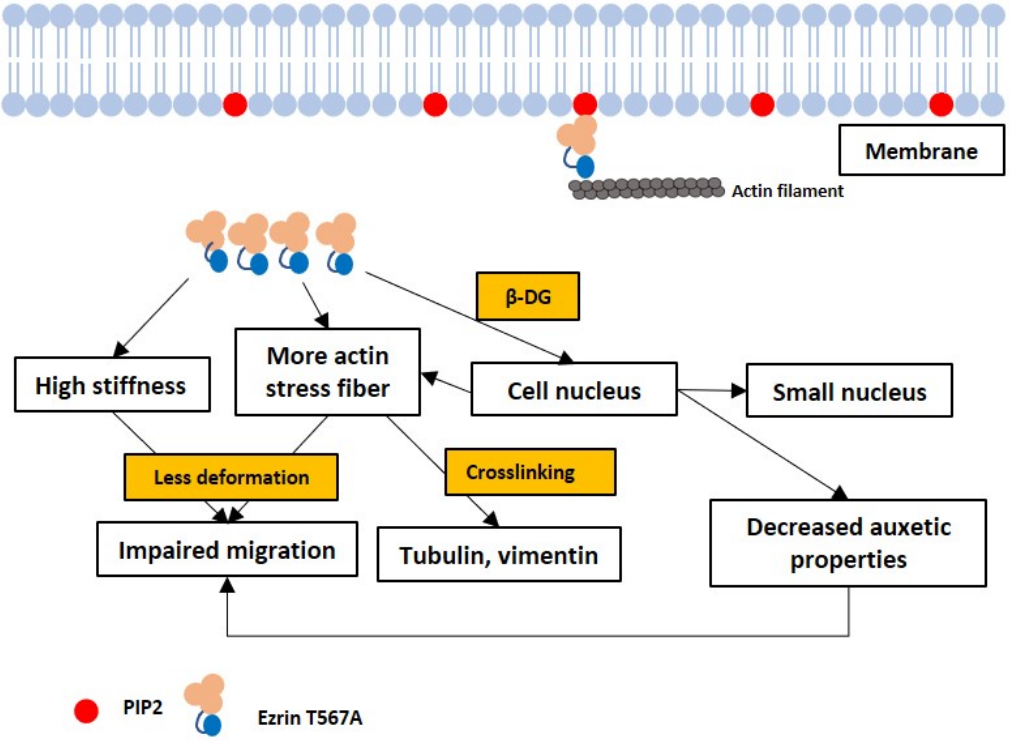

Figure 6.15: Effect of Ezrin T567A on cell's function. The main effects of Ezrin T567A on cell migration, cell mechanical properties and cell cytoskeleton are summarized and the potential molecular pathways are indicated in the orange boxes.

6.3.4 FERM domain affects cytoskeleton organization significantly

The most interesting results were from the cells expressing FERM domain, as FERM domain was reported to compete with endogenous ERM proteins for PIP2 binding and act as a dominant negative Ezrin mutant. However, FERM domains are present in a variety of proteins. The impact of expression of FERM domain may be more complicated than inhibition of ERM proteins. As shown in the last two chapters that transfection of FERM domain had little inhibitory effect on cell migration or cell mechanical properties. This chapter, however, demonstrates that FERM domain has marked effect on cell morphology as well as three types of cytoskeleton. Similar with reports which inhibited Ezrin expression by siRNA [402], cells transfected with FERM domain, which have smaller cell area, exhibit elongated shape with more filopodium formation. Others have reported that an increase in the amount of stress fiber was observed in N-terminal domain of Ezrin transfected cells [48]. As supplementary, instead of increased actin fiber, cells transfected with FERM domain displayed an increase in fiber length, fiber

thickness and fiber alignment. These observations maybe result from deletion of α helical domain and C-terminal domain which are involved in the regulation of actin filament structure as well as actin filament binding [403]. Or FERM domain could inhibit the formation of branched actin filaments by completing with FAK, as it has been reported that the FERM domain of FAK binds directly to Arp3 subunit, enhancing Arp2/3-dependent actin polymerization [404]. This could be assessed by inhibiting Arp2/3 complex activity and checking the effects of inhibition. Also the interaction between Arp2/3 complex and FERM domain can be investigated by pull-down assays. Therefore, cells would form more unbranched actin filaments, which explains the increased amount of stress fiber and longer and more aligned stress fiber (Figure6.16). What's more, the transfection of FERM domain displays paralleled effects on the microstructure of tubulin and vimentin fibers. Therefore, it is likely that the strengthening of the overall cytoskeleton structure observed here leads to slower cell migration.

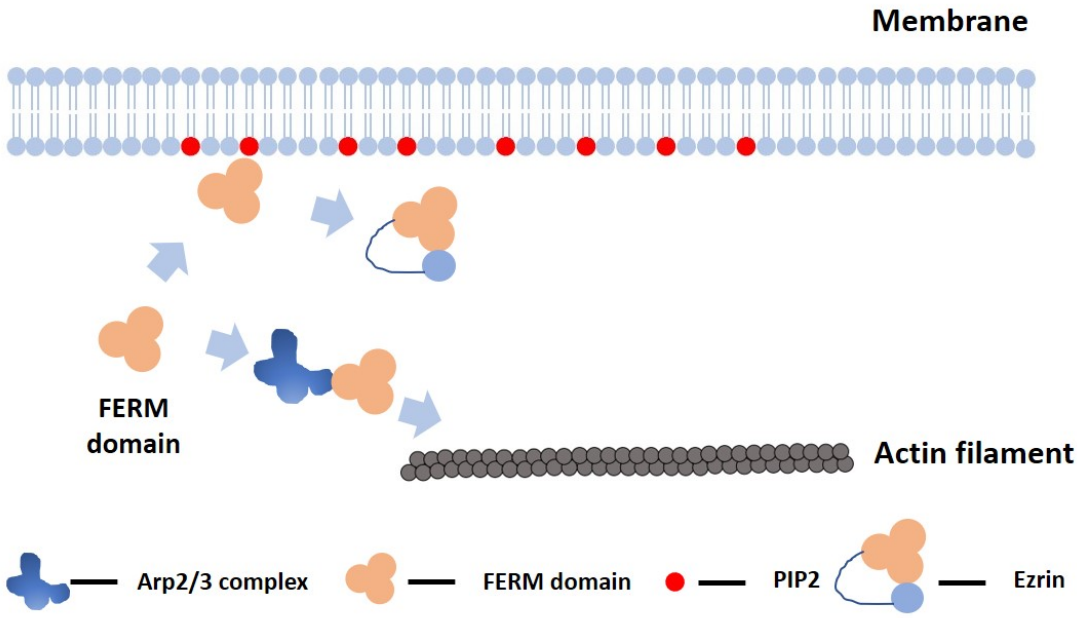

Figure 6.16: Effect of FERM domain on cell's function. The transfected FERM domain would compete with endogenous Ezrin for PIP2 binding, leaving Ezrin inactive. Or FERM domain would bind to Arp2/3 complex, disrupting the formation of branched actin filaments, resulting in formation of unbranched, longer actin filaments.

The results also suggest that the actin filaments, microtubules and vimentin are not independent. In fact, they can affect each other through crosstalk. Because transfection of active Ezrin T567D had limited effect on actin filament. As a result, the effects of Ezrin T567D on microtubules and vimentin were also moderate. On the contrary, FERM domain changed the actin filaments dramatically. At the same time, the effects of FERM domain on microtubules and vimentin were significant, too. Therefore it is possible that an increase in the assembly of one particular cytoskeletal network will result in an increase in other networks too.

6.3.5 Effect of Ezrin mutants on nuclear properties

Nucleus, which contains genetic material and transcriptional machineryis the largest organelle of the cell. The cytoskeleton and the nucleus are physically connected, allowing cells to gather surrounding physical information by their cytoskeleton and transfer it to the nucleus for physiological responses [405]. Therefore, alterations in Ezrin, the actin-membrane linking protein, could affect nuclear morphology and mechanical properties.

Nucleus in cells expressing Ezrin T567D has larger volume, smaller Poisson's ratio and condensed chromatin. One requirement of fast migration is to efficiently push the nucleus forward, or deform it through the pores in the particular situation of 3D migration. Accordingly, the results for T567D suggest the reinforced cytoskeleton indicated by increased cytoskeletal Young's modulus could pull the nucleus for the increased volume. What's more, the increased auxetic properties of the nucleus in Ezrin T567D transfection permits larger deformation of the nucleus during cell migration and against extracellular forces. This could protect the nucleus better as large nuclear deformations by extracellular forces increase the risk of disrupting the integrity of the nuclear envelop and causing DNA damage [406].

On the other hand, the decreased volume of nucleus in cells transfected with Ezrin T567A results in more condensed chromatin. Also the decreased auxetic properties indicates that the nucleus is less deformable. It is possible that it results from the perinuclear distribution pattern of transfected Ezrin T567A.

Lastly, it was also pointed out in our previous work [345] that vimentin has large contribution to cell volume, Poisson's ratio and stiffness, which is in agreement with the results in this study. Transfection of FERM domain have huge effect on vimentin cytoskeleton, accompanied by large change in nuclear state. It has been reported that transfection of N-terminal of Ezrin caused DNA condensation

[369]. Different with their report, FERM domain show no effect on chromatin condensation.

Our group has reported that nuclear volume, Poisson's ratio and elastic modulus increase with increasing cell spread area [345]. However, not all results obtained here follow this trend as cells expressing FERM domain have decreased cell area but display decreased nuclear volume and increased Poisson's ratio. It is possible that the transfection of Ezrin and its mutant has complex impact on biological and biophysical properties.

6.4 Summary

In summary, this chapter demonstrated that Ezrin and its mutants have pronounced effects on actin, tubulin and vimentin structure. What's more, nuclear properties are influenced by Ezrin transfection. These results may provide explanations on migratory and mechanical changes caused by Ezrin and its mutant. Main changes due to different Ezrin mutations measured by image quantification approaches are summarized in Table 6.1.

Table 6.1: Summary of main changes due to different Ezrin mutations measured in this study. (+) indicates significant increase, (-) indicates significant decrease and (=) indicates no significant changes.

	Biophysical parameter	T567D	T567A	FERM
Morphology	Cell area	-	=	-
	Aspect ratio	+	+	+
	Membrane Projections	+	+	+
Actin Filament	fibre assembly	=	+	=
	Fiber length	=	+	+
	Fiber thickness	+	=	+
	Fiber spread	+	=	+
	Alignment	=	=	+
	Curvature	=	=	+
	Fiber peak	-	=	-
	Chirality	=	+	+
Tubulin	Microtubules assembly	=	=	+
	Fiber length	=	=	+
	Fiber thickness	=	=	+
	Fiber spread	+	+	+
	Alignment	=	=	+
	Curvature	=	=	+
	Fiber peak	=	=	+
	Chirality	=	=	+
Vimentin	Vimentin assembly	=	=	+
	Fiber length	+	+	+
	Fiber thickness	=	=	+
	Fiber spread	=	=	=
	Alignment	=	+	+
	Curvature	=	=	+
	Fiber peak	=	=	+
	Chirality	=	=	=
Nucleus	Nuclear volume	+	-	-
	Nuclear auxetic properties	+	-	-
	Stiffness	+	=	+

Chapter 7

Sandwich model for bleb based migration

7.1 Introduction

In previous chapter, the role of Ezrin and its mutant was investigated in cell migration and it established that the expression of Ezrin T567D could increase cell migratory capacity significantly compared with other mutants. These results are in line with the reports that cancer cells expressing high level of phosphorylated T567 Ezrin have more potential to metastasize. However, the experiments were conducted in a two-dimensional (2D) environment growing cells as a monolayer on plastic or glass, which has several disadvantages. One is that 2D cell culture doesn't mimic the natural structures of tissues where cell-cell and cell-extracellular environment interactions are different [407]. Another drawback is that cells grown as monolayer are more sensitive to drug test, which has misleading effect in clinical investigations. What's more, it has been reported that cancer cells are able to switch to bleb based migration as an alternative to lamellipodium based migration after protease inhibition. Bleb based migration, another migration type relying on blebbing formation, allows cancer cells to move from one location to another without the aid of proteases [408]. As discussed above, Ezrin is one of the regulators in bleb based migration. The aim of this chapter is to construct a sandwich model in which cells can migrate with blebbing.

7.2 Results

7.2.1 Construct a sandwich model to study cell migration in a confined environment

Bleb based migration is characterized by low adherent to the substrate and fast migration. In this case, polyacrylamide gels without ECM proteins coating were prepared to study adhesion-independent motility. Also, instead of using NIH 3T3 cells, U937 cells were chosen to conduct this experiment for the following reasons. First of all, U937 cells grow suspended in the medium and they are non-adherent to culture dishes as well as the gel, which makes it more suitable for bleb based migration study. Secondly, U937 cells are easier to form blebbings than 3T3 cells. Lastly, it is relatively easier to manipulate U937 cells during culture and subculture, saving time for the preparation procedure. To mimic a confined 3D environment where cells have to migrate through pores in the ECM, U937 cells were sandwiched between a top and bottom polyacrylamide gels without any coating. Four different models were proposed aiming to create an optimum gap between two gels as shown in Figure 7.1.

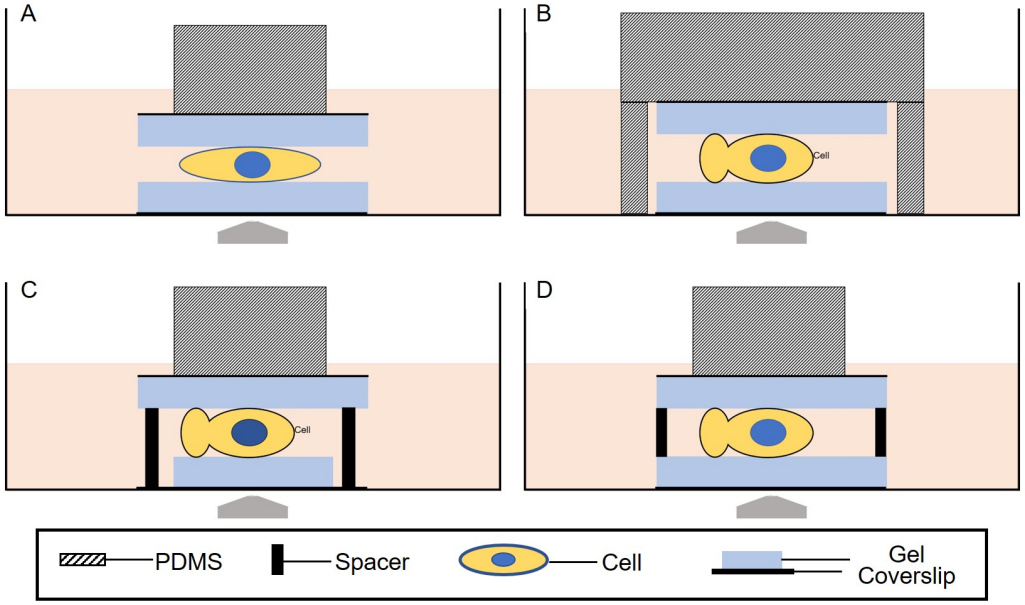

Figure 7.1: Schematic drawing of the four sandwich models. A. Model one: no gap; B. Model two: extension of the PDMS works like spacer; C. Model three: spacers are put inside the between gel on the top and the coverslip on the bottom; D. Model four: spacers like microbeads, fiber or ring, are put between two gels.

Four models were tested to see in which model U937 cells would migrate in bleb based mode. The diameter of the U937 cells are around 13 μm according to the

bright field images. So gap sizes around this value were tried and the size of 12 μm was found to work the best. The four models are individually described as follows:

Sandwich model one: This model was used as a control, which is also the simplest one, as cells were simply placed between two gels with a PDMS block on the top. No spacer was placed between the two gels, leaving the cells compressed with no other structural support. It was found that the cells cultured between the two gels were no longer healthy and died after few hours (Figure 7.2). It is most likely because without a gap between two gels, there was not enough supply of oxygen and nutrition to maintain the cells' normal living.

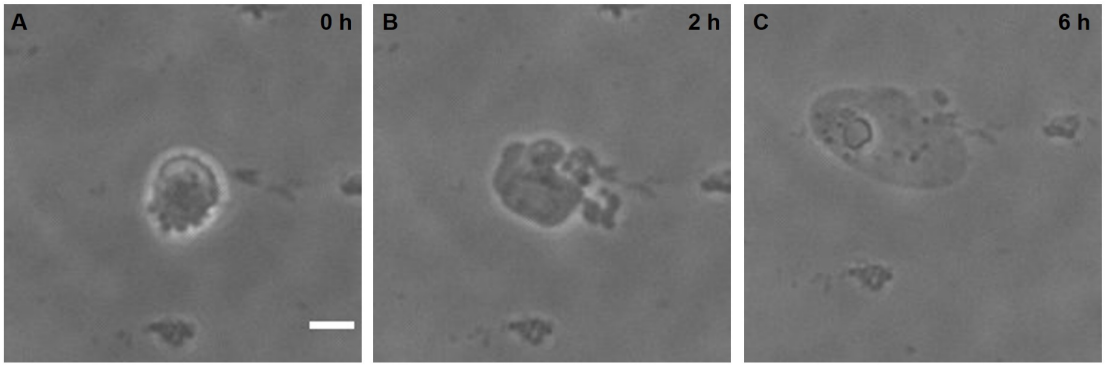

Figure 7.2: Sandwich model one without spacer. Bright field images of the same location but at different time. A. The image of the cell was taken at time 0; B. The image of the cells was taken 2h after. C. The image of the cell was taken 6 h later. The cell died without gap between two gels as no supply for air and nutrition. Scale bar: 10 μm

Sandwich model two: In this model, a bigger gap between the two gels was created by using a specially designed PDMS block with a rectangular groove obtained from a 3D printed mould (Figure 7.3). The top gel was fixed to the bottom side of the PDMS with superglue. The gap size was calculated by subtracting the two gel thickness from the depth of the groove. Nevertheless, bleb based migration was not able to be observed maybe due to the unstable system as the precision of the 3D printing was not good enough to achieve μm level.

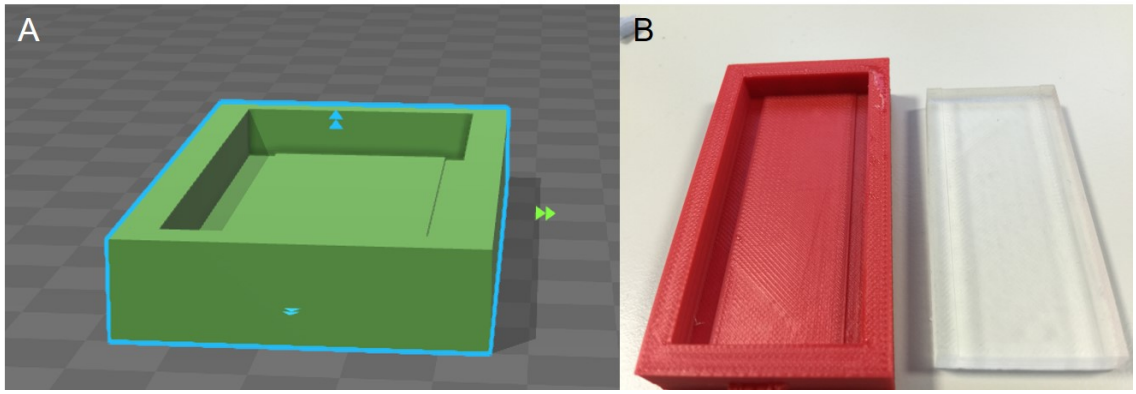

Figure 7.3: 3D printed mould used in model two. A. The design images of the 3D mould. B. On the left, the mould printed; on the right, the PDMS gels made from the mould.

Sandwich model three: Similar to the second model, the bottom gel was made with smaller diameter and placed a spacer around the bottom gel in contact with the coverslip. Then the top gel was placed on top of the spacer. The gap size was calculated by subtracting the thickness of bottom gel from the the height of the spacer. Although cell blebbing was observed, the movement was not significant (Figure 7.4). The challenge was that due to the slippery nature of the gel surface, it was difficult to keep the bottom coverslip and the spacer stay still.

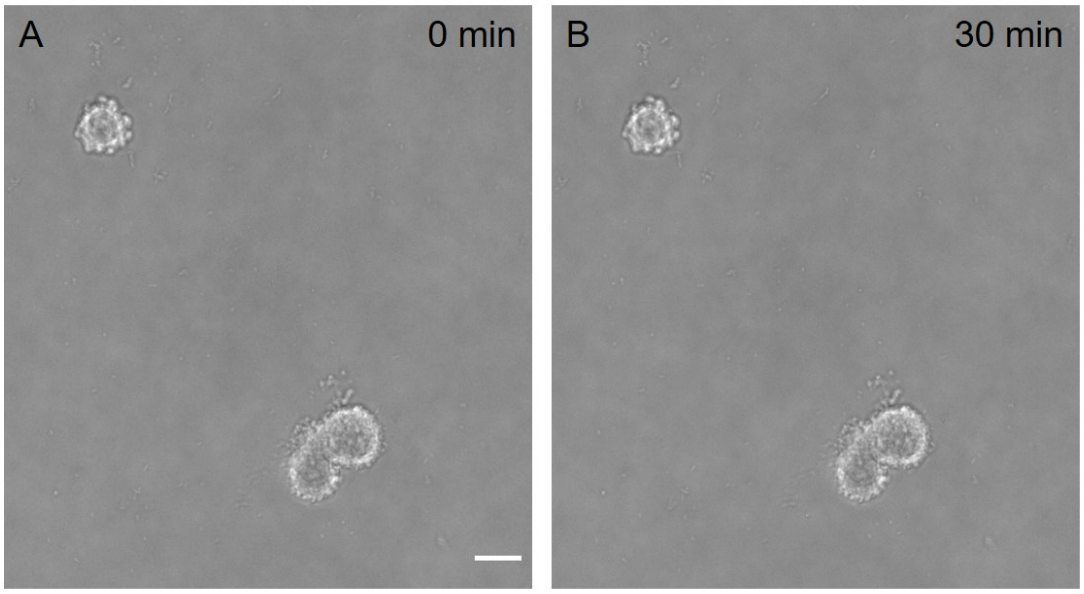

Figure 7.4: Cells in sandwich model three. Bright field images of the same location but with different time: A. at time 0; B. at time 30 min. There was no significant cell movement during the 30 min. Scale bar: 10 μm

Sandwich model four: For further improvement, the spacer was placed between two gels and the height of the spacer was the gap size. Three different types

of spacers were tested separately, namely micro-beads, fibers and ring-shaped spacers. As a result, the ring-shaped spacer was found to work the best among the three. Bleb based migration was successfully observed within this model and preliminary results were acquired, which will be presented in the next section. Tests with the other two spacers, however, did not work well. The diameter of the micro-beads was found to be too small to create a gap for the cells and they were also unable to stay still (Figure 7.5). While the fibers were found to be too thick making it difficult to find the same focal plane for all cells, as demonstrated in Figure 7.6 showing cells at two different focal planes. In addition, both micro-beads and fiber couldn't create an even gap as only the area near the beads or fibers had wide gap but the area away from the them did not.

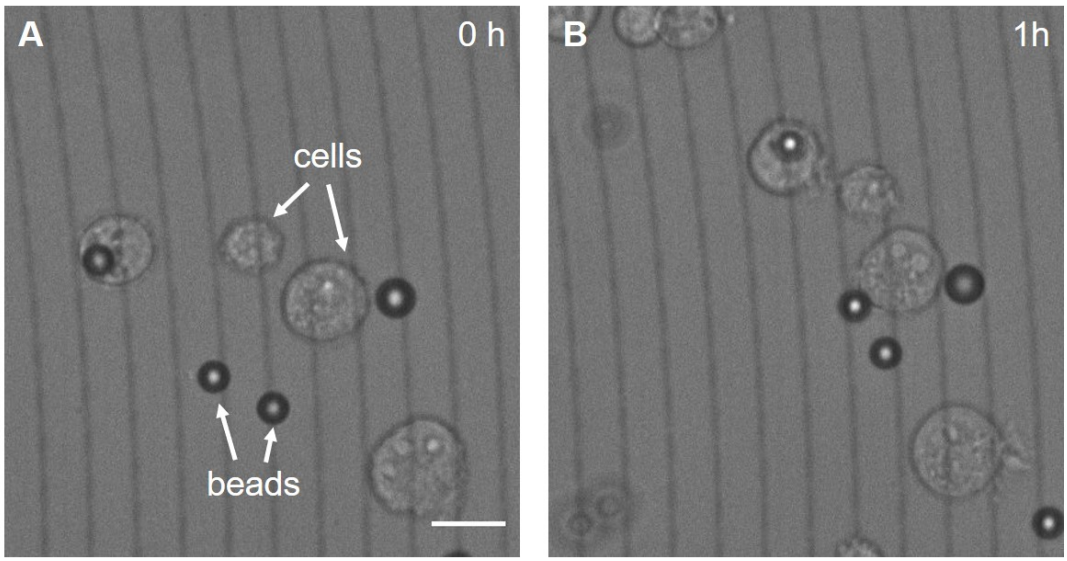

Figure 7.5: Sandwich model four with microbeads as spacer. Bright field images of the same location: A. 0 h; and B. 1h later. The system was not stable as the location of both beads and cells changed with time. Scale bar: 10 μm

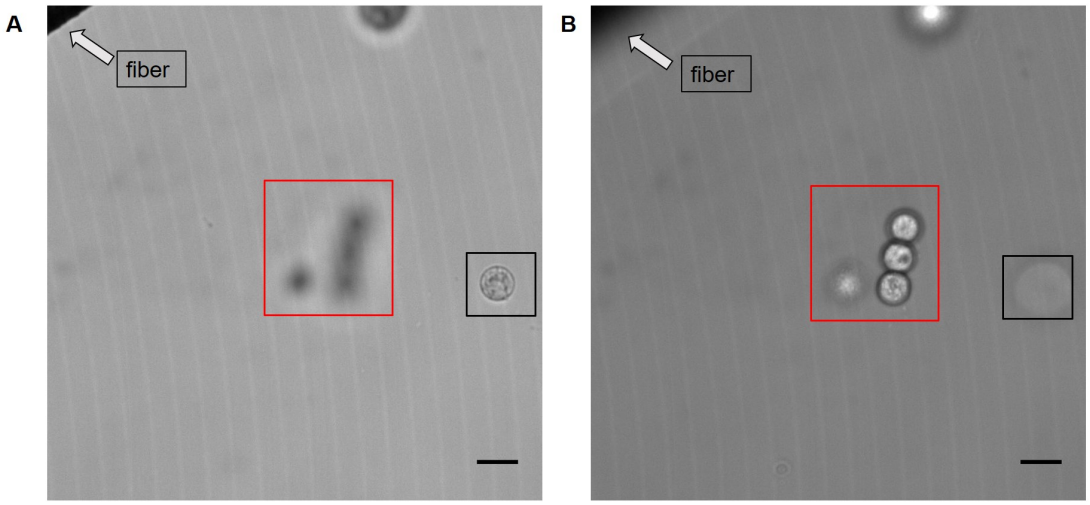

Figure 7.6: Sandwich model four with fibers as spacer. Bright field images of the same location but with different focuses. A. The focus was on the fiber. The arrow indicates the location of the fiber in the right up corner. At the same time, the cell in the black rectangle was in focus. B. The focus was on the cells in the red rectangle this time. The fiber and the cell were blurred. Scale bar: 10 μm

7.2.2 Characterization of bleb based migration using sandwich model four

a. Cell morphology

By using the ring-shaped spacer in model four, cell migration with blebbings was successfully observed. As cell shape changed rapidly during migration, bright field images of the cells were taken every 5 s for 30 min. According to the videos, the morphology of the migrating cell could be divided into two groups (Figure 7.7): in group one, cells with elongated shape, display polarized blebbings at the leading edge (Figure 7.7 A); while cells in group two form blebs at all directions, displaying a round shape (Figure 7.7 B). Furthermore, the results of aspect ratio in Figure 7.7 C also shows that polarized cells with an aspect ratio of around 1.6 are much longer than unpolarized cells with a ratio of around 1.2.

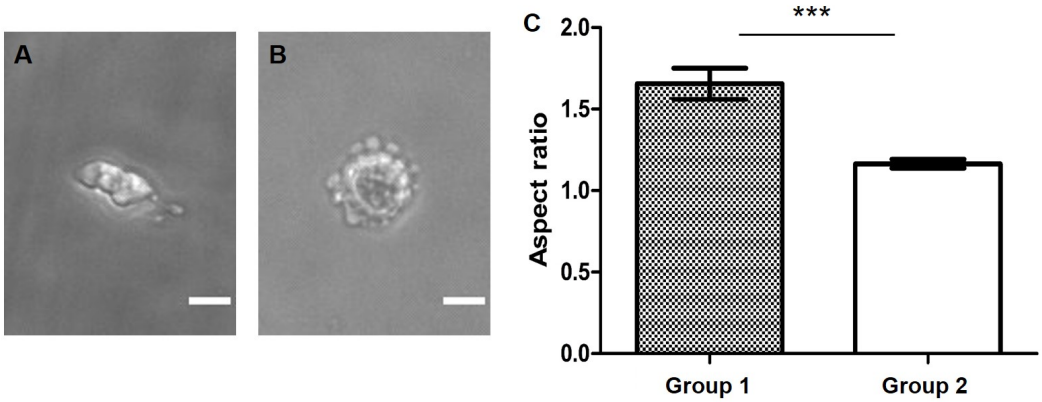

Figure 7.7: Two types of blebbing in sandwich model four. A. In group one, cells had elongated shape with blebbing at one direction; B. In group two, cells were round with blebbing at all directions; Scale bar: 10 μm, C. Box plot of the aspect ratio from group one and group two; group one (n=15), group two (n=17) , ***p $<$0.001 according to t test.

b. Migration speed

Next the migration speed of the two types of confined cells was investigated. Surprisingly, no significant difference is found in migration speed between these two group cells, all migrating at around 2 μm/min (Figure 7.8 C). Even though they have the same migration speed, from Figure 7.8 A and B, it is obvious that cells with polarized blebbings (A) have travelled longer distance. While cells with unpolarized blebbings (B) kept moving with the same speed but changed migrating directions whenever new bleb formed. These cells came back to the same location ultimately. These results demonstrate that polarization is an essential step not only in lamellipodia based migration but also in bleb based migration.

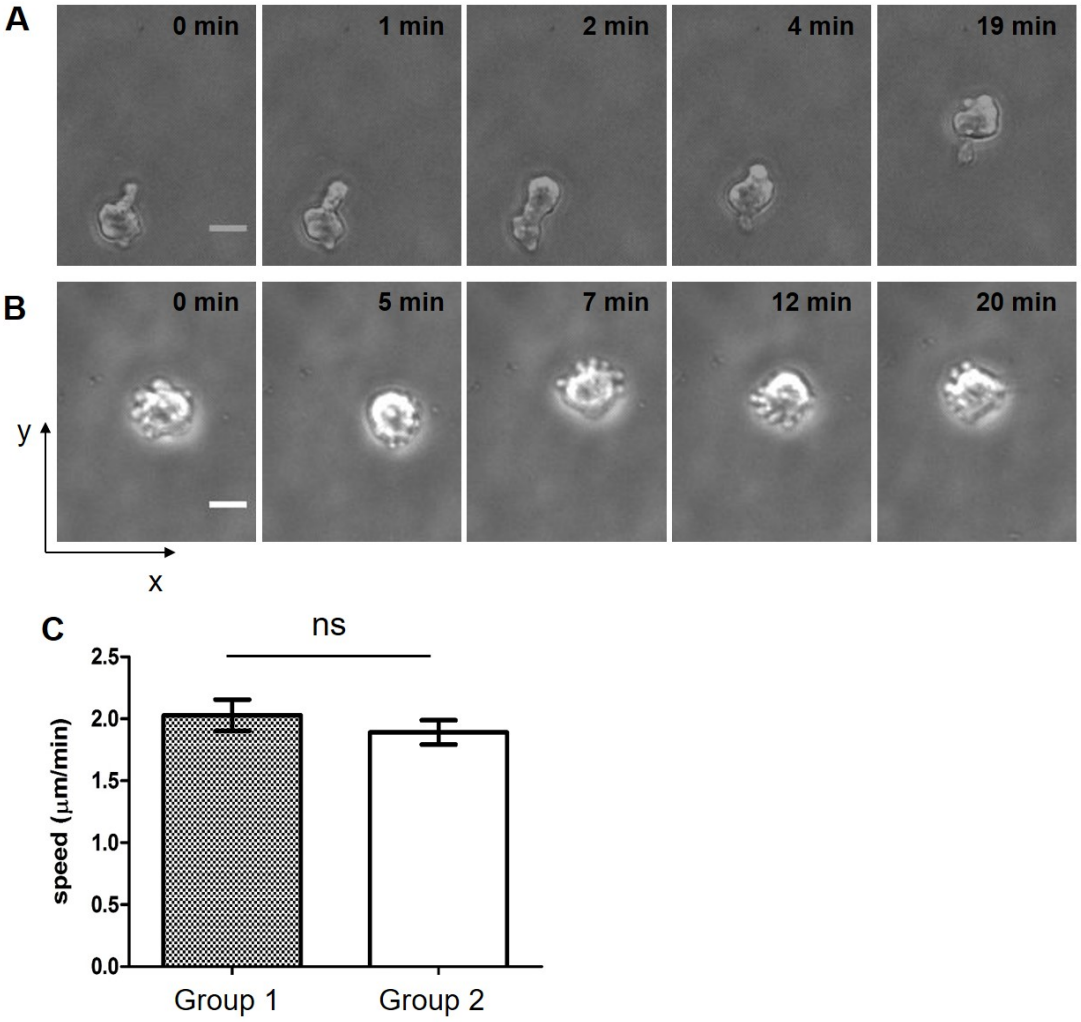

Figure 7.8: Migration Behavior of two group cells for migration speed. Time-lapse sequences of bleb based migration for a typical group one cell (A) and group two cell (B). Scale bar: 10 μm. Box plot of the migration speed of two group cells. n.s no significant difference.

c. Migration persistence

If comparing between these two groups, the Euclidean distance (straight distance between start and end point of cell trajectory) of the two group were significantly different, which means the randomness of these two migration types is different. Figure 7.9 A and B show the representative trajectories of single cells for 31 cells with polarized blebbings and 68 cells with unpolarized blebbings. The trajectories indicate that migration persistence of these two groups were markedly different. Two methods were used to describe the persistence: one is Euclidean distance divided by total migration length, another one is maximum distance from origin divided by total migration length. Both methods give the similar results, which indicates that cells with polarized blebbings migrate with larger persistence than

cells with unpolarized blebbings (Figure 7.9 C and D).

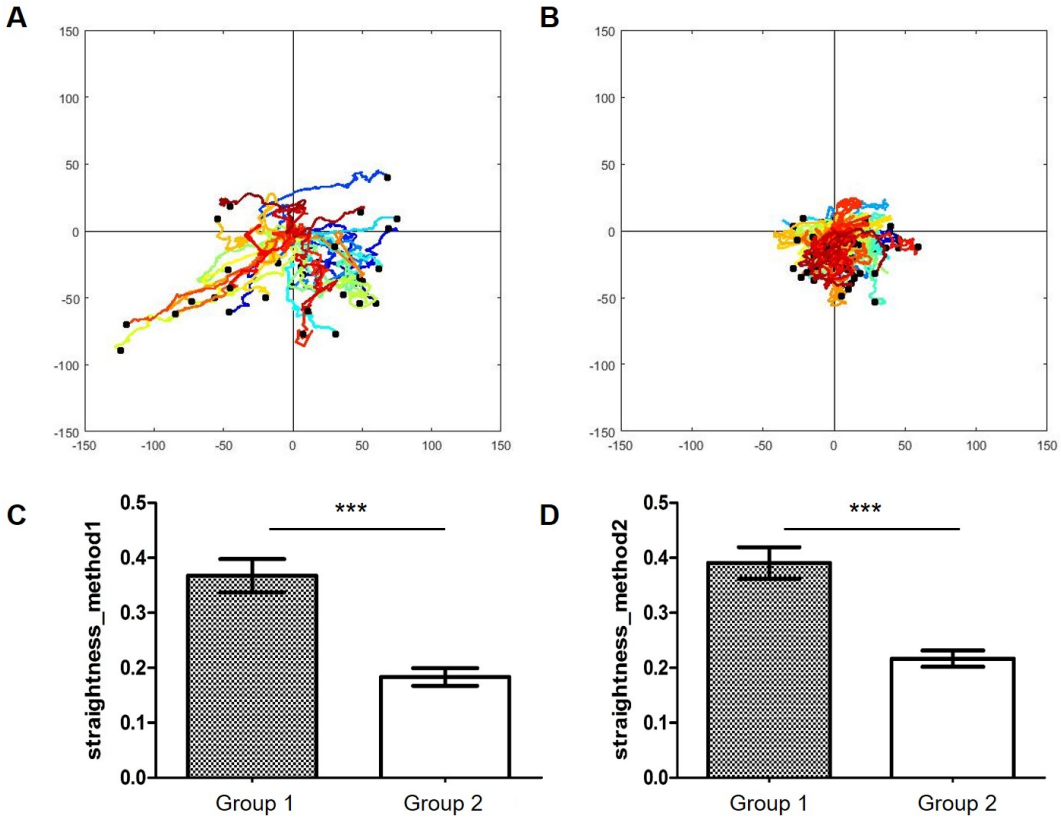

Figure 7.9: Migration Behavior of two group cells for straightness. Representative trajectories of 31 cells with polarized blebbings (A) and 68 cells with unpolarized blebbings (B) recorded for 30 min. The starting position of each cell were registered to the center of the plot. Box plot shows the migration straightness of two group cells by two methods, method one (C) and method two (D), ***p $<$0.001 according to t test.

d. Polarized blebbings

Polarized blebbings were observed under a higher magnification, in order to obtain detailed morphology information. Figure 7.10 shows time-lapse sequences of the polarized bleb based migration. The images show that cells occasionally form a large bleb at the leading edge. The rest of the cytosol flows into the bleb, driving the cell to move forward (at 2 min). While for the rest of the time, cells form several small blebs at the leading edge, one on top of another (at 4min). Cells move forward with the retraction of the rear.

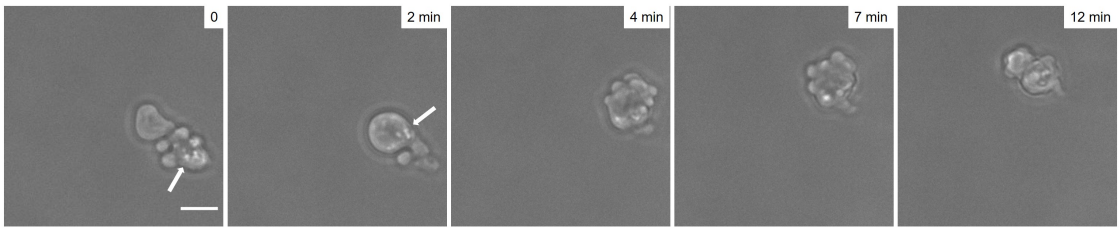

Figure 7.10: Time-lapse sequences of the polarized bleb based migration. Bright field images were taken with 40x objective to get more detailed information of cellular movement. The arrow indicates the same components inside the cell at different time points. Scale bar: 10 μm.

Blebbing has also been considered as a hallmark for apoptosis by forming one of the most spectacular features of the execution phase of apoptosis [409]. Figure 7.11 shows an example of cell blebbing during apoptosis. The Cell forms large blebs at all directions, even at the top of the cell body and does not migrate during the course of imaging. More importantly, the formed blebs could last for more than 30 min with no sign to retract. These results suggest that the blebbing observed in the confined gels is a new type of blebbing, which is considered as healthy.

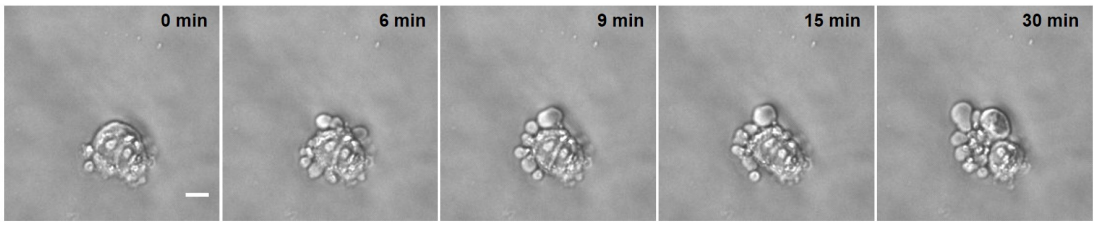

Figure 7.11: Time-lapse sequences of a typical apoptosis cells confined in two gels. Scale bar: 10 μm

7.3 Discussion

7.3.1 Sandwich model set-up and control

In this chapter, a sandwich model in which U937 cells are confined between opposing surfaces of two pieces of polyacrylamide gels, is set up and used to characterize the mechanics of bleb based migration. A ring-sized spacer with specified thickness is placed between two gels to make a gap for cells to migrate. Compared with other models tried in this study, a uniform and stable gap created by the spacer is essential for this set-up. Another requirement for bleb based

migration is the absence of focal adhesions. Without any coating on the polyacrylamide gels, cells are not able to form persistent protrusions and stress fibers, as it has been reported that integrin expression inhibits bleb based migration [410].

One of the advantages of this set-up is that polyacrylamide gels are a highly swollen network of cross-linked acrylamide units and the stiffness of gels can be tuned by changing the amount of bis-acrylamide cross-linker and total acrylamide monomers in the gel precursor solution [411]. Therefore polyacrylamide gels are widely used as cell culture substrates to study how cells sense and respond to the physical characteristics of their microenvironment [412]. The stiffness of polyacrylamide gels can be adjusted according to the studies required. Another advantage is that, cells are confined between two pieces of polyacrylamide gels to mimic the real biological situations, unlike other set-up reported by others that cells are placed between glass and agarose [413], or petri dish and PDMS [414]. Also the polyacrylamide gels can also be used to study the traction force in bleb based migration.

7.3.2 Polarized blebbing and cell migration

A wide range of studies have reported that cancer cells could switch to bleb based migration from lamellipodium based migration when the environment changes, such as protease inhibition [415]. As a result, an increasing number of studies have turned their attention to bleb based migration as an important motility mechanism and a common alternative to lamellipodium based migration in 3D environment. However the molecular mechanisms of bleb based migration is still not as clear as lamellipodium based migration.

In this chapter, U937 cells were confined in the sandwich model and bleb based migration of U937 cells was investigated. Firstly, two types of blebbings were observed in the sandwich model: one was polarized blebbings towards one part of the cell; another was multiple small blebbings at all directions. As discussed in previous chapter, polarization is required for effective migration to form distinct leading and rear edge [416]. As a result, cells with polarized blebbings have larger displacement and migrating persistence, even though two types of cells had similar migration speed. In contrast, cells forming multiple small blebs at all directions, did not have a defined front, as each bleb generates its own force pulling the cell in the direction of bleb growth, resulting in little displacement during the whole movement. The fact that cells need to create polarized blebbings at the leading edge is an important step for blebbing transferring to cellular movement, as polarization determines the direction of movement.

Cellular morphology has been reported during bleb based migration as a round cell body with a small leading edge or an elongated ellipsoid cell body with a large uropod [414]. A little different from other reports, polarized blebbings are found to assist cell migration in two modes, either forming large blebbing at the leading edge or forming multiple small blebbings at the leading edge. The difference may be due to different cell types used in the experiment. In the absence of adhesions, the migration in the confinement is termed 'chimneying', in reference to a technique used by mountain climbers [417]. During bleb based migration, cell exerts forces perpendicularly to the surfaces such that it can squeeze itself forward by blebbing [144].

7.3.3 Potential role of Ezrin in bleb based migration

As one main difference between motile and non-motile blebbing cells is that motile blebbing cells form blebs primarily at their leading edge. If blebs nucleate through the local detachment of the membrane from the actin cortex, polarization could result from a localized weakening of membrane-cortex attachments or a local increase in the pressure that is exerted on the membrane. This could be achieved by polarizing the distribution of the actin–membrane linker protein, ERM proteins, to the rear of the cell [144]. Therefore membrane-cortex attachment plays a central role in controlling the ability of cells to form blebs [158]. Also it has been reported that melanoma cells, which can migrate in a rounded amoeboid-type mode, have an ezrin-rich uropod like structure (ERULS) which could reduce membrane blebbing and thus determine the direction of a moving cell through localized inhibition of membrane blebbing [418].

Ezrin has been reported to be involved in the cycle of bleb formation, where Ezrin is recruited to the membrane first, followed by actin, actin-bundling proteins during cortex assembly under newly formed bleb [148]. As already shown before, phosphorylated Ezrin T567D localized at the cell rear during cell migration in 2D. In addition, there is a linear relationship, which is the more Ezrin T567D concentrated at the rear, the faster the cells migrated. It is interesting to investigate how Ezrin and its mutant affect bleb based migration and compare the different function of Ezrin in bleb based migration and mesenchymal migration.

7.3.4 Application of sandwich model

As basic properties of bleb based migration has been characterized in this study, it is worthy to investigate more about bleb based migration by the sandwich model.

Firstly, several studies have shown that a retrograde flow of actin is responsible for cell movement independently of adhesion in bleb based migration [414, 419]. Actin filaments assemble into a fibrous cortex that was absent from the cell front and become progressively denser to the cell rear. Actin polymerization at the front and depolymerization at the back makes a strong retrograde flow in the central part of the cell [414]. Though the role of actin filaments in bleb based migration is well studied, how other cytoskeleton, microtubules and intermediate filaments, function in this mode of migration is unknown. So with the sandwich model, the whole picture of cytoskeleton in bleb based migration can be studied.

Secondly, as discussed above that Ezrin is involved in bleb based migration, cells expressing Ezrin and its mutant, including Ezrin, Ezrin T567D, Ezrin T567A, and FERM, can be confined in the sandwich model to investigate the role of Ezrin in this kind of migration. The relationship between Ezrin localization and cell polarization during bleb based migration is also interesting to explore. However, in order to image transfected cells, modifications of the model are needed to obtain higher quality images. The transparency of petri dish bottom, the coverslip, as well as the superglue will all affect the quality of fluorescent images.

Furthermore, since Some cancer cells use membrane blebbing as a mode of motility during metastasis [420], the sandwich model also can be used to study cancer cell migration in the absence of adherence, especially the role of Ezrin in this kind of motility during cancer metastasis. It is necessary to change another cell type, such as walker carcinosarcoma cells [421], instead of using U937 cells. At the same time, the surface of the gel needs to be coated with a hydrophobic chemical to study the adhesion independent migration, if the new cell type is adherent dependent.

Lastly, the orientation and the magnitude of the traction forces exerted by cells during bleb based migration is quite different from lamellipodium based migration [157]. So fluorescent micro-beads could be added to polyacrylamide gels during the mixing step. In this way, the traction force of the moving cells in bleb based mode is able to be investigated by comparing the magnitude and direction of the traction force with classic migration mode, lamellipodium based migration. Again, the role of Ezrin and its mutant on traction force during bleb based migration can be explored, at the same time.

7.4 Summary

Altogether, a sandwich model was constructed by confining cells between two gels (Figure 7.12) in this chapter. A brief characterization of bleb based migration was assessed by this model. More improvements are needed to use this model to study the role of Ezrin and mutants in bleb based migration.

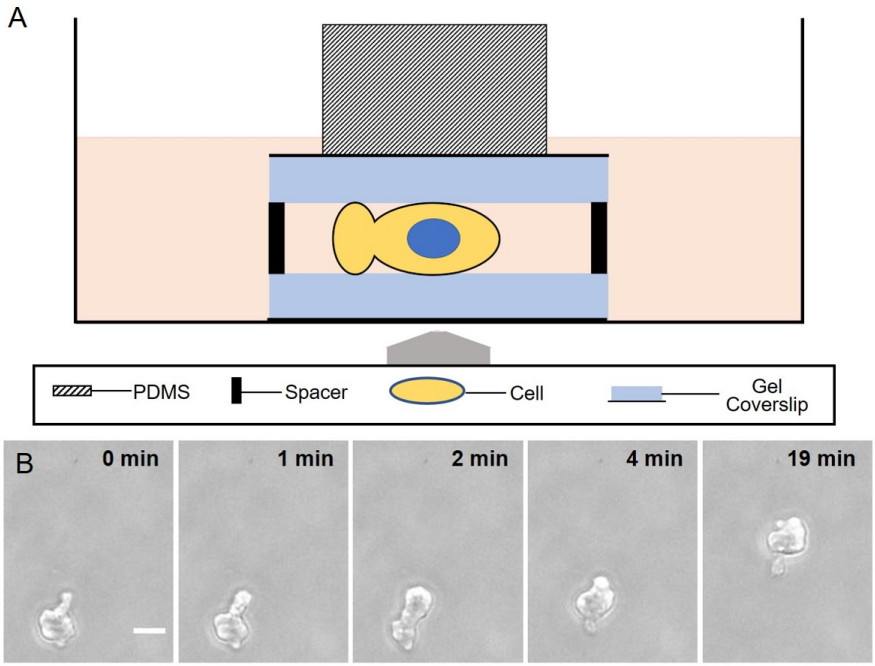

Figure 7.12: Sandwich model and bleb based migration in this study. A. Sandwich model where cells can migrate in blebbing way. B. An example of bleb based migration. Scale bar: 10 μm

Chapter 8

Conclusions and Future work

8.1 General conclusions

In this study, a comprehensive review of literature on the structure and function of Ezrin and its relationship with cancer has been presented. In order to find out the role of Ezrin phosphorylation at T567, a combination of methods including long-term live-cell imaging, AFM and image quantification approaches were applied to cells transfected with Ezrin, and its mutants: phosphomimetic mutant Ezrin T567D, phosphodeficient mutant Ezrin T567A and dominant negative FERM domain. Concluding remarks are summarized as follows:

1. Expression of phosphorylated Ezrin at t567 resulted in increased cell migration in a more directional manner. In addition, cell rear accumulation of Ezrin T567D induces quicker migration. Results from AFM and image quantification approaches results suggest that the expression of Ezrin T567D is associated with a reorganization of the cellular cytoskeleton, which leads to a decrease in cortical stiffness and an increase in cytoskeleton stiffness. Collectively, these biophysical changes support a more migratory phenotype.

2. Though expression of Ezrin T567A does not impair cell migration, it leads to a significant buildup of actin fibers, a decrease in nuclear volume, and an increase in cytoskeletal stiffness. Also nuclear periphery distribution suggests that Ezrin may have other functions in inactive state.

3. Transfection of FERM domain induces significant morphological and nuclear changes. The effects on actin fibers extend to microtubules and the intermediate filament vimentin, resulting in cytoskeletal fibers that are longer, thicker, and more aligned.

4. A sandwich model was developed and bleb based migration was successfully

observed within this model. Two types of blebbings were observed: one forms at the leading edge, leading to effective migration and larger straightness; and the other forms at all directions of the cell, resulting in smaller displacement and directionality.

Collectively, the results suggest that ezrin's phosphorylation state and its intracellular localization plays a pivotal role in cell migration, modulating also biophysical properties, such as membrane–cortex linkage, cytoskeletal and nuclear organization, and the mechanical properties of cells. These findings highlight the importance of phosphorylated Ezrin as a biomarker for cancer metastasis diagnosis. Even though further studies are still needed to understand the molecular mechanism in detail, results in this study suggest that Ezrin phosphorylation might be a promising molecular target for cancer therapy, especially to suppress cancer invasion and metastasis.

8.2 Future work

Based on the results and conclusions of this thesis, future works on further investigation of Ezrin phosphorylation and sandwich model are listed as followings,

1. Utilization of epithelial or metastatic cancer cells

This study was carried out in fibroblasts, which is due to their mesenchymal nature. When cultured in sparse conditions, they become well spread and display a strong migratory phenotype. This makes them a suitable model to study the relationship between cell migration direction and cytoskeletal organization or intracellular distribution of proteins. Additional studies on epithelial cells should provide a further understanding on the role of ezrin's phosphorylation in cell monolayer models, where cell-cell adhesions play a key role or where ETM transitions may be studied. Moreover, studies on metastatic cancer cells, such as hepatocellular carcinoma cells which has been reported to have higher metastasis ability and higher phosphorylation Ezrin expression, could provide more information. Expression level of phosphorylated Ezrin and Ezrin can be determined by qPCR and western blot. The differences in cell migration, cell mechanical as well as cytoskeleton organization between cells can be investigated by our experimental techniques.

2. Additional experiments to study the underlying mechanism

In this study, cytoskeleton characterization was carried out in fixed cells. It would be better to know how cytoskeleton changes within time, as the cytoskeleton

changes are dynamic process. Double transfection of cells with reporters for cytoskeleton and Ezrin mutants could be carried out in order to monitor the effect of Ezrin and its mutant on cytoskeleton dynamics during cell migration. To do this, cells with lower transfection ratio should be selected to ensure the viability of the cells.

Due to time restrictions, the molecular mechanism underlying the effects of Ezrin and its mutant could not be assessed. One possibility is that Ezrin affects the cytoskeleton directly. This could be assessed by inhibiting Ezrin activity by siRNA or chemicals like NSC305787 and NSC668394. Effects of inhibitors could be compared after rescued by reexpressing Ezrin or washing out the chemicals. Another possibility is that Ezrin regulates the cytoskeleton through other proteins, such as Rho family GTPases. As described in the previous, Rho family GTPases works closely with ERM family. Also Rho proteins are involved in regulating cytoskeletal dynamics. This could be assessed by pull-down assay to find out the proteins that interacts with Ezrin and select those that have potential influence on cytoskeleton.

3. In vivo experiment for further investigation

As all the experiments were carried out in vitro, whether or not active Ezrin T567D could promote cells metastasis ability in vivo remains to be answered. So if it is possible, a metastasis assay is needed by using immunodeficient mice. Briefly, cells transfected with Ezrin and its mutants will be injected into the circulation of immunodeficient mice through their tail veins. A small number of cells could survive and grow as metastases in internal organs, such as lung. Then the injected mice need to be dissected and tissue distribution of metastases is determined after a certain period. The number of metastases in a specific tissue directly correlates with the metastatic ability of the injected transfected cells. By doing this, the role of Ezrin phosphorylation in cell metastasis can be determined.

4. Sandwich model used for Ezrin and bleb based migration

With this model, bleb based migration can be further studied thoroughly, such as the distribution and function of three types of cytoskeleton structures and the traction force during bleb based migration if the gels are embedded with fluorescent beads. In addition, the migration state of cells transfected with Ezrin and its mutants can be investigated, such as whether Ezrin phosphorylation at T567 could promote fast bleb based migration or the distribution of Ezrin during the bleb based migration. What's more, it is worth comparing the ability of transferring to bleb based migration between cancer cells and normal cells from different patients given the condition that lamellipodium based migration is inhibited.

Appendix A

Publications and conferences

A.1 List of publications

1. **X Zhang**, L Flores, M Keeling, K Sliogeryte, N Gavara, Ezrin Phosphorylation at T567 Modulates Cell Migration, Mechanical Properties, and Cytoskeletal Organization, International Journal of Molecular Sciences, 2020, 21.2, 435.

2. J Molina, **X Zhang**, M Borghesan, J Silva, M Awan, B Fuller, N Gavara, C Selden, Extracellular fluid viscosity enhances liver cancer cell mechanosensing and migration, Biomaterials, 2018, 177, 113-124.

3. J Xu, A Nyga, W Li, **X Zhang**, N Gavara, M Knight, J C Shelton, "Cobalt ions stimulate a fibrotic response through matrix remodelling, fibroblast contraction and the release of pro-fibrotic signals from macrophages" E Cells and Materials, 2018, Eur Cell Mater vol. 36, 142-155.

4. L Flores, M Keeling, **X Zhang**, K Sliogeryte, N Gavara,"Lifeact-GFP alters F-actin organization, cellular morphology and biophysical behaviour", Scientific Reports, 2019 9(1):3241.

5. M Bai, H Kazi, **X Zhang**, J Liu, T Hussain, Robust Hydrophobic Surfaces from Suspension HVOF Thermal Sprayed Rare-Earth Oxide Ceramics Coatings, Scientific Reports, 2018, 8:6973.

6. M Bai, H Kazi, **X Zhang**, J Liu, B Song, T Hussain, "Hydrophobicity of Suspension HVOF Sprayed Rare Earth Oxide Coatings", Thermal Spray Bulletin, 2018, 45084. (Best paper award at ITSC 2018 with $500 cash award)

A.2 List of conferences

1. 8th World Congress of Biomechanics 2018

(Dublin, Ireland, 2018.7.08-12)

Session: Cell biomechanics and oncology 2

Oral Presentation: ”The effect of Ezrin mutations on actin cytoskeleton and cell mechanical properties”

2. Forces in cancer: interdisciplinary approaches in tumour mechanobiology

(London, UK, 2018.6.18-19)

Appendix B

Example of cell phenotype and associated morphometric descriptor values

B.1 Examples of cell phenotypes and associated morphometric descriptor values

Example cells highlighting the morphological appearance of each computed parameter were human mesenchymal stem cells transfected with LifeAct-GFP [346]. Mesenchymal stem cells have larger spread area as well as more clear cytoskeleton structure than NIH 3T3 cells for presenting better examples of computed parameters. For each parameter, two cells corresponding to low and high value ranges are pictured, with specific values included. Scale bars are 30 μmm for all cells plotted.

1.Cell area (μm^2): 0-∞

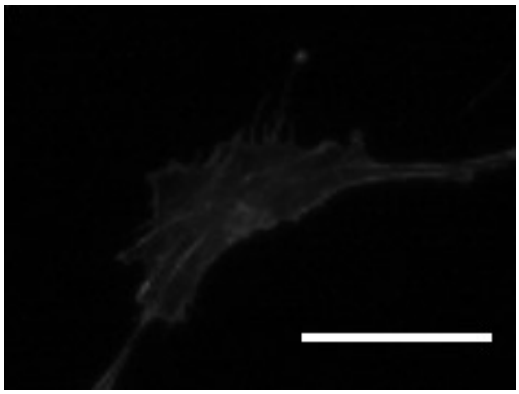

(a) Cell area=686 μm^2

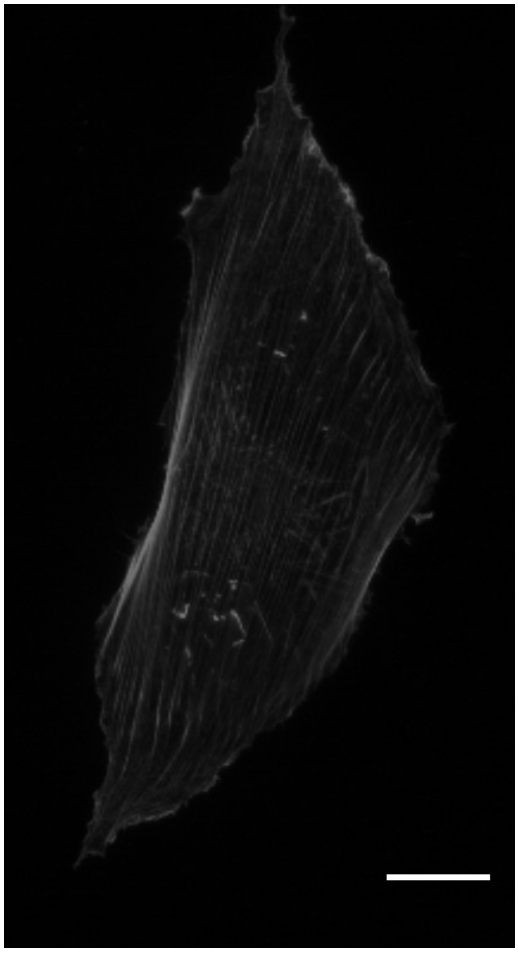

(b) Cell area=12292 μm^2

2. Aspect ratio: 1-∞

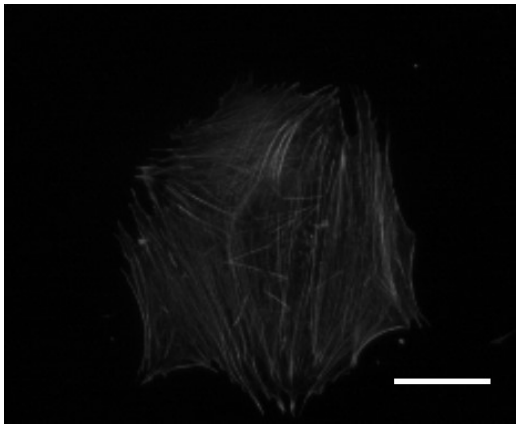

(a) Aspect ratio=1.13

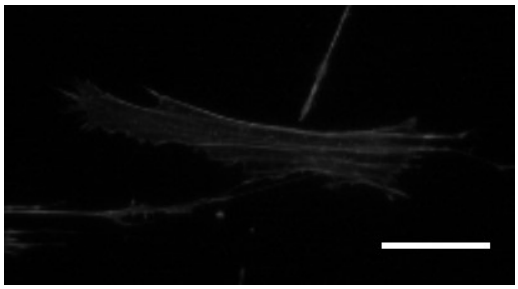

(b) Aspect ratio=5.89

3. Stellate factor:0-∞ (typically 0.1-0.8)

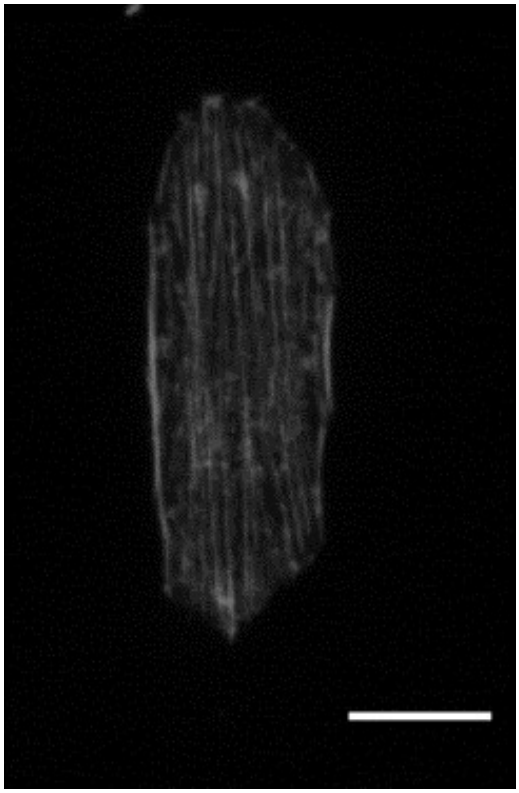

(a) Stellate factor=0.11

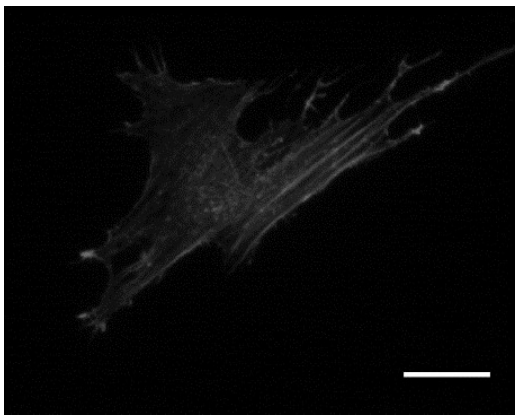

(b) Stellate factor=0.62

4. Total fiber intensity (AU): 1-∞

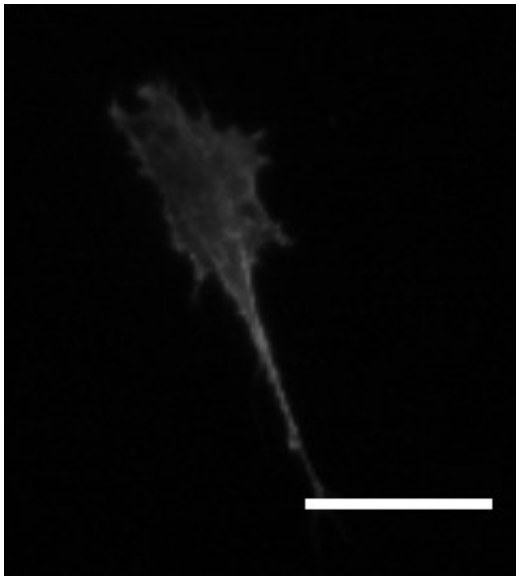

(a) Total fiber intensity=3.1X10^5

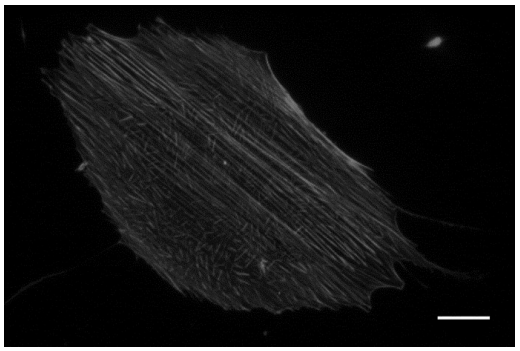

(b) Total fiber intensity=1.3X10^7

5. Fiber thickness (AU): 1-∞

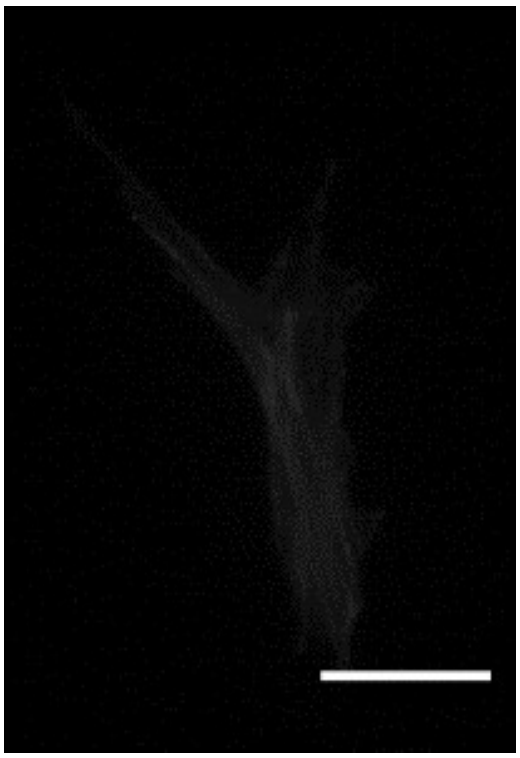

(a) Fiber thickness=65

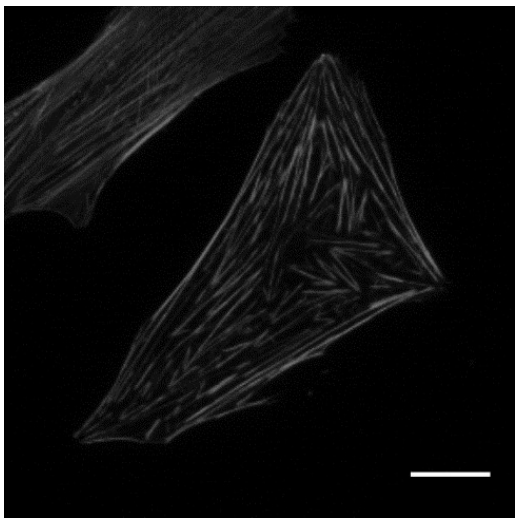

(b) Fiber thickness=425

6. Variability in fiber thickness (%): 0-∞ (typically 50-200%)

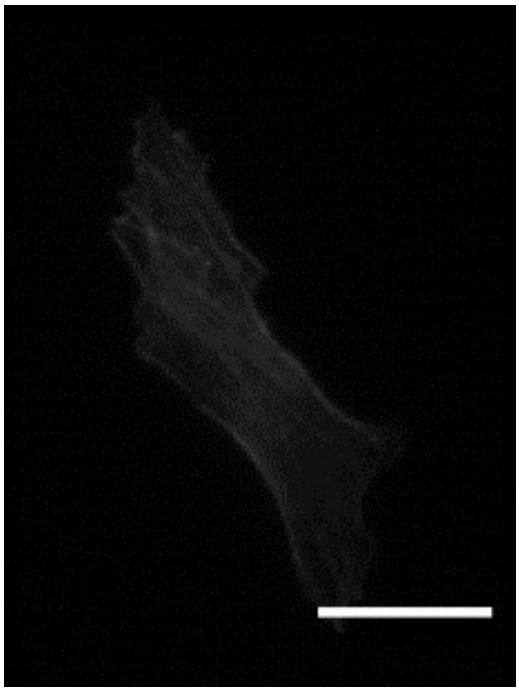

(a) Variability in fiber thickness=81%

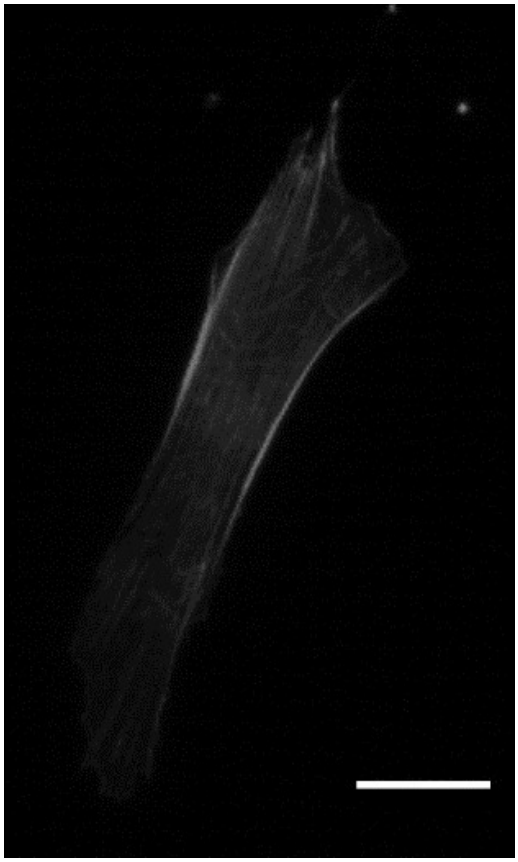

(b) Variability in fiber thickness= 149%

7. Alignment: 0-1 (typically 0.6-1)

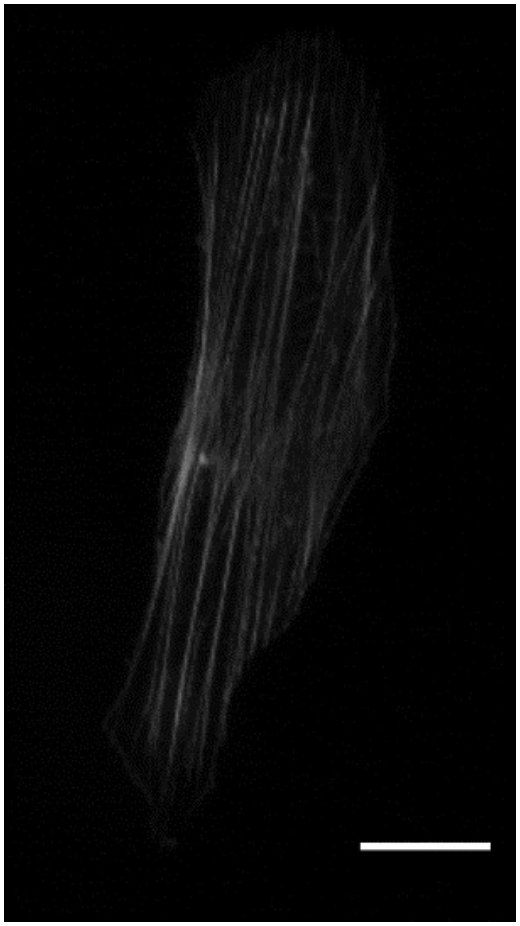

(a) Alignment=0.74

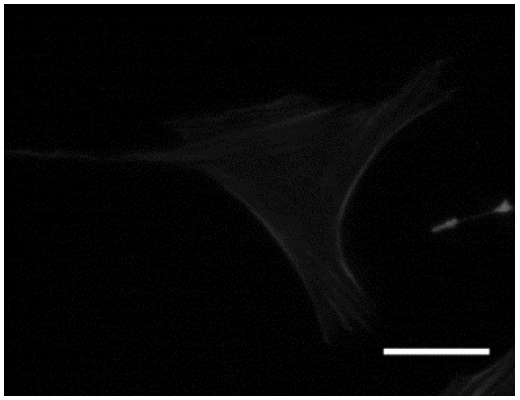

(b) Alignment=0.96

8. Curvature: 0-1 (typically 0-0.6)

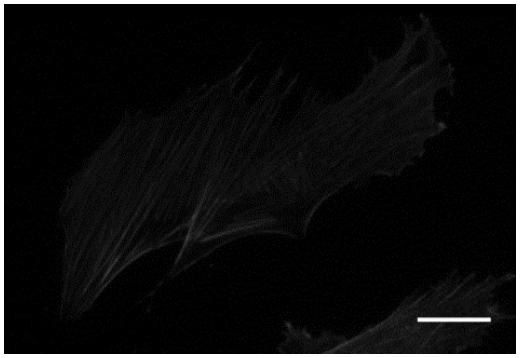

(a) Curvature=0.074

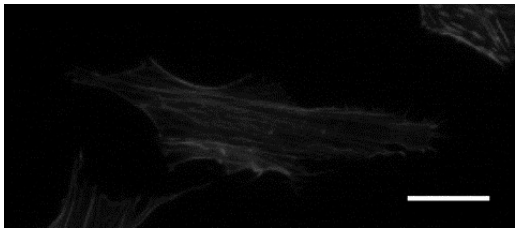

(b) Curvature=0.418

9. Location of fiber peak: 0-1

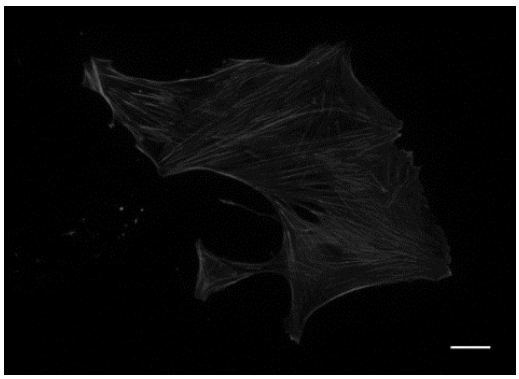

(a) Location of fiber peak=0.036

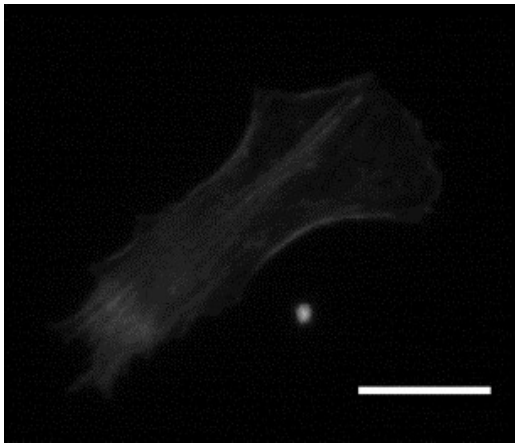

(b) Location of fiber peak=0.27147

10. Fiber spread: 0-1 (typically 0.1-0.3)

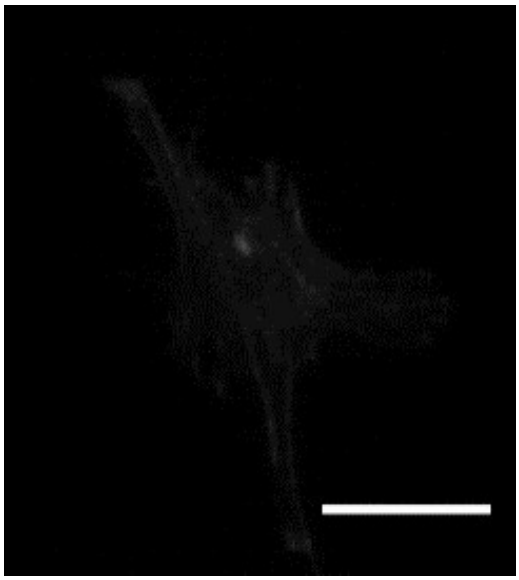

(a) Fiber spread=0.10267

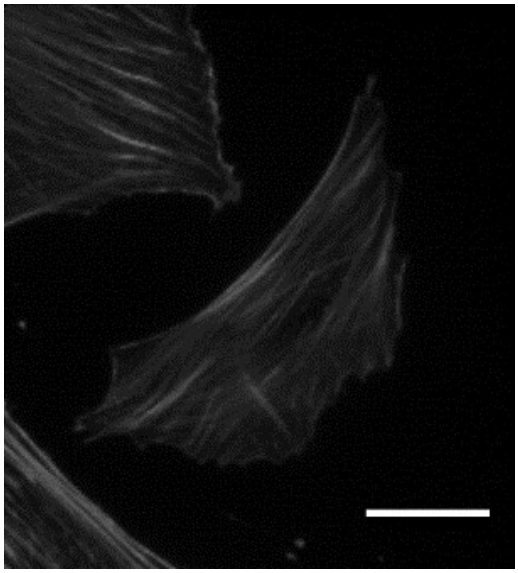

(b) Fiber spread=0.27147

11. Length (AU): 0-∞

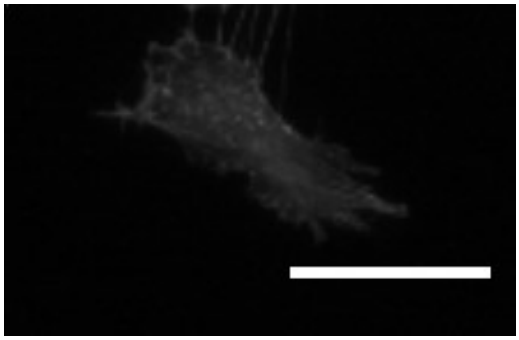

(a) Length=19.47

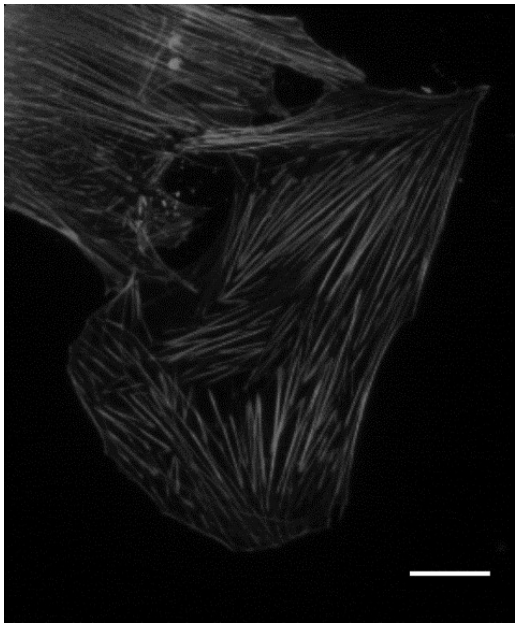

(b) Length=103.68

12. Variability in fiber length ($\%$): 0-∞

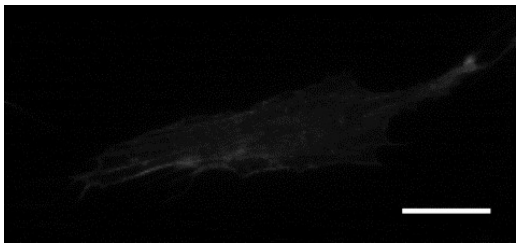

(a) Variability in fiber length=71.3$\%$

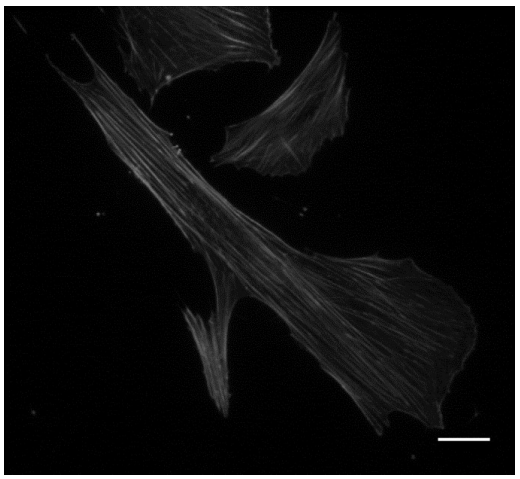

(b) Variability in fiber length=247.7$\%$

13. Chirality (deg): 0-90

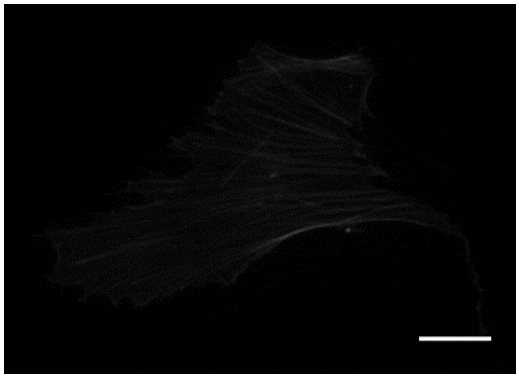

(a) Chirality=35.2 deg

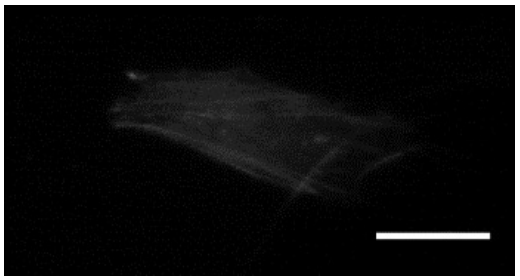

(b) Chiralit=89.6 deg

14. Variability in chirality (deg^2): 0-8100

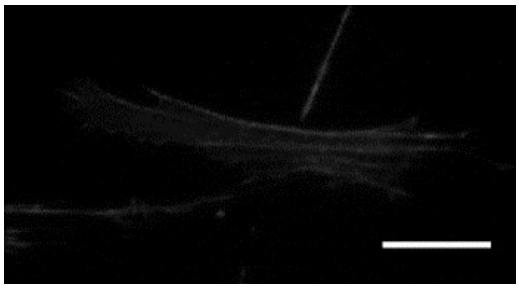

(a) Variability in chirality=239.8 deg^2

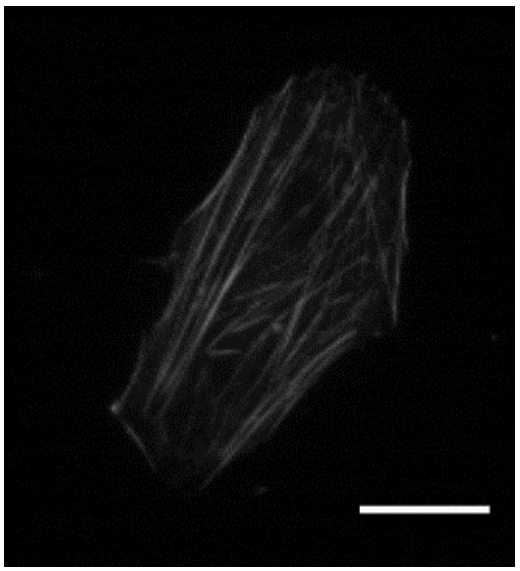

(b) Variability in chirality=772.5 deg^2

Appendix C

Matlab codes

C.1 Matlab code for migration trajectory

```
clear all
clc

T=readtable('migration-trajectory.xlsx');
%File name for the excel input
p=1;
cc=jet(11);
%Number of cells and colours for trajectory
figure;
hold on
%Create a plain image for trajectory
plot([-600 600],[0 0],'k-')
plot([0 0],[-600 600],'k-')
axis([-600 600 -600 600])
box on
for j=1:11
n=sum(T.CellID==j);
x=zeros(1,n-1);
y=zeros(1,n-1);
for i=(1:(n-1))
x(i)=T.x_coordinate_pixel_(p+i)-T.x_coordinate_pixel_(p);
```

```
y(i)=T.y_coordinate_pixel_(p+i)-T.y_coordinate_pixel_(p);
end;
f1=['x',num2str(j),'.png']
plot(x,y,'color',cc(j,:),'LineWidth',2)
plot(x(n-1),y(n-1),'k.','MarkerSize',20)
p=p+n;
end;
```

C.2 Migration straightness one

$$\text{Straightness one}=\frac{\text{Euclidean distance}}{\text{Total migration length}}$$

```
clear all
clc
T=readtable('migration-trajectory.xlsx');
%File name for the excel input
p=0;
x=zeros(1,300)
e=zeros(1,300)
for j=1:9
n=sum(T.CellID==j);
d=0;
for i=(1:(n-1))
s=(T.x_coordinate_pixel_(p+i+1)-T.x_coordinate_pixel_(p+i))^2+...
(T.y_coordinate_pixel_(p+i+1)-T.y_coordinate_pixel_(p+i))^2;
d=d+sqrt(s);
%Calculate the total migration length
end;
x(j)=sqrt((T.x_coordinate_pixel_(p+n)-T.x_coordinate_pixel_(p+1))^2+...
(T.y_coordinate_pixel_(p+n)-T.y_coordinate_pixel_(p+1))^2)/d;
%Calculate the straightness
p=p+n;
e(j)=d;
end;
x=x';
```

```
e=e';
writetable(table(x), 'fastmigration_straightness.xls');
%Output straightness one
writetable(table(e), 'fastmigration_straightness.xls');
%Output the total migration length
```

C.3 Migration straightness two

$$\text{Straightness two} = \frac{\text{Maximum distance from origin}}{\text{Total migration length}}$$

```
clear all
clc
T=readtable('migration-trajectory.xlsx');
p=0;
x=zeros(1,300);
c=0;
for j=1:11
n=sum(T.CellID==j);
a=(T.x_coordinate_pixel_(p+2)-T.x_coordinate_pixel_(p+1))^2+...
(T.y_coordinate_pixel_(p+2)-T.y_coordinate_pixel_(p+1))^2;
for i=(1:(n-2))
b=(T.x_coordinate_pixel_(p+i+2)-T.x_coordinate_pixel_(p+1))^2+...
(T.y_coordinate_pixel_(p+i+2)-T.y_coordinate_pixel_(p+1))^2;
a=max(a,b);
%Find the maximum distance from origin
end;
x(j)=sqrt(a);
p=p+n;
end;
x=x';
writetable(table(x),'fastmigration_directness.xls');
%Output the maximum distance from origin
```

Bibliography

[1] J. Clucas and F. Valderrama. ERM proteins in cancer progression. *Journal of Cell Science*, 128(6):1253–1253, 2015.

[2] Qing Luo, Dongdong Kuang, Bingyu Zhang, and Guanbin Song. Cell stiffness determined by atomic force microscopy and its correlation with cell motility. *BBA - General Subjects*, 1860(9):1953–1960, 2016.

[3] Xiaoli Zhang, Luis R Flores, Michael C Keeling, Kristina Sliogeryte, and Núria Gavara. Ezrin phosphorylation at t567 modulates cell migration, mechanical properties, and cytoskeletal organization. *International Journal of Molecular Sciences*, 21(2):435, 2020.

[4] Bruno Fiévet, Daniel Louvard, and Monique Arpin. ERM proteins in epithelial cell organization and functions. *Biochimica et Biophysica Acta - Molecular Cell Research*, 1773(5):653–660, 2007.

[5] Athar H Chishti, Anthony C Kim, Shirin M Marfatia, Mohini Lutchman, Manjit Hanspal, Hitesh Jindal, Shih-Chun Liu, Philip S Low, Guy A Rouleau, Narla Mohandas, et al. The ferm domain: a unique module involved in the linkage of cytoplasmic proteins to the membrane. *Trends in biochemical sciences*, 23(8):281–282, 1998.

[6] Kosei Takeuchi, Naruki Sato, Hideko Kasahara, Noriko Funayama, Akira Nagafuchi, Shigenobu Yonemura, and Sachiko Tsukita. Perturbation of cell adhesion and microvilli formation by antisense oligonucleotides to erm family members. *The Journal of cell biology*, 125(6):1371–1384, 1994.

[7] Mark Berryman, Zsofia Franck, and Anthony Bretscher. Ezrin is concentrated in the apical microvilli of a wide variety of epithelial cells whereas moesin is found primarily in endothelial cells. *Journal of cell science*, 105(4):1025–1043, 1993.

[8] M Amieva, O Turumen, A Vaheri, D Louvard, and M Arpin. Radixin ls a component of hepatocyte microvilli in situ. *Exp. Cell Res*, 210:140–144, 1994.

[9] A. Bretscher. Purification of an 80,000-dalton protein that is a component of the isolated microvillus cytoskeleton, and its localization in nonmuscle cells. *The Journal of cell biology*, 97(2):425–432, 1983.

[10] Kathleen L Gould, Jonathan A Cooper, Anthony Bretscher, and Tony Hunter. The protein-tyrosine kinase substrate, p81, is homologous to a chicken microvillar core protein. *The Journal of cell biology*, 102(2):660–669, 1986.

[11] R Gary and A Bretscher. Ezrin self-association involves binding of an N-terminal domain to a normally masked C-terminal domain that includes the F-actin binding

site. *Molecular biology of the cell*, 6(8):1061–75, aug 1995.

[12] M. Algrain, O. Turunen, A. Vaheri, D. Louvard, and M. Arpin. Ezrin contains cytoskeleton and membrane binding domains accounting for its proposed role as a membrane-cytoskeletal linker. *Journal of Cell Biology*, 120(1):129–140, 1993.

[13] Ossi Turunen, Torsten Wahlström, and Antti Vaheri. Ezrin has a COOH-terminal actin-binding site that is conserved in the ezrin protein family. *Journal of Cell Biology*, 126(6):1445–1453, 1994.

[14] Matthew A. Pearson, David Reczek, Anthony Bretscher, and P. Andrew Karplus. Structure of the ERM protein moesin reveals the FERM domain fold masked by an extended actin binding tail domain. *Cell*, 101(3):259–270, 2000.

[15] Sachiko Tsukita, Kumiko Oishi, Naruki Sato, Junji Sagara, Akihiko Kawai, and Shoichiro Tsukita. ERM family members as molecular linkers between the cell surface glycoprotein CD44 and actin-based cytoskeletons. *Journal of Cell Biology*, 126(2):391–401, 1994.

[16] S. Yonemura, A. Nagafuchi, N. Sato, and S. Tsukita. Concentration of an integral membrane protein, CD43 (leukosialin, sialophorin), in the cleavage furrow through the interaction of its cytoplasmic domain with actin-based cytoskeletons. *Journal of Cell Biology*, 120(2):437–449, 1993.

[17] T. S. Helander, O. Carpen, O. Turunen, P. E. Kovanen, A. Vaheri, and T. Timonen. ICAM-2 redistributed by ezrin as a target for killer cells. *Nature*, 382(6588):265–268, 1996.

[18] David Reczek, Mark Berryman, and Anthony Bretscher. Identification of ebp50: A pdz-containing phosphoprotein that associates with members of the ezrin-radixin-moesin family. *The Journal of cell biology*, 139(1):169–179, 1997.

[19] Edward J. Weinman, Randy A. Hall, Peter A. Friedman, Lee-Yuan Liu-Chen, and Shirish Shenolikar. the Association of Nherf Adaptor Proteins With G Protein–Coupled Receptors and Receptor Tyrosine Kinases. *Annual Review of Physiology*, 68(1):491–505, 2006.

[20] Ofelia Maniti, Nada Khalifat, Kriti Goggia, Fabien Dalonneau, Christophe Guérin, Laurent Blanchoin, Laurence Ramos, and Catherine Picart. Binding of moesin and ezrin to membranes containing phosphatidylinositol (4,5) bisphosphate: A comparative study of the affinity constants and conformational changes. *Biochimica et Biophysica Acta - Biomembranes*, 1818(11):2839–2849, 2012.

[21] Henri S. Saleh, Ulrike Merkel, Katja J. Geißler, Tobias Sperka, Antonio Sechi, Constanze Breithaupt, and Helen Morrison. Properties of an Ezrin Mutant Defective in F-actin Binding. *Journal of Molecular Biology*, 385(4):1015–1031, 2009.

[22] Qianzhi Li, Mark R. Nance, Rima Kulikauskas, Kevin Nyberg, Richard Fehon, P. Andrew Karplus, Anthony Bretscher, and John J.G. Tesmer. Self-masking in an Intact ERM-merlin Protein: An Active Role for the Central α-Helical Domain. *Journal of Molecular Biology*, 365(5):1446–1459, 2007.

[23] Motohiro Hirao, Naruki Sato, Takahisa Kondo, Shigenobu Yonemura, and Morito

Monden. Regulation Mechanism of ERM (Ezrin / Radixin / Moesin) Protein / Plasma Membrane Association : Possible Involvement of Phosphatidylinositol Turnover and Rho-dependent Signaling Pathway. *Journal of Cell Biology*, 135(1):37–51, 1996.

[24] Verena Niggli, Christophe Andréoli, Christian Roy, and Paul Mangeat. Identification of a phosphatidylinositol-4, 5-bisphosphate-binding domain in the n-terminal region of ezrin. *Febs Letters*, 376(3):172–176, 1995.

[25] Cécile Barret, Christian Roy, Philippe Montcourrier, Paul Mangeat, and Verena Niggli. Mutagenesis of the phosphatidylinositol 4, 5-bisphosphate (pip2) binding site in the nh2-terminal domain of ezrin correlates with its altered cellular distribution. *The Journal of cell biology*, 151(5):1067–1080, 2000.

[26] Matthias Janke, Alexander Herrig, Judith Austermann, Volker Gerke, Claudia Steinem, and Andreas Janshoff. Actin binding of ezrin is activated by specific recognition of pip2-functionalized lipid bilayers. *Biochemistry*, 47(12):3762–3769, 2008.

[27] Laiqiang Huang, Teresa YW Wong, Richard CC Lin, and Heinz Furthmayr. Replacement of threonine 558, a critical site of phosphorylation of moesin in vivo, with aspartate activates f-actin binding of moesin regulation by conformational change. *Journal of Biological Chemistry*, 274(18):12803–12810, 1999.

[28] T Matsui, M Maeda, Y Doi, S Yonemura, M Amano, K Kaibuchi, S Tsukita, and S Tsukita. Rho-kinase phosphorylates COOH-terminal threonines of ezrin/radixin/moesin (ERM) proteins and regulates their head-to-tail association. *The Journal of cell biology*, 140(3):647–57, feb 1998.

[29] Tony Ng, Maddy Parsons, William E Hughes, James Monypenny, Daniel Zicha, Alexis Gautreau, Monique Arpin, Steve Gschmeissner, Peter J Verveer, Philippe IH Bastiaens, et al. Ezrin is a downstream effector of trafficking pkc–integrin complexes involved in the control of cell motility. *The EMBO journal*, 20(11):2723–2741, 2001.

[30] Harn Shiue, Mark W. Musch, Yingmin Wang, Eugene B. Chang, and Jerrold R. Turner. Akt2 phosphorylates ezrin to trigger NHE3 translocation and activation. *Journal of Biological Chemistry*, 280(2):1688–1695, 2005.

[31] Bruno T Fievet, Alexis Gautreau, Christian Roy, Laurence Del Maestro, Paul Mangeat, Daniel Louvard, and Monique Arpin. Phosphoinositide binding and phosphorylation act sequentially in the activation mechanism of ezrin. *The Journal of cell biology*, 164(5):653–659, 2004.

[32] Julia A Braunger, Bastian R Brückner, Stefan Nehls, Anna Pietuch, Volker Gerke, Ingo Mey, Andreas Janshoff, and Claudia Steinem. Phosphatidylinositol 4, 5-bisphosphate alters the number of attachment sites between ezrin and actin filaments a colloidal probe study. *Journal of Biological Chemistry*, 289(14):9833–9843, 2014.

[33] David N Chambers and Anthony Bretscher. Ezrin mutants affecting dimerization

and activation. *Biochemistry*, 44(10):3926–3932, 2005.

[34] Victoria Shabardina, Corinna Kramer, Benjamin Gerdes, Julia Braunger, Andrea Cordes, Jonas Schäfer, Ingo Mey, David Grill, Volker Gerke, and Claudia Steinem. Mode of ezrin-membrane interaction as a function of pip2 binding and pseudophosphorylation. *Biophysical journal*, 110(12):2710–2719, 2016.

[35] Anthony Bretscher, Kevin Edwards, and Richard G. Fehon. ERM proteins and merlin: Integrators at the cell cortex. *Nature Reviews Molecular Cell Biology*, 3(8):586–599, 2002.

[36] J Krieg and Tony Hunter. Identification of the two major epidermal growth factor-induced tyrosine phosphorylation sites in the microvillar core protein ezrin. *Journal of Biological Chemistry*, 267(27):19258–19265, 1992.

[37] Tiziana Crepaldi, Alexis Gautreau, Paolo M Comoglio, Daniel Louvard, and Monique Arpin. Ezrin is an effector of hepatocyte growth factor–mediated migration and morphogenesis in epithelial cells. *The Journal of cell biology*, 138(2):423–434, 1997.

[38] Alexis Gautreau, Patrick Poullet, Daniel Louvard, and Monique Arpin. Ezrin, a plasma membrane–microfilament linker, signals cell survival through the phosphatidylinositol 3-kinase/akt pathway. *Proceedings of the National Academy of Sciences*, 96(13):7300–7305, 1999.

[39] Matti Autero, Leena Heiska, Lars Rönnstrand, Antti Vaheri, Carl G Gahmberg, and Olli Carpén. Ezrin is a substrate for lck in t cells. *FEBS letters*, 535(1-3):82–86, 2003.

[40] Leena Heiska and Olli Carpén. Src phosphorylates ezrin at tyrosine 477 and induces a phosphospecific association between ezrin and a kelch-repeat protein family member. *Journal of Biological Chemistry*, 280(11):10244–10252, 2005.

[41] J Srivastava, BE Elliott, D Louvard, and M Arpin. Src-dependent ezrin phosphorylation in adhesion-mediated signaling. *Molecular biology of the cell*, 16(3):1481–1490, 2005.

[42] Alexandra Naba, Celine Reverdy, Daniel Louvard, and Monique Arpin. Spatial recruitment and activation of the fes kinase by ezrin promotes hgf-induced cell scattering. *The EMBO journal*, 27(1):38–50, 2008.

[43] Hannah Mak, Alexandra Naba, Sonal Varma, Colleen Schick, Andrew Day, Sandip K SenGupta, Monique Arpin, and Bruce E Elliott. Ezrin phosphorylation on tyrosine 477 regulates invasion and metastasis of breast cancer cells. *BMC cancer*, 12(1):82, 2012.

[44] Eeva Auvinen, Niina Kivi, and Antti Vaheri. Regulation of ezrin localization by Rac1 and PIPK in human epithelial cells. *Experimental Cell Research*, 313(4):824–833, 2007.

[45] S Hiscox and W G Jiang. Ezrin regulates cell-cell and cell-matrix adhesion, a possible role with E-cadherin/beta-catenin. *Journal of cell science*, 112 Pt 18(October):3081–3090, 1999.

[46] Max Koltzscher, Claudia Neumann, Simone Kö, and Volker Gerke. Ezrin regulates e-cadherin-dependent adherens junction assembly through rac1 activation. *Molecular Biology of the Cell*, 14(February):2372–2384, 2003.

[47] Jean Paul ten Klooster, Marnix Jansen, Jin Yuan, Viola Oorschot, Harry Begthel, Valeria Di Giacomo, Frédéric Colland, John de Koning, Madelon M. Maurice, Peter Hornbeck, and Hans Clevers. Mst4 and Ezrin Induce Brush Borders Downstream of the Lkb1/Strad/Mo25 Polarization Complex. *Developmental Cell*, 16(4):551–562, 2009.

[48] T Crepaldi, A Gautreau, P Comoglio, D Louvard, and M Arpin. Ezrin is an effector of hepotocyte growth factor-mediated migration and morphogeneis in epithelial cells. *J. Cell Biol.*, 138(2):423–434, 1997.

[49] Nicoletta Filigheddu, Viola F Gnocchi, Marco Coscia, Miriam Cappelli, Paolo E Porporato, and Riccardo Taulli. Activated ezrin promotes cell migration through recruitment of the GEF Dbl to lipid rafts and preferential downstream activation of Cdc42. *Molecular biology of the cell*, 18(December):986–994, 2007.

[50] Verena Niggli and Jérémie Rossy. Ezrin/radixin/moesin: Versatile controllers of signaling molecules and of the cortical cytoskeleton. *International Journal of Biochemistry and Cell Biology*, 40(3):344–349, 2008.

[51] Yi Zheng. Dbl family guanine nucleotide exchange factors. *Trends in Biochemical Sciences*, 26(12):724–732, 2001.

[52] Sun Young Moon and Yi Zheng. Rho GTPase-activating proteins in cell regulation. *Trends in Cell Biology*, 13(1):13–22, 2003.

[53] Anja Schmidt and Alan Hall. Guanine nucleotide exchange factors for Rho GTPases: Turning on the switch. *Genes and Development*, 16(13):1587–1609, 2002.

[54] S. Huveneers and E. H. J. Danen. Adhesion signaling - crosstalk between integrins, Src and Rho. *Journal of Cell Science*, 122(8):1059–1069, 2009.

[55] Paschal A Oude Weernink, Konstantinos Meletiadis, Silvia Hommeltenberg, Matthias Hinz, Hisamitsu Ishihara, Martina Schmidt, and Karl H Jakobs. Activation of type i phosphatidylinositol 4-phosphate 5-kinase isoforms by the rho gtpases, rhoa, rac1, and cdc42. *Journal of Biological Chemistry*, 279(9):7840–7849, 2004.

[56] Kazuo Takahashi, Takuya Sasaki, Akiko Mammoto, Kenji Takaishi, Takaaki Kameyama, Sachiko Tsukita, Shoichiro Tsukita, and Yoshimi Takai. Direct interaction of the Rho GDP dissociation inhibitor with ezrin/radixin/moesin initiates the activation of the Rho small G protein. *Journal of Biological Chemistry*, 272(37):23371–23375, 1997.

[57] Hi-Su Yang and Philip W Hinds. Phosphorylation of ezrin by cyclin-dependent kinase 5 induces the release of rho gdp dissociation inhibitor to inhibit rac1 activity in senescent cells. *Cancer research*, 66(5):2708–2715, 2006.

[58] Tobias Sperka, Katja J. Geißler, Ulrike Merkel, Ingmar Scholl, Ignacio Rubio, Peter Herrlich, and Helen L. Morrison. Activation of ras requires the ERM-dependent link of actin to the plasma membrane. *PLoS ONE*, 6(11), 2011.

[59] Romina d'Angelo, Sandra Aresta, Anne Blangy, Laurence Del Maestro, Daniel Louvard, and Monique Arpin. Interaction of ezrin with the novel guanine nucleotide exchange factor plekhg6 promotes rhog-dependent apical cytoskeleton rearrangements in epithelial cells. *Molecular biology of the cell*, 18(12):4780–4793, 2007.

[60] Anastassia Hatzoglou, Isabelle Ader, Anne Splingard, James Flanders, Evelyne Saade, Ingrid Leroy, Sabine Traver, Sandra Aresta, and Jean De Gunzburg. Gem associates with ezrin and acts via the rho-gap protein gmip to down-regulate the rho pathway. *Molecular biology of the cell*, 18(4):1242–1252, 2007.

[61] Junjie Piao, Shusen Liu, Yunjie Xu, Changan Wang, Zhenhua Lin, Yunzhi Qin, and Shuangping Liu. Ezrin protein overexpression predicts the poor prognosis of pancreatic ductal adenocarcinomas. *Experimental and Molecular Pathology*, 98(1):1–6, 2015.

[62] Jienan Kong, Yan Li, Shuangping Liu, Haidan Jin, Yongjun Shang, Chengshi Quan, Yulin Li, and Zhenhua Lin. High expression of ezrin predicts poor prognosis in uterine cervical cancer. *BMC Cancer*, 13(1):1, 2013.

[63] Premila D Leiphrakpam, Ashwani Rajput, Michelle Mathiesen, Ekta Agarwal, Audrey J Lazenby, Chandrakanth Are, Michael G Brattain, and Sanjib Chowdhury. Ezrin expression and cell survival regulation in colorectal cancer. *Cellular signalling*, 26(5):868–879, 2014.

[64] Chand Khanna, Xiaolin Wan, Seuli Bose, Ryan Cassaday, Osarenoma Olomu, Arnulfo Mendoza, Choh Yeung, Richard Gorlick, Stephen M. Hewitt, and Lee J. Helman. The membrane-cytoskeleton linker ezrin is necessary for osteosarcoma metastasis. *Nature Medicine*, 10(2):182–186, 2004.

[65] Endi Wang, Qingchang Li, Hui Gao, Hongtao Xu, Xin Wang, Yongqi Pan, Fengxia Hao, Xueshan Qiu, Maggie Stoecker, and Enhua Wang. Expression of ezrin correlates with malignant phenotype of lung cancer, and in vitro knockdown of ezrin reverses the aggressive biological behavior of lung cancer cells. *Tumor Biology*, 33(5):1493–1504, 2012.

[66] Yong Chen, Dongmei Wang, Zhen Guo, Jun Zhao, Bing Wu, Hui Deng, Ti Zhou, Hongjun Xiang, Fei Gao, Xue Yu, Jian Liao, Tarsha Ward, Peng Xia, Chibuzo Emenari, Xia Ding, Winston Thompson, Kelong Ma, Jingde Zhu, Felix Aikhionbare, Kefen Dou, Shi-Yuan Cheng, and Xuebiao Yao. Rho kinase phosphorylation promotes ezrin-mediated metastasis in hepatocellular carcinoma. *Cancer research*, 71(5):1721–9, mar 2011.

[67] Yin Choy Chuan, See Tong Pang, Angel Cedazo-Minguez, Gunnar Norstedt, Åke Pousette, and Amilcar Flores-Morales. Androgen induction of prostate cancer cell invasion is mediated by ezrin. *Journal of Biological Chemistry*, 281(40):29938–29948, 2006.

[68] L. Ren, S. H. Hong, J. Cassavaugh, T. Osborne, A. J. Chou, S. Y. Kim, R. Gorlick, S. M. Hewitt, and C. Khanna. The actin-cytoskeleton linker protein ezrin is regulated during osteosarcoma metastasis by PKC. *Oncogene*, 28(6):792–802,

2009.

[69] David Sarrió, Socorro María Rodríguez-Pinilla, Ana Dotor, Francisco Calero, David Hardisson, and José Palacios. Abnormal ezrin localization is associated with clinicopathological features in invasive breast carcinomas. *Breast Cancer Research and Treatment*, 98(1):71–79, Jul 2006.

[70] Jingchun Jin, Tiefeng Jin, Meiling Quan, Yingshi Piao, and Zhenhua Lin. Ezrin overexpression predicts the poor prognosis of gastric adenocarcinoma. *Diagnostic Pathology*, 7(1):1, 2012.

[71] Jienan Kong, Chunchan Di, Junjie Piao, Jie Sun, Longzhe Han, Liyan Chen, Guanghai Yan, and Zhenhua Lin. Ezrin contributes to cervical cancer progression through induction of epithelial-mesenchymal transition. *Oncotarget*, 7(15), 2016.

[72] Raghu Kalluri and Robert A Weinberg. The basics of epithelial-mesenchymal transition. *The Journal of clinical investigation*, 119(6):1420–1428, 2009.

[73] Bruce E. Elliott, Hui Qiao, Daniel Louvard, and Monique Arpin. Co-operative effect of c-Src and ezrin in deregulation of cell-cell contacts and scattering of mammary carcinoma cells. *Journal of Cellular Biochemistry*, 92(1):16–28, 2004.

[74] Qiong Li, Mingfu Wu, Hui Wang, Gang Xu, Tao Zhu, Yongtao Zhang, Ping Liu, Anping Song, Chen Gang, Zhiqiang Han, Jianfeng Zhou, Li Meng, Yunpin Lu, Shixuan Wang, and Ding Ma. Ezrin silencing by small hairpin RNA reverses metastatic behaviors of human breast cancer cells. *Cancer Letters*, 261(1):55–63, 2008.

[75] Zhaojin Yu, Mingli Sun, Feng Jin, Qinghuan Xiao, Miao He, Huizhe Wu, Jie Ren, Lin Zhao, Haishan Zhao, Weifan Yao, Fengping Shan, Yaming Cao, and Minjie Wei. Combined expression of ezrin and E-cadherin is associated with lymph node metastasis and poor prognosis in breast cancer. *Oncology Reports*, 34(1):165–174, 2015.

[76] Jie Mao, Xian-rui Yuan, Shan-shui Xu, Xiao-chun Jiang, and Xin-tong Zhao. Expression and functional significance of ezrin in human brain astrocytoma. *Cell biochemistry and biophysics*, 67(3):1507–1511, 2013.

[77] Bruce E Elliott, Jalna A Meens, Sandip K SenGupta, Daniel Louvard, and Monique Arpin. The membrane cytoskeletal crosslinker ezrin is required for metastasis of breast carcinoma cells. *Breast cancer research*, 7(3):R365, 2005.

[78] David Sarrió, Socorro María Rodríguez-Pinilla, Ana Dotor, Francisco Calero, David Hardisson, and José Palacios. Abnormal ezrin localization is associated with clinicopathological features in invasive breast carcinomas. *Breast cancer research and treatment*, 98(1):71–79, 2006.

[79] Sophya Konstantinovsky, Ben Davidson, and Reuven Reich. Ezrin and bcar1/p130cas mediate breast cancer growth as 3-d spheroids. *Clinical & experimental metastasis*, 29(6):527–540, 2012.

[80] Qiong Li, Mingfu Wu, Hui Wang, Gang Xu, Tao Zhu, Yongtao Zhang, Ping Liu, Anping Song, Chen Gang, Zhiqiang Han, et al. Ezrin silencing by small hairpin rna reverses metastatic behaviors of human breast cancer cells. *Cancer letters*,

261(1):55–63, 2008.

[81] Abdi Ghaffari, Victoria Hoskin, Alvin Szeto, Maaike Hum, Navid Liaghati, Kanji Nakatsu, Yolanda Madarnas, Sandip Sengupta, and Bruce E Elliott. A novel role for ezrin in breast cancer angio/lymphangiogenesis. *Breast Cancer Research*, 16(5):438, 2014.

[82] Zhaojin Yu, Mingli Sun, Feng Jin, Qinghuan Xiao, Miao He, Huizhe Wu, Jie Ren, Lin Zhao, Haishan Zhao, Weifan Yao, et al. Combined expression of ezrin and e-cadherin is associated with lymph node metastasis and poor prognosis in breast cancer. *Oncology reports*, 34(1):165–174, 2015.

[83] Nan Li, Jienan Kong, Zhenhua Lin, Yang Yang, Tiefeng Jin, Ming Xu, Jie Sun, and Liyan Chen. Ezrin promotes breast cancer progression by modulating akt signals. *British journal of cancer*, 120(7):703–713, 2019.

[84] Victoria Hoskin, Alvin Szeto, Abdi Ghaffari, Peter A Greer, Graham P Côté, and Bruce E Elliott. Ezrin regulates focal adhesion and invadopodia dynamics by altering calpain activity to promote breast cancer cell invasion. *Molecular biology of the cell*, 26(19):3464–3479, 2015.

[85] Bruce E Elliott, Hui Qiao, Daniel Louvard, and Monique Arpin. Co-operative effect of c-src and ezrin in deregulation of cell–cell contacts and scattering of mammary carcinoma cells. *Journal of cellular biochemistry*, 92(1):16–28, 2004.

[86] Abdi Ghaffari, Victoria Hoskin, Gulisa Turashvili, Sonal Varma, Jeff Mewburn, Graeme Mullins, Peter A Greer, Friedemann Kiefer, Andrew G Day, Yolanda Madarnas, et al. Intravital imaging reveals systemic ezrin inhibition impedes cancer cell migration and lymph node metastasis in breast cancer. *Breast Cancer Research*, 21(1):12, 2019.

[87] Jienan Kong, Chunchan Di, Junjie Piao, Jie Sun, Longzhe Han, Liyan Chen, Guanghai Yan, and Zhenhua Lin. Ezrin contributes to cervical cancer progression through induction of epithelial-mesenchymal transition. *Oncotarget*, 7(15):19631, 2016.

[88] E Auvinen, O Carpen, T Korpela, M Ronty, A Vaheri, and J Tarkkanen. Altered expression of ezrin, e-cadherin and β-catenin in cervical neoplasia. *Neoplasma*, 60(1):56–61, 2013.

[89] Marcelo Patara, Erika Maria Monteiro Santos, Renata de Almeida Coudry, Fernando Augusto Soares, Fábio Oliveira Ferreira, and Benedito Mauro Rossi. Ezrin expression as a prognostic marker in colorectal adenocarcinoma. *Pathology & Oncology Research*, 17(4):827–833, 2011.

[90] Li-Juan Lin and Li-Tian Chen. Association between ezrin protein expression and the prognosis of colorectal adenocarcinoma. *Molecular medicine reports*, 8(1):61–66, 2013.

[91] Adam Elzagheid, Eija Korkeila, Riyad Bendardaf, Abdelbaset Buhmeida, Suvi Heikkilä, Antti Vaheri, Kari Syrjänen, Seppo Pyrhönen, and Olli Carpén. Intense cytoplasmic ezrin immunoreactivity predicts poor survival in colorectal cancer. *Hu-*

man pathology, 39(12):1737–1743, 2008.

[92] Martin Köbel, Tina Langhammer, Stefan Hüttelmaier, Wolfgang D Schmitt, Karen Kriese, Jürgen Dittmer, Hans-Georg Strauss, Christoph Thomssen, and Steffen Hauptmann. Ezrin expression is related to poor prognosis in figo stage i endometrioid carcinomas. *Modern pathology*, 19(4):581–587, 2006.

[93] Jian-Jun Xie, Li-Yan Xu, Yang-Min Xie, Hai-Hua Zhang, Wei-Jia Cai, Fei Zhou, Zhong-Ying Shen, and En-Min Li. Roles of ezrin in the growth and invasiveness of esophageal squamous carcinoma cells. *International journal of cancer*, 124(11):2549–2558, 2009.

[94] Jian-Jun Xie, Li-Yan Xu, Zhi-Yong Wu, Qing Zhao, Xiu-E Xu, Jian-Yi Wu, Qiao Huang, and En-Min Li. Prognostic implication of ezrin expression in esophageal squamous cell carcinoma. *Journal of surgical oncology*, 104(5):538–543, 2011.

[95] Zhi-Qiang Ling, Ken-ichi Mukaisho, Hiroto Yamamoto, Kuan-Hao Chen, Shinji Asano, Yoshio Araki, Hiroyuki Sugihara, Wei-Min Mao, and Takanori Hattori. Initiation of malignancy by duodenal contents reflux and the role of ezrin in developing esophageal squamous cell carcinoma. *Cancer science*, 101(3):624–630, 2010.

[96] Shota Saito, Hiroto Yamamoto, Ken-ichi Mukaisho, Sho Sato, Tomoki Higo, Takanori Hattori, Gaku Yamamoto, and Hiroyuki Sugihara. Mechanisms underlying cancer progression caused by ezrin overexpression in tongue squamous cell carcinoma. *PloS one*, 8(1), 2013.

[97] Jingchun Jin, Tiefeng Jin, Meiling Quan, Yingshi Piao, and Zhenhua Lin. Ezrin overexpression predicts the poor prognosis of gastric adenocarcinoma. *Diagnostic pathology*, 7(1):135, 2012.

[98] Li Li, Yuan-Yu Wang, Zhong-Sheng Zhao, and Jie Ma. Ezrin is associated with gastric cancer progression and prognosis. *Pathology & Oncology Research*, 17(4):909–915, 2011.

[99] Hong Jian Wang, Jin Shui Zhu, Qiang Zhang, Hua Guo, Yun Hai Dai, and Xiao Peng Xiong. Rnai-mediated silencing of ezrin gene reverses malignant behavior of human gastric cancer cell line sgc-7901. *Journal of digestive diseases*, 10(4):258–264, 2009.

[100] Prabhu Arumugam, Stefano Partelli, Stacey J Coleman, Ivana Cataldo, Stefania Beghelli, Claudio Bassi, Nilukushi Wijesuriya, Jo-Anne Chin Aleong, Fieke EM Froeling, Aldo Scarpa, et al. Ezrin expression is an independent prognostic factor in gastro-intestinal cancers. *Journal of Gastrointestinal Surgery*, 17(12):2082–2091, 2013.

[101] Yu-Ching Wei, Chien-Feng Li, Shih-Chen Yu, Fong-Fu Chou, Fu-Min Fang, Hock-Liew Eng, Yih-Huei Uen, Yu-Fang Tian, Jing-Mei Wu, Shau-Hsuan Li, et al. Ezrin overexpression in gastrointestinal stromal tumors: an independent adverse prognosticator associated with the non-gastric location. *Modern Pathology*, 22(10):1351–1360, 2009.

[102] Fabiana C Morales, Jennifer R Molina, Yuho Hayashi, and Maria-Magdalena

Georgescu. Overexpression of ezrin inactivates nf2 tumor suppressor in glioblastoma. *Neuro-oncology*, 12(6):528–539, 2010.

[103] Yong Chen, Dongmei Wang, Zhen Guo, Jun Zhao, Bing Wu, Hui Deng, Ti Zhou, Hongjun Xiang, Fei Gao, Xue Yu, et al. Rho kinase phosphorylation promotes ezrin-mediated metastasis in hepatocellular carcinoma. *Cancer research*, 71(5):1721–1729, 2011.

[104] Yan Zhang, Mei-Yu Hu, Wei-Zhong Wu, Zhi-Jun Wang, Kang Zhou, Xi-Liang Zha, and Kang-Da Liu. The membrane-cytoskeleton organizer ezrin is necessary for hepatocellular carcinoma cell growth and invasiveness. *Journal of cancer research and clinical oncology*, 132(11):685–697, 2006.

[105] Ahmed Musa Hago, Yaser Gamallat, Salma Abdi Mahmoud, Yuhong Huang, Jun Zhang, Yousra Khidir Mahmoud, Jingwen Wang, Yuanyi Wei, Li Wang, Shuting Zhou, et al. Ezrin expression is altered in mice lymphatic metastatic hepatocellular carcinoma and subcellular fractions upon annexin 7 modulation in-vitro. *Biomedicine & Pharmacotherapy*, 85:209–217, 2017.

[106] See-Tong Pang, Xioalei Fang, Alexander Valdman, Gunnar Norstedt, Åke Pousette, Lars Egevad, and Peter Ekman. Expression of ezrin in prostatic intraepithelial neoplasia. *Urology*, 63(3):609–612, 2004.

[107] X Wang, M Liu, CY Zhao, et al. Expression of ezrin and moesin related to invasion, metastasis and prognosis of laryngeal squamous cell carcinoma. *Genet Mol Res*, 13(3):8002–8013, 2014.

[108] Qingchang Li, Hui Gao, Hongtao Xu, Xin Wang, Yongqi Pan, Fengxia Hao, Xueshan Qiu, Maggie Stoecker, Endi Wang, and Enhua Wang. Expression of ezrin correlates with malignant phenotype of lung cancer, and in vitro knockdown of ezrin reverses the aggressive biological behavior of lung cancer cells. *Tumor Biology*, 33(5):1493–1504, 2012.

[109] Xiyun Deng, Sarah H Tannehill-Gregg, Murali VP Nadella, Guangchun He, Andrea Levine, Ya Cao, and Thomas J Rosol. Parathyroid hormone-related protein and ezrin are up-regulated in human lung cancer bone metastases. *Clinical & experimental metastasis*, 24(2):107–119, 2007.

[110] Wen-Hui Weng, Jan Åhlén, Kristina Åström, Weng-Onn Lui, and Catharina Larsson. Prognostic impact of immunohistochemical expression of ezrin in highly malignant soft tissue sarcomas. *Clinical Cancer Research*, 11(17):6198–6204, 2005.

[111] Hsuan-Ying Huang, Chien-Feng Li, Fu-Min Fang, Jen-Wei Tsai, Shau-Hsuan Li, Yuan-Ting Lee, and Huei-Min Wei. Prognostic implication of ezrin overexpression in myxofibrosarcomas. *Annals of surgical oncology*, 17(12):3212–3219, 2010.

[112] Liang Wang, Gui-Nan Lin, Xiang-Li Jiang, and Yue Lu. Expression of ezrin correlates with poor prognosis of nasopharyngeal carcinoma. *Tumor Biology*, 32(4):707–712, 2011.

[113] Tiefeng Jin, Jingchun Jin, Xiangyu Li, Songnan Zhang, Yun Ho Choi, Yingshi Piao, Xionghu Shen, and Zhenhua Lin. Prognostic implications of ezrin and phospho-

rylated ezrin expression in non-small cell lung cancer. *BMC cancer*, 14(1):191, 2014.

[114] Ho Won Lee, Eui Han Kim, and Mee-Hye Oh. Clinicopathologic implication of ezrin expression in non-small cell lung cancer. *Korean journal of pathology*, 46(5):470, 2012.

[115] Xiao-Qin Zhang, Guo-Ping Chen, Tao Wu, Jian-Ping Yan, and Jian-Ying Zhou. Expression and clinical significance of ezrin in non–small-cell lung cancer. *Clinical lung cancer*, 13(3):196–204, 2012.

[116] Chand Khanna, Xiaolin Wan, Seuli Bose, Ryan Cassaday, Osarenoma Olomu, Arnulfo Mendoza, Choh Yeung, Richard Gorlick, Stephen M Hewitt, and Lee J Helman. The membrane-cytoskeleton linker ezrin is necessary for osteosarcoma metastasis. *Nature medicine*, 10(2):182–186, 2004.

[117] Jian Zhang, Jianhong Zuo, Mingsheng Lei, Song Wu, Xiaofang Zang, and Chaoyue Zhang. Ezrin promotes invasion and migration of the mg63 osteosarcoma cell. *Chinese medical journal*, 127(10):1954–1959, 2014.

[118] Sébastien Salas, Catherine Bartoli, Jean-Laurent Deville, Jean Gaudart, Fréderic Fina, Arlette Calisti, Gérard Bollini, Georges Curvale, Jean-Claude Gentet, Florence Duffaud, et al. Ezrin and alpha-smooth muscle actin are immunohistochemical prognostic markers in conventional osteosarcomas. *Virchows Archiv*, 451(6):999–1007, 2007.

[119] Chan Kim, Eunah Shin, Soojung Hong, Hong Jae Chon, Hye Ryun Kim, Jung Ryun Ahn, Min Hee Hong, Woo Ick Yang, Jae Kyung Roh, and Sun Young Rha. Clinical value of ezrin expression in primary osteosarcoma. *Cancer research and treatment: official journal of Korean Cancer Association*, 41(3):138, 2009.

[120] Min Suk Kim, Won Seok Song, Wan Hyeong Cho, Soo-Yong Lee, and Dae-Geun Jeon. Ezrin expression predicts survival in stage iib osteosarcomas. *Clinical Orthopaedics and Related Research®*, 459:229–236, 2007.

[121] L Ren, SH Hong, J Cassavaugh, T Osborne, AJ Chou, SY Kim, Richard Gorlick, SM Hewitt, and C Khanna. The actin-cytoskeleton linker protein ezrin is regulated during osteosarcoma metastasis by pkc. *Oncogene*, 28(6):792–802, 2009.

[122] Stefano Ferrari, Licciana Zanella, Marco Alberghini, Emanuela Palmerini, Eric Staals, and Patrizia Bacchini. Prognostic significance of immunohistochemical expression of ezrin in non-metastatic high-grade osteosarcoma. *Pediatric blood & cancer*, 50(4):752–756, 2008.

[123] Martin Köbel, Elise Gradhand, Katharina Zeng, Wolfgang D Schmitt, Karen Kriese, Tilmann Lantzsch, Matthias Wolters, Jürgen Dittmer, Hans G Strauss, Christoph Thomssen, et al. Ezrin promotes ovarian carcinoma cell invasion and its retained expression predicts poor prognosis in ovarian carcinoma. *International journal of gynecological pathology*, 25(2):121–130, 2006.

[124] Yunxiao Meng, Zhaohui Lu, Shuangni Yu, Qiang Zhang, Yihui Ma, and Jie Chen. Ezrin promotes invasion and metastasis of pancreatic cancer cells. *Journal of*

translational medicine, 8(1):61, 2010.

[125] Hemant M Kocher, Jennifer Sandle, Tariq A Mirza, Ningfeng F Li, and Ian R Hart. Ezrin interacts with cortactin to form podosomal rosettes in pancreatic cancer cells. *Gut*, 58(2):271–284, 2009.

[126] Yazhou Cui, Tianliang Li, Denglu Zhang, and Jinxiang Han. Expression of ezrin and phosphorylated ezrin (pezrin) in pancreatic ductal adenocarcinoma. *Cancer investigation*, 28(3):242–247, 2010.

[127] Junjie Piao, Shusen Liu, Yunjie Xu, Changan Wang, Zhenhua Lin, Yunzhi Qin, and Shuangping Liu. Ezrin protein overexpression predicts the poor prognosis of pancreatic ductal adenocarcinomas. *Experimental and molecular pathology*, 98(1):1–6, 2015.

[128] Yin Choy Chuan, D Iglesias-Gato, L Fernandez-Perez, A Cedazo-Minguez, ST Pang, G Norstedt, Å Pousette, and Amilcar Flores-Morales. Ezrin mediates c-myc actions in prostate cancer cell invasion. *Oncogene*, 29(10):1531–1542, 2010.

[129] Fredrik Jörgren, Mef Nilbert, Eva Rambech, Pär-Ola Bendahl, and Gudrun Lindmark. Ezrin expression in rectal cancer predicts time to development of local recurrence. *International journal of colorectal disease*, 27(7):893–899, 2012.

[130] Gustav Andersson, Christoffer Wennersten, Alexander Gaber, Karolina Boman, Björn Nodin, Mathias Uhlén, Ulrika Segersten, Per-Uno Malmström, and Karin Jirström. Reduced expression of ezrin in urothelial bladder cancer signifies more advanced tumours and an impaired survival: validatory study of two independent patient cohorts. *BMC urology*, 14(1):36, 2014.

[131] Jienan Kong, Yan Li, Shuangping Liu, Haidan Jin, Yongjun Shang, Chengshi Quan, Yulin Li, and Zhenhua Lin. High expression of ezrin predicts poor prognosis in uterine cervical cancer. *BMC cancer*, 13(1):520, 2013.

[132] Teemu Makitie, Olli Carpén, Antti Vaheri, and Tero Kivela. Ezrin as a prognostic indicator and its relationship to tumor characteristics in uveal malignant melanoma. *Investigative ophthalmology & visual science*, 42(11):2442–2449, 2001.

[133] Yanlin Yu, Javed Khan, Chand Khanna, Lee Helman, Paul S Meltzer, and Glenn Merlino. Expression profiling identifies the cytoskeletal organizer ezrin and the developmental homeoprotein six-1 as key metastatic regulators. *Nature medicine*, 10(2):175–181, 2004.

[134] Peter Friedl and Katarina Wolf. Plasticity of cell migration: a multiscale tuning model. *The Journal of cell biology*, 188(1):11–19, 2010.

[135] Pieta K Mattila and Pekka Lappalainen. Filopodia: molecular architecture and cellular functions. *Nature reviews Molecular cell biology*, 9(6):446, 2008.

[136] Benoit Ladoux and Alice Nicolas. Physically based principles of cell adhesion mechanosensitivity in tissues. *Reports on Progress in Physics*, 75(11):116601, 2012.

[137] K Paňková, D Rösel, M Novotnỳ, and Jan Brábek. The molecular mechanisms of transition between mesenchymal and amoeboid invasiveness in tumor cells. *Cel-*

lular and molecular life sciences, 67(1):63–71, 2010.

[138] Miguel Vicente-Manzanares, Colin Kiwon Choi, and Alan Rick Horwitz. Integrins in cell migration–the actin connection. *Journal of cell science*, 122(2):199–206, 2009.

[139] Nathalie Q Balaban, Ulrich S Schwarz, Daniel Riveline, Polina Goichberg, Gila Tzur, Ilana Sabanay, Diana Mahalu, Sam Safran, Alexander Bershadsky, Lia Addadi, et al. Force and focal adhesion assembly: a close relationship studied using elastic micropatterned substrates. *Nature cell biology*, 3(5):466, 2001.

[140] Leann Norman, Kheya Sengupta, and Helim Aranda-Espinoza. Blebbing dynamics during endothelial cell spreading. *European journal of cell biology*, 90(1):37–48, 2011.

[141] Heiko Blaser, Michal Reichman-Fried, Irinka Castanon, Karin Dumstrei, Florence L Marlow, Koichi Kawakami, Lilianna Solnica-Krezel, Carl-Philipp Heisenberg, and Erez Raz. Migration of zebrafish primordial germ cells: a role for myosin contraction and cytoplasmic flow. *Developmental cell*, 11(5):613–627, 2006.

[142] Amine Sadok, Afshan McCarthy, John Caldwell, Ian Collins, Michelle D Garrett, Maggie Yeo, Steven Hooper, Erik Sahai, Sandra Kuemper, Faraz K Mardakheh, et al. Rho kinase inhibitors block melanoma cell migration and inhibit metastasis. *Cancer research*, 75(11):2272–2284, 2015.

[143] Guillaume T Charras, Margaret Coughlin, Timothy J Mitchison, and L Mahadevan. Life and times of a cellular bleb. *Biophysical journal*, 94(5):1836–1853, 2008.

[144] Guillaume Charras and Ewa Paluch. Blebs lead the way: how to migrate without lamellipodia. *Nature reviews Molecular cell biology*, 9(9):730, 2008.

[145] Jianwu Dai and Michael P Sheetz. Membrane tether formation from blebbing cells. *Biophysical journal*, 77(6):3363–3370, 1999.

[146] Guillaume T Charras, Justin C Yarrow, Mike A Horton, L Mahadevan, and TJ Mitchison. Non-equilibration of hydrostatic pressure in blebbing cells. *Nature*, 435(7040):365, 2005.

[147] Jean-Yves Tinevez, Ulrike Schulze, Guillaume Salbreux, Julia Roensch, Jean-François Joanny, and Ewa Paluch. Role of cortical tension in bleb growth. *Proceedings of the National Academy of Sciences*, 106(44):18581–18586, 2009.

[148] Guillaume T Charras, Chi-Kuo Hu, Margaret Coughlin, and Timothy J Mitchison. Reassembly of contractile actin cortex in cell blebs. *The Journal of cell biology*, 175(3):477–490, 2006.

[149] Erik Sahai and Christopher J Marshall. Differing modes of tumour cell invasion have distinct requirements for rho/rock signalling and extracellular proteolysis. *Nature cell biology*, 5(8):711, 2003.

[150] Ann R Kennedy. Prevention of carcinogenesis by protease inhibitors. *Cancer Research*, 54(7 Supplement):1999s–2005s, 1994.

[151] Colin D Paul, Panagiotis Mistriotis, and Konstantinos Konstantopoulos. Cancer cell motility: lessons from migration in confined spaces. *Nature Reviews Cancer*, 17(2):131, 2017.

[152] Peter Friedl, Stefan Borgmann, and Eva-B Bröcker. Amoeboid leukocyte crawling through extracellular matrix: lessons from the dictyostelium paradigm of cell movement. *Journal of leukocyte biology*, 70(4):491–509, 2001.

[153] Sunil K Shaw, Paul S Bamba, Brandy N Perkins, and Francis W Luscinskas. Real-time imaging of vascular endothelial-cadherin during leukocyte transmigration across endothelium. *The Journal of Immunology*, 167(4):2323–2330, 2001.

[154] Jochen Guck, Franziska Lautenschläger, Stephan Paschke, and Michael Beil. Critical review: cellular mechanobiology and amoeboid migration. *Integrative biology*, 2(11-12):575–583, 2010.

[155] Ewa K Paluch and Erez Raz. The role and regulation of blebs in cell migration. *Current opinion in cell biology*, 25(5):582–590, 2013.

[156] Martin Bergert, Anna Erzberger, Ravi A Desai, Irene M Aspalter, Andrew C Oates, Guillaume Charras, Guillaume Salbreux, and Ewa K Paluch. Force transmission during adhesion-independent migration. *Nature cell biology*, 17(4):524, 2015.

[157] Ai Kia Yip, Keng-Hwee Chiam, and Paul Matsudaira. Traction stress analysis and modeling reveal that amoeboid migration in confined spaces is accompanied by expansive forces and requires the structural integrity of the membrane–cortex interactions. *Integrative Biology*, 7(10):1196–1211, 2015.

[158] Tim Lämmermann and Michael Sixt. Mechanical modes of 'amoeboid'cell migration. *Current opinion in cell biology*, 21(5):636–644, 2009.

[159] R Ilona Linnoila, Harry R Keiser, Seth M Steinberg, and Ernest E Lack. Histopathology of benign versus malignant sympathoadrenal paragangliomas: clinicopathologic study of 120 cases including unusual histologic features. *Human pathology*, 21(11):1168–1180, 1990.

[160] Leonard Maurice Franks and Natalie M Teich. *Introduction to the cellular and molecular biology of cancer*. Oxford University Press, USA, 1997.

[161] Yingqun Wang. Breast cancer metastasis driven by erbb2 and 14-3-3ξ: A division of labor. *Cell adhesion & migration*, 4(1):7–9, 2010.

[162] Michael L De Ieso and Andrea J Yool. Mechanisms of aquaporin-facilitated cancer invasion and metastasis. *Frontiers in chemistry*, 6:135, 2018.

[163] G Breier. Angiogenesis in embryonic development—a review. *Placenta*, 21:S11–S15, 2000.

[164] Marcia G Tonnesen, Xiaodong Feng, and Richard AF Clark. Angiogenesis in wound healing. In *Journal of Investigative Dermatology Symposium Proceedings*, volume 5, pages 40–46. Elsevier, 2000.

[165] Marek Zygmunt, Friederike Herr, Karsten Münstedt, Uwe Lang, and Olin D Liang. Angiogenesis and vasculogenesis in pregnancy. *European Journal of Obstetrics & Gynecology and Reproductive Biology*, 110:S10–S18, 2003.

[166] Talia N Crawford, III Alfaro, John B Kerrison, Eric P Jablon, et al. Diabetic retinopathy and angiogenesis. *Current diabetes reviews*, 5(1):8–13, 2009.

[167] Eugene WM Ng and Anthony P Adamis. Targeting angiogenesis, the underlying

disorder in neovascular age-related macular degeneration. *Canadian Journal of Ophthalmology*, 40(3):352–368, 2005.

[168] Robert S Kerbel. Tumor angiogenesis: past, present and the near future. *Carcinogenesis*, 21(3):505–515, 2000.

[169] Mihaela Skobe, Patricia Rockwell, Neil Goldstein, Silvia Vosseler, and Norbert E Fusenig. Halting angiogenesis suppresses carcinoma cell invasion. *Nature medicine*, 3(11):1222–1227, 1997.

[170] Judah Folkman. Tumor angiogenesis: therapeutic implications. *New england journal of medicine*, 285(21):1182–1186, 1971.

[171] Peter Carmeliet. Vegf as a key mediator of angiogenesis in cancer. *Oncology*, 69(Suppl. 3):4–10, 2005.

[172] Noboru Sato, JG Beitz, Junji Kato, Mikio Yamamoto, JW Clark, Paul Calabresi, A Raymond, and AR Frackelton Jr. Platelet-derived growth factor indirectly stimulates angiogenesis in vitro. *The American journal of pathology*, 142(4):1119, 1993.

[173] Y Kitadai, Y Takahashi, K Haruma, K Naka, K Sumii, H Yokozaki, W Yasui, N Mukaida, Y Ohmoto, G Kajiyama, et al. Transfection of interleukin-8 increases angiogenesis and tumorigenesis of human gastric carcinoma cells in nude mice. *British journal of cancer*, 81(4):647–653, 1999.

[174] Jiao Yue, Kun Zhang, and JianFeng Chen. Role of integrins in regulating proteases to mediate extracellular matrix remodeling. *Cancer Microenvironment*, 5(3):275–283, 2012.

[175] Judah Folkman. Angiogenesis in cancer, vascular, rheumatoid and other disease. *Nature medicine*, 1(1):27–30, 1995.

[176] Takayuki Asahara, Donghui Chen, Tomono Takahashi, Koshi Fujikawa, Marianne Kearney, Meredith Magner, George D Yancopoulos, and Jeffrey M Isner. Tie2 receptor ligands, angiopoietin-1 and angiopoietin-2, modulate vegf-induced postnatal neovascularization. *Circulation research*, 83(3):233–240, 1998.

[177] Safiyyah Ziyad and M Luisa Iruela-Arispe. Molecular mechanisms of tumor angiogenesis. *Genes & cancer*, 2(12):1085–1096, 2011.

[178] Tracey A Martin, Lin Ye, Andrew J Sanders, Jane Lane, and Wen G Jiang. Cancer invasion and metastasis: molecular and cellular perspective. In *Madame Curie Bioscience Database [Internet]*. Landes Bioscience, 2013.

[179] Guido Giordano, Antonio Febbraro, Michele Venditti, Serena Campidoglio, Nunzio Olivieri, Katia Raieta, Pietro Parcesepe, Giusy Carmen Imbriani, Andrea Remo, and Massimo Pancione. Targeting angiogenesis and tumor microenvironment in metastatic colorectal cancer: role of aflibercept. *Gastroenterology research and practice*, 2014, 2014.

[180] Hwajin Son and Aree Moon. Epithelial-mesenchymal transition and cell invasion. *Toxicological research*, 26(4):245–252, 2010.

[181] Brigitt D Angst, Cristiana Marcozzi, and Anthony I Magee. The cadherin superfamily: diversity in form and function. *Journal of cell science*, 114(4):629–641, 2001.

[182] Anne-Karina Perl, Petra Wilgenbus, Ulf Dahl, Henrik Semb, and Gerhard Christofori. A causal role for e-cadherin in the transition from adenoma to carcinoma. *Nature*, 392(6672):190–193, 1998.

[183] Kris Vleminckx, L Vakaet Jr, Marcus Mareel, Walter Fiers, and Frans Van Roy. Genetic manipulation of e-cadherin expression by epithelial tumor cells reveals an invasion suppressor role. *Cell*, 66(1):107–119, 1991.

[184] Geert Berx and Frans Van Roy. The e-cadherin/catenin complex: an important gatekeeper in breast cancer tumorigenesis and malignant progression. *Breast Cancer Research*, 3(5):289, 2001.

[185] Xin Liu and Kent-Man Chu. E-cadherin and gastric cancer: cause, consequence, and applications. *BioMed research international*, 2014, 2014.

[186] Masahiro Yanagisawa and Panos Z Anastasiadis. p120 catenin is essential for mesenchymal cadherin–mediated regulation of cell motility and invasiveness. *The Journal of cell biology*, 174(7):1087–1096, 2006.

[187] Alexandros Glentis, Vasily Gurchenkov, and Danijela Matic Vignjevic. Assembly, heterogeneity, and breaching of the basement membranes. *Cell adhesion & migration*, 8(3):236–245, 2014.

[188] Sophia Havaki, Mirsini Kouloukoussa, Kawther Amawi, Yiannis Drosos, Leonidas D Arvanitis, Nikos Goutas, Dimitrios Vlachodimitropoulos, Stamatis D Vassilaros, Eleni Z Katsantoni, Irene Voloudakis-Baltatzis, et al. Altered expression pattern of integrin alphavbeta3 correlates with actin cytoskeleton in primary cultures of human breast cancer. *Cancer Cell International*, 7(1):16, 2007.

[189] Yves A DeClerck, Arthur M Mercurio, M Sharon Stack, Harold A Chapman, Mary M Zutter, Ruth J Muschel, Avraham Raz, Lynn M Matrisian, Bonnie F Sloane, Agnes Noel, et al. Proteases, extracellular matrix, and cancer: a workshop of the path b study section. *The American journal of pathology*, 164(4):1131–1139, 2004.

[190] Kai Kessenbrock, Vicki Plaks, and Zena Werb. Matrix metalloproteinases: regulators of the tumor microenvironment. *Cell*, 141(1):52–67, 2010.

[191] Susan A Brooks, Hannah J Lomax-Browne, Tracey M Carter, Chloe E Kinch, and Debbie MS Hall. Molecular interactions in cancer cell metastasis. *Acta histochemica*, 112(1):3–25, 2010.

[192] Jeffrey B Wyckoff, Yarong Wang, Elaine Y Lin, Jiu-feng Li, Sumanta Goswami, E Richard Stanley, Jeffrey E Segall, Jeffrey W Pollard, and John Condeelis. Direct visualization of macrophage-assisted tumor cell intravasation in mammary tumors. *Cancer research*, 67(6):2649–2656, 2007.

[193] Tim Molloy and Laura J van't Veer. Recent advances in metastasis research. *Current opinion in genetics & development*, 18(1):35–41, 2008.

[194] GF Nash, LF Turner, MF Scully, and AK Kakkar. Platelets and cancer. *The lancet oncology*, 3(7):425–430, 2002.

[195] Ann F Chambers, Alan C Groom, and Ian C MacDonald. Dissemination and growth of cancer cells in metastatic sites. *Nature Reviews Cancer*, 2(8):563–572, 2002.

[196] Ramin Shayan, Marc G Achen, and Steven A Stacker. Lymphatic vessels in cancer metastasis: bridging the gaps. *Carcinogenesis*, 27(9):1729–1738, 2006.

[197] Brunhilde Felding-Habermann, Timothy E O'Toole, Jeffrey W Smith, Emilia Fransvea, Zaverio M Ruggeri, Mark H Ginsberg, Paul E Hughes, Nisar Pampori, Sanford J Shattil, Alan Saven, et al. Integrin activation controls metastasis in human breast cancer. *Proceedings of the National Academy of Sciences*, 98(4):1853–1858, 2001.

[198] Scott Valastyan and Robert A Weinberg. Tumor metastasis: molecular insights and evolving paradigms. *Cell*, 147(2):275–292, 2011.

[199] Stephan Braun, Florian D Vogl, Bjørn Naume, Wolfgang Janni, Michael P Osborne, R Charles Coombes, Günter Schlimok, Ingo J Diel, Bernd Gerber, Gerhard Gebauer, et al. A pooled analysis of bone marrow micrometastasis in breast cancer. *New England journal of medicine*, 353(8):793–802, 2005.

[200] Rosandra N Kaplan, Rebecca D Riba, Stergios Zacharoulis, Anna H Bramley, Loïc Vincent, Carla Costa, Daniel D MacDonald, David K Jin, Koji Shido, Scott A Kerns, et al. Vegfr1-positive haematopoietic bone marrow progenitors initiate the premetastatic niche. *Nature*, 438(7069):820–827, 2005.

[201] Stephen Paget. The distribution of secondary growths in cancer of the breast. *Lancet*, pages 571–573, 1889.

[202] Hui Wang, Weili Fu, Jae Hong Im, Zengyi Zhou, Samuel A Santoro, Vandana Iyer, C Mike DiPersio, Qian-Chun Yu, Vito Quaranta, Abu Al-Mehdi, et al. Tumor cell $\alpha 3\beta 1$ integrin and vascular laminin-5 mediate pulmonary arrest and metastasis. *The Journal of cell biology*, 164(6):935–941, 2004.

[203] LiKang Chin, Yuntao Xia, Dennis E Discher, and Paul A Janmey. Mechanotransduction in cancer. *Current opinion in chemical engineering*, 11:77–84, 2016.

[204] Arlizan B Ariffin, Patrick F Forde, Saleem Jahangeer, Declan M Soden, and John Hinchion. Releasing pressure in tumors: what do we know so far and where do we go from here? a review. *Cancer research*, 74(10):2655–2662, 2014.

[205] Shom Goel, Dan G Duda, Lei Xu, Lance L Munn, Yves Boucher, Dai Fukumura, and Rakesh K Jain. Normalization of the vasculature for treatment of cancer and other diseases. *Physiological reviews*, 91(3):1071–1121, 2011.

[206] Carl-Henrik Heldin, Kristofer Rubin, Kristian Pietras, and Arne Östman. High interstitial fluid pressure—an obstacle in cancer therapy. *Nature Reviews Cancer*, 4(10):806–813, 2004.

[207] Rakesh K Jain, John D Martin, and Triantafyllos Stylianopoulos. The role of mechanical forces in tumor growth and therapy. *Annual review of biomedical engineering*, 16:321–346, 2014.

[208] Stephane Ferretti, Peter R Allegrini, Mike M Becquet, and Paul MJ McSheehy. Tumor interstitial fluid pressure as an early-response marker for anticancer therapeutics. *Neoplasia (New York, NY)*, 11(9):874, 2009.

[209] Jennifer L Leight, Michele A Wozniak, Sophia Chen, Michelle L Lynch, and Christo-

pher S Chen. Matrix rigidity regulates a switch between tgf-β1–induced apoptosis and epithelial–mesenchymal transition. *Molecular biology of the cell*, 23(5):781–791, 2012.

[210] Takae Ebihara, Narayanan Venkatesan, Ryoichi Tanaka, and Mara S Ludwig. Changes in extracellular matrix and tissue viscoelasticity in bleomycin–induced lung fibrosis: Temporal aspects. *American journal of respiratory and critical care medicine*, 162(4):1569–1576, 2000.

[211] Robert W Tilghman, Edik M Blais, Catharine R Cowan, Nicholas E Sherman, Pablo R Grigera, Erin D Jeffery, Jay W Fox, Brett R Blackman, Daniel J Tschumperlin, Jason A Papin, et al. Matrix rigidity regulates cancer cell growth by modulating cellular metabolism and protein synthesis. *PloS one*, 7(5), 2012.

[212] Tony Yeung, Penelope C Georges, Lisa A Flanagan, Beatrice Marg, Miguelina Ortiz, Makoto Funaki, Nastaran Zahir, Wenyu Ming, Valerie Weaver, and Paul A Janmey. Effects of substrate stiffness on cell morphology, cytoskeletal structure, and adhesion. *Cell motility and the cytoskeleton*, 60(1):24–34, 2005.

[213] Joseph W O'Connor and Esther W Gomez. Biomechanics of tgfβ-induced epithelial-mesenchymal transition: implications for fibrosis and cancer. *Clinical and translational medicine*, 3(1):1–13, 2014.

[214] Cyrus M Ghajar and Mina J Bissell. Extracellular matrix control of mammary gland morphogenesis and tumorigenesis: insights from imaging. *Histochemistry and cell biology*, 130(6):1105, 2008.

[215] Spencer C Wei, Laurent Fattet, Jeff H Tsai, Yurong Guo, Vincent H Pai, Hannah E Majeski, Albert C Chen, Robert L Sah, Susan S Taylor, Adam J Engler, et al. Matrix stiffness drives epithelial–mesenchymal transition and tumour metastasis through a twist1–g3bp2 mechanotransduction pathway. *Nature cell biology*, 17(5):678–688, 2015.

[216] Jörg Schrader, Timothy T Gordon-Walker, Rebecca L Aucott, Mariëlle van Deemter, Alexander Quaas, Shaun Walsh, Daniel Benten, Stuart J Forbes, Rebecca G Wells, and John P Iredale. Matrix stiffness modulates proliferation, chemotherapeutic response, and dormancy in hepatocellular carcinoma cells. *Hepatology*, 53(4):1192–1205, 2011.

[217] Mingshu Pang, Yao Teng, Jianyong Huang, Yuan Yuan, Feng Lin, and Chunyang Xiong. Substrate stiffness promotes latent tgf-β1 activation in hepatocellular carcinoma. *Biochemical and biophysical research communications*, 483(1):553–558, 2017.

[218] Yinying Dong, Qiongdan Zheng, Zhiming Wang, Xiahui Lin, Yang You, Sifan Wu, Yaohui Wang, Chao Hu, Xiaoying Xie, Jie Chen, et al. Higher matrix stiffness as an independent initiator triggers epithelial-mesenchymal transition and facilitates hcc metastasis. *Journal of hematology & oncology*, 12(1):112, 2019.

[219] Andrew D Hughes and Michael R King. Nanobiotechnology for the capture and manipulation of circulating tumor cells. *Wiley Interdisciplinary Reviews: Nanomedicine*

and Nanobiotechnology, 4(3):291–309, 2012.

[220] Donald Elliott Brooks. The biorheology of tumor cells. *Biorheology*, 21(1-2):85–91, 1984.

[221] Peter F Davies, Jos A Spaan, and Robert Krams. Shear stress biology of the endothelium. *Annals of biomedical engineering*, 33(12):1714–1718, 2005.

[222] Vijayalakshmi Thamilselvan, David H Craig, and Marc D Basson. Fak association with multiple signal proteins mediates pressure-induced colon cancer cell adhesion via a src-dependent pi3k/akt pathway. *The FASEB Journal*, 21(8):1730–1741, 2007.

[223] Anke von Sengbusch, Peter Gassmann, Katja M Fisch, Andreas Enns, Garth L Nicolson, and Jörg Haier. Focal adhesion kinase regulates metastatic adhesion of carcinoma cells within liver sinusoids. *The American journal of pathology*, 166(2):585–596, 2005.

[224] L. R. Otterbein, P. Graceffa, and R. Dominguez. The crystal structure of uncomplexed actin in the ADR state. *Science*, 293(5530):708–711, 2001.

[225] T. D. Pollard and G. G. Borisy. Cellular Motility Driven by Assembly and Disassembly of Actin Filaments. *Cell*, 21:453–465, 2003.

[226] C. G. Dos Remedios, D. Chhabra, M. Kekic, I. V. Dedova, M. Tsubakihara, D. A. Berry, and N. J. Nosworthy. Actin Binding Proteins: Regulation of Cytoskeletal Microfilaments. *Physiological Reviews*, 83(2):433–473, 2003.

[227] Elif Nur Firat-Karalar and Matthew D. Welch. New mechanisms and functions of actin nucleation. *Current Opinion in Cell Biology*, 23(1):4–13, 2011.

[228] Bruce Alberts, Alexander Johnson, Julian Lewis, Martin Raff, Keith Roberts, and Peter Walter. The self-assembly and dynamic structure of cytoskeletal filaments. In *Molecular Biology of the Cell. 4th edition*. Garland Science, 2002.

[229] Erin D. Goley and Matthew D. Welch. The ARP2/3 complex: An actin nucleator comes of age. *Nature Reviews Molecular Cell Biology*, 7(10):713–726, 2006.

[230] Jasmine V.G. Abella, Chiara Galloni, Julien Pernier, David J. Barry, Svend Kjær, Marie France Carlier, and Michael Way. Isoform diversity in the Arp2/3 complex determines actin filament dynamics. *Nature Cell Biology*, 18(1):76–86, 2016.

[231] R Dyche Mullins, John A Heuser, and Thomas D Pollard. The interaction of arp2/3 complex with actin: nucleation, high affinity pointed end capping, and formation of branching networks of filaments. *Proceedings of the National Academy of Sciences*, 95(11):6181–6186, 1998.

[232] Luke A. Helgeson and Brad J. Nolen. Mechanism of synergistic activation of Arp2/3 complex by cortactin and N-WASP. *eLife*, 2013(2):1–26, 2013.

[233] Shiro Suetsugu. Activation of nucleation promoting factors for directional actin filament elongation: Allosteric regulation and multimerization on the membrane. *Seminars in Cell and Developmental Biology*, 24(4):267–271, 2013.

[234] Bruce L. Goode and Michael J. Eck. Mechanism and Function of Formins in the Control of Actin Assembly. *Annual Review of Biochemistry*, 76(1):593–627, 2007.

[235] Sally H. Zigmond. Formin-induced nucleation of actin filaments. *Current Opinion in Cell Biology*, 16(1):99–105, 2004.

[236] Yingwu Xu, James B. Moseley, Isabelle Sagot, Florence Poy, David Pellman, Bruce L. Goode, and Michael J. Eck. Crystal structures of a formin homology-2 domain reveal a tethered dimer architecture. *Cell*, 116(5):711–723, 2004.

[237] Aditya Paul and Thomas Pollard. The Role of the FH1 Domain and Profilin in Formin-Mediated Actin-Filament Elongation and Nucleation. *Current Biology*, 18(1):9–19, 2008.

[238] GEOFFREY M Cooper and RE Hausman. A molecular approach. *The cell. 2nd ed. Sunderland, MA: Sinauer Associates*, 2000.

[239] Ikuko Fujiwara, Shin Takahashi, Hisashi Tadakuma, Takashi Funatsu, and Shin'ichi Ishiwata. Microscopic analysis of polymerization dynamics with individual actin filaments. *Nature Cell Biology*, 4(9):666–673, 2002.

[240] J Victor Small, Theresia Stradal, Emmanuel Vignal, and Klemens Rottner. The lamellipodium: where motility begins. *Trends in cell biology*, 12(3):112–120, 2002.

[241] Pieta K. Mattila and Pekka Lappalainen. Filopodia: Molecular architecture and cellular functions. *Nature Reviews Molecular Cell Biology*, 9(6):446–454, 2008.

[242] Gaëlle Letort, Hajer Ennomani, Laurène Gressin, Manuel Théry, and Laurent Blanchoin. Dynamic reorganization of the actin cytoskeleton. *F1000Research*, 4, 2015.

[243] Tetsuro Wakatsuki, Bill Schwab, Nathan C Thompson, and Elliot L Elson. Effects of cytochalasin d and latrunculin b on mechanical properties of cells. *Journal of cell science*, 114(5):1025–1036, 2001.

[244] S. Tojkander, G. Gateva, and P. Lappalainen. Actin stress fibers - assembly, dynamics and biological roles. *Journal of Cell Science*, 125(8):1855–1864, 2012.

[245] Louise P Cramer, Margaret Siebert, and Timothy J Mitchison. Identification of novel graded polarity actin filament bundles in locomoting heart fibroblasts: implications for the generation of motile force. *The Journal of cell biology*, 136(6):1287–1305, 1997.

[246] J. Victor Small, K. Rottner, I. Kaverina, and K. I. Anderson. Assembling an actin cytoskeleton for cell attachment and movement. *Biochimica et Biophysica Acta - Molecular Cell Research*, 1404(3):271–281, 1998.

[247] Sari Tojkander, Gergana Gateva, Galina Schevzov, Pirta Hotulainen, Perttu Naumanen, Claire Martin, Peter W. Gunning, and Pekka Lappalainen. A molecular pathway for myosin II recruitment to stress fibers. *Current Biology*, 21(7):539–550, 2011.

[248] Pirta Hotulainen and Pekka Lappalainen. Stress fibers are generated by two distinct actin assembly mechanisms in motile cells. *Journal of Cell Biology*, 173(3):383–394, 2006.

[249] S. B. Khatau, C. M. Hale, P. J. Stewart-Hutchinson, M. S. Patel, C. L. Stewart, P. C. Searson, D. Hodzic, and D. Wirtz. A perinuclear actin cap regulates nuclear shape. *Proceedings of the National Academy of Sciences*, 106(45):19017–19022, 2009.

[250] Lysianne Follonier Castella, Lara Buscemi, Charles Godbout, Jean-Jacques Meister, and Boris Hinz. A new lock-step mechanism of matrix remodelling based on subcellular contractile events. *J Cell Sci*, 123(10):1751–1760, 2010.

[251] John A. Hammer and James R. Sellers. Walking to work: Roles for class v myosins as cargo transporters. *Nature Reviews Molecular Cell Biology*, 13(1):13–26, 2012.

[252] Amit D Mehta, Ronald S Rock, Matthias Rief, James A Spudich, Mark S Mooseker, and Richard E Cheney. Myosin-v is a processive actin-based motor. *Nature*, 400(6744):590, 1999.

[253] Chalfie M and Thomson JN. Structural and functional diversity in the neuronal microtubules of C. elegans. *Journal of Cell Biology*, 93:15–23, 1982.

[254] Lewis G. Tilney, Joseph Bryan, Doris J. Bush, Keigi Fujiwara, Mark S. Mooseker, Douglas B. Murphy, and Daniel H. Snyder. Microtubules: Evidence for 13 protofilaments. *Journal of Cell Biology*, 59(2):267–275, 1973.

[255] Harish C. Joshi. Microtubule organizing centers and γ-tubulin. *Current Opinion in Cell Biology*, 6(1):55–62, 1994.

[256] Harvey Lodish, Arnold Berk, S Lawrence Zipursky, Paul Matsudaira, David Baltimore, James Darnell, et al. *Molecular cell biology*, volume 7. WH freeman New York, 2013.

[257] Anna Akhmanova and Michel O Steinmetz. Control of microtubule organization and dynamics: two ends in the limelight. *Nature reviews Molecular cell biology*, 16(12):711, 2015.

[258] Timothy J Mitchison and M Kirschner. dynamic instability of microtubule growth. *Nature Publishing Group*, 312(5991):237–242, 1984.

[259] Hugo Bowne-Anderson, Marija Zanic, Monika Kauer, and Jonathon Howard. Microtubule dynamic instability: A new model with coupled GTP hydrolysis and multistep catastrophe. *BioEssays*, 35(5):452–461, 2013.

[260] Tetsuya Horio and Takashi Murata. The role of dynamic instability in microtubule organization. *Frontiers in Plant Science*, 5(October):1–10, 2014.

[261] Harvey Lodish, Arnold Berk, S Lawrence Zipursky, Paul Matsudaira, David Baltimore, and James Darnell. Microtubule dynamics and associated proteins. In *Molecular Cell Biology. 4th edition*. WH Freeman, 2000.

[262] Chris M Coppin, J T Finer, J a Spudich, and Ronald D Vale. Detection of sub-8-nm movements of kinesin by high-resolution optical-trap microscopy. *Proceedings of the National Academy of Sciences*, 93(5):1913–1917, 1996.

[263] S Block, B Schnapp, K Svoboda, and C Schmidt. Direct observation of kinesin stepping by optical trapping interferometry. *Nature*, 365(October):721–727, 1993.

[264] Nobutaka Hirokawa. Kinesin and dynein superfamily proteins and the mechanism of organelle transport. *Science*, 279(5350):519–526, 1998.

[265] Arne Gennerich and Ronald D. Vale. Walking the walk: how kinesin and dynein coordinate their steps. *Current Opinion in Cell Biology*, 21(1):59–67, 2009.

[266] Susan L Kline-Smith and Claire E Walczak. Mitotic Spindle Assembly and Chro-

mosome Segregation. *Molecular Cell*, 15(3):317–327, 2004.

[267] Juraj Simunić and Iva M. Tolić. Mitotic Spindle Assembly: Building the Bridge between Sister K-Fibers. *Trends in Biochemical Sciences*, 41(10):824–833, 2016.

[268] RE Palmer, DS Sullivan, T Huffaker, and D Koshland. Role of astral microtubules and actin in spindle orientation and migration in the budding yeast, saccharomyces cerevisiae. *The Journal of cell biology*, 119(3):583–593, 1992.

[269] D. N. Mastronarde, K. L. McDonald, R. Ding, and J. R. McIntosh. Interpolar spindle microtubules in PTK cells. *Journal of Cell Biology*, 123(6 I):1475–1489, 1993.

[270] Susan L Kline-Smith and Claire E Walczak. Mitotic spindle assembly and chromosome segregation: refocusing on microtubule dynamics. *Molecular cell*, 15(3):317–327, 2004.

[271] Ye Zhai, Paul J. Kronebusch, Patrick M. Simon, and Gary G. Borisy. Microtubule dynamics at the G2/M transition: Abrupt breakdown of cytoplasmic microtubules at nuclear envelope breakdown and implications for spindle morphogenesis. *Journal of Cell Biology*, 135(1):201–214, 1996.

[272] Ekaterina L Grishchuk and J Richard McIntosh. Microtubule depolymerization can drive poleward chromosome motion in fission yeast. *The EMBO journal*, 25(20):4888–4896, 2006.

[273] Marileen Dogterom, Jacob W.J. Kerssemakers, Guillaume Romet-Lemonne, and Marcel E. Janson. Force generation by dynamic microtubules. *Current Opinion in Cell Biology*, 17(1):67–74, 2005.

[274] Clare M. Waterman-Storer, Rebecca A. Worthylake, Betty P. Liu, Keith Burridget, and E. D. Salmon. Microtubule growth activates Rac1 to promote lamellipodial protrusion in fibroblasts. *Nature Cell Biology*, 1(1):45–50, 1999.

[275] Irina Kaverina, Klemens Rottner, and J. Victor Small. Targeting, capture, and stabilization of microtubules at early focal adhesions. *Journal of Cell Biology*, 142(1):181–190, 1998.

[276] Paul M. Miller, Andrew W. Folkmann, Ana R.R. Maia, Nadia Efimova, Andrey Efimov, and Irina Kaverina. Golgi-derived CLASP-dependent microtubules control Golgi organization and polarized trafficking in motile cells. *Nature Cell Biology*, 11(9):1069–1080, 2009.

[277] Anutosh Ganguly, Hailing Yang, Ritu Sharma, Kamala D. Patel, and Fernando Cabral. The role of microtubules and their dynamics in cell migration. *Journal of Biological Chemistry*, 287(52):43359–43369, 2012.

[278] Harald Herrmann and Ueli Aebi. Intermediate filaments: structure and assembly. *Cold Spring Harbor Perspectives in Biology*, 8(11):a018242, 2016.

[279] Norbert Geisler and Klaus Weber. The amino acid sequence of chicken muscle desmin provides a common structural model for intermediate filament proteins. *The EMBO journal*, 1(12):1649–1656, 1982.

[280] Peter Soellner, Roy A Quinlan, and Werner W Franke. Identification of a distinct soluble subunit of an intermediate filament protein: tetrameric vimentin from living

cells. *Proceedings of the National Academy of Sciences*, 82(23):7929–7933, 1985.

[281] Harald Herrmann and Ueli Aebi. Intermediate Filaments: Molecular Structure, Assembly Mechanism, and Integration Into Functionally Distinct Intracellular Scaffolds. *Annual Review of Biochemistry*, 73(1):749–789, 2004.

[282] Sarah Köster, David A. Weitz, Robert D. Goldman, Ueli Aebi, and Harald Herrmann. Intermediate filament mechanics in vitro and in the cell: From coiled coils to filaments, fibers and networks. *Current Opinion in Cell Biology*, 32:82–91, 2015.

[283] Yosef Gruenbaum and Roland Foisner. Lamins: Nuclear Intermediate Filament Proteins with Fundamental Functions in Nuclear Mechanics and Genome Regulation. *Annual Review of Biochemistry*, 84(1):131–164, 2015.

[284] Paul A Janmey, Ursula Euteneuer, Peter Traub, and Manfred Schliwa. Viscoelastic properties of vimentin compared with other filamentous biopolymer networks. *The Journal of cell biology*, 113(1):155–160, 1991.

[285] L. Kreplak, H. Bär, J. F. Leterrier, H. Herrmann, and U. Aebi. Exploring the mechanical behavior of single intermediate filaments. *Journal of Molecular Biology*, 354(3):569–577, 2005.

[286] Florian Huber, Adeline Boire, Magdalena Preciado López, and Gijsje H. Koenderink. Cytoskeletal crosstalk: When three different personalities team up. *Current Opinion in Cell Biology*, 32:39–47, 2015.

[287] Gerhard Wiche, Selma Osmanagic-Myers, and Maria J. Castañón. Networking and anchoring through plectin: A key to IF functionality and mechanotransduction. *Current Opinion in Cell Biology*, 32:21–29, 2015.

[288] Veena Prahlad, Miri Yoon, Robert D. Moir, Ronald D. Vale, and Robert D. Goldman. Rapid movements of vimentin on microtubule tracks: Kinesin-dependent assembly of intermediate filament networks. *Journal of Cell Biology*, 143(1):159–170, 1998.

[289] Brian T. Helfand, Atsushi Mikami, Richard B. Vallee, and Robert D. Goldman. A requirement for cytoplasmic dynein and dynactin in intermediate filament network assembly and organization. *Journal of Cell Biology*, 157(5):795–806, 2002.

[290] P J Hollenbeck, A D Bershadsky, O Y Pletjushkina, and J M Vasiliev. Intermediate filament collapse is an ATP-dependent and actin-dependent process. *Journal of Cell Science*, pages 621–632, 1985.

[291] I S Tint, P J Hollenbeck, A B Verkhovsky, I G Surgucheva, and A D Bershadsky. Evidence that intermediate filament reorganization is induced by ATP-dependent contraction of the actomyosin cortex in permeabilized fibroblasts. *Journal of cell science*, 98 (Pt 3):375–84, 1991.

[292] Werner W Franke, Michaela Hergt, and Christine Grund. Rearrangement of the vimentin cytoskeleton during adipose conversion: formation of an intermediate filament cage around lipid globules. *Cell*, 49(1):131–141, 1987.

[293] B Eckes, D Dogic, E Colucci-Guyon, N Wang, A Maniotis, D Ingber, A Merckling, F Langa, M Aumailley, A Delouvée, V Koteliansky, C Babinet, and T Krieg. Impaired mechanical stability, migration and contractile capacity in vimentin-deficient

fibroblasts. *Journal of cell science*, 111:1897–1907, 1998.

[294] O. E. Nekrasova, M. G. Mendez, I. S. Chernoivanenko, P. A. Tyurin-Kuzmin, E. R. Kuczmarski, V. I. Gelfand, R. D. Goldman, and A. A. Minin. Vimentin intermediate filaments modulate the motility of mitochondria. *Molecular Biology of the Cell*, 22(13):2282–2289, 2011.

[295] Ya Sheng Gao and Elizabeth Sztul. A novel interaction of the Golgi complex with the vimentin intermediate filament cytoskeleton. *Journal of Cell Biology*, 152(5):877–893, 2001.

[296] G V Tolstonog, E Mothes, R L Shoeman, and P Traub. Isolation of SDS-stable complexes of the intermediate filament protein vimentin with repetitive, mobile, nuclear matrix attachment region, and mitochondrial {DNA} sequence elements from cultured mouse and human fibroblasts. *DNA Cell Biol*, 20(9):531–554, 2001.

[297] Johanna Ivaska, Hanna-Mari Pallari, Jonna Nevo, and John E Eriksson. Novel functions of vimentin in cell adhesion, migration, and signaling. *Experimental cell research*, 313(10):2050–2062, 2007.

[298] Q. S. Li, G. Y H Lee, C. N. Ong, and C. T. Lim. AFM indentation study of breast cancer cells. *Biochemical and Biophysical Research Communications*, 374(4):609–613, 2008.

[299] Wenwei Xu, Roman Mezencev, Byungkyu Kim, Lijuan Wang, John McDonald, and Todd Sulchek. Cell Stiffness Is a Biomarker of the Metastatic Potential of Ovarian Cancer Cells. *PLoS ONE*, 7(10), 2012.

[300] Alperen N. Ketene, Eva M. Schmelz, Paul C. Roberts, and Masoud Agah. The effects of cancer progression on the viscoelasticity of ovarian cell cytoskeleton structures. *Nanomedicine: Nanotechnology, Biology, and Medicine*, 8(1):93–102, 2012.

[301] Meenakshi Prabhune, Gazanfer Belge, Andreas Dotzauer, Jörn Bullerdiek, and Manfred Radmacher. Comparison of mechanical properties of normal and malignant thyroid cells. *Micron*, 43(12):1267–1272, 2012.

[302] Eric M Darling and Dino Di Carlo. High-throughput assessment of cellular mechanical properties. *Annual review of biomedical engineering*, 17:35–62, 2015.

[303] Igor Titushkin and Michael Cho. Distinct membrane mechanical properties of human mesenchymal stem cells determined using laser optical tweezers. *Biophysical journal*, 90(7):2582–2591, 2006.

[304] Gerd Binnig, Calvin F Quate, and Ch Gerber. Atomic force microscope. *Physical review letters*, 56(9):930, 1986.

[305] Daniel J Müller and Yves F Dufrene. Atomic force microscopy as a multifunctional molecular toolbox in nanobiotechnology. In *Nanoscience And Technology: A Collection of Reviews from Nature Journals*, pages 269–277. World Scientific, 2010.

[306] Yves F Dufrêne, Toshio Ando, Ricardo Garcia, David Alsteens, David Martinez-Martin, Andreas Engel, Christoph Gerber, and Daniel J Müller. Imaging modes of atomic force microscopy for application in molecular and cell biology. *Nature nanotechnology*, 12(4):295, 2017.

[307] Kai-Chih Chang, Yu-Wei Chiang, Chin-Hao Yang, and Je-Wen Liou. Atomic force microscopy in biology and biomedicine. *Tzu Chi Medical Journal*, 24(4):162–169, 2012.

[308] S Rao and KD Costa. Atomic force microscopy (afm) in biomedical research. In *Biomedical Imaging*, pages 41–64. Elsevier, 2014.

[309] MK Khan, QY Wang, and ME Fitzpatrick. Atomic force microscopy (afm) for materials characterization. In *Materials Characterization Using Nondestructive Evaluation (NDE) Methods*, pages 1–16. Elsevier, 2016.

[310] Yongho Seo and Wonho Jhe. Atomic force microscopy and spectroscopy. *Reports on Progress in Physics*, 71(1):016101, 2007.

[311] JKP Instruments. *NanoWizard AFM Handbook*. JKP Instruments, 2016.

[312] JKP Instruments. *NanoWizard AFM Handbook*. JKP Instruments, 2016.

[313] 4PK Hansma, JP Cleveland, M Radmacher, DA Walters, PE Hillner, M Bezanilla, M Fritz, D Vie, HG Hansma, CB Prater, et al. Tapping mode atomic force microscopy in liquids. *Applied Physics Letters*, 64(13):1738–1740, 1994.

[314] William B. McConnaughey and Nils O. Petersen. Cell poker: An apparatus for stress-strain measurements on living cells. *Review of Scientific Instruments*, 51(5):575–580, 1980.

[315] B. Daily, E. L. Elson, and G. I. Zahalak. Cell poking. Determination of the elastic area compressibility modulus of the erythrocyte membrane. *Biophysical Journal*, 45(4):671–682, 1984.

[316] Kazuo Tanishita and Kimiko Yamamoto. *Vascular Engineering: New Prospects of Vascular Medicine and Biology with a Multidiscipline Approach*. Springer, 2016.

[317] Nader Jalili and Karthik Laxminarayana. A review of atomic force microscopy imaging systems: Application to molecular metrology and biological sciences. *Mechatronics*, 14(8):907–945, 2004.

[318] Chao Min Cheng, Robert L. Steward, and Philip R. LeDuc. Probing cell structure by controlling the mechanical environment with cell-substrate interactions. *Journal of Biomechanics*, 42(2):187–192, 2009.

[319] A. E. Smith, Z. Zhang, C. R. Thomas, K. E. Moxham, and A. P. J. Middelberg. The mechanical properties of Saccharomyces cerevisiae. *Proceedings of the National Academy of Sciences*, 97(18):9871–9874, 2000.

[320] Steven M Block. Making light work with optical tweezers. *Nature*, 360(6403):493–495, 1992.

[321] Emad Moeendarbary and Andrew R. Harris. Cell mechanics: Principles, practices, and prospects. *Wiley Interdisciplinary Reviews: Systems Biology and Medicine*, 6(5):371–388, 2014.

[322] Bruno Pontes, Yareni Ayala, Anna Carolina C Fonseca, Luciana F Romão, Racκele F Amaral, Leonardo T Salgado, Flavia R Lima, Marcos Farina, Nathan B Viana, Vivaldo Moura-Neto, et al. Membrane elastic properties and cell function. *PLoS One*, 8(7):e67708, 2013.

[323] Y. Liu, D. K. Cheng, G. J. Sonek, M. W. Berns, C. F. Chapman, and B. J. Tromberg. Evidence for localized cell heating induced by infrared optical tweezers. *Biophysical Journal*, 68(5):2137–2144, 1995.

[324] Andreas R. Bausch, Winfried Möller, and Erich Sackmann. Measurement of local viscoelasticity and forces in living cells by magnetic tweezers. *Biophysical Journal*, 76(1 I):573–579, 1999.

[325] Ning Wang and Donald E Ingber. Probing transmembrane mechanical coupling and cytomechanics using magnetic twisting cytometry. *Biochemistry and Cell Biology*, 73(7-8):327–335, 1995.

[326] Monica Tanase, Nicolas Biais, and Michael Sheetz. Magnetic Tweezers in Cell Biology. *Methods in Cell Biology*, 83(07):473–493, 2007.

[327] Marina Puig-De-Morales, Mireia Grabulosa, Jordi Alcaraz, Joaquim Mullol, Geoffrey N. Maksym, Jeffrey J. Fredberg, and Daniel Navajas. Measurement of cell microrheology by magnetic twisting cytometry with frequency domain demodulation. *Journal of Applied Physiology*, 91(3):1152–1159, 2001.

[328] Deok-Ho Kim, Pak Kin Wong, Jungyul Park, Andre Levchenko, and Yu Sun. Microengineered Platforms for Cell Mechanobiology. *Annual Review of Biomedical Engineering*, 11(1):203–233, 2009.

[329] Keir C Neuman and Attila Nagy. Single-molecule force spectroscopy: optical tweezers, magnetic tweezers and atomic force microscopy. *Nature methods*, 5(6):491, 2008.

[330] Lap Man Lee and Allen P. Liu. The Application of Micropipette Aspiration in Molecular Mechanics of Single Cells. *Journal of Nanotechnology in Engineering and Medicine*, 5(4):040902, 2014.

[331] Kristina Sliogeryte, Stephen D. Thorpe, David A. Lee, Lorenzo Botto, and Martin M. Knight. Stem cell differentiation increases membrane-actin adhesion regulating cell blebability, migration and mechanics. *Scientific Reports*, 4:1–9, 2014.

[332] Robert M. Hochmuth. Micropipette aspiration of living cells. *Journal of Biomechanics*, 33(1):15–22, 2000.

[333] Denis Wirtz. Particle-Tracking Microrheology of Living Cells: Principles and Applications. *Annual Review of Biophysics*, 38(1):301–326, 2009.

[334] Section Ii and Section Iv. Methods of Digital Video Microscopy for Colloidal Studies. *Journal of Colloid and Interface Science*, 310(179):298–310, 1996.

[335] Lara Selvaggi, Marinella Salemme, Carmen Vaccaro, Giuseppe Pesce, Giulia Rusciano, Antonio Sasso, Chiara Campanella, and Rosa Carotenuto. Multiple-Particle-Tracking to investigate viscoelastic properties in living cells. *Methods*, 51(1):20–26, 2010.

[336] Pietro Cicuta and Athene M Donald. Microrheology: a review of the method and applications. *Soft matter*, 3(12):1449–1455, 2007.

[337] SLOJVPKM Alexander, Louis Hellemans, Othmar Marti, Jason Schneir, Virgil Elings, Paul K Hansma, Matt Longmire, and John Gurley. An atomic-resolution

atomic-force microscope implemented using an optical lever. *Journal of Applied Physics*, 65(1):164–167, 1989.

[338] Núria Gavara and Richard S. Chadwick. Relationship between cell stiffness and stress fiber amount, assessed by simultaneous atomic force microscopy and live-cell fluorescence imaging. *Biomechanics and Modeling in Mechanobiology*, 15(3):511–523, 2016.

[339] Núria Gavara and Richard S. Chadwick. Determination of the elastic moduli of thin samples and adherent cells using conical atomic force microscope tips. *Nature Nanotechnology*, 7(11):733–736, 2012.

[340] Katarzyna Pogoda, Justyna Jaczewska, Joanna Wiltowska-Zuber, Olesya Klymenko, Kazimierz Zuber, Maria Fornal, and Malgorzata Lekka. Depth-sensing analysis of cytoskeleton organization based on AFM data. *European Biophysics Journal*, 41(1):79–87, 2012.

[341] Luciana Magalhaes Rebelo, Jeanlex Soares de Sousa, Jose Mendes Filho, and Manfred Radmacher. Comparison of the viscoelastic properties of cells from different kidney cancer phenotypes measured with atomic force microscopy. *Nanotechnology*, 24(5):055102, 2013.

[342] Jeffrey M Levsky and Robert H Singer. Gene expression and the myth of the average cell. *Trends in cell biology*, 13(1):4–6, 2003.

[343] Alex K Shalek and Mikael Benson. Single-cell analyses to tailor treatments. *Science translational medicine*, 9(408), 2017.

[344] Emir Hodzic. Single-cell analysis: Advances and future perspectives. *Bosnian journal of basic medical sciences*, 16(4):313, 2016.

[345] Michael C. Keeling, Luis R. Flores, Asad H. Dodhy, Elizabeth R. Murray, and Núria Gavara. Actomyosin and vimentin cytoskeletal networks regulate nuclear shape, mechanics and chromatin organization. *Scientific Reports*, 7(1):5219, 2017.

[346] Luis R Flores, Michael C Keeling, Xiaoli Zhang, Kristina Sliogeryte, and Núria Gavara. Lifeact-gfp alters f-actin organization, cellular morphology and biophysical behaviour. *Scientific reports*, 9(1):3241, 2019.

[347] A Zemel, F Rehfeldt, AEX Brown, DE Discher, and SA Safran. Optimal matrix rigidity for stress-fibre polarization in stem cells. *Nature physics*, 6(6):468, 2010.

[348] Filippo Piccinini, Alexa Kiss, and Peter Horvath. Celltracker (not only) for dummies. *Bioinformatics*, 32(6):955–957, 2015.

[349] Peter Friedl. Prespecification and plasticity: shifting mechanisms of cell migration. *Current opinion in cell biology*, 16(1):14–23, 2004.

[350] Miaojuan Chen, Tengfei Liu, Lina Xu, Xuejuan Gao, Xiaohui Liu, Cuihua Wang, Qingyu He, Gong Zhang, and Langxia Liu. Direct interaction of 14-3-3ζ with ezrin promotes cell migration by regulating the formation of membrane ruffle. *Journal of Molecular Biology*, 426(18):3118–3133, 2014.

[351] James W Legg, Charlotte A Lewis, Maddy Parsons, Tony Ng, and Clare M Isacke. A novel pkc-regulated mechanism controls cd44–ezrin association and directional

cell motility. *Nature cell biology*, 4(6):399, 2002.

[352] Y. Meng, Z. Lu, S. Yu, Q. Zhang, Y. Ma, and J. Chen. Ezrin promotes invasion and metastasis of pancreatic cancer cells. *Journal of Translational Medicine*, 8:1–14, 2010.

[353] Yin Liu, Natalya V. Belkina, Chung Park, Raj Nambiar, Scott M. Loughhead, Genaro Patino-Lopez, Khadija Ben-Aissa, Jian Jiang Hao, Michael J. Kruhlak, Hai Qi, Ulrich H. Von Andrian, John H. Kehrl, Matthew J. Tyska, and Stephen Shaw. Constitutively active ezrin increases membrane tension, slows migration, and impedes endothelial transmigration of lymphocytes in vivo in mice. *Blood*, 119(2):445–453, 2012.

[354] Sibylla Martinelli, Emily J H Chen, Fiona Clarke, Ruth Lyck, Sarah Affentranger, Janis K. Burkhardt, and Verena Niggli. Ezrin/radixin/moesin proteins and flotillins cooperate to promote uropod formation in T cells. *Frontiers in Immunology*, 4(APR):1–16, 2013.

[355] Anna Huttenlocher. Cell polarization mechanisms during directed cell migration. *Nature cell biology*, 7(4):336, 2005.

[356] Wouter-Jan Rappel and Leah Edelstein-Keshet. Mechanisms of cell polarization. *Current opinion in systems biology*, 3:43–53, 2017.

[357] Priyamvada Chugh and Ewa K. Paluch. The actin cortex at a glance. *Journal of Cell Science*, 131(14):jcs186254, 2018.

[358] Matthew F Krummel, Frederic Bartumeus, and Audrey Gérard. T cell migration, search strategies and mechanisms. *Nature Reviews Immunology*, 16(3):193, 2016.

[359] Germán Reig, Eduardo Pulgar, and Miguel L Concha. Cell migration: from tissue culture to embryos. *Development*, 141(10):1999–2013, 2014.

[360] Jose Javier Bravo-Cordero, Louis Hodgson, and John Condeelis. Directed cell invasion and migration during metastasis. *Current opinion in cell biology*, 24(2):277–283, 2012.

[361] Chun-Min Lo, Denis B Buxton, Gregory CH Chua, Micah Dembo, Robert S Adelstein, and Yu-Li Wang. Nonmuscle myosin iib is involved in the guidance of fibroblast migration. *Molecular biology of the cell*, 15(3):982–989, 2004.

[362] Harrison V Prentice-Mott, Yasmine Meroz, Andreas Carlson, Michael A Levine, Michael W Davidson, Daniel Irimia, Guillaume T Charras, L Mahadevan, and Jagesh V Shah. Directional memory arises from long-lived cytoskeletal asymmetries in polarized chemotactic cells. *Proceedings of the National Academy of Sciences*, 113(5):1267–1272, 2016.

[363] Katarina Wolf, Mariska te Lindert, Marina Krause, Stephanie Alexander, Joost te Riet, Amanda L. Willis, Robert M. Hoffman, Carl G. Figdor, Stephen J. Weiss, and Peter Friedl. Physical limits of cell migration: Control by ECM space and nuclear deformation and tuning by proteolysis and traction force. *Journal of Cell Biology*, 201(7):1069–1084, 2013.

[364] Alejandra Vásquez-Limeta, Kylie M. Wagstaff, Arturo Ortega, Dorothy H. Crouch,

David A. Jans, and Bulmaro Cisneros. Nuclear import of β-dystroglycan is facilitated by ezrin-mediated cytoskeleton reorganization. *PLoS ONE*, 9(3), 2014.

[365] Alexis Gautreau, Daniel Louvard, and Monique Arpin. Morphogenic effects of ezrin require a phosphorylation-induced transition from oligomers to monomers at the plasma membrane. *The Journal of cell biology*, 150(1):193–204, 2000.

[366] C Tran Quang, a Gautreau, M Arpin, and R Treisman. Ezrin function is required for ROCK-mediated fibroblast transformation by the Net and Dbl oncogenes. *The EMBO journal*, 19(17):4565–4576, 2000.

[367] Shigenobu Yonemura, Takeshi Matsui, Shoichiro Tsukita, and Sachiko Tsukita. Rho-dependent and -independent activation mechanisms of ezrin/radixin/moesin proteins: an essential role for polyphosphoinositides in vivo. *Journal of cell science*, 115(Pt 12):2569–80, 2002.

[368] Lixin Zhu, Rihong Zhou, Shelley Mettler, Tim Wu, Aennes Abbas, Joseph Delaney, and John G Forte. High turnover of ezrin t567 phosphorylation: conformation, activity, and cellular function. *American Journal of Physiology-Cell Physiology*, 293(3):C874–C884, 2007.

[369] Sunil C. Kaul, Rena Kawai, Hitoshi Nomura, Youji Mitsui, Roger R. Reddel, and Renu Wadhwa. Identification of a 55-kDa ezrin-related protein that induces cytoskeletal changes and localizes to the nucleolus. *Experimental Cell Research*, 250(1):51–61, 1999.

[370] Margaret C Frame, Hitesh Patel, Bryan Serrels, Daniel Lietha, and Michael J Eck. The ferm domain: organizing the structure and function of fak. *Nature reviews Molecular cell biology*, 11(11):802–814, 2010.

[371] Marisa A Gallicchio, E Anne McRobert, Anjali Tikoo, Mark E Cooper, and Leon A Bach. Advanced glycation end products inhibit tubulogenesis and migration of kidney epithelial cells in an ezrin-dependent manner. *Journal of the American Society of Nephrology*, 17(2):414–421, 2006.

[372] Hans I.Chen Harn, Yang Kao Wang, Chao Kai Hsu, Yen Ting Ho, Yi Wei Huang, Wen Tai Chiu, Hsi Hui Lin, Chao Min Cheng, and Ming Jer Tang. Mechanical coupling of cytoskeletal elasticity and force generation is crucial for understanding the migrating nature of keloid fibroblasts. *Experimental Dermatology*, 24(8):579–584, 2015.

[373] Bingyu Zhang, Qing Luo, Xinjian Mao, Baiyao Xu, Li Yang, Yang Ju, and Guanbin Song. A synthetic mechano-growth factor E peptide promotes rat tenocyte migration by lessening cell stiffness and increasing F-actin formation via the FAK-ERK1/2 signaling pathway. *Experimental Cell Research*, 322(1):208–216, 2014.

[374] Cosmin Mihai, Shengying Bao, Ju-Ping Lai, Samir N Ghadiali, and Daren L Knoell. Pten inhibition improves wound healing in lung epithelia through changes in cellular mechanics that enhance migration. *American Journal of Physiology-Heart and Circulatory Physiology*, 2011.

[375] Tatsuro Watanabe, Hiromi Kuramochi, Atsushi Takahashi, Kazue Imai, Naoko Kat-

suta, Tomonobu Nakayama, Hirota Fujiki, and Masami Suganuma. Higher cell stiffness indicating lower metastatic potential in b16 melanoma cell variants and in (-)-epigallocatechin gallate-treated cells. *Journal of cancer research and clinical oncology*, 138(5):859–866, 2012.

[376] Vinay Swaminathan, Karthikeyan Mythreye, E Tim O'Brien, Andrew Berchuck, Gerard C Blobe, and Richard Superfine. Mechanical stiffness grades metastatic potential in patient tumor cells and in cancer cell lines. *Cancer research*, 71(15):5075–5080, 2011.

[377] M Yokokawa, K Takeyasu, and SH Yoshimura. Mechanical properties of plasma membrane and nuclear envelope measured by scanning probe microscope. *Journal of microscopy*, 232(1):82–90, 2008.

[378] Andrew G. Clark, Kai Dierkes, and Ewa K. Paluch. Monitoring actin cortex thickness in live cells. *Biophysical Journal*, 105(3):570–580, 2013.

[379] Antje Schaefer, Joost te Riet, Katja Ritz, Mark Hoogenboezem, Eloise C Anthony, Frederik PJ Mul, Carlie J de Vries, Mat J Daemen, Carl G Figdor, Jaap D van Buul, et al. Actin-binding proteins differentially regulate endothelial cell stiffness, icam-1 function and neutrophil transmigration. *J Cell Sci*, 127(20):4470–4482, 2014.

[380] Mientao A Tsai, Richard E Waugh, and Peter C Keng. Passive mechanical behavior of human neutrophils: effects of colchicine and paclitaxel. *Biophysical Journal*, 74(6):3282–3291, 1998.

[381] Christian Rotsch and Manfred Radmacher. Drug-induced changes of cytoskeletal structure and mechanics in fibroblasts: an atomic force microscopy study. *Biophysical journal*, 78(1):520–535, 2000.

[382] Kristina Haase and Andrew E Pelling. The role of the actin cortex in maintaining cell shape. *Communicative & integrative biology*, 6(6):e26714, 2013.

[383] Margaret Clarke and James A Spudich. Nonmuscle contractile proteins: the role of actin and myosin in cell motility and shape determination. *Annual review of biochemistry*, 46(1):797–822, 1977.

[384] Gilles Weder, Mariëlle C Hendriks-Balk, Rita Smajda, Donata Rimoldi, Martha Liley, Harry Heinzelmann, André Meister, and Agnese Mariotti. Increased plasticity of the stiffness of melanoma cells correlates with their acquisition of metastatic properties. *Nanomedicine: Nanotechnology, Biology and Medicine*, 10(1):141–148, 2014.

[385] Sarah E. Cross, Yu Sheng Jin, Jianyu Rao, and James K. Gimzewski. Nanomechanical analysis of cells from cancer patients. *Nature Nanotechnology*, 2(12):780–783, 2007.

[386] Kimberly A Ward, Wen-I Li, Stephen Zimmer, and Tom Davis. Viscoelastic properties of transformed cells: role in tumor cell progression and metastasis formation. *Biorheology*, 28(3-4):301–313, 1991.

[387] Malgorzata Lekka, Piotr Laidler, Dorota Gil, Janusz Lekki, Zbigniew Stachura, and AZ Hrynkiewicz. Elasticity of normal and cancerous human bladder cells studied by scanning force microscopy. *European Biophysics Journal*, 28(4):312–316, 1999.

[388] Xinyi Guo, Keith Bonin, Karin Scarpinato, and Martin Guthold. The effect of neighboring cells on the stiffness of cancerous and non-cancerous human mammary epithelial cells. *New Journal of Physics*, 16(10):105002, 2014.

[389] Rehana Afrin, Takafumi Yamada, and Atsushi Ikai. Analysis of force curves obtained on the live cell membrane using chemically modified afm probes. *Ultramicroscopy*, 100(3-4):187–195, 2004.

[390] Anne Simon and Marie-Christine Durrieu. Strategies and results of atomic force microscopy in the study of cellular adhesion. *Micron*, 37(1):1–13, 2006.

[391] Sarah E Cross, Yu-Sheng Jin, Julianne Tondre, Roger Wong, JianYu Rao, and James K Gimzewski. Afm-based analysis of human metastatic cancer cells. *Nanotechnology*, 19(38):384003, 2008.

[392] L Sirghi, J Ponti, F Broggi, and F Rossi. Probing elasticity and adhesion of live cells by atomic force microscopy indentation. *European Biophysics Journal*, 37(6):935–945, 2008.

[393] Linda M Griffith and Thomas D Pollard. Evidence for actin filament-microtubule interaction mediated by microtubule-associated proteins. *The Journal of cell biology*, 78(3):958–965, 1978.

[394] Alperen N Ketene, Eva M Schmelz, Paul C Roberts, and Masoud Agah. The effects of cancer progression on the viscoelasticity of ovarian cell cytoskeleton structures. *Nanomedicine: Nanotechnology, Biology and Medicine*, 8(1):93–102, 2012.

[395] Stella M Hurtley. Cell biology of the cytoskeleton, 1998.

[396] Daniel A Fletcher and R Dyche Mullins. Cell mechanics and the cytoskeleton. *Nature*, 463(7280):485–492, 2010.

[397] Xavier Trepat, Zaozao Chen, and Ken Jacobson. Cell migration. *Comprehensive Physiology*, 2(4):2369–2392, 2012.

[398] Bo Chen, Girish Kumar, Carlos C Co, and Chia-Chi Ho. Geometric control of cell migration. *Scientific reports*, 3(1):1–7, 2013.

[399] Kouichi Tachibana, Seyed Mohammad Ali Haghparast, and Jun Miyake. Inhibition of cell adhesion by phosphorylated ezrin/radixin/moesin. *Cell adhesion & migration*, 9(6):502–512, 2015.

[400] Richard HJ Bruijns and Hidde Bult. Effects of local cytochalasin d delivery on smooth muscle cell migration and on collar-induced intimal hyperplasia in the rabbit carotid artery. *British journal of pharmacology*, 134(3):473–483, 2001.

[401] David A Knecht, Rebecca A LaFleur, Alem W Kahsai, Christian E Argueta, Anwar B Beshir, and Gabriel Fenteany. Cucurbitacin i inhibits cell motility by indirectly interfering with actin dynamics. *PLoS One*, 5(11), 2010.

[402] Chunji Quan, Yan Yan, Zhaoping Qin, Zhenhua Lin, and Taihao Quan. Ezrin regulates skin fibroblast size/mechanical properties and YAP-dependent proliferation. *Journal of Cell Communication and Signaling*, pages 1–12, 2017.

[403] M R Amieva, P Litman, L Huang, E Ichimaru, and H Furthmayr. Disruption of dynamic cell surface architecture of NIH3T3 fibroblasts by the N-terminal domains

of moesin and ezrin: in vivo imaging with GFP fusion proteins. *Journal of cell science*, 112 (Pt 1:111–125, 1999.

[404] Bryan Serrels, Alan Serrels, Valerie G Brunton, Mark Holt, Gordon W McLean, Christopher H Gray, Gareth E Jones, and Margaret C Frame. Focal adhesion kinase controls actin assembly via a ferm-mediated interaction with the arp2/3 complex. *Nature cell biology*, 9(9):1046–1056, 2007.

[405] Tristan P Driscoll, Brian D Cosgrove, Su-Jin Heo, Zach E Shurden, and Robert L Mauck. Cytoskeletal to nuclear strain transfer regulates yap signaling in mesenchymal stem cells. *Biophysical journal*, 108(12):2783–2793, 2015.

[406] Xian Wang, Haijiao Liu, Min Zhu, Changhong Cao, Zhensong Xu, Yonit Tsatskis, Kimberly Lau, Chikin Kuok, Tobin Filleter, Helen McNeill, et al. Mechanical stability of the cell nucleus–roles played by the cytoskeleton in nuclear deformation and strain recovery. *J Cell Sci*, 131(13):jcs209627, 2018.

[407] Marta Kapałczyńska, Tomasz Kolenda, Weronika Przybyła, Maria Zajaczkowska, Anna Teresiak, Violetta Filas, Matthew Ibbs, Renata Bliźniak, Łukasz Łuczewski, and Katarzyna Lamperska. 2d and 3d cell cultures–a comparison of different types of cancer cell cultures. *Archives of medical science: AMS*, 14(4):910, 2018.

[408] Katarina Wolf, Irina Mazo, Harry Leung, Katharina Engelke, Ulrich H Von Andrian, Elena I Deryugina, Alex Y Strongin, Eva-B Bröcker, and Peter Friedl. Compensation mechanism in tumor cell migration: mesenchymal–amoeboid transition after blocking of pericellular proteolysis. *The Journal of cell biology*, 160(2):267–277, 2003.

[409] Mathew L Coleman, Erik A Sahai, Margaret Yeo, Marta Bosch, Ann Dewar, and Michael F Olson. Membrane blebbing during apoptosis results from caspase-mediated activation of rock i. *Nature cell biology*, 3(4):339, 2001.

[410] NO Carragher, SM Walker, LA Scott Carragher, F Harris, TK Sawyer, VG Brunton, BW Ozanne, and MC Frame. Calpain 2 and src dependence distinguishes mesenchymal and amoeboid modes of tumour cell invasion: a link to integrin function. *Oncogene*, 25(42):5726–5740, 2006.

[411] Justin R Tse and Adam J Engler. Preparation of hydrogel substrates with tunable mechanical properties. *Current protocols in cell biology*, 47(1):10–16, 2010.

[412] Aleksandra K Denisin and Beth L Pruitt. Tuning the range of polyacrylamide gel stiffness for mechanobiology applications. *ACS applied materials & interfaces*, 8(34):21893–21902, 2016.

[413] Martin Bergert, Stanley D Chandradoss, Ravi A Desai, and Ewa Paluch. Cell mechanics control rapid transitions between blebs and lamellipodia during migration. *Proceedings of the National Academy of Sciences*, 109(36):14434–14439, 2012.

[414] Yan-Jun Liu, Maël Le Berre, Franziska Lautenschlaeger, Paolo Maiuri, Andrew Callan-Jones, Mélina Heuzé, Tohru Takaki, Raphaël Voituriez, and Matthieu Piel. Confinement and low adhesion induce fast amoeboid migration of slow mesenchymal cells. *Cell*, 160(4):659–672, 2015.

[415] Katarina Wolf, Regina Müller, Stefan Borgmann, Eva-B Bröcker, and Peter Friedl. Amoeboid shape change and contact guidance: T-lymphocyte crawling through fibrillar collagen is independent of matrix remodeling by mmps and other proteases. *Blood*, 102(9):3262–3269, 2003.

[416] Joseph P Campanale, Thomas Y Sun, and Denise J Montell. Development and dynamics of cell polarity at a glance. *J Cell Sci*, 130(7):1201–1207, 2017.

[417] Stephen E Malawista, Anne de Boisfleury Chevance, and Laurence A Boxer. Random locomotion and chemotaxis of human blood polymorphonuclear leukocytes from a patient with leukocyte adhesion deficiency-1: Normal displacement in close quarters via chimneying. *Cell motility and the cytoskeleton*, 46(3):183–189, 2000.

[418] Anna Lorentzen, Jeffrey Bamber, Amine Sadok, Ilan Elson-Schwab, and Christopher J Marshall. An ezrin-rich, rigid uropod-like structure directs movement of amoeboid blebbing cells. *J Cell Sci*, 124(8):1256–1267, 2011.

[419] Jörg Renkawitz, Kathrin Schumann, Michele Weber, Tim Lämmermann, Holger Pflicke, Matthieu Piel, Julien Polleux, Joachim P Spatz, and Michael Sixt. Adaptive force transmission in amoeboid cell migration. *Nature cell biology*, 11(12):1438–1443, 2009.

[420] Chris D Madsen, Steven Hooper, Melda Tozluoglu, Andreas Bruckbauer, Georgina Fletcher, Janine T Erler, Paul A Bates, Barry Thompson, and Erik Sahai. Stripak components determine mode of cancer cell migration and metastasis. *Nature cell biology*, 17(1):68–80, 2015.

[421] J Sroka, M Von Gunten, GA Dunn, and HU Keller. Phenotype modulation in non-adherent and adherent sublines of walker carcinosarcoma cells: the role of cell-substratum contacts and microtubules in controlling cell shape, locomotion and cytoskeletal structure. *The international journal of biochemistry & cell biology*, 34(7):882–899, 2002.